UNIVERSIDAD DE GRANADA

PROGRAMA OFICIAL DE DOCTORADO EN BIOMEDICINA

MECHANISMS MEDIATING T LYMPHOCYTE INDUCED PATHOLOGICAL CARDIAC REMODELING IN HEART FAILURE

MECANISMOS MEDIADOS POR LINFOCITOS T IMPLICADOS EN EL REMODELADO CARDIACO PATOLOGICO EN INSUFICIENCIA CARDIACA

Presentado por:

ANE MIREN SALVADOR GARICANO

Directoras de tesis:

Dra. Pilar Alcaide y Dra. Ana C. Abadía

TESIS DOCTORAL

Granada

2017

Editor: Universidad de Granada. Tesis Doctorales
Autora: Ane Miren Salvador Garicano
ISBN: 978-84-9163-199-6
URI: http://hdl.handle.net/10481/46428

El doctorando / The *doctoral candidate* **[Ane Miren Salvador Garicano]** y los directores de la tesis / and the thesis supervisor/s: **[Ana Clara Abadia Molina y Maria Pilar Alcaide Alonso]**

Garantizamos, al firmar esta tesis doctoral, que el trabajo ha sido realizado por el doctorando bajo la dirección de los directores de la tesis y hasta donde nuestro conocimiento alcanza, en la realización del trabajo, se han respetado los derechos de otros autores a ser citados, cuando se han utilizado sus resultados o publicaciones.

/

Guarantee, by signing this doctoral thesis, that the work has been done by the doctoral candidate under the direction of the thesis supervisor/s and, as far as our knowledge reaches, in the performance of the work, the rights of other authors to be cited (when their results or publications have been used) have been respected.

Lugar y fecha / Place and date:

Granada, 30 de enero de 2017

Director/es de la Tesis / *Thesis supervisor/s;*	Doctorando / *Doctoral candidate*:
	
Firma / Signed	Firma / Signed

El trabajo presentado en la presente Tesis Doctoral ha sido publicado y expuesto en:

PUBLICACIONES:

- **Salvador AM**, Nevers T, Velázquez F, Aronovitz M, Wang B, Abadía Molina A, Jaffe IZ, Karas RH, Blanton RM, Alcaide P. *Intercellular Adhesion Molecule 1 Regulates Left Ventricular Leukocyte Infiltration, Cardiac Remodeling, and Function in Pressure OverloadInduced Heart Failure.* J Am Heart Assoc. 2016 Mar 15;5(3):e003126. doi: 10.1161/JAHA.115.003126.
- Nevers T, **Salvador AM**, Grodecki-Pena A, Knapp A, Velázquez F, Aronovitz M, Kapur NK, Karas RH, Blanton RM, Alcaide P. *Left Ventricular T-Cell Recruitment Contributes to the Pathogenesis of Heart Failure.* Circ Heart Fail. 2015 Jul; 8(4):776-87. doi: 10.1161/CIRCHEARTFAILURE.115.002225.

ASISTENCIA Y EXPOSICION EN CONGRESOS:

- Experimental Biology meeting 2015, Boston, MA (USA). Oral presentation. Intercelullar Adhesion Molecule 1 (ICAM-1) regulates cardiac remodeling and function in pressure overload induced heart failure. *The FASEB Journal 29 (1 Supplement), 46.3.*
    - Additional oral presentation in special session of “Highlights: Graduate Student research in pathology”.

- Basic Cardiovascular Sciences conference 2015, New Orleans, LA, (USA). Poster presentation. Intercellular Adhesion Molecule 1 Regulates Cardiac Remodeling and Function and T Cell Recruitment to the Heart in Pressure Overload Induced Heart Failure. *Circulation Research 117 (Suppl 1), A211-A211.*
    - Awarded with New Investigator Travel Award.

- Experimental Biology meeting 2016, San Diego, CA (USA). Oral presentation. Intercellular Adhesion Molecule 1 Regulates Left Ventricular Leukocyte Recruitment, Cardiac Remodeling and Function in Pressure Overload Induced Heart Failure. *The FASEB Journal 30 (1 Supplement), 306.6-306.6.*
    - Trainee Travel Award (Sobel Scholar) from the American Society for Investigative Pathology

- Additional oral presentation in special session of “Highlights: Graduate Student research in pathology”.

- Basic Cardiovascular Sciences conference 2016, Phoenix, AZ (USA). Poster presentation. The role of the chemokine receptor CXCR3 - LFA1 integrin – ICAM1 axis in T lymphocyte mediated cardiac inflammation in pressure overload induced heart failure.

TABLE OF CONTENTS

1 NON STANDARD ABBREVIATIONS AND ACRONYMS

ACE: Angiotensin Converting Enzyme

ANP: Atrial Natriuretic Peptide

APC: Antigen Presenting Cell

ARB: Angiotensin Receptor Blocker

BNP: Brain Natriuretic Peptide

CAD: Coronary Artery Disease

CAM: Cell Adhesion Molecule

CaMKII: Ca2+/Calmodulin-dependent Protein Kinase II

Cas9: CRISPR associated protein 9

CFB: Cardiac Fibroblasts

CLR: C-type Lectin Receptor

CRISPR: Clustered Regularly Interspaced Short Palindromic Repeats

CM: Cardiac Myocyte

CVD: Cardiovascular Disease

DAMP: Damage-Associated Molecular Patterns

DCM: Dilated Cardiomyopathy

DM: Diabetes Mellitus

DS: Downstream

EC: Endothelial Cell

ECM: Extracellular Matrix

EC-MR: Endothelial Cell Mineralocorticoid Receptor

EDD: End Diastolic Diameter

EDP: End Diastolic Pressure

ESD: End Systolic Diameter

ETB: Endothelin Receptor type B

FoxP3: Forkhead box P3

FS: Fractional Shortening

GATA3: GATA binding protein 3

GPCR: G Protein-Coupled Receptors

HF: Heart Failure

HFrEF: Heart Failure with reduced Ejection Fraction

HFpEF: Heart Failure with preserved Ejection Fraction

H&E: Hematoxylin and Eosin

ICAM1: Intercellular Adhesion Molecule 1

IFNγ: Interferon gamma

Ig: Immunoglobulin

IHC: Immunohistochemistry

IL: Interleukin

iNOS: inducible Nitric Oxide Synthase

IR: Ischemia-Reperfusion injury

KI: Knock In

KO: Knock Out

LFA1: Lymphocyte Function-associated Antigen 1

loxP: locus of X-over P1

LV: Left Ventricle

LVP: Left Ventricular Pressure

LVV: Left Ventricular Volume

Mac1: Macrophage-1 antigen

MCP1: Monocyte Chemoattractant Protein 1

MHC: Major Histocompatibility Complex

MHCα: Myosin Heavy Chain alpha isoform

MHCβ: Myosin Heavy Chain beta isoform

MI: Myocardial Infarction

MLN: Mediastinal Lymph Nodes

MMP: Matrix Metalloproteases

MR: Mineralocorticoid Receptor

NF- κB: Nuclear Factor-κB

NK: Natural Killer cells

NLR: NOD-like Receptor

PAMP: Pathogen-Associated Molecular Patterns

pDC: plasmacitoid Dendritic Cell

PECAM1: Platelet/Endothelial Cell Adhesion Molecule 1

PRR: Pattern Recognition Receptor

PS: Picrosirius Red

RAAS: Renin Angiotensin Aldosterone System

RORγt: Retinoic acid receptor-related Orphan Receptor gamma-T

RV: Right Ventricle

SAN: Sinoatrial Node

sgRNA: Short guide RNA

sICAM1: soluble Intercellular Adhesion Molecule 1

SMC: Smooth Muscle Cell

SMAα: Smooth Muscle Actin alpha

STAT3: Signal Transducer and Activator of Transcription 3

TAC: Transverse Aortic Constriction

Tbet: T-box transcription factor

Treg: Regulatory T cell

TGFβ: Tumor Growth Factor beta

TCR: T Cell Receptor

TLR: Toll-like Receptor

TNFα: Tumor Necrosis Factor alpha

US: Upstream

VCAM1: Vascular Cell Adhesion Molecule 1

VLA4 : Very Late Antigen 4

VP: Ventricular Pressure

VV: Ventricular Volume

WT : Wild-type

2 ABSTRACT

Despite the emerging association between heart failure and chronic inflammation, the specific immune and inflammatory mechanisms involved remain to be investigated. In the current doctoral thesis dissertation, we hypothesize that in response to left ventricular pressure overload, the adaptive immune response gets activated, CD4+ lymphocytes differentiate into their effector subsets and are recruited into the left ventricle through specific mechanisms, contributing to pathological cardiac remodeling and heart failure.

Initially, a temporal correlation between T lymphocyte recruitment and cardiac hypertrophy, fibrosis and dysfunction is observed in WT mice, while none of these pathological features is observed in mice lacking T lymphocytes. Additionally, we show that the adhesion molecule ICAM1 plays a key role in T lymphocyte recruitment in response to pressure overload; $ICAM1^{-/-}$ mice have reduced left ventricular T lymphocyte recruitment as compared to WT mice, and are protected from developing a pathological cardiac remodeling phenotype, characterized by a lack of both cardiac fibrosis and dysfunction, despite having the same degree of lymphocyte activation.

When investigating the inducers of ICAM1 upregulation in the left ventricle in response to pressure overload, we observe that the pro-inflammatory cytokines overexpressed in the myocardium likely mediate the activation of the cardiac endothelium, independently of aldosterone signaling through endothelial cell mineralocorticoid receptor. Our experimental data using mice lacking selectively endothelial cell mineralocorticoid receptor indicate that this last one is not essential for either ICAM1 upregulation or LV leukocyte recruitment; however, it does seem to have certain relevance in systolic function in response to pressure overload.

Next, when examining T cell chemotaxis mechanisms taking place in response to pressure overload, we have found an increase in both the expression of the chemokines CXCL9 and CXCL10 in the left ventricle, and in the percent of T lymphocytes expressing their receptor CXCR3 in the mediastinal lymph nodes that drain the myocardium. Additionally, CXCR3+ T lymphocytes express higher levels of the integrin LFA1, ICAM1's main ligand. In line with this, our *in vitro* studies indicate that CXCR3+ lymphocyte adhesion to ICAM1 is increased in the presence of these chemokines, in a LFA1 dependent manner.

With the aim of determining the role of ICAM1 expressed in the different cell types involved in heart failure development, we have begun to develop a mouse in which the gene encoding for ICAM1 is flanked with loxP sites using CRISPR/Cas9 technology, with the goal of generating cell specific ICAM1 knock-out mice.

In summary, in this doctoral thesis dissertation we describe the T lymphocyte mediated immune response, the inflammatory mechanisms, the endothelial cell adhesion molecules and the chemokines that mediate T lymphocyte cardiotropism during heart failure development, being many of these mechanisms potential targets for the treatment of this chronic disease.

3 SUMMARY-*RESUMEN*

Heart failure (HF) is a chronic pathological condition in which the myocardium modifies its phenotype in response to a variety of insults (ischemia, hypertension, autoimmunity and metabolic diseases, among others) with the aim of maintaining an adequate contractile function. Such phenotypical changes include cardiac hypertrophy, cardiac fibrosis and candiac inflammation, which initially contribute to the maintenance of the contractile function, but in the long term are insufficient and lead to HF.

Given the fact that HF is a complex pathology, many mechanisms have been investigated in the last decades with the aim of understanding the disrupted systems that underlay in HF development. Among those factors, the immune system and pro-inflammatory mechanisms have recently started to be associated with the progression of HF. However, clinical trials blocking the systemic immune response have resulted inefficient, highlighting the need for a better understanding of the specific immune and inflammatory mechanisms involved in HF.

With this aim, in the current doctoral thesis dissertation we hypothesize that in response to left ventricular (LV) pressure overload, the adaptive immune response becomes activated, CD4+ lymphocytes differentiate into their effector subsets and are recruited into the LV through specific mechanisms, contributing to pathological cardiac remodeling and HF. To test this hypothesis, we have used the Transverse Aortic Constriction (TAC) mouse model of LV pressure overload, in mice lacking T lymphocytes ($TCR\alpha^{-/-}$), the adhesion molecule ICAM1 ($ICAM1^{-/-}$) or the Mineralocorticoid Receptor specifically in Endothelial Cells ($EC\text{-}MR^{-/-}$), in order to investigate the role of these molecules and cell types in HF development. For quantifying lymphocyte activation in mediastinal lymph nodes and in circulation as well as their recruitment into the myocardial tissue, flow cytometry has been used in addition

to histological techniques. For analyzing parameters of pathological cardiac remodeling as cardiac hypertrophy, fibrosis, inflammation and dysfunction, qRT-PCR, histological techniques and cardiac function study methods, as non-invasive echocardiography and invasive pressure-volume loops, have been used. For evaluating the adhesion molecules and chemokines involved in lymphocyte recruitment *in vitro*, a parallel flow chamber apparatus attached to a microscope for live cell imaging has been utilized. Finally, for the generation of the knock-in mice with the gene encoding for ICAM1 flanked by loxP sites, we have based our approach in the CRISPR-Cas9 technology for designing the sgRNA sequences that guide Cas9 and the oligonucleotide sequences to be inserted in the 5' and 3' regions of the ICAM1 gene; for the validation of the insertion, specific genotyping methods have been used.

Initially, we describe the role T lymphocytes in pathological cardiac remodeling in response to LV pressure overload, in which we observe a temporal correlation between lymphocyte recruitment and cardiac dysfunction, as well as phenotypical changes as ventricular hypertrophy and fibrosis. The role of T lymphocytes in these pathological processes is highlighted in the experimental observations using TCR$\alpha^{-/-}$ mice, which in response to the same pressure overload insult, have preserved ventricular function, and do not develop either cardiac hypertrophy or fibrosis.

Next, we determined the recruitment mechanisms that mediate T lymphocyte infiltration into the LV after TAC. In these studies, we observe an LV upregulation of the adhesion molecule ICAM1, which plays an essential role in T lymphocyte recruitment in response to pressure overload, since in the absence of ICAM1 (ICAM1$^{-/-}$ mice), T lymphocyte recruitment is significantly lower than in mice that do express ICAM1. Additionally, ICAM1$^{-/-}$ mice are protected from developing a pathological cardiac

remodeling phenotype, characterized by a lack of both cardiac fibrosis and dysfunction, despite having the same degree of lymphocyte activation.

When investigating the factors that induce ICAM1 upregulation in the endothelial cells in response to pressure overload, our observations suggest that probably the pro-inflammatory cytokines IL-6 and IL-1β overexpressed in the myocardium are the responsible of activating the cardiac endothelium, and not hormonal mechanisms as the signaling that occurs upon aldosterone binding to the mineralocorticoid receptor in the endothelium (EC-MR). Our experimental data using mice lacking EC-MR indicate that this last one is not essential for either ICAM1 upregulation or T lymphocyte and pro-inflammatory monocyte LV recruitment; however, EC-MR does seem to have certain relevance in systolic function in response to pressure overload.

Lastly, we evaluate the chemokine receptors and their ligands involved in T lymphocyte chemotaxis and LV tropism during HF development. In response to pressure overload the expression of the chemokines CXCL9 and CXCL10 is upregulated in the LV, as well as the percent of T lymphocytes expressing their receptor CXCR3 in the mediastinal lymph nodes that drain the myocardium. Additionally, CXCR3+ T cells express higher levels of the integrin LFA1, ICAM1's main ligand. In line with this, our *in vitro* studies indicate that CXCR3+ lymphocyte adhesion to ICAM1 is increased in the presence of the chemokines CXCL9 and CXCL10, in a LFA1 dependent manner.

Given the fact that several cell types express ICAM1 in addition to endothelial cells, and with the aim of determining the role of ICAM1 in the different cell types involved in the pathological mechanisms associated to HF, we have begun to develop a mouse in which the gene encoding for ICAM1 is flanked with loxP sites with the goal of generating tissue or cell specific ICAM1 knock-out mice. For this purpose, we have

taken advantage of the emergent CRISPR/Cas9 technology, based on which we have designed and microinjected oligonucleotides containing homologous regions and loxP sequences for their insertion by recombination in the upstream (US) and downstream (DS) sites of the ICAM1 gene. Given the low degree of successful insertions we got using that initial strategy, we have considered an alternative approach based on a single plasmid that includes both the US and the DS loxP insertion sequences that flank exon 1 of the ICAM1 encoding gene, which once microinjected will ideally be inserted in a single step, thus increasing the percent of successful insertions and leading to the generation of the *ICAM1*$^{fl/fl}$ mouse.

The results of this doctoral thesis dissertation indicate that a T lymphocyte mediated immune response occurs during HF development. The fact that the cytokine IFNγ, the transcription factor Tbet and the chemokine receptor CXCR3 are upregulated in the LV in mice undergoing TAC suggest that the immune response is mediated by Th1 lymphocytes. The mechanisms that initiate the adaptive immune response remain to be explored; a classical T lymphocyte response could be considered, responding to either cardiac antigens exposed due to the lack of immune tolerance in the context of pressure overload or non-cardiac antigens that activate T lymphocytes. Alternatively, T lymphocytes could also get activated in response to Damage Associated Molecular Patterns (DAMP). Future studies using mice lacking key molecules of both antigen-specific and non-antigen-specific immune responses will shed some light to the antigen specificity and/or non-antigen specificity of the adaptive immune response in HF. Our results also indicate that the adhesion molecule ICAM1 plays an important role in T lymphocyte recruitment to the LV, whose endothelial upregulation is EC-MR independent and possibly mediated by pro-inflammatory cytokines released in the

myocardium in response to pressure overload. Given the lack of cardiac dysfunction in ICAM1$^{-/-}$ mice, future experiments will explore the possibility of ICAM1 becoming upregulated in the cardiac myocytes in response to hemodynamic stress, through which infiltrated T lymphocytes come into contact with cardiac myocytes, leading to cardiac dysfunction. In the near future, taking advantage of the *ICAM1*$^{fl/fl}$ mice, currently under development, we will be able to describe in depth the role of extra-endothelial ICAM1 and the necessity of a direct interaction between infiltrated T lymphocytes and cardiac resident cells leading to pathological cardiac remodeling. Furthermore, the specific mechanisms through which EC-MR mediates cardiac systolic function remain to be described; these mechanisms could involve an improved coronary vessel function in the absence of EC-MR, which could partially explain the beneficial therapeutic effect of MR antagonists, independently of the development of cardiac fibrosis and leukocyte infiltration to the LV in HF.

In summary, in this doctoral thesis dissertation we describe the adaptive immune response, the inflammatory mechanisms, the endothelial cell adhesion molecules and the chemokines that mediate T lymphocyte cardiotropism during HF development, being many of them potential targets for the treatment of this chronic disease.

La insuficiencia cardíaca (IC) es una patología crónica en la cual el tejido miocárdico modifica su fenotipo en respuesta a una variedad de factores (isquemia, hipertensión, autoinmunidad, enfermedades metabólicas etc.) con el objetivo de mantener una función contráctil adecuada. Estos cambios fenotípicos incluyen procesos de hipertrofia, fibrosis e inflamación cardíaca, los cuales en un inicio resultan suficientes para mantener una función cardíaca adecuada, pero que a largo plazo resultan ineficientes y llevan a IC crónica.

Al tratarse de una patológica compleja, son muchos los mecanismos que han sido investigados en las últimas décadas con el objetivo de comprender los sistemas disfuncionales que subyacen en el desarrollo de IC crónica. Entre estos factores, el sistema inmunitario y mecanismos pro-inflamatorios relacionados con él han sido recientemente asociados con el desarrollo de esta patología. Sin embargo, ensayos clínicos basados en inhibir la respuesta inflamatoria de forma sistémica han resultado ineficaces, subrayando la necesidad de investigar y comprender de forma específica los mecanismos inmunes e inflamatorios implicados en IC.

Con este objetivo, en la presente tesis doctoral postulamos la hipótesis de que en respuesta a sobrecarga de presión en el ventrículo izquierdo del corazón, el sistema inmunitario adaptativo se activa, con ello los linfocitos CD4+ se diferencian a sus subtipos efectores y se reclutan mediante mecanismos específicos al ventrículo izquierdo, contribuyendo al remodelado cardíaco patológico e IC. Para probar dicha hipótesis, hemos hecho uso del modelo de ratón basado en la constricción quirúrgica de la aorta transversa (TAC), la cual induce una sobrecarga de presión en el ventrículo izquierdo. Hemos aplicado dicha cirugía a ratones deficientes en linfocitos T (TCR$\alpha^{-/-}$), deficientes en la molécula de adhesión ICAM1 (ICAM1$^{-/-}$) o deficientes en el receptor

mineralocorticoide selectivamente en células endoteliales (EC-MR$^{-/-}$), para determinar el papel de estos tipos celulares y moléculas en el desarrollo de IC. Con el objetivo de cuantificar la activación linfocitaria en ganglios linfáticos mediastínicos y en circulación sanguínea, así como su infiltración al ventrículo izquierdo, hemos hecho uso de técnicas histológicas y de citometría de flujo. Los parámetros de remodelado cardíaco patológico, como hipertrofia, fibrosis, inflamación y disfunción cardíaca, han sido analizados mediante PCR cuantitativa, técnicas histológicas, ecocardiografía no-invasiva y curvas hemodinámicas presión-volumen invasivas. Para la evaluación de moléculas de adhesión y quimioquinas implicadas en el reclutamiento linfocitario in vitro, hemos hecho uso de la cámara paralela de flujo laminar adosada a microscopio. Finalmente, para la creación del ratón knock-in, conteniendo secuencias loxP flanqueando el gen que codifica para ICAM1, nos hemos basado en la tecnología CRISPR-Cas9 para el diseño de por un lado las secuencias sgRNA que guían a Cas9, y por otro lado, de las secuencias de oligonucleótidos a insertar en los extremos 5' y 3' del gen que codifica para ICAM1; para la validación de presencia de la inserción hemos hecho uso de métodos de genotipado específicos.

Inicialmente, describimos el papel esencial de los linfocitos T en el remodelado ventricular patológico en respuesta de sobrecarga de presión del ventrículo izquierdo, donde se observa una correlación temporal entre el reclutamiento linfocitario y la disfunción miocárdica, junto con cambios fenotípicos como hipertrofia y fibrosis ventricular. Además, se enaltece la importancia de los linfocitos T en estos procesos patológicos en las observaciones experimentales en ratones deficientes en linfocitos T, los cuales en respuesta al mismo insulto de sobrecarga de presión, mantienen una correcta función ventricular, sin desarrollar ni hipertrofia ni fibrosis.

Tras ello, determinamos los mecanismos de reclutamiento utilizados por los linfocitos T en su migración al ventrículo izquierdo. En estos estudios, observamos que la expresión endotelial de la molécula de adhesión ICAM1 está incrementada y juega un papel esencial en el reclutamiento de linfocitos T al miocardio como respuesta a la sobrecarga de presión, ya que en ausencia de ICAM1 (ratones ICAM1$^{-/-}$) el número de linfocitos reclutados al ventrículo izquierdo es significativamente inferior a ratones que expresan ICAM1. Además de ello, los ratones deficientes en ICAM1 están protegidos de desarrollar remodelado cardiaco patológico, caracterizado por ausencia de fibrosis y disfunción cardíaca, a pesar del mismo grado de activación linfocitaria.

Al determinar los factores que llevan a un incremento de expresión endotelial de ICAM1 en el contexto de sobrecarga de presión, observamos que probablemente las citoquinas pro-inflamatorias IL-6 e IL-1β sobre-expresadas en el miocardio están implicadas en la activación endotelial, y no mecanismos endocrinológicos como la señalización que ocurre cuando la hormona aldosterona se une al receptor mineralocorticoide en el endotelio vascular (EC-MR). Nuestros resultados en ratones deficientes en dicho receptor exclusivamente en células endoteliales indican que EC-MR no es esencial en el incremento de expresión de ICAM1 ni en el reclutamiento de células T y monocitos pro-inflamatorios al miocardio, a pesar de que presenta cierta importancia en la función sistólica en respuesta a sobrecarga de presión.

Adicionalmente, indicamos los receptores de quimioquinas y sus ligandos implicados en la quimiotaxis y el tropismo de los linfocitos T hacia el ventrículo izquierdo en el desarrollo de IC. Dentro del contexto de sobrecarga de presión, la expresión ventricular de las quimioquinas CXCL9 y CXCL10 se encuentra incrementado, al igual que el porcentaje de linfocitos T que expresan su correspondiente receptor CXCR3 en

los nódulos linfáticos que drenan el miocardio. Además, los linfocitos T CXCR3+ expresan mayores niveles de la integrina LFA1, principal ligando de ICAM1. Estudios in vitro indican que en presencia de dichas quimioquinas la adhesión de linfocitos CXCR3+ a ICAM1 está incrementada, la cual resulta ser dependiente de LFA1.

Dado que otros tipos celulares expresan ICAM1 además de las células endoteliales, y con el objetivo de determinar el papel de ICAM1 en los diferentes tipos celulares implicados en los fenómenos patológicos asociados a IC, hemos comenzado a desarrollar el ratón con el gen que codifica para ICAM1 flanqueado por secuencias loxP, para así poder generar ratones deficientes en ICAM1 específicamente en diferentes tipos celulares. Para ello, hemos hecho uso de la tecnología CRISPR/Cas9 emergente, mediante la cual hemos inicialmente microinyectado oligonucleótidos con secuencias homólogas y loxP para su inserción por recombinación en las regiones 5' y 3' del gen que codifica ICAM1. Dado el bajo nivel de rendimiento de esta estrategia también hemos considerado la producción de un único plásmido que incluya ambas regiones loxP de inserción, que flanqueen el exón 1 del gen que codifica ICAM1, para así una vez microinyectado, la inserción se produzca en un único paso y con ello idealmente se aumente el porcentaje de inserción exitosa y generemos el ratón $ICAM1^{fl/fl}$.

Los resultados de esta tesis doctoral indican que existe una clara respuesta inmunitaria durante el desarrollo de IC mediada por linfocitos T. El hecho de que la citoquina IFNγ, el factor de transcripción Tbet y el receptor de quimioquinas CXCR3 se encuentren incrementados en el ventrículo izquierdo de ratones con IC sugiere que la respuesta es mediada por células Th1. Los mecanismos que inician dicha respuesta también quedan por explorar, pudiéndose considerar una respuesta T clásica hacia

antígenos cardíacos que queden expuestos debido a la ausencia de tolerancia inmunológica en el contexto de sobrecarga de presión miocárdica, o a antígenos no cardíacos que activen a los linfocitos T. No hay que descartar la posibilidad de que los linfocitos T se activen en respuesta a patrones moleculares asociadas a daño tisular (DAMP). Futuros estudios en ratones deficientes en moléculas clave en el desarrollo de respuestas dependiente e independientes de antígeno determinaran el tipo de linfocitos T, la especificidad de antígeno y si además existe una activación independiente de antígeno en la respuesta inmunitaria durante la IC. Nuestros resultados además indican el papel esencial de ICAM1 en el reclutamiento de linfocitos T al ventrículo izquierdo, cuya sobreexpresión endotelial en el miocardio es independiente de EC-MR y posiblemente mediada por citoquinas pro-inflamatorias producidas de forma local en el miocardio en IC. Dada la ausencia de disfunción cardíaca de los ratones deficientes en ICAM1, queda por explorar la posibilidad de que los cardiomiocitos expresen ICAM1 en respuesta al estrés hemodinámico, y mediante ella medien la interacción de linfocitos T infiltrados y cardiomiocitos, llevando a disfunción miocárdica. En un futuro próximo, mediante el uso de los ratones ICAM1$^{fl/fl}$ que estamos desarrollando, podremos describir en mayor profundidad el papel extra-endotelial de ICAM1 y con ello la necesidad de interacción directa entre linfocitos T infiltrados y células cardíacas que lleven al remodelado cardíaco patológico. Adicionalmente, quedan por describir los mecanismos específicos mediante los cuales EC-MR regula la función sistólica, los cuales posiblemente estén relacionados con la mejora de la función coronaria en ausencia de EC-MR y explique parcialmente el beneficio terapéutico de los fármacos antagonistas de MR, independientemente del desarrollo de fibrosis y reclutamiento leucocitario al ventrículo izquierdo en IC.

En resumen, en la presente tesis doctoral describimos el papel de la respuesta inmunitaria adaptativa, los mecanismos inflamatorios, las moléculas de adhesión endotelial y las quimioquinas que median el cardiotropismo de los linfocitos T durante el desarrollo de IC, muchos de ellos potenciales dianas para el tratamiento de esta crónica enfermedad.

4 BACKGROUND

4.1 Cardiac anatomy and physiology

The cardiac tissue consists on a muscular pump associated to the pulmonary and systemic circulatory systems, which synchronized maintain and regulate a correct nutrient and oxygen supply to all tissues and organs of the body and transport carbon dioxide back to the lungs (1).

The myocardium relies on a variety of cells encompassed on a network that ensure adequate cardiac function: contracting cardiac myocytes (CM), which provide the power to pump the blood through the circulatory system (2), together with vascular smooth muscle cell (SMC), endothelial cells (EC) and cardiac fibroblasts (CFB). More recently, we have learned that other cells non-classically known to be part of the heart, such as macrophages, regulatory T cells and B cells, are present in the myocardium and contribute to cardiac structure and homeostasis (Figure 4.1) (3-7). Self-excitable CM contractility is initiated in a regular manner and at an appropriate rate by pacemaker cells that compose the sinoatrial node (SAN). Gap junctions and Purkinje fibers enable synchronized electric and mechanical conductance to the entire myocardial tissue; in addition, CM interactions with the rest of cardiac resident cells that create the extracellular matrix (ECM) ensure the optimal myocardial contraction and relaxation functions, as well as contribute to biochemical, structural, mechanical and electrical properties (3, 8).

The normal human and murine adult heart consists of four functionally and spatially distinct chambers, two atria and two ventricles, separated on right and left heart muscular pumps (Figure 4.1). The right heart, composed by the right atrium and right ventricle, drives deoxygenated blood from the vena cava through the pulmonary artery to the lungs, which once enriched in oxygen, the pulmonary aorta drives the oxygenated

blood to the left heart. This last one, composed by the left atria and left ventricle (LV), pump the blood out through the aorta in a regular late, thus providing metabolic substrates and oxygen to the different organs and tissues in the organism. In order to ensure the one-way flow, each atrium is separated from the correspondent ventricle by the tricuspid and mitral valve, in the right and left heart respectively.

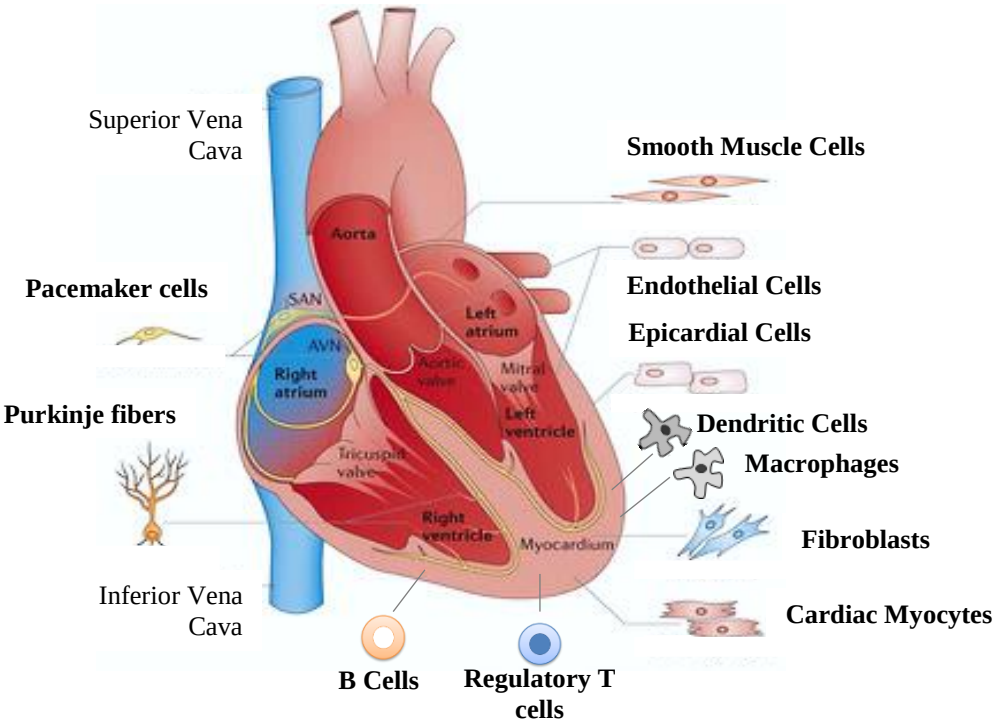

Figure 4.1. Cardiac anatomy and cell composition of the heart (3, 4).

The cardiac cycle, defined as the lapse of time required for each heartbeat, is separated in the systolic or contractile and diastolic or relaxation phases. In the systolic period, the CM membrane depolarizes and allows calcium entrance in the cytoplasm, resulting in maximal mechanical contraction. During the diastolic period the CM membrane repolarizes, calcium levels in the cytoplasm decrease and therefore the myocardium relaxes from the end systolic maximal contraction state to the resting state.

In each cardiac cycle, the LV undergoes modifications in pressure (LVP) and volume (LVV) to regulate unidirectional blood flow (Figure 4.2).

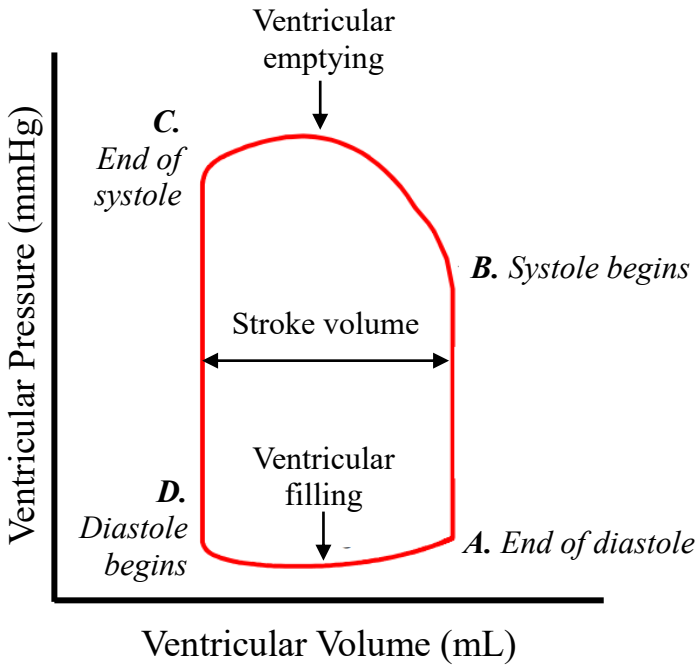

Figure 4.2. Diagram representing the events taking place in each cardiac cycle. During the diastole, time *D*, the ventricle filling takes place, increasing the LVV, while the LVP remains relatively constant. At time *A* the contractile phase begins, LVP increases reaching a higher pressure than the atria but still lower than the aorta; thus the mitral valve closes and the isovolumetric ventricular contraction occurs. When LVP exceeds aortic pressure, time *B*, the aortic valve opens and the blood is ejected from the LV out to the aorta and LVV decreases. As the cardiac contractile phase comes to an end, LVP decreases below aortic pressure (time *C*) and the aortic valve closes. The relaxation process continues while the LVP continues dropping but the LVV remains constant, having both mitral and aortic valves closed; this period is called isovolumetric relaxation. Eventually, LVP drops below the atrial pressure and the mitral valve opens (time *D*), initiating the filling phase. Thus, blood flows from the atrium into the ventricle, increasing the LVV and therefore initiating another cardiac cycle.

When alterations of the different steps involved in the cardiac cycle occur, systolic, diastolic or both functions are affected resulting in cardiac dysfunction and heart failure.

4.2 Pathological ventricular remodeling and heart failure

Heart failure (HF), frequently referred as congestive heart failure (CHF), is a complex pathological condition in which the heart cannot pump oxygen-rich blood to meet the body's needs efficiently. HF was first described centuries ago but still remains one of the most common causes of hospitalization in both Europe (9) and US (10). No curative treatment has been found to date, thus nowadays HF affects more than 26 million people worldwide (11), 6.5 million Europeans and 5.7 million Americans, with increasing prevalence estimated in 46% between years 2012 and 2030. Even though relevant improvements have been done in the therapeutics to either prevent or treat HF, 2% to 17% of patients die in the first admission, 17%-45% within the first year after the admission and more than 50% within five years, indicating a poor prognosis of patients after the first admission (12).

4.2.1 Classification of heart failure

The complex syndrome of HF can be classified in different subtypes based on either the patients' symptomatology, the ability of the heart chambers to efficiently eject blood in each cardiac cycle, or the etiology leading to the inability of the heart to function correctly that results in HF:

4.2.1.1 New York Heart Association Functional Classification

This HF classification in based on the limitations the patients have when subjected to physical activity at the time of diagnosis, and it classifies the patients in four numerical categories that range from less to more severe HF (13). This classification was first

published in 1928 by the New York Heart Association; it has been updated in seven subsequent editions, being the ninth edition “Nomenclature and Criteria for Diagnosis of Diseases of the Heart and Great Vessels” (Little, Brown & Co) the latest one revised by the Criteria Committee of the American Heart Association and released on 1994:

I. NYHA Class I: patients can perform ordinary physical activity that does not cause fatigue, dyspnea or palpitations.
II. NYHA Class II: these patients are comfortable at rest but present slight limitations when doing physical activity, resulting in fatigue, shortness of breath and palpitations.
III. NYHA Class III: these patients are comfortable at rest but present severe limitations when doing physical activity; even doing low amount of activity results in fatigue, shortness of breath or palpitations.
IV. NYHA Class IV: patients classified in this class are not able to do physical activity without discomfort. They present fatigue, shortness of breath or palpitations at rest, all symptoms of HF.

4.2.1.2 Heart Failure classification based on ejection fraction

The ejection fraction (EF) is an important measurement determined by non-invasive echocardiography that indicates the efficacy of the heart pumping blood out in each cardiac cycle. It consists on the ratio between the volume of blood pumped out from the LV in systole (stroke volume), relative to the total volume of blood in the LV at the end of the diastole. Thus, this parameter can be used for diagnosing and tracking HF progression (14):

I. Heart failure with reduced ejection fraction (HFrEF): also known as systolic HF, refers to the condition in which the heart does not contract effectively and the volume of oxygen-rich blood pumped out to the body is reduced (≤40% of the blood volume in the ventricle is pumped out). Therefore, symptomatology becomes noticeable even during rest. During the last decades, various treatment strategies have been proposed to treat patients with HFrEF, by blocking the renin-angiotensin-aldosterone system (RAAS) with either angiotensin-converting enzyme (ACE) inhibitors, angiotensin receptor blockers (ARBs) or mineralocorticoid receptor (MR) antagonists, in combination with neprilisin inhibitors or diuretics. The different strategies aim to reduce blood pressure, by inducing vasodilation and diuresis, and therefore decreasing cardiac workload. Other therapeutic options for HFrEF, target cardiac contractility and heart rate, by either increasing the heart´s capacity to contract properly (digoxin) or decreasing the heart rate and therefore lowering the myocardium´s oxygen needs (β-blockers and ion channel-blockers) (15).

II. Heart failure with preserved ejection fraction (HFpEF): also referred as diastolic dysfunction. Under this condition, the heart contracts effectively and a normal volume of oxygenated blood is pumped out from the heart (EF between 50-70%); however, the ventricles do not relax as they should during the diastole or ventricular filling period. The diagnosis of HFpEF is often challenging since it results from excluding other non-cardiac causes of symptoms suggestive of HF. Thus, an efficient therapy for HFpEF remains to be identified to date.

4.2.1.3 Heart Failure classification based on the etiology

Several alterations in the heart can lead to cardiac dysfunction and HF. Some of these include structural defects, cardiac injury or infection and toxins damaging the heart. Some patients have spontaneous HF from unknown causes, so called idiopathic HF. For the purpose of the current dissertation, the different causes that lead to HF are classified based on the presence or absence of an immune and inflammatory component initiating the pathology:

I. Heart failure as a result of infection, autoimmunity or injury:

   i. Viral and autoimmune myocarditis: inflammatory disease of the myocardium mainly caused by viral infections and also due to an autoimmune response of unknown origin through autoantibodies targeting the myocardium. Coxsackievirus B is the main infectious organism that causes viral myocarditis; however, for the last years adenovirus and parvovirus are becoming more prevalent (16, 17). Infection prevalence in HF patients with dilated cardiomyopathy (DCM) is high since viral genomes can be detected in around 64% of these patients. Thus, as T cells clear virus infected cells, close to 50% of patients with DCM show cardiac T lymphocyte recruitment, indicating a chronic inflammatory process taking place (18). However, the adaptive immune response can also target self-antigens on uninfected cells that have molecular mimicry with the virus (cross-reactive immune determinants) (19, 20). The ventricular function in these patients correlates with the persistence of the immune response or clearance of viral presence in the myocardium. On the other hand, there is clinical evidence of cardiac autoantibody deposition initiating or maintaining

inflammation and therefore promoting HF (21). Indeed, HF patients have elevated levels of self-antibodies that target CM antigens, such as troponin I, actin, Na/K ATPase, M2 muscarinic receptor and β1 adrenergic receptor (21).

ii. Chagas disease: chronic Chagas disease associated DCM is considered an important cause of death in Central and South America, yet it is relatively uncommon in Europe and North America (22). Between 10 to 30 % of the people infected with the protozoan parasite *Trypanosoma Cruzi* develop symptomatic Chagas disease, including biventricular hypertrophy, reduction of the ventricular wall thickness, apical aneurysms and mural thrombi. The myocardial conduction is often altered, leading to right bundle-branch block, left anterior fascicular block, or even complete atrioventricular block (23). The cardiomyopathy observed in Chagas disease is cataloged within post-infectious autoimmunity due to molecular mimicry between cardiac myosin and the immunodominant B13 protein in *Trypanosoma Cruzi*, leading to a cardiac immune damage (24, 25).

iii. Ischemic heart failure: myocardial infarction (MI) is one of the leading causes of HF with reduced ejection fraction (HFrEF). The ventricular remodeling taking place after the occlusion of a coronary vessel, and concomitant perfusion interruption can be divided in stages. Early on after the onset of the ischemic event CM death occurs, via either necrosis, apoptosis or maybe autophagy. Dead CM release their intracellular proteins into the extracellular space and circulation, initiating an inflammatory response. As a result, both innate and adaptive immune cells are recruited to the infarcted myocardial tissue and remove the dead CM. Later, as part of

the healing stage, CFB proliferate and create the fibrotic scar, replacing dead CM with ECM proteins, as collagen I. Finally, the wall stress progressively enhances, CM hypertrophy around the infarcted area, wall thickness decreases and ventricular chamber dilates, resulting in reduced EF (26).

II. Non-classically autoimmune, injury or infection triggered heart failure:

i. Hypertension induced heart failure: elevated blood pressure is considered the most important risk factor for HF; approximately ¾ of patients with HF have hypertension antecedents in their clinical history (12). In response to the pressure-overload induced by the chronic hypertension, CM undergo hypertrophic mechanisms, resulting in ventricular wall thickening, decreasing both wall stress and oxygen demand (27). However, when the pressure stress is chronic the myocardial adaptive remodeling decompensates and transitions to clinical HF.

ii. Valvular heart disease: pathological condition that involves one or more of the four valves in the heart, resulting in valvular stenosis, regurgitation or atreasia. Stenosis results from valve thickening, stiffening or fusing together; thus, the valve is prevented from fully opening, and fewer blood flows through it. Regurgitation occurs when the valve does not close tightly, resulting in the blood leaking back to the chamber. Finally, atresia occurs when the cardiac valve lacks an opening for the blood to pass through. Valve problems may be congenital or acquired, secondary to valve calcification processes, endocarditis or Rheumatic fever, among others. All pathological valvular heart condition may lead to HF symptomatology, such as dyspnea and palpitations (28).

iii. Heart failure associated with metabolic diseases: patients with certain metabolic pathologies, such as diabetes mellitus (DM) and obesity, show increased risk of suffering from coronary artery disease, high blood pressure and HF (29). In healthy individuals, the myocardium metabolizes mainly fatty acids and glucose to satisfy its metabolic needs. However, under insulin resistance and obesity caused type II DM conditions, fatty acid use increases coupled to mitochondrial dysfunction due to the increased lipid load in the heart; this condition leads to DCM, CM hypertrophy and dead, interstitial collagen deposition and diastolic dysfunction (30).

iv. Heart failure induced by cardiac toxins: the classic toxins that lead to LV dysfunction and HF include recreational drugs as alcohol and cocaine, as well as drugs used for cancer therapy. Long term alcoholism is one of the most important causes leading to DCM (31), which is diagnosed in heavy drinkers with persistent biventricular dysfunction and dilation in the absence of other known causes of myocardial disease (32). Chronic abuse of cocaine may result in DCM even without coronary artery disease (CAD), MI or vasculitis, with 4 to 18% of asymptomatic cocaine abusers reporting reduced LV function (33). A variety of cytotoxic antineoplastic drugs are cardiotoxic and result in long-term cardiac disease; these drugs include anthracyclines, monoclonal antibodies as trastuzumab, taxoids, high doses of cyclophosphamide, mitomycin-C, 5-fluorouracil and the interferons (34).

v. Idiopathic heart failure: many cases of HF are due to idiopathic DCM, which by definition has no known cause. The diagnosis of idiopathic cardiomyopathy involves first excluding known causes that lead to DCM, which may or may not be reversible. These patients usually present an EF

inferior than 45%, and/or a fractional shortening below 25%. The LV end diastolic diameter is greater than 117% of the expected value corrected by patient´s age and body surface area (35). The treatment of idiopathic DCM is similar to the one applied in HFrEF.

Fortunately, we nowadays count with experimental models of HF induced by the different etiologies mentioned above that allow the study of specific mechanism involved in the complex syndrome of HF. Patients suffering from HF, present an increased LV pressure, reaching 140 mm Hg. Based on this pathophysiological feature, the Transverse Aortic Constriction (TAC) experimental mouse model is widely used in pre-clinical studies, which is based on a surgical procedure constricting the transverse aorta, and thus mimicking the LV pressure overload observed in HF patients. The TAC model allows the study of the phenotypical, functional and mechanistical changes involved in non-ischemic HF progression, as it is indicated in the current doctoral thesis dissertation.

4.2.2 Hallmarks of pathological cardiac remodeling and heart failure

In the context of cardiac disease, the LV undergoes a series of modifications in its structure and functionality in a plastic manner. This pathological cardiac remodeling is partially a consequence of several transcriptional, signaling, structural, electrophysiological and functional responses occurring in the CM. However, other cardiac resident cells also contribute to the remodeling, as CFB promoting ECM deposition and thus fibrosis, SMC contributing to vascular stiffness, EC promoting vascular dysfunction and immune cells inducing cardiac inflammation. The classical features of pathological cardiac remodeling are expanded below:

4.2.2.1 Cardiomyocyte hypertrophy

In response to both developmental signals and workload increases the myocardium can undergo hypertrophic mechanisms (from Greek excess nourishment), aiming to decrease heart ventricular wall stress and keep an adequate pump function. Mammalians' CM become terminally differentiated after birth and therefore lose their proliferative capacity. Thus, the main cause of cardiac mass increase is due to an enlargement of individual CM; on a lower extent, CFB proliferation and progenitor cell activity can also contribute to an increased ventricular mass. Cardiac hypertrophy can be both physiological and pathological, being adaptive or maladaptive, respectively.

In response to exercise or pregnancy, the myocardial tissue undergoes adaptive eccentric cardiac hypertrophy due to volume overload, which consists on increased perfusion and metabolism and where no cardiac disease is developed (Figure 4.3) (1, 36). Even though the myocardial tissue can tolerate an increased workload compensating a diversity of pathological stress conditions and pressure overload by adaptation mechanisms as developing concentric hypertrophy, eventually the heart fails to maintain the appropriate cardiac function, leading to dilated cardiomyopathy and a wide variety of cardiac dysfunction conditions (Figure 4.3).

4.2.2.2 Cardiac fibrosis

In response to pathological conditions in which the heart is subjected to a demand increase, such as chronic hypertension and MI of coronary arteries, the cardiac ventricle undergoes remodeling and dilation mechanisms (37). Thus, CFB differentiate to myofibroblasts (Figure 4.3), in a process mediated by TGFβ, endothelin-1 and angiotensin-II, increasing collagen production and contributing to myocardial stiffness (38). Collagen deposition leads to loss of CM by apoptosis or necrosis, which are later

on replaced by CFB and extracellular collagen. Vascular SMC can also produce collagen in response to oxidative and mechanical stress, ischemia and inflammation, promoting vascular stiffness.

4.2.2.3 Electrophisiological remodeling

Either early after ischemic events take place, when the ventricular remodeling happens, or later after injury, sustained ventricular tachycardia or ventricular fibrillation can occur as a result of modifications of the expression and function of important ion channels and Ca^{2+}-handling proteins; these alterations impact the CM action potential duration and their intracellular Ca^{2+} transients. Indeed, ventricular arrhythmia is considered one of the main conditions leading to cardiac dysfunction and HF (Figure 4.3) (39).

4.2.2.4 Coronary microvascular rarefaction and endothelial dysfunction

Microvascular rarefaction defined as the decline in blood vessel numbers (40), is often associated with conditions of vascular EC inflammation and dysfunction, pathological features observed in both HFrEF and HFpEF patients (41). As a consequence of the reduction of the coronary microvascular density, coronary flow reserve and therefore oxygen distribution within the myocardial tissue are impaired, affecting the LV systolic and diastolic functions. Furthermore, vascular EC contribute to endothelial dysfunction and leukocytes, both cardiac resident and recruited as a result of the insult, activate inflammatory mechanisms via cytokine and chemokine release.

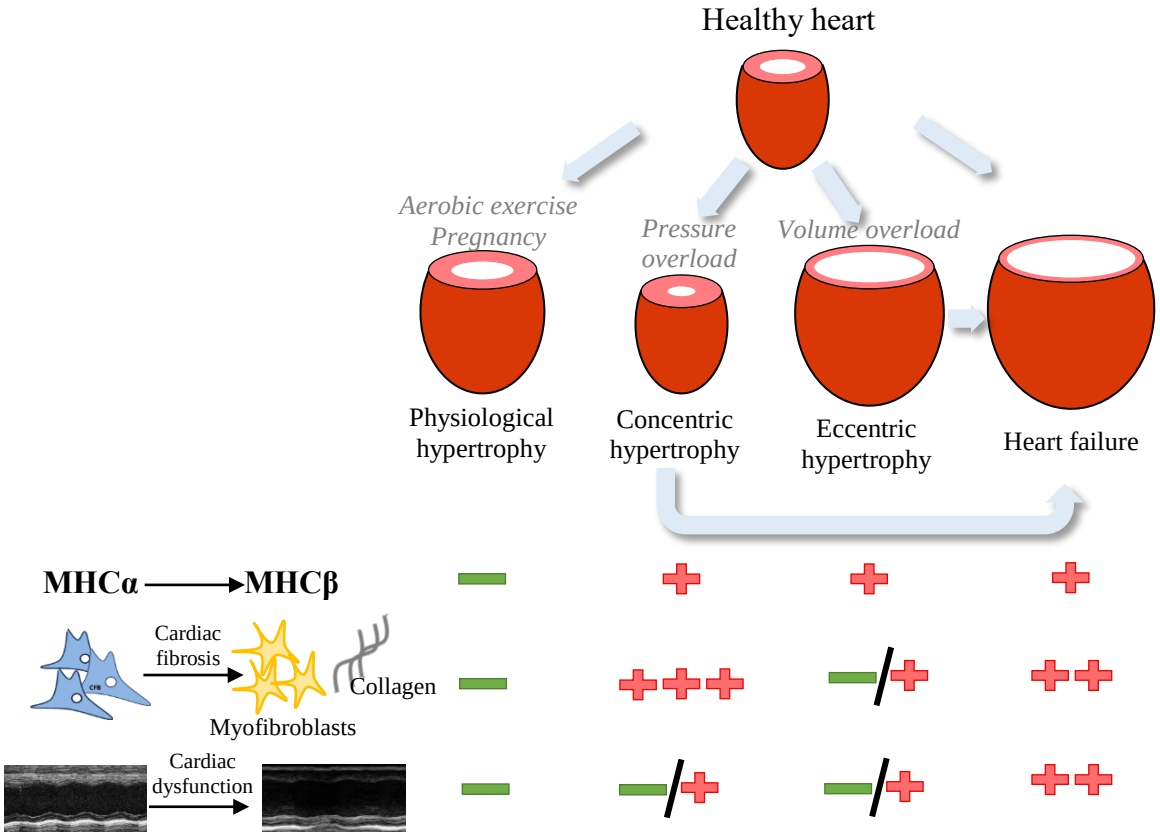

Figure 4.3. Stimulus-specific cardiac remodeling response.

Altogether, maladaptive cardiac remodeling, characterized by increased myocardial stiffness and reduced contractile function, predispose to cardiovascular morbidity and mortality, and results in HF (37).

4.3 New players in heart failure: immune system and the inflammatory response

4.3.1 Innate and adaptive cardiac immune responses

Myocardial injury caused by pathogens or environmental stress (as ischemic events or hemodynamic overload) can activate both the innate and the adaptive immune systems. A hallmark in the activation of the immune response is the release of pro-inflammatory cytokines, which have been associated with HF of all different etiologies (42). On the

one hand, the innate immune response provides a global, non-antigen specific protection against pathogens and injury. On the other hand, the adaptive immune response provides a highly antigen-specific response, which is mediated by T and B lymphocytes.

4.3.1.1 Innate immune myocardial responses

Myocardial innate immune response consists mainly in homeostatic and tissue repair responses. These non-specific immune responses are initiated in response to pathogen-associated molecular patterns (PAMPs) or damage-associated molecular patterns (DAMPs) that are recognized by a series of germ-line encoded pattern recognition receptor (PRRs), which include Toll like receptors (TLR), C-type lectin receptors (CLR) and NOD-like receptors (NLR). In addition to infection associated PAMPs, cardiac PRRs can as well recognize molecular patterns of endogenous host molecules released by injured CM or during apoptotic and necrotic events (DAMPs), including endogenous TLR-agonists, NLR-agonists and alarmins, which upon recognition by PRRs, sterile inflammatory responses begin (Figure 4.4). Upon molecular pattern recognition by PRRs, intracellular signaling cascades are initiated activating nuclear factor-κB (NF-κB), interferon regulatory factor and activator protein 1 transcription factors, which regulate genes that encode for pro-inflammatory cytokines and interferons in the myocardium (43). Regardless of the cause of the cardiac cell injury, polymorphonuclear cells are first recruited to the injured area, followed by the monocytes.

Other cardiac PRRs instead, mediate the clustering of cytoplasmatic protein structures termed inflammasomes; these protein complexes convert procaspase-1 in the

catalytically active protease caspase-1, which is the responsible of IL-1β and IL-18 production that initiate inflammatory mechanisms in the myocardium (Figure 4.4) (44).

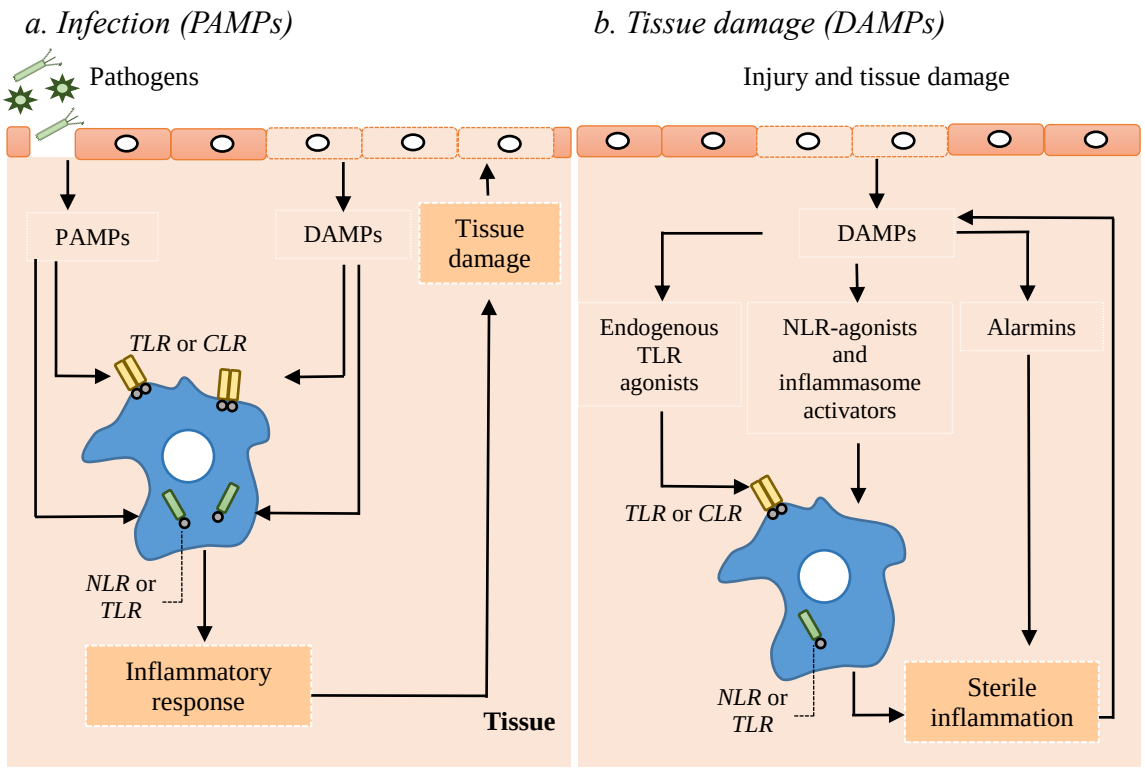

Figure 4.4. PAMP and DAMP mediated activation of the immune response.

Either when the myocardial inflammation is caused by pathogenic or non-pathogenic injury, the main aim of the inflammatory response is to clear the origin of the disturbance, aiding the cardiac tissue to adapt to the unusual circumstances first, and later on bringing back homeostatic conditions and optimal cardiac function. In cases where the anomalous conditions are kept in time and the myocardium is unable to restore homeostasis, a long-term inflammatory state remains in the heart, leading to chronic low-grade inflammation, which could contribute to disease progression.

Activated by molecular patterns, macrophages play an important role both in homeostatic functions and innate immunity, where they control tissue remodeling and metabolic functions on one hand, and are essential in host defense against pathogens

and inflammatory processes on the other hand. In response to different inflammatory stimuli, as IFN, TLR activation or IL-4/IL-13 signaling, macrophages undergo activation into M1 (classical) or M2 (alternative) subtypes respectively, which consist on continuous states of activation (45). M1 macrophages express high levels of pro-inflammatory cytokines, promote Th1 response, release reactive oxygen and nitrogen species and present a strong tumoricidal and microbicidal activity (46). M2 macrophages instead, promote tissue remodeling and tumor progression and regulate parasite containment (47). Besides their role in host defense and tissue homeostasis, macrophages are critical players in the pathophysiological processes induced in the context of ischemic heart disease (48, 49).

In addition to PAMPs, DAMPs and macrophage mediated innate immune responses, the activation of neurohormonal systems during cardiac dysfunction conditions, as the adrenergic nervous system and the RAAS, can end up promoting inflammation in the myocardium and leading to a low-grade inflammatory state (50, 51). In Section 4.3.2.3 of the current dissertation the role of RAAS and the mineralocorticoid receptor expressed in endothelial cells (EC-MR) in cardiovascular disease and vascular dysfunction will further be described.

4.3.1.2 T lymphocyte mediated adaptive immune responses: T lymphocyte subsets

In addition to innate immune responses, the adaptive immune system plays an important role in a variety of cardiovascular diseases. B and T lymphocytes are the main components of the adaptive immune system, and among the different T lymphcoytes types, CD4+ T helper cells play an important role in immune surveillance; aiding B lymphocytes produce antibodies, increasing the microbicide activity of macrophages, recruiting eosinophils, basophils and neutrophils to the infectious or inflammatory sites,

and finally via cytokine and chemokine production, regulating a variety of immune responses (52). CD4+ T cells can be classified in a variety of subsets depending on the signaling pattern received during the interaction between naïve CD4+ T cells and a specific antigen. Four main CD4+ T cell subsets are distinguished, even if more minor subsets have recently been described. These four populations include Th1, Th2, Th17 and induced regulatory T (iTreg) cells (Figure 4.5).

I. Th1: Th1 cells regulate intracellular pathogen clearance and are involved in tissue-specific autoimmune responses (53). IL-12 and interferon γ (IFNγ) are the two essential cytokines responsible of initiating the intracellular signaling cascade that leads to Th1 development and their signature transcription factor is T-box (Tbet), which regulates the Th1 cell signature cytokine IFNγ and also inhibits the maturation of opposing T cell lineages (Th2 and Th17).

II. Th2: Th2 cell mediated immune response targets extracellular parasites and plays an essential role in the initiation and persistence of asthmatic and allergic reactions and some of the cytokines produced such as IL-4 and IL-13 are considered pro-fibrotic (54, 55). The signature transcription factor of Th2 cells is GATA3 (GATA binding protein 3), which enhances Th2 differentiation and cytokine release.

III. Th17: Th17 cells mediate immune responses targeting extracellular bacteria and fungi, in addition to autoimmune pathologies. IL-17A, IL-17F, IL-21 and IL-22 are considered to be main effector cytokines; interestingly, the first two share the receptor through which they signal, IL-17RA, which is expressed in a variety of tissues (such as skin, lung, intestine, joints and hematopoietic tissue) and therefore produce inflammatory reactions that exceed T lymphocytes mediates

responses (56). Th17 cell maturation requires the signaling mediated by the cytokines IL-6 and TGFβ for differentiation, IL-21 during self-amplification and IL-23 for cell stabilization. Retinoic acid receptor-related orphan receptor gamma-T (RORγt) is considered their signature transcription factor (57, 58).

IV. Treg: Treg suppress effector T cell mediated immune responses in autoimmunity and therefore are involved in immune tolerance to self-antigens. FOXP3 (Forkhead box P3) is considered CD4+CD25+Treg cells' signature transcription factor. While natural Treg express FOXP3 when released from the thymus, induced Treg (iTreg) require the antigen priming to fully develop in the peripheral lymphoid organs (59).

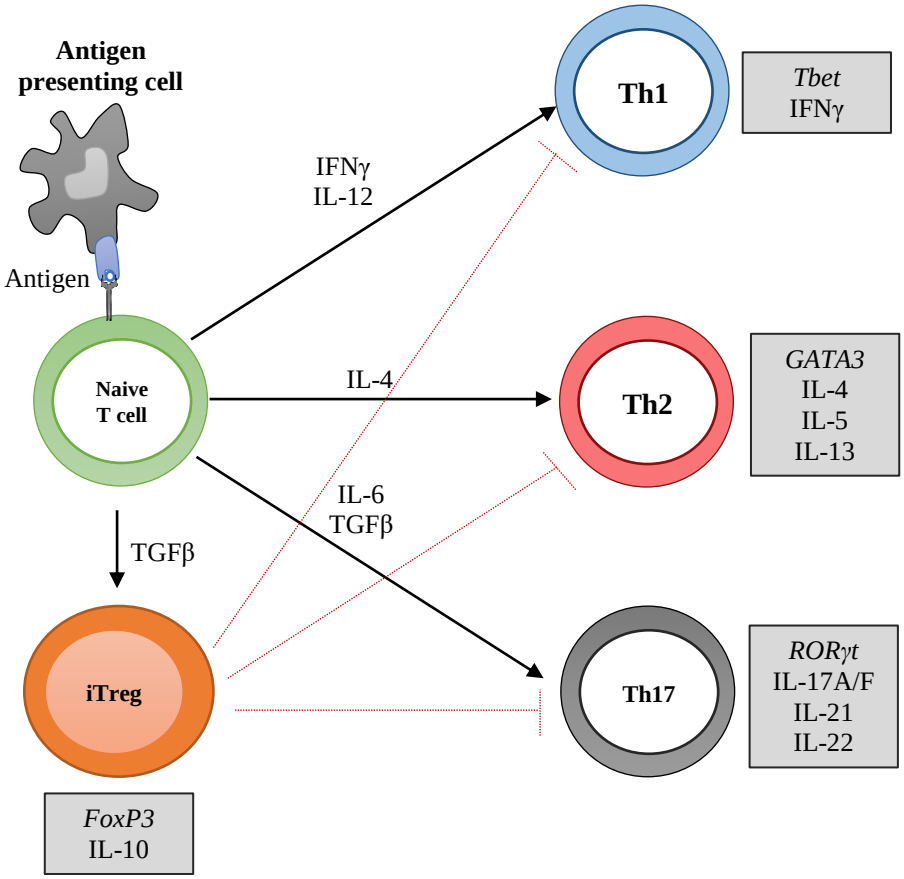

Figure 4.5. CD4+ T cell subsets: cytokines that induce their differentiation from naïve T cells, and signature transcription factors and cytokines of each subset.

Given that this doctoral thesis dissertation digs on the role of the previously mentioned T lymphocyte subsets during pathological cardiac remodeling in HF, the current knowledge in T lymphocyte mediated immune responses in LV remodeling will further be explained extensively in Chapter 4.4 below.

4.3.2 Vascular activation and leukocyte recruitment

4.3.2.1 Cell adhesion molecules

Cells' interaction with their ECM allows their growth, differentiation and migration. Cell adhesion between each other, their ECM and endothelial surfaces are mediated by a variety of cell membrane proteins named cell adhesion molecules (CAMs). CAMs are protein structures expressed by cells of all tissues in their membrane, functioning as receptors that initiate intracellular signaling pathways and regulate basic vital processes, as interactions between cells, with the ECM, and regulate their trafficking (60).

CAMs can be classified in immunoglobulin gene superfamily members, integrins, cadherins and selectins (Figure 4.6).

I. Immunoglobulin Superfamily: protein family with one or more immunoglobulin (Ig)-like domains, homologous to antibody's basic structural unit (61). As type I membrane protein, immunoglobulin superfamily protein CAMs consist on an amino N-terminal extracellular site, one transmembrane domain and a carboxyl C-terminal cytoplasmatic domain (62). These CAMs have weak interaction with their ligands, which can be other Ig-like domains, integrins and carbohydrates. A good example of Ig-like CAM is CD54 or Intercellular Adhesion Molecule-1 (ICAM1), which is constitutively expressed in a certain percentage by EC, but becomes upregulated in cultured EC after IL-1β or TNFα stimulation and is

permanently expressed in chronic inflammatory pathologies (63). Upon upregulation, ICAM1 mediates leukocyte firm arrest to the EC and signals favoring their transendothelial migration, as it is further explained below in Section 4.3.2.2.

II. Integrins: these CAMs consist on transmembrane heterodimeric non-covalently bound α and β glycoprotein subunits (64). Integrins display three different activation states: inactive (bent over, low affinity), active (upright, high affinity due to full exposure of the ligand-binding pocket) and ligand occupied (65, 66). Stable integrin-ligand binding requires the cytoplasmatic domains to be anchored in the cytoskeleton; thus, upon integrin-ligand adhesion, integrins cluster in the cell membrane, recruit enzymes and adaptor molecules that create adhesion sites linking integrins and the cellular cytoskeleton (64). As an example of integrins within CAMs, lymphocyte function-associated antigen 1 (LFA1) could be mentioned, which is ICAM1's main ligand, and therefore is an important player in leukocyte firm arrest to the endothelium.

III. Cadherins: cadherins are the CAMs family responsible for Ca^{2+}-dependent homophilic cell-cell interactions, which have an important role in tissue differentiation. As an example, VE-Cadherin is an adhesion molecule that maintains and controls specifically endothelial cells in contact (67).

IV. Selectins: this CAM family is specific for leukocyte-vascular cell interactions. Cell extravasation requires the creation and breakage of leukocyte-EC interactions in a successive manner. Selectins interact in a Ca^{2+}-dependent manner with sugar sites on mucin-like adhesion molecules through their distal domain, mediating heterophilic cell-cell interactions (68).

There are three types of selectins. (1) L-Selectin, which is expressed on all monocytes and granulocytes and on most lymphocytes. (2) P-selectin which is stored in Weibel-Palade bodies on EC and in α-granules of platelets, and is translocated to the surface of activated vascular ECs and platelets, playing an important role in the recruitment of immune cells into inflamed tissues. (3) E-Selectin is just expressed by skin microvessels under baseline conditions, while it gets rapidly upregulated by inflammatory cytokines in all the other tissues (69).

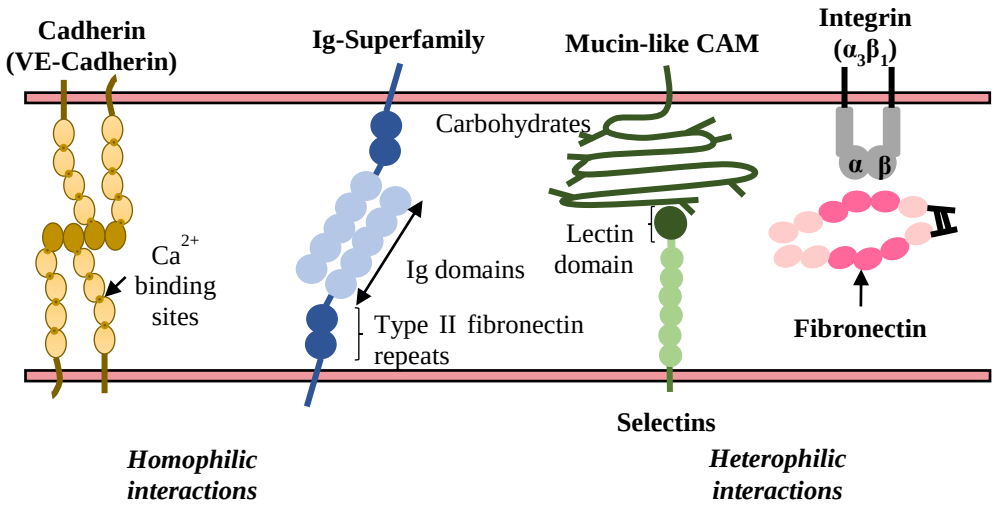

Figure 4.6. Diagram showing the structure and domains of each CAM family.

Interestingly, some of these CAMs are implicated in cellular interactions that are essential for homeostasis, immune cell surveillance, vascular integrity and leukocyte-EC interactions both in physiologic and pathological conditions (as inflammation and immune response). Within the cell interactions involved in the immune responses, CAMs are involved in all the steps: selection in the thymus, antigen priming, antigen recognition, immune cell activation, cytotoxic responses and T lymphocyte circulation. Furthermore, in the inflammatory mechanisms taking place in a variety of pathologies,

as cardiovascular diseases, CAMs are involved in endothelial activation and dysfunction, as observed in atherosclerosis, coronary disease and hypertrophic cardiomyopathy, among others (70).

4.3.2.2 Endothelial cell activation and leukocyte recruitment

Vascular ECs play an essential role in the inflammatory response regulation. All the CAMs mentioned above (Ig receptors, selectins, integrins and cadherins) are expressed by the ECs; under homeostatic conditions they mediate EC interactions and control vascular permeability. However, during inflammatory processes and cytokine release the expression of CAMs on the EC surface is modified and they mediate the interactions between the activated endothelium and circulating leukocytes. Leukocyte trafficking within microvessels is essential for an optimal immune surveillance. Immune cell recruitment is a tightly regulated process (Figure 4.7), involving consecutive expression and activation of specific CAMs both on leukocytes and EC.

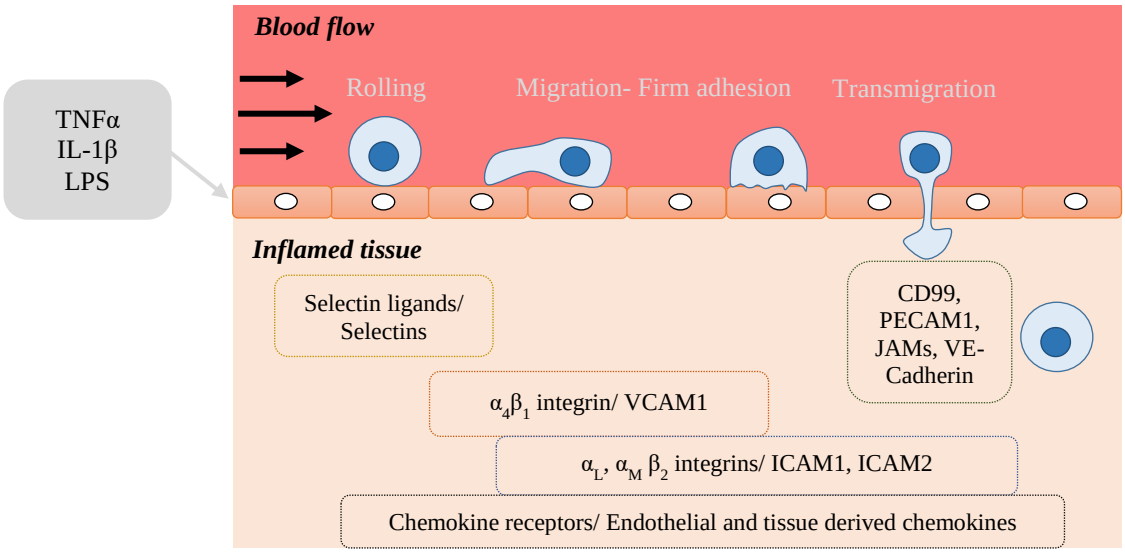

Figure 4.7. Leukocyte recruitment cascade, in which the different steps and adhesion molecules involved are indicated.

Within the leukocyte recruitment cascade, each CAM mediates a precise step: initial leukocyte rolling over the EC is mediated by selectins (E- and P-Selectin), followed by firm adhesion and immune cell transmigration regulated by glycoprotein integrins (LFA1, MAC1 and VLA4) and Ig-superfamily (ICAM1, VCAM1 and PECAM1). While the initial rolling interactions are taking place, tethered leukocytes are exposed to chemoattractants and other inflammatory molecules that induce further leukocyte activation and induce integrin:Ig-superfamily adhesion molecule interaction, and subsequent L-Selectin downregulation. After firm leukocyte adhesion to ECs is stablished, active immune cells locomote toward EC junctions and transmigrate by diapedesis to the inflammatory site following chemotactic signals, although transcellular diapedesis has also been reported (71).

Among the pathologies that present an immune and inflammatory component, several studies indicate that chronic cardiac low grade inflammation is present in patients with dilated DCM, myocarditis and ischemic heart disease, contributing to structural and functional cardiac failure. Furthermore, the study of the expression of vascular CAM and the inflammatory reaction taking place in congestive HF is gaining considerable relevance in the last years. It was first described two decades ago that the vascular ECs were activated (determined by ICAM1 upregulation) and CD3 T lymphocytes were present in hearts of patients with DCM (72, 73). In addition, in rodent non-ischemic HF models it was not only observed that ICAM1 expression was increased in the intramyocardial arterioles, but also it was determined to regulate macrophage infiltration, TGFβ production and myocardial fibrosis (74).

Besides the membrane bound CAM form, several stimuli and enzymes have been reported to mediate ICAM1 cleavage from the EC, such as TNFα and IFNγ (75-77) and

proteases such as matrix metalloproteases (MMP) (78) and elastase (79). ICAM1's circulating form consists on the five extracellular Ig-domains, lacking the transmembrane domain and cytoplasmatic tail of the membrane bound form. Soluble adhesion molecules are often considered as biomarkers of vascular disease. sICAM1 for instance, has been found increased in serum of patients with CVD (80-82), cancer (83) and autoimmune diseases. Several studies have determined that sICAM1 can both induce and inhibit the inflammatory response. In the first one, sICAM1 in physiological concentrations can activate pro-inflammatory signaling cascades leading to chemokine release and angiogenesis (84), thus contributing to chronic inflammatory diseases. On the contrary, sICAM1 in high concentrations has been reported to bind in a competitive manner to membrane bound ICAM1's ligands (LFA1 and MAC1) and therefore potentially block immune cell – EC interactions (85).

4.3.2.3 Hormonal regulation of inflammation

In addition to soluble forms of adhesion molecules, circulating levels of the mineralocorticoid hormone aldosterone are also increased in patients suffering from either HFrEF or HFpEF, and predicts mortality risk (86, 87). Aldosterone is a major endocrine regulator of sodium homeostasis in the organism, since it inhibits natriuresis (sodium excretion in the urine), as part of the RAAS. Aldosterone binds to MR in the kidney to regulate sodium balance (88) and in SMC to regulate vascular tone and constriction (89) thereby contributing to volume overload and increased systemic vascular resistance, important contributors to HF pathophysiology. MR antagonists, such as spironolactone and eplerenone, are an effective therapeutic option for reducing blood pressure in patients with hypertension. Clinical trials have demonstrated that aldosterone antagonism increases survival in patients with systolic HF (HFrEF) (90-92).

Over the past decades, it has been demonstrated that MR is expressed and is functional in other cells and tissues outside the kidney. Indeed, within the cardiac resident cells, MR is expressed by CM (93) and CFB (94), vascular SMC (95), ECs (96), and infiltrated immune cells (97). The DOCA/Salt model of hypertension was used for studying myeloid cell MR's role in cardiac remodeling, where its absence showed to be protective from developing cardiac fibrosis and increasing blood pressure (98, 99). This model was used to investigate the role of EC-MR in myocardial remodeling as well, using a transgenic mouse that lacked MR also in the myelid cells, showing that MR deletion from EC decreased cardiac inflammation and pathological remodeling (100, 101).

Aldosterone-MR binding promotes inflammatory pathways via NF κB by increasing pro-inflammatory cytokines IL-1β, IL-6 as well as TNFα expression (102) and ICAM1 upregulation in human coronary EC *in vitro* (96). As indicated above, systemic inflammatory markers are elevated in patients with HF, and various reports using various HF models (induced by ischemia, autoimmunity, infection, hypertension or pressure overload) suggest different mechanisms taking place that may link the aldosterone-MR pathway with inflammation and HF (103).

4.3.2.4 Chemokines and chemokine receptors in leukocyte recruitment

Chemokines are a group of small glycoprotein cytokines, which upon binding to G protein-coupled receptors (GPCR), present chemotactic properties that mediate leukocyte locomotion and migration to inflamed tissues. Furthermore, chemokines can also have other effects not exclusively chemotactic, since they increase inflammatory cytokine production and reactive oxygen species in leukocytes. In addition to immune cells, chemokines have also been shown to interact with CFB, vascular SMC, EC and

CM, modulating these last ones' function and contributing to cardiac dysfunction (104). Experimental evidence suggest that chemokine mediated mechanisms may also be involved in the pathogenesis of HF.

Myocardial dysfunction is associated with increased circulating chemokine concentrations in both humans and experimental rodent models (105, 106). Several chemokines have been detected in various models of myocardial injury mainly mediating inflammatory leukocyte recruitment; among those, IL-8 may induce neutrophil infiltration when upregulated in the infarcted area and MCP1 (Monocyte Chemoattractant Protein 1) may regulate monocyte and lymphocyte recruitment to the ischemic region (107). The chemokine CXCL10 is also found induced in the infarcted area and prevents fibrous tissue deposition in a CXCR3-independent manner (107-110).

Interestingly, chemokine receptors have been found expressed by CM, indicating that chemokines not exclusively have an inflammatory role but also are involved in cardiovascular biology. Among those receptors, CXCR2, CCR2 and CXCR4 could be mentioned, which are constitutively expressed by CM and become upregulated in response to oxidative stress (111, 112). In this context, chemokine receptors mainly regulate leukocyte recruitment, but also cardiac function, TNFα production and cellular apoptosis (113). The chemokines, and their respective receptors involved in CVD are listed in Table 4.1 below.

Chemokine	**Receptor**	**Main function**	**Associated cardiac disease**	**Reference**
CCL2	CCR2	Monocyte, memory T cell and dendritic cell recruitment	Myocardial IR injury, remodeling, HF	(114, 115)

CCL3	CCR1	Neutrophil activation, induction of cytokine production	Myocardial IR injury	(116)
CCL4	CCR1, CCR5			
CCL5	CCR5	Leukocyte recruitment	Myocardial ischemia and post-infarction HF	(117)
CCL11	CCR2-3-5	Modulation of macrophage function in the atherosclerotic plaque	Atherosclerosis cardiac ischemia	(118)
CCL18	CCR8, GPR30, PITPNM3	Adaptive immune system cell recruitment	Acute coronary syndrome	(119)
CCL21	CCR7	Adaptive immune system cell recruitment, vascular inflammation, cell proliferation, matrix remodeling	Ventricular remodeling in response to aortic stenosis	(120, 121)
CXCL1	CXCR2	Chemotaxis of neutrophils	Myocardial ischemia	(122)
CXCL2		Chemotaxis of neutrophils and hematopoietic stem cells	Cardiac reperfusion injury, cardiac infarction	(112, 116)
CXCL5	CXCR2	Chemotaxis of neutrophils, angiogenesis	HF	(123)

CXCL8	CXCR1, CXCR2	Chemotaxis of neutrophils	Cardiac IR injury, cardiac arrhythmia, HF	(123-125)
CXCL9	CXCR3	Chemotaxis of T cells	Chagas cardiomyopathy	(126)
CXCL10		Chemotaxis of monocytes/macrophages, T cell adhesion to endothelial cells, angiogenesis	Pressure overload induced cardiac remodeling, Chagas cardiomyopathy	(126, 127)
CXCL12	CXCR4	Stem cell mobilization from bone marrow	Hypertrophic cardiomyopathy, fibrosis and remodeling, HF	(128)
CXCL13	CXCR5	B cell homing, monocyte activation, apoptosis	Cardiac matrix remodeling	(129)
CXCL16	CXCR6	T cell and NKT cell migration, stimulation of SLRP production by fibroblasts	Matrix remodeling and HF	(127)
CX3CL1	CX3CR1	Chemotaxis of T cells and monocytes	Rejection of transplanted heart and HF	(130, 131)
XCL1 and 2	XCR1	Chemotaxis of T cells	Heart transplantation	(131)

Table 4.1. Chemokines and chemokines receptors involved in CVD.

In the present doctoral thesis dissertation, we have focused on the chemokine receptor CXCR3, which is expressed mainly by CD4+ Th1 cells, in addition to CD8 cytotoxic T cells, Natural Killer (NK) cells, NK T cells and plasmacytoid Dendritic Cells (pDC) (132). As recently reported, a subset of regulatory T cells (Tregs) also express CXCR3 allowing Treg mediated control of Th1 responses in inflamed tissues (133). CXCR3 ligands are known to target activated lymphocytes specifically. Upon release, CXCL9, CXCL10 and CXCL11 chemoattract CD3-stimulated CXCR3 expressing T cells and induce their adhesion and transendothelial migration through human endothelial cells (134, 135). CXCR3 ligand mediated lymphocyte recruitment could further be mediated by endothelial ICAM1 and VCAM1 adhesion molecules, since T cell adhesion to these last ones is enhanced in static conditions in the presence of CXCR3 ligands (135). Furthermore, in addition to chemotactic effects, CXCL9 and CXCL10 have also been reported to stimulate T lymphocyte proliferation, Th1 differentiation and optimal effector cytokine production (136, 137).

As indicated in Table 4.1 above, CXCR3 has been reported to play a role in T cell chemotaxis in relation with non-ischemic HF. In the myocardium of patients with chronic Chagas cardiomyopathy, CXCR3+ mononuclear cells are detected, and the mRNA expression of its chemokine ligands CXC9 and CXCL10 is found upregulated; interestingly, the mRNA expression of CXCL9 directly correlates with the intensity of the myocarditis (126). In a mouse model of pressure-overload induced right ventricular (RV) remodeling induced by pulmonary banding, CXCL10 is found upregulated in the RV and it mediates the reduction of the expression of collagen network regulators in cardiac fibroblasts (127). In line with this, CXCL10 has been shown to be upregulated and to have anti-fibrotic effects in the healing heart after MI and in isolated CFB, thus

attenuating pathological cardiac remodeling; however, these effects are independent of CXCR3 and may be mediated by proteoglycans, indicating that in ischemic heart disease CXCR3 signaling is not critical for cardiac remodeling and dysfunction (110, 138). In addition to HF, interactions between CXCR3 and its ligands have also been linked to other cardiovascular and metabolic pathologies (139).

4.4 Chronic inflammation and adaptive immune responses in heart failure

HF was initially considered a disease of the cardiac muscle impacted by alterations in the neurohormonal and sympathetic nervous system axis (140), but there is now growing awareness of inflammation playing a direct role in the development and progression of HF. It is a well stablished fact that in both HF with reduced and preserved ejection fraction (HFrEF and HFpEF, respectively) there is a direct correlation between increased circulating pro-inflammatory cytokine levels (such as TNFα, IL-1, IL-6, galectin 3, TNF receptor 1 and 2) and adverse clinical outcomes (141-143).This observation suggests that low-grade chronic inflammation may be an important regulatory component to the maintenance or detrimental prognosis of patients with diagnosed HF. Indeed, it is believed that both tissue injury and the subsequent repair are regulated in a significant degree by resident and infiltrating innate and adaptive immune cells, which promote inflammatory and reparative mechanisms. The balance between pathological and physiological/reparative inflammatory pathways determine HF progression.

It was first observed in experimental investigations in dogs that TNFα injections contribute to LV dysfunction; subsequent studies in rodents showed that circulating

TNF, in similar concentration to the one found in patients with HF, produced persistent negative inotropic effects in the myocardium (144-146). Furthermore, cardiac overexpression of TNF was found to reduce LV EF in mice (147), in addition to NF-κB activation leading to IL-1β and VCAM1 upregulation in human CM (148). Additionally, some pro-inflammatory cytokines, such as IL-6 and IL-1, have also shown to induce negative inotropic effects (149).

Based on the above mentioned clinical and experimental evidence, multicenter clinical trials using TNFα inhibitors were performed in an attempt to block inflammation in patients with moderate to advanced HF (150, 151); however, they failed to improve HF outcomes, since the TNFα neutralizing approach was either negative respecting the primary endpoints of the study, worsened HF or increased death rates among participants (150, 151). Interestingly, on another clinical trial in which IL-1 receptor antagonist Anakinra was tested, a reduction of the systemic inflammatory response was observed in patients with acute decompensated HF (152). Nonetheless, it remains to be studied whether the anti-inflammatory effect of IL-1 receptor blockers translates into improved clinical outcomes, and therefore emphasizes the need for a better understanding of the mechanisms by which systemic inflammation influences the pathogenesis of HF using different experimental mouse models of HF.

Using the mouse model of HF induced by Transverse Aortic Constriction (TAC), which is also used in the current dissertation (Methods Section 6.2.1 below), it has recently been reported that IL-6 mediates LV hypertrophy, cellular apoptosis and dysfunction in response to TAC, via CaMKII (Ca2+/calmodulin-dependent protein kinase II)-dependent STAT3 activation (153). On the contrary, some cytokines have been reported to have beneficial effects in HF progression: IL-2 for instance, increases Treg

population in spleen and lungs of HF mice, which due to their capacity to suppress inflammatory responses, effectively attenuate pulmonary inflammation, RV hypertrophy and LV dysfunction after TAC (154). The role of inflammatory cytokines has also been studied in HF models other than TAC, showing that chronically elevated IL-4 induces cardiac fibrosis in the angiotensin-II induced hypertension and cardiac damage mouse model (155). In the context of autoimmune myocarditis, Th17 cells' signature cytokine IL-17 has been implicated in CFB stimulation that leads to the production of chemokines and cytokines critical for neutrophil and $Ly6C^{hi}$ monocytes, contributing to the development of DCM (156). Additionally, in a mouse model of ischemic HF induced by MI, it has been observed that IL-1 mediates the inflammatory response and cardiac remodeling post-infarction, favoring the reparative response during the infarct healing phase (157).

Not only the myocardium is targeted by inflammatory cytokines; endothelial cell function has also been shown to be affected by pro-inflammatory mediators. TNF present in serum of patients with HF has been observed to reduce constitutive endothelial nitric oxide (NO) synthase expression and correlate inversely with peak blood flow (158).

As indicated in Section 4.3.1.2, T lymphocytes play a key role in chronic inflammation and adaptive immune response. From the clinical perspective, it has been documented that patients suffering from chronic HF have decreased frequencies of circulating CD4+CD25+Foxp3+ Tregs, with compromised immune suppressive function (159). Additionally, a Th17/Treg imbalance has been observed in patients diagnosed with both HFpEF and HFrEF (160). The role of the adaptive immune response has been studied in mice lacking both T and B cells ($Rag\text{-}1^{-/-}$ mice) using the angiotensin-II induced

hypertension and vascular dysfunction model, in which protection from pathological features was observed. This investigation suggested that blood pressure regulation may be an important mechanisms through which lymphocytes modulate cardiac hypertrophy and remodeling (161). Using various experimental mouse models of ischemic and hypertension induced cardiac disease, Th1 effector lymphocytes have been shown to be detrimental, opposite to Foxp3+ Tregs, which have been shown to be beneficial and reduce cardiac damage. In the context of ischemic myocardial injury induced by coronary ligation, it has been observed that T cells numbers in the heart increase 5 to 10 fold as compared to steady state, being CD4+IFNγ+ Th1 and FoxP3+ T cells the principal T cell subsets been recruited (162). In this model, CD4+IFNγ+ T cells were found to enhance ischemia-reperfusion injury, opposite to FoxP3+CD4+ Treg cells which were found to favor healing after MI by regulating monocyte/macrophage differentiation (163). Furthermore, adoptive transfer of Tregs reduced both angiotensin II and pressure-overload induced cardiac hypertrophy and pathological cardiac remodeling, also decreasing T cell and macrophage populations in the heart (164, 165). Thus, the role of T cells in chronic HF is an emerging field with clinical data suggesting that T cells are central regulators of the pathophysiology of heart disease (166).

Despite having clinical and experimental evidence associating T cell mediated immune responses with cardiac remodeling in HF caused by different etiologies, the specific role of T lymphocytes in the heart, the mechanisms of recruitment and adhesion molecules and chemokines involved in pathological ventricular cardiac remodeling, the hormonal effect in T cell mediated immune response, and their overall impact in non-ischemic HF progression remains to be characterized. The current thesis dissertation aims to better understand the role of T cells in non-ischemic HF and define the specific mechanisms

regulating their trafficking to the heart and their impact in cardiac remodeling and dysfunction that leads to HF. We have postulated the hypothesis and aims indicated in Chapter 5 below, to expand on the knowledge of the adaptive immune mechanisms contributing to the development of the HF that will help with potential new treatments for this deadly syndrome.

5 HYPOTHESIS AND AIMS

Cardiac dysfunction and HF are currently one of the main morbidity and mortality causes worldwide. The causative role of the endocrine system and the autonomous nervous system, among others, has thoroughly been studied. However, even if experimental and clinical observations suggest that inflammatory and immune mechanisms play a role in HF development, the importance of the adaptive immune response in pathological cardiac remodeling remains to be explored. In the current doctoral thesis we hypothesize that T lymphocytes play a key role in cardiac inflammation, hypertrophy, fibrosis and dysfunction in response to pressure overload; further, T cell immune responses are facilitated by ICAM1 mediated recruitment and CXCR3 chemokine regulated chemoattraction to the LV during HF progression.

In order to test the above indicated hypothesis, the specific aims of this work were the following:

1. Determine the role effector CD4+ T lymphocytes play in pressure overload induced HF.
2. Characterize the role of intercellular adhesion molecule 1 (ICAM1) in T cell activation and LV recruitment in HF.
3. Investigate the role of endothelial cell mineralocorticoid receptor (EC-MR) in cardiac remodeling and dysfunction during HF progression.
4. Investigate the chemotactic molecules involved in T cell LV recruitment in response to pressure overload.
5. Generate a new mouse strain, in which the *icam1* gene is flanked by loxP sites, allowing the generation of tissue specific ICAM1$^{-/-}$ mice.

6 MATERIALS AND METHODS

6.1 MATERIALS

6.1.1 Mice

Mice were bred and maintained under pathogen-free conditions and treated in compliance with the *Guide for the Care and Use of Laboratory Animals* (National Academy of Science). Male C57BL/6 wild-type (WT), male TCR$\alpha^{-/-}$ mice (*Tcra*^{tm1Mjo}) (provided by Christophe Benoist, Harvard Medical School, Boston) , male ICAM1$^{-/-}$ mice (*Icam1*^{tm1Bay}) (167) (provided by Dan Bullard, University of Alabama, Birmingham) and endothelial cell specific mineralocorticoid receptor knock-out EC-MR$^{-/-}$ (MR$^{f/f}$-VECad-Cre+) and EC-MR$^{+/+}$ (MR$^{f/f}$-VECad-Cre-) male littermates (168) (provided by Iris Jaffe, Tufts Medical Center, Boston) were euthanized at 10-14 weeks of age for tissue collection. The total numbers of mice used per experiment are indicated in the figure legends. All mice were bred in the Tufts campus animal facilities and all protocols were approved by the Tufts Medical Center and Tufts University Institutional Animal Care and Use Committee.

6.1.2 Primer sequences for Polymerase Chain Reaction (PCR) amplification of the NR3C2 gene

Primer	Sequence
MR-3	CTG TGA TGC GCT CGG AAA CGG
MR-4	CCA CTT GTA TCG GCA ATA CAG TTT AGT GTC
MR-5	CAC ATT GCA TGG GGA CAA CTG ACT TC

Table 6.1. Primer sequences used for PCR amplification of the gene encoding for MR.

6.1.3 Primer sequences for PCR amplification of the insertions upstream and downstream the ICAM1 mice

Primer name	5'→3' sequence
ICAM1 US Forward primer	CCCTGGGGTTCCACTACTGT
ICAM1 US Reverse primer	AGAGGTCTCAGCTCCACACTC TC
ICAM1 DS Forward primer	TGGAACTGCACGTGCTGTGT
ICAM1 DS Reverse primer	TTTCTTGGCTGAAGGTCCAC

Table 6.2. Primer sequences used for genotyping the upstream (US) and downstream (DS) regions of the gene encoding for *icam1*.

6.1.4 RNA Reverse transcription

Component	Reference	Manufacturer
25mM $MgCl_2$	361691	Life Technologies
10X PCR Buffer I	4486218	Life Technologies
DEPC water	R0601	ThermoFisher Scientific
dNTP´s (10mM)	362275	Life Technologies
RNase Inhibitor	100021540	Life Technologies
Random hexamers	100026484	Invitrogen
MuLV RT	100023379	Life Technologies

Table 6.3. Reagents used for reverse transcription of RNA to complementary DNA. Concentration and manufacturers' reference are indicated.

6.1.5 qRT-PCR primers' sequences

All primers indicated below were purchased from Integrated DNA Technologies (IDT).

Gene	Forward	Reverse
icam1	5' -GCT GTG CTT TGA GAA CTG TG -3'	5' -GTG AGG TCC TTG CCT ACT TG -3'
nppb	5' -CAC CGC TGG GAG GTC ACT -3'	5' -GTG AGG CCT TGG TCC TTC AA -3'
nppa	5' -GAG AGA CGG CAG TGC TTC TAG GC -3'	5' -CGT GAC ACA CCA CAA GGG CTT AGG -3'
col1a1	5' -AAG GGT CCC TCT GGA GAA CC -3'	5' -TCT AGA GCC AGG GAG ACC CA -3'
tgfb1	5' -CAC CGG AGA GCC CTG GAT A -3'	5' -TGC CGC ACA CAG CAG TTC -3'
acta2	5' -GCA TCC ACG AAA CCA CCT A -3',	5' -CAC GAG TAA CAA ATC AAA GC -3'
myh6	5'-CCT AGC CAA CTC CCC GTT CT -3'	5' –GCC AAT GAG TAC CGC GTG A -3'
myh7	5'-TGA GCC TTG GAT TCT CAA ACG T -3'	5' –AGG TGG CTC CGA GAA AGG AA -3'
il1b	5'- ACT CCT TAG TCC TCG GCC A –3'	5'-TGG TTT CTT GTG ACC CTG AGC -3'
il6	5' –TGA TGG ATG CTA CCA AAC TGG-3'	5'-TTC ATG TAC TCC AGG TAG CTA TGG -3'
tnfa	5' –GCA CAG AAA GCA TGA CCC G -3'	5' –GCC CCC CAT CTT TTG GG -3'
nos2	5'-GCC ACC AAC AAT GGC AAC A -3'	5' –CGT ACC GGA TGA GCT GTG AAT T -3'
arg1	5'-TTG CGA GAC GTA GAC CCT GG -3'	5' –CAA AGC TCA GGT GAA TCG GC -3'
ednrb	5' –GTG GCT TCT TGG GGG TAT GG -3'	5' –TCT TAG TGG GTG GCG TCA TTA -3'

cxcl9	5′-CTT GAG CCT AGT CGT GAT AAC -3′	5′-CCA GCT TGG TGA GGT CTA TC-3′
cxcl10	5’- ATG ACG GGC CAG TGA GAA TG-3’	5’- ATT CTT TTT CAT CGT GGC AAT GA-3’
vcam1	5’- ACT CCT TAG TCC TCG GCC A –3’	5’-TGG TTT CTT GTG ACC CTG AGC -3’
tbx21	5’- CAA CAA CCC CTT TGC CAA AG -3’	5’- TCC CCC AAG CAG TTG ACA GT -3’
ifng	5’- AAC GCT ACA CAC TGC ATC TTG G-3’	5’- GCC GTG GCA GTA ACA GCC -3’
gapdh	5’-ACC ACA GTC CAT GCC ATC AC -3’	5’ –TCC ACC ACC CTG TTG CTG TA – 3’

Table 6.4. Primer sequences used for determining the expression of the genes indicated.

6.1.6 Immunohistochemistry antibodies

Antibody	Clone	Manufacturer
anti-mouse CD54	YN1/1.7.4	BioLegend
anti-mouse CD31	MEC13.3	BioLegend
anti-mouse CD4	GK1.5	BioLegend
anti-mouse CD8	53-6.7	BioLegend
anti-mouse CD11b	M1/70	BioLegend
anti-mouse Gr1	RB6-8C5	BioLegend

Table 6.5. Antibodies used for frozen tissue staining. Clone and manufacturer are indicated.

6.1.7 Immunohistochemistry buffers

0.1M Acetate buffer pH 5.2 (Vt= 500 mL)

Chemical	MW	Molarity	Volume
$CH_3COONa\ 3{\cdot}H_2O$	136.08	0.2M	197.5mL
CH_3COOH glacial	60.08	0.2M	52.5 mL
Distilled water	-	-	250 mL

Table 6.6. Chemical reagents and their concentration are indicated. V_t= total volume. MW= molecular weight.

3-Amino-9-ethylcarbazole (AEC) Solution (Vt=100mL)

Chemical	MW	mmol/L	Mass/ Volume
3-Amino-9-ethylcarbazole	210.27	0.02M	0.4 g
N,N-Dimethylformamide	73.09	-	100mL

Table 6.7. Chemical reagents and their concentration are indicated. V_t= total volume. MW= molecular weight.

6.1.8 Left Ventricle (LV) digestion buffer

Chemical	MW	mmol/L	g/mg for 1L diH_2O
NaCl	58.44	120	7.0128 g
KCl	74.55	5.4	402.57 mg

NaH_2PO_4	120	1.2	144 mg
$NaHCO_3$	84.01	20	1.6802 g
Glucose	180.2	5.6	1.0091 g
Taurine	125.15	5	625.75 mg
$MgCl_2$	95.21	1.6	152.336 mg
2,3-butanodione monoxime	101.1	10	1.011 g

Table 6.8. Chemical reagents and their concentration are indicated.

6.1.9 Flow cytometry antibodies

Antibody	Clone	Manufacturer
anti-mouse CD45.2-**PE**	104	BioLegend
anti-mouse CD45.2-**APC**	104	BioLegend
anti-mouse Ly-6C- **APC-Cy7**	HK1.4	BioLegend
anti-mouse CD4-**FITC**	GK1.5	BioLegend
anti-mouse CD4-**APC-Cy7**	GK1.5	BioLegend
anti-mouse CD3e-**FITC**	145-2C11	BioLegend
anti-mouse CD11b- **PerCP**	M1/70	BioLegend
anti-mouse CD44-**APC-Cy7**	IM7	BioLegend
anti-mouse CD62L-**PE**	MEL-14	BioLegend

anti-mouse CXCR3-**APC**	CXCR3-173	BioLegend
anti-mouse CD11a-**FITC**	2D7	BioLegend
anti-mouse IFNγ-**PE**	XMG1.2	BioLegend
anti-mouse IL17-**PE**	TC11-18H10.1	BioLegend

Table 6.9. Antibodies used for cell suspension staining. Clone and manufacturer are indicated.

6.2 METHODS

6.2.1 Mouse model of Transverse Aortic Constriction

Left ventricular pressure overload was induced by constricting the transverse aorta of 8-10 week old male mice (169). 2.5% Isoflurane carried in 100% oxygen was used to induce anesthesia and to maintain the anesthesia while the mice were on the respirator. The mice were placed in a supine position and the chest cavity was accessed through the intercostal space. Transverse Aortic Constriction (TAC) was performed between the two common carotid arteries by ligating a 7-0 nylon suture material against a 25-gauge needle (Figure 6.1, Figure 6.2) (169). Sham operated mice underwent the same procedure but without ligation. 1.0 mg/kg Buprenorphine SR (sustained released) was administrated subcutaneously with a 20-gauge needle using a Hamilton micro syringe as post-operatory analgesia. 48h, 1, 2 or 4 weeks after TAC, mice were euthanized and tissue was harvested for further analysis as described (170).

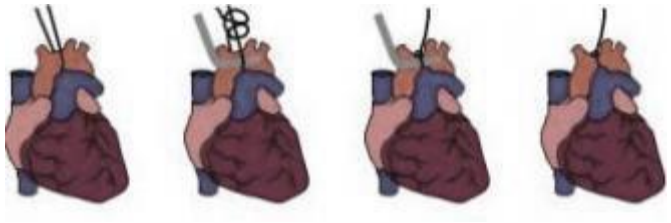

Figure 6.1. Sequential schematic diagram of the transverse aortic constriction surgery**.**

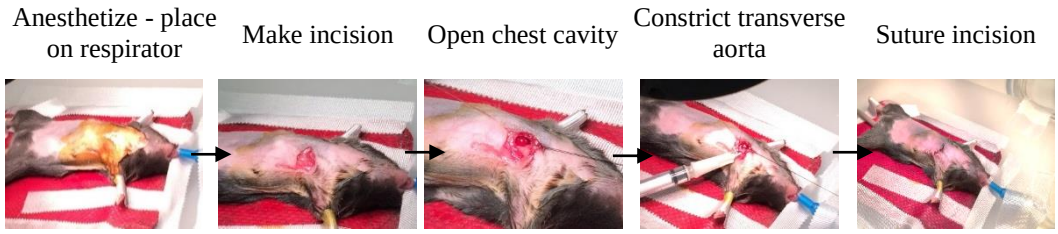

Figure 6.2. Sequential steps of the transverse aortic constriction surgery.

6.2.2 PCR analysis of Nr3c2 genomic DNA to confirm EC-specific recombination

Right ventricle, lungs, and lymph nodes were isolated from EC-MR$^{-/-}$ and MR-intact littermates and frozen in liquid nitrogen. DNA was extracted from each tissue with the DNeasy kit (Qiagen) and PCR was performed as previously described (89) using a combination of three primers indicated above in Section 6.1.2 PCR products were run on a 1.5% agarose gel.

6.2.3 CRISPR/Cas9 validation

In order to test and validate sgRNA's target specificity Cas9 mediated cleavage, US and DS sgRNAs were transfected into mouse Neuro2A cells stably expressing Cas9 (171) and genomic DNA was harvested 24 hours after the transfection. This DNA was used as template for a mismatch sensitive PCR assay to detect CRISPR/Cas9 mediated mutations (Figure 6.3).

A.

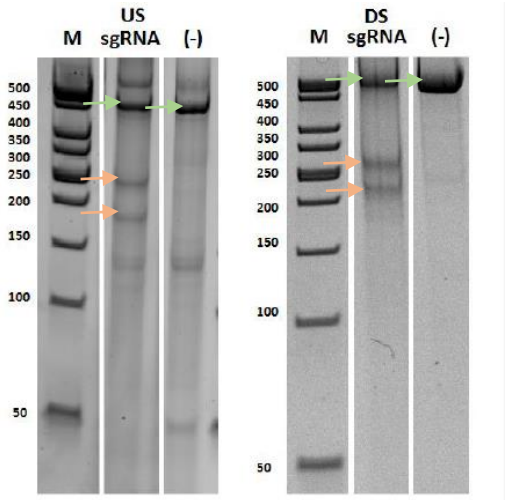

B.

	US sgRNA	DS sgRNA
Wild-type band	448bp	499bp
Cleavage bands	251bp + 197bp	266bp + 233bp

Figure 6.3. CRISPR/Cas9 specific enzymatic activity validation. **A.** Agarose gel showing the CRISPR/Cas9 mediated cleavage of the targeted DNA template. M= molecular weight marker. US and DS sgRNA columns show the WT (green arrow) and Cas9 mediated cleaved bands (orange arrow). The third column (-) is a negative control, where just the WT bands (green arrow) are observed with no Cas9 mediated DNA cleavage. **B.** Table indicating the nucleic base pairs of both WT and cleaved DNA bands for the US and DS regions respectively.

6.2.4 *icam1* gene targeting sgRNA/Cas9/loxP oligo microinjection into C57BL/6 mouse blastocysts

Once the components of the microinjection were designed and validated, 0.5 days post coitum C57BL/6 mouse fertilized oocytes were injected in either the cytoplasm or pronuclei using an Eppendorf Transjector 5246 with in-house pulled glass capillaries, which contained the microinjection buffer. The microinjection reagents, sequences and the procedure to prepare them as indicated below:

- US sgRNA at 1µg/µl (sgRNA/*PAM* site: TACCTCAATTCACTTAGTCT*CGG*)
- DS sgRNA at 1µg/µl (sgRNA/*PAM* site:AGGCAGGAGTCTCATCCAGC*AGG*)

- Cas9 mRNA at 1µg/µl
- Oligonucleotides used for loxP insertion at 1µg/µl
    - US donor sequence:

      GAGTGGTGGTACAGTCTGTAATTCCAGCCAAAGAAGGAGACTGGCA
      AGGCTGAGGCTAGCCGAGAATAACTTCGTATAATGTATGCTATACG
      AAGTTATCTCGAGCTAAGTGAATTGAGGTATGCAAAACTAAGCTGC
      ACTTGTGTCAAAACTCCAAGACTAATCCATGA

    - DS donor sequence:

      GTTACAGAAGGCTCAGGAGGAGGCCATAAAACTCAAGGGACAAGCC
      CCACCTCCCTGAGCCTGCTCGAGATAACTTCGTATAGCATACATTATA
      CGAAGTTATGGATGAGACTCCTGCCTGGACCCCCTGCAGGGCAACAG
      CTGCTGCTGCTTTTGAACAGAATGGTA

Microinjections were prepared by adding Cas9 mRNA (final concentration 60ng/µL) and both sgRNA (final concentration 15ng/µL) to IDTE buffer (10 mM Tris, 0.1 mM EDTA, pH 8.0) and run through the sgRNA renature PCR reaction: 90C-1min, 80C-1min, 70C-1min, 60C-1min, 50C-1min, 40C-1min, 30C-1min, 20C-1min, 10C-1min, 4C-hold. The upstream and downstream donor oligonucleotides (final concentration 10ng/µl each) and 40U RNAsin were added. The sample was centrifuged for 10 minutes at 14,000rpm at 4C and proceeded with the microinjection.

After the injection, zygotes were incubated at 37C, 5%CO_2 until implantation into the pseudopregnant surrogate mother's oviducts the same day.

6.2.5 DNA isolation from pups derived from injected oocytes

Mouse toe clips from pups derived from injected embryos were incubated in lysis buffer containing 4% of proteinase K at 60C overnight, precipitated with an equal volume of

cold isopropanol, and pelleted by centrifugation. The DNA pellet was washed with 200µl of 70% ethanol, air dried, and resuspended in Tris-EDTA buffer pH8.

6.2.6 Genotyping of founder pups

DNA isolated from mice generated from the injection of CRISPR/Cas9 reagents was amplified using GoTaq® Green Master Mix (Promega M712) and the primer pairs listed in Table 6.2 according to the cycling conditions indicated in Table 6.10 and Table 6.11 below. All PCR reactions were run on a 1% agarose gel for 1h at 100V to visualize the products.

Reaction components	Volume (µL)	Final concentration
DNA template	1	-
Forward primer	0.5	20µM
20µM Reverse primer	0.5	20µM
2X GoTaq® Green Master Mix, Promega (M712)	10	1X
Water	8	-

Table 6.10. PCR reaction components and their final concentration used for the PCR reactions.

Cycle steps	Temperature (C)	Time	
1	94	2 min	
2	94	30 s	x 30 cycles
3	58	30 s	
4	72	120 s	

5	72	5 min	
6	10	∞	

Table 6.11. PCR reaction cycling conditions.

Insertion was confirmed by digesting 4.5µL of each amplyfied PCR product with 0.5µL of XhoI (R016S, New England BioLabs) and 1.0µL of 10X CutSmart buffer (B7204S, New England BioLabs) in a 10µL reaction for 30 minutes at 37C.

6.2.7 RNA isolation

For isolating RNA of *in vitro* cultured cells, 1mL of TRIzol™ LS Reagent (ThermoFisher 10-296-028) were added into each cell containing well and after scrapping the surface, the resultant solution was harvested to proceed with the RNA isolation. When RNA from the whole LV tissue was isolated, 500µL of TRIzol were added to the tube containing the LV tissue, and using a plastic pistil the LV was digested. When a homogeneous digestion was achieved, the samples were kept for 3 minutes at room temperature (RT), and 500µL of Trizol were added to the suspension, up to 1mL.

For RNA extraction from both *in vitro* cultured cells and tissues, the protocol followed was the same. Phase separation was performed by adding 0.2 mL of chloroform per 1 mL of TRIzol. Samples were vortexed vigorously for 15 seconds, incubated at RT for 2 to 3 minutes and centrifuged at 12,500rpm for 15 minutes at 4C. As a result of the centrifugation, the phases were separated into a lower red, phenol-chloroform phase, an interphase, and a colorless upper aqueous phase in which the RNA remained. For precipitating the RNA from the aqueous phase, the upper phase containing it was transferred to a RNAse-free fresh tube, followed by adding half of the volume of the

aqueous phase of isopropyl alcohol (440µL/2=220µL). Samples were incubated at RT for 10 minutes and centrifuged at 12,500rpm for 10 minutes at 4C. The precipitated RNA, often invisible before centrifugation, forms a gel-like pellet on the side and bottom of the tube. The supernatant was carefully removed and 1 mL of 75% ethanol per 1 ml of TRIzol Reagent used for the initial homogenization were added. The samples were mixed and centrifuged at 9,500rpm for 5 minutes at 4C. Upon removal of the supernatant RNA pellet was air-dry at RT for 5-10 minutes, resuspended in 30µL RNA-ase free water (DEPC-treated water) and incubated for 10 minutes at 55-60C.

The quality and the concentration of the RNA was determined through the Thermo Scientific NanoDrop 2000c UV-Vis spectrophotometer. RNA concentration and purity were determined by measuring optical density (OD) at 260 nm and 280 nm. The convention 1 optical density (OD) at 260 equals 40 µg /ml RNA was applied. 260/280 nm ratio values ranging from 1.8 to 2.0 were considered adequate to proceed with the reverse transcription of the RNA samples.

6.2.8 Reverse transcription

For synthetizing cDNA (complementary DNA) from template RNA, the following volumes of each reagent were added per 1µg of template RNA:

Component	Volume	Final Concentration
25mM $MgCl_2$	4µL	5mM
10X PCR Buffer II	2µL	1X
DEPC water	Variable	-
dNTP´s (10mM)	2µL	1mM

RNase Inhibitor	1µL	1U/µL
Random hexamers	1µL	2.5µM
MuLV RT	1µL	2.5U/µL
RNA template sample	Variable (max. is 9µL)	1µg
Final volume	20µL	

Table 6.12. Reagents and final concentration used for reverse transcription reactions.

RNA was then reverse-transcribed to cDNA following Applied Biosystems' protocol, based on 10 minute cycle at 25C, 20 minutes at 42C, 5 minutes at 99C, finalized by holding the samples at 4C.

6.2.9 Real-time Quantitative Polymerase Chain Reaction (RT-PCR)

In order to determine gene expression through mRNA levels, 3µL of each 1/10 diluted cDNA sample were mixed with 1.25µL 10µM forward primer, 1.25µL 10µM reverse primer, 12.5µL of SYBR Green (QuantiTect®SYBR® Green PCR Master Mix, Qiagen 1020722) and 8µL of RNase free water.

Samples were quantified in triplicate in 384-well plates using 40 cycles performed at 94°C for 30 seconds, 60°C for 45 seconds, 72°C for 45 seconds using an ABI Prism® 7900 Sequence Detection System.

6.2.10 Cardiac tissue staining

Heart samples were excised and the LV was separated from the right ventricle. Sections of the LV were immediately embedded in OCT or fixed in 10% formalin, embedded in paraffin, and cryostat cut into 5µm LV sections.

Immunohistochemistry

The ABC Elite peroxidase method was used for immune cell and adhesion molecule staining of OCT frozen LV tissue sections. Samples were thawed, fixed with acetone (6 minute incubation) and incubated for 10 minutes with 10% goat serum in PBS (corresponding to the specie in which the secondary antibody was produced). Next, Avidin and Biotin (Vector SP-2001) mediated blocking was performed by incubating the sections for 10 minutes with each solution. After blocking, samples were incubated with the 100µL of primary antibody (1:500 in PBS without Ca/Mg) for 1 hour at RT, followed by a 40 minute incubation at RT with the goat anti-rat biotinylated secondary antibody (1:300, in 6µL of 2% mouse serum and 300µL PBS without Ca/Mg per secondary antibody µL). After the antibody incubations, sections were washed with 1% H_2O_2 in PBS without Ca/Mg for 10 minutes at RT, in order to inactivate endogenous non-specific peroxidase activity of the tissue. Next, 30µL of ABC complexes per section were added and incubated for 40 minutes at RT light protected: for preparing the complexes 100µL PBS without Ca/Mg with 1µL solution A and 1µL solution B, from Vectastain Elite ABC HRP Kit (Peroxidase, Standard, Catalog Number: PK-6100) were mixed and kept light protected for at least 30 minutes before incubating the sections. After the incubation with the ABC complexes, sections were washed with 0.1M acetate buffer for 4 minutes at RT, followed by a 10 minute incubation with AEC buffer (300mL acetate buffer pH 5.2 + 15mL AEC stock solution + 150µL 30% H_2O_2, filtered through No. 1 Whatman Filter paper). Upon a second wash with 0.1M acetate buffer for 3 minutes, followed by a wash in distilled water, sections were incubated in filtered Gill´s hematoxylin solution for 1 minute. Finally, sections were washed thoroughly with warm water and covered with glycerin and capped with a glass coverslip. Numbers of

cells positively stained with the marker of interest were quantified across the whole ventricular section per mouse.

Hematoxylin and eosin and Picrosirius red staining

Hematoxylin and Eosin dyes were used for staining of the nucleus and cytoplasm of 5μm LV sections embedded in paraffin. The staining was initiated by heating the sections for 20 minutes at 60C, followed by washes with xylene, 100% alcohol, 95% alcohol and water. Hematoxylin (Richard-Allan Scientific™ Signature Series Hematoxylin 7211, ThermoFisher Scientific) staining was done for 2 minutes, followed by water washes, 1 minute incubation with Clarifier 2 to remove background staining, bluing to enhance the color of the nuclei after hematoxylin staining and 30 second wash with 95% alcohol. Next, alcoholic eosin staining was done for 2 minutes, providing delineation of cytoplasmic components. Staining was finalized by doing several washes with 95% and 100% alcohol, and xylene, and placing a coverslip on top of the sections. Cardiomyocyte size was determined in H&E stained LV cross sections by measuring the area of 10-20 myocytes per mouse LV using the NIS-Elements AR 4.51.00 software. Percent leukocyte infiltration was quantified using Image J by dividing each 40x representative picture in 30 grids and counting the number of grids containing leukocytes infiltrated (%= positive grids/30 x 100).

Picrosirius red staining was used to visualize collagen deposition in paraffin-embedded LV sections. The staining was initiated by heating the sections for 40 minutes at 60C, followed by washes with xylene, 100% alcohol and 85% alcohol. Sections were next incubated in 0.2% phosphomoybdic acid for 5 minutes, followed by deionized water rinsing. Picrosirius Red staining was done by incubating the sections with 0.1% Picrosirius solution (Direct Red 80, Sigma-Aldrich 365548) for 60 minutes. After the

incubation, sections were briefly rinsed and washed with 0.01N HCl. Finally, stained tissues were rinsed with deionized water, air dried, placed in xylene and covered with a coverslip. Collagen deposition was quantified in Picrosirius red stained LV cross sections by determining the intensity of the staining in 5-7 representative fields per LV using Image J.

ApopTag® Peroxidase In-Situ Apoptosis Detection

The ApopTag® Peroxidase In-Situ Apoptosis Detection Kit (EMD Millipore S7100) detects apoptotic cells in situ by labeling and detecting DNA strand breaks by utilizing the terminal deoxynucleotidyl transferase (TdT) (TUNEL method). 5μm frozen LV cross-sections were first fixed in 1% paraformaldehyde in PBS for 10 minutes at RT, followed by two washes with PBS for 5 minutes each. Next, sections were incubated for 5 minutes in precooled ethanol: acetic acid 2:1 for at -20C, followed by two washes with PBS for 5 minutes each. Immediately after, equilibration buffer was applied on the sections for 10 minutes at RT, in a 75 μL/5 cm^2 volume/tissue surface area ratio. Immediately next, 55μL/5 cm^2 of working strength TdT enzyme was added on the sections and incubated for 1h at 37C in a humidified chamber. After the incubation, the sections were immersed in stop/wash buffer and agitated for 15 seconds, followed by a 10 minute incubation at RT. Next, after 3 washes with PBS, anti-Digoxigenin peroxidase was applied on the sections in a 65 μL/5 cm^2 volume/tissue sections area ratio and incubated 30 minutes at RT. Following 4 washes with PBS for 2 minutes each, Peroxidase substrate was applied on the sections, on a 75 μL/5cm^2 volume/tissue section area ratio, and incubated for 6 minutes at RT. Finally, the sections were washed 3 times in distilled water for 1 minute each, followed by 5 minute incubation at RT in distilled water, and mounted on a DAPI containing mounting media (Vectashield, H-1200,

Vector Laboratories). Representative pictures were adquired using a Nikon NIS-Elements AR 4.51.00 software.

6.2.11 Quantitative flow cytometry

Flow cytometry was performed to analyze the immune profile present in response to TAC.

Prior to staining the LV tissues, these where digested based on the following protocol. PBS perfused hearts were chopped with razors, collected in 5mL digestion buffer (composition indicated in Section 6.1.8) containing collagenase type II (0.895mg/mL) and protease XIV (0.5mg/mL). Cell suspensions were incubated at 37C in a water bath for 30 minutes with intermittent shaking and triturated with a cannula. The resulting digests were filtered through a 40μm cell strainer, followed by centrifuging at 1500rpm for 5 minutes. The pellets were resuspended in 200μL FACS buffer (PBS without Ca/Mg, plus 2% FBS) and staining was initiated.

Digested LV suspensions and lymphoid organs harvested from Sham and TAC mice and surface stained with the monoclonal antibodies (mAbs) indicated in Section 6.1.9 above. Cells were surface stained by incubation with the relevant antibodies diluted 1:100 in phosphate buffered saline (PBS) + 2% FBS for 20 minutes at room temperature light protected, followed by two washes with PBS 2% FBS.

When intracellular staining of signature cytokines was performed, cell suspensions were initially incubated for 3-5 hours at 37C with RPMI T cell media containing 0.1% ionomycin (Sigma-Aldrich**,** I0634***)***, 0.1% brefeldin A (BioLegend, 420601), 0.1% monensin (BioLegend, 420701) and 0.5% 1/100 diluted PMA (Phorbol Myristate Acetate, Sigma-Aldric P8139). Ionomycin in conjunction with PMA

stimulates the intracellular production of the cytokines. Brefeldin A causes disassembly of the Golgi complex and accumulation of secretory proteins in the endoplasmic reticulum. After the incubation, surface staining was performed as indicated above, followed by cell fixation for 15 minutes at RT light protected with fixation buffer (BD Biosciences, 554655). Upon fixation and washes with PBS 2% FBS, cell suspensions were permeabilized with 1X wash/permeabilization buffer (BD Biosciences, 554723, diluted in distilled water), and the intracellular staining was performed for 20 minutes at RT light protected.

The data was acquired on a BD LSRII and analyzed using FlowJo software.

6.2.12 Adult mouse cardiac myocyte isolation

Cardiac myocytes were isolated from WT and ICAM1$^{-/-}$ hearts 4 weeks after TAC as previously described (22). Briefly, mice were administered heparin (200U ip) and euthanized. The hearts were rapidly excised, cannulated via the aorta and perfused in the Langendorff mode with perfusion buffer (113mM NaCl, 4.7mM KCl, 0.6mM NaH_2PO_4, 12mM $NaHCO_3$, 0.6mM KH_2PO_4, 10mM HEPES, 1.2mM $MgSO_4$-$7H_2O$, 30mM Taurine, 10 mM 2,3 butane-dione monoxime and 5.5mM glucose, pH 7.46, at 35 °C). Hearts were then digested with perfusion buffer containing 773.78µg/mL Collagenase type 2 and 0.14mg/mL Trypsin. After 5 minute digestion the LV was separated, minced, and gently agitated in stopping buffer, which consists on perfusion buffer containing 10%FBS and 12.5µM $CaCl_2$, allowing the myocytes to be dispersed. The cells were subsequently resuspended in stopping buffer with gradually increasing Ca^{2+} concentrations (0.062, 0.112, 0.212, 0.5, and 1.0 mM [Ca^{2+}]). Cardiac myocytes plated on laminin coated wells were imaged with a 20x magnification and width and length were determined using the Nikon NIS-Elements AR 4.51.00 software.

6.2.13 Bone marrow (BM) monocyte isolation and M1 or M2 differentiation

WT and ICAM1$^{-/-}$ BM cells were collected from femur and tibias by flushing them with buffer (PBS with 0.5% BSA and 2mM EDTA) using a 25G needle. BM cells were disaggregated and passed through a 40μm cell strainer. From the resulting BM cell suspension, the Miltenyi Biotec's isolation kit (Cambridge, MA) was used to isolate BM derived monocytes, which were incubated for three days with 1μg/ml LPS (Santa Cruz Biotechnology sc-3535) or 20ng/ml of IL-4 (PeproTech 214-14) for differentiation to M1 or M2 monocytes, respectively. RNA was isolated using the Qiagen kit and iNOS and Arginase I expressions were determined through qRT-PCR for identifying the M1 and M2 monocyte populations.

6.2.14 Cardiac fibroblast isolation and differentiation to myofibroblast

Perfused hearts from 8-10 week old male WT and ICAM1$^{-/-}$ mice were digested with Liberase DL (Roche) for 25min at 37C. The resulting cell suspension was cultured in Fibroblast Growth Media on 1% gelatin coated plates. Purified cardiac fibroblast in passages 2-3 were treated with TGFβ (100ng/mL for 16h) to induce fibroblast transition to myofibroblasts, which was determined by measuring mRNA levels of SMAα.

6.2.15 LV *in vivo* hemodynamic studies

In vivo LV function was assessed by Pressure-Volume (PV) loop analysis in mice anesthetized with 2.5% isofluorane, which was reduced to 2.0% for PV loop data measurement recording and occlusions. A fully calibrated 1-French PV catheter (PVR-1045; AD Instruments) was advanced through the right carotid artery and across the aortic valve into the LV. The absolute volume was calibrated, and PV data were assessed at steady state and during preload reduction. Hemodynamics were recorded

and analyzed with IOX version 2.8.0.19 software (EMKA Instruments, Falls Church, VA) (23).

6.2.16 *In vivo* transthoracic echocardiography

Transthoracic echocardiography was performed under light sedation with 1.5% isoflurane administered via nose cone while the core body temperature was maintained at 37.0 ± 0.2°C. M Mode and 2-dimensional images were obtained from the short-axis view, as described previously (19;23). Left ventricular end-diastolic and end-systolic diameters (EDDs and ESDs, respectively) and heart rate were measured by averaging values obtained from 5 cardiac cycles. Fractional shortening was calculated using the following standard equation: FS%=([EDD−ESD]/EDD) × 100. The investigators were blinded to genotype during data acquisition and analysis.

6.2.17 Preparation of effector T cells

CD4+ cells were isolated from spleen and lymph node suspensions of WT mice through using immunomagnetic bead mediated positive selection (L3T4, Miltenyi Biotec, Germany). Naïve CD4 T cells were differentiated into Th1 by stimulating them with anti-CD3 (5µg/mL) and anti-CD28 (1µg/mL) in the presence of IL-12 (0.01µg/mL), IL-2 (25U/mL) and anti-IL-4 (0.5µg/mL). On day 3 of stimulation, Th1 and Th17 cultures were split 1:1 with fresh medium containing IL-2 (25U/mL) and IL-23 (40ng/mL), respectively. Differentiated T cells were harvested on day 4 and immediately used for experiments (Figure 6.4).

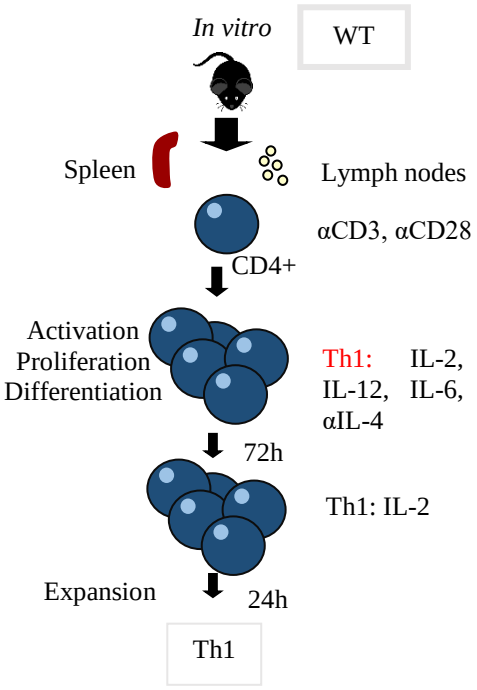

Figure 6.4. Diagram showing the *in vitro* CD4+ naïve T cell polarization protocol into Th1 cells.

6.2.18 Measurement of interactions of effector T cells with ICAM1 under defined flow conditions *in vitro*

Th1 cell interactions with immobilized ICAM1 were observed by videomicroscopy (×20 objective) under defined laminar flow conditions in a parallel plate apparatus using the Nikon NIS-Elements AR 4.51.00 software. Interactions of T cells with immobilized ICAM1 were measured in eight different fields of view after the initial minute of each flow rate (shear stress 0.8 dyne/cm^2 and 1 dyne/cm^2) as previously described. Where indicated, T cells were stimulated with either PMA (50ng/mL), CXCL9 (100ng/mL) or CXCL10 (100ng/mL) for 5 minutes at 37C before T cells were perfused in the flow chamber. For LFA1 blocking, T cells were incubated for 30 min with 40µg/mL αLFA1 (M17/4, Biolegend) at 37C, prior to the chemokine stimulation. Immobilized ICAM1 was incubated when indicated with CXCL9 or CXCL10 (2µg/mL) for 15minutes at

37C, before placing the coverslip containing the immobilized protein in the parallel plate apparatus (Figure 6.5, Figure 6.6).

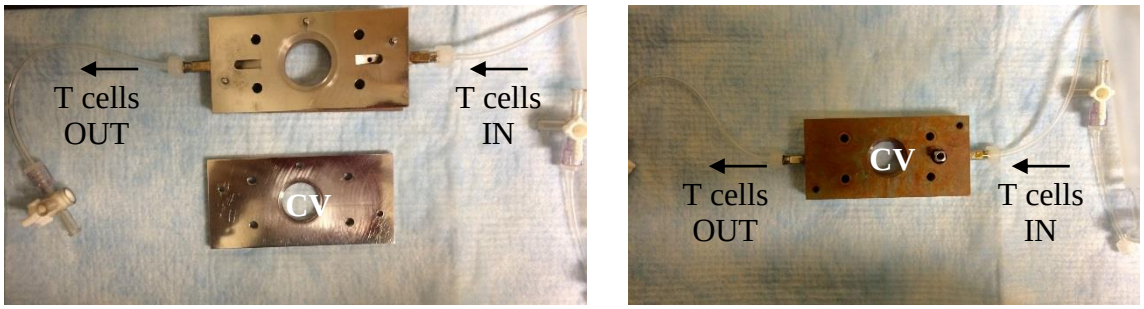

Figure 6.5. Parallel flow chamber set up; the coverslip is first placed centered on one side on the chamber (left). Then, chamber is closed and sealed (right) preventing T cell and buffer leaks. Arrows indicate the directionality of the T cells flown through the chamber.

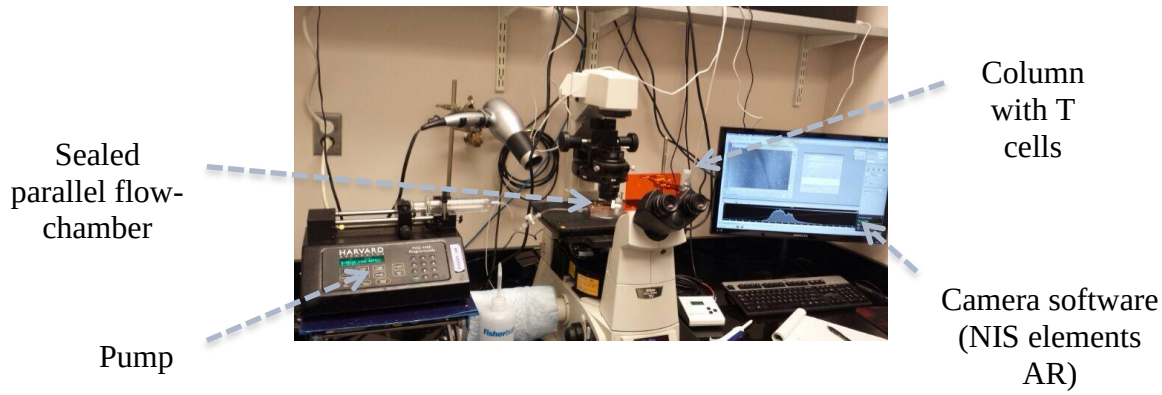

Figure 6.6. Parallel flow chamber set up once placed on the microscope and connected to the pump.

6.2.19 Statistical Analysis

Data are represented as the mean ± SEM. Statistical analyses were done by student unpaired *t* test or non-parametric Mann-Whitney test where indicated, using GraphPad Prism software (GraphPad). When unpaired *t* test was used, the outcome was confirmed

to be normally distributed. Differences were considered statistically significant at $p \leq 0.05$ and are indicated with an (*).

7 RESULTS

7.1 T cell mediated adaptive immune response in heart failure

Several clinical and experimental reports suggest that adaptive immune responses contribute to pathological cardiac remodeling during HF progression (172). However, the specific effect of T lymphocytes in the detrimental ventricular remodeling and the mechanisms involved remain to be elucidated. We used the well-stablished Transverse Aortic Constriction (TAC) mouse model to induce ventricular pressure overload, cardiac remodeling and failure, and thus to characterize the role of effector T cells in non-ischemic HF, using both wild type (WT) and transgenic mice lacking T cells.

7.1.1 CD3+ T lymphocytes, including CD4+ helper T cells, and CD11b+ myeloid cells are recruited into the LV in response to TAC

Permanent constriction of the transversal aorta induced increased LV recruitment of total CD45.2+ leukocytes (Figure 7.1A) , and specifically CD3+ T cells and CD11b+ myeloid cells 4 weeks after TAC as measured by flow cytometry, which determined a two and three-fold increased infiltration as compared to Sham operated control mice (Figure 7.1B-D). On the contrary, no significant increase in Gr1+ neutrophil and F4/80 macrophage infiltration into the LV was observed (Figure 7.1D). Within the CD3+ T lymphocytes recruited to the LV, CD4+ helper T cell numbers were found increased in LV cross-sections stained for its specific epitope (Figure 7.1E-F).

Furthermore, qRT-PCR studies demonstrated elevated LV expression of Tbet and RORγT, the signature transcription factors of Th1 and Th17 cells, respectively, in TAC vs Sham mice. In contrast, Foxp3, the signature transcription factor for regulatory T cells, remained unchanged between Sham and TAC mice (Figure 7.1G).

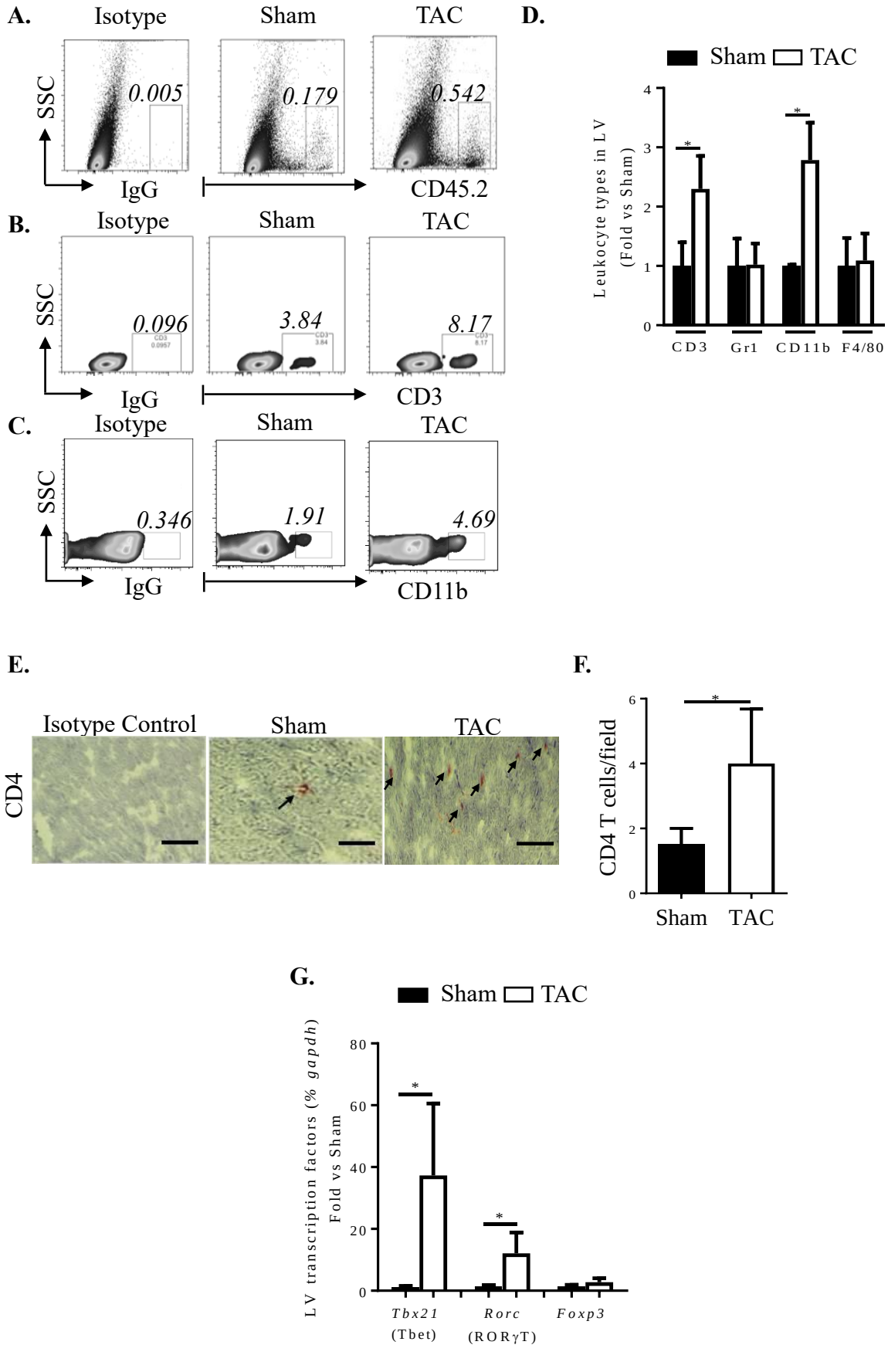
A.
Isotype
Sham
TAC
SSC
0.005
0.179
0.542
IgG
CD45.2
B.
Isotype
Sham
TAC
SSC
0.096
3.84
8.17
IgG
CD3
C.
Isotype
Sham
TAC
SSC
0.346
1.91
4.69
IgG
CD11b
D.
Sham
TAC
Leukocyte types in LV
(Fold vs Sham)
CD3
Gr1
CD11b
F4/80
E.
Isotype Control
Sham
TAC
CD4
F.
CD4 T cells/field
Sham
TAC
G.
Sham
TAC
LV transcription factors (% gapdh)
Fold vs Sham
Tbx21
(Tbet)
Rorc
(RORγT)
Foxp3

Figure 7.1. Pro-inflammatory leukocytes are recruited to the LV in response to 4 weeks TAC. Representative flow cytometry plots for **(A)** total CD45.2+ leukocytes, **(B)** CD3+ T cells and **(C)** CD11b+ myeloid cells infiltrated into the LV after 4 weeks from TAC. Numbers represent the percent of positive cells in the indicated gate. **D.** Quantification of CD3+ T cells, Gr1+ neutrophils, CD11b+ myeloid cells and F4/80 macrophage infiltrates into the LV after 4 weeks TAC, represented as fold change compared to Sham control. **E.** Representative immunohistochemistry pictures of LV cross-sections from 4 week TAC or Sham operated mice stained for CD4+ T cells. **F.** Quantitative analysis of CD4+ T cells per field of view is represented on the right, scale bar 100μm. Mean ± SEM of independent experimental replicates is represented. Statistics unpaired t-test. **G.** qRT-PCR of CD4+ T lympjocyte subsets' signature transcription factors, represented as fold change vs Sham. n= 4 Sham, 7 TAC. Mean ± SEM from a single qRT-PCR run containing samples collected in independent experimental replicates is represented. Statistics Mann-Whitney test.

Thus, in response to 4 week TAC, CD3+ T lymphocytes and pro-inflammatory CD11b+ myeloid cells infiltrated the LV, and the signature transcription factors for the CD4+ T lymphocyte subsets Th1 and Th17 were also found increased in the LV.

7.1.2 Sequential CD3+ T lymphocyte ventricular recruitment correlates with LV hypertrophy and dysfunction

Temporal quantification of LV CD3+ T lymphocyte recruitment after 48h, 2 and 4 weeks from TAC, revealed that early after TAC induction (48h), CD3+ T lymphocytes were recruited to the LV in similar quantity as Sham operated mice (Figure 7.2A). This correlated with the pre-hypertrophic state when the LV mass remained unchanged (Figure 7.2B) and there were not any variations in systolic function determined by echocardiography (Figure 7.2C). However, after 2 weeks from surgery, CD3+ T lymphocyte LV recruitment was found increased in comparison to Sham mice;

interestingly, the elevated lymphocyte infiltration coincided in time with increased LV weight and worsening of systolic function determined by decrease a in the percent fractional shortening (%FS) measured by echocardiography. The association between CD3+ T lymphocyte recruitment, LV hypertrophy and systolic dysfunction was further confirmed 4 weeks after TAC, when the significant increase in lymphocyte recruitment correlated with a further increase in LV hypertrophy and decrease in %FS.

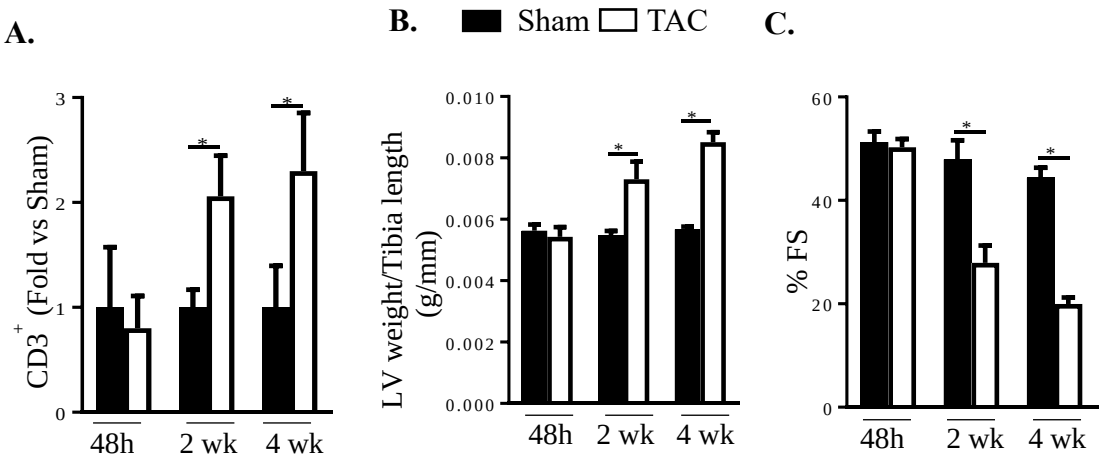

Figure 7.2. Time course of CD3+ T lymphocyte recruitment into the LV and its correlation with LV hypertrophy and systolic dysfunction in pressure overload–induced HF. Wild-type (WT) mice were subjected to Sham or TAC surgery and euthanized at the indicated time points. **A.** Quantification of CD3+ T lymphocyte infiltrates into the LV, represented as fold change compared to Sham control. **B.** LV weight normalized to tibia length. **C.** Systolic function measured by echocardiography, %FS= [(EDD-ESD)/EDD] x 100. n= 3-11 Sham, 5-16 TAC. Mean ± SEM of independent experimental replicates is represented. Statistics unpaired t-test.

7.1.3 Endothelial cell adhesion molecules become upregulated in the LV in response to pressure overload induced by TAC

Next, we characterized the endothelial cell adhesion molecules that could potentially aid and contribute to T lymphocyte mediated pathological cardiac remodeling. TAC surgery

induced an upregulation of mRNA levels of the endothelial cell adhesion molecules, vascular cell adhesion molecule-1 (VCAM1), E-selectin, and intercellular adhesion molecule 1 (ICAM1) (Figure 7.3A), Thus, these findings demonstrated that pressure overload induced the intramyocardial upregulation of ICAM1 and other endothelial cell adhesion molecules that could mediate effector T lymphocyte recruitment to the LV.

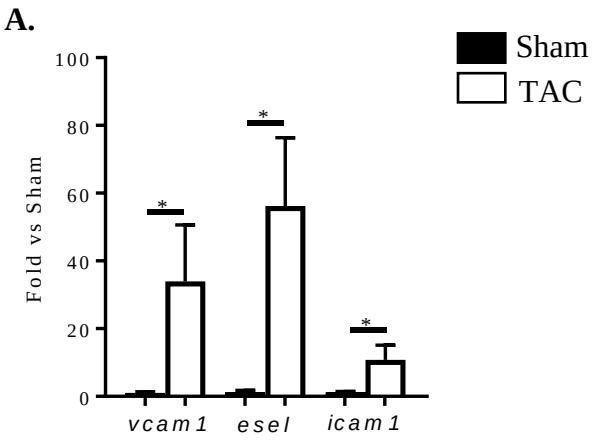

Figure 7.3. TAC induced intramyocardial endothelial cell activation. A. RNA was extracted from the LV of 4 week TAC and Sham mice and the expression of the indicated adhesion molecules was analyzed by qRT-PCR. n= 4 Sham, 10 TAC. Mean ± SEM from a single qRT-PCR run containing samples collected in independent experimental replicates is represented. Statistics Mann-Whitney test.

7.1.4 Mice lacking T lymphocytes have preserved cardiac function and increased survival in response to pressure overload induced by TAC as compared to WT mice

Having observed the association between CD3+ T lymphocyte recruitment and cardiac dysfuntion in response to TAC (Figure 7.2), we next evaluated the cardiac function phenotype of TCR$\alpha^{-/-}$ mice, which lack the α chain of the T cell receptor (TCR) and therefore lack αβ T cells, and compared to WT mice in response to 4 weeks TAC.

Non invasive echocardiographic studies determined that while the %FS was significantly decreased in WT mice 4 weeks after TAC, TCR$\alpha^{-/-}$ mice showed completely preserved %FS (Figure 7.4A-B) in response to same degree of pressure overload over 4 weeks (Figure 7.4C).

Invasive hemodynamic studies further characterized cardiac function and demonstrated that while stroke volume was decreased two fold in WT mice, TCR$\alpha^{-/-}$ mice preserved similar values of blood volume ejected out in each cardiac cycle after TAC when compared to Sham operated mice (Figure 7.4D). The End Diastolic Pressure (EDP) which was three-fold elevated in WT TAC mice, was found to be significantly lower in TCR$\alpha^{-/-}$ TAC mice when compared to WT TAC mice, and similar to TCR$\alpha^{-/-}$ Sham mice, indicating a preserved ejection capacity and therefore a lower blood volume remaining in the LV after each cardiac cycle (Figure 7.4E). Contractile and relaxation functions determined using the dP/dt_{max} and dP/dt_{min} index, respectively, were both preserved in TCR$\alpha^{-/-}$ mice after TAC, opposite to the phenotype observed in WT mice, in which dP/dt_{max} and dP/dt_{min} were significantly decreased (Figure 7.4F-G).

Interestingly, along the four weeks that these studies lasted, all TCR$\alpha^{-/-}$ mice survived to the TAC induced HF, while 25% mortality was observed in WT mice (Figure 7.4H). Altogether, TCR$\alpha^{-/-}$ mice had preserved cardiac function in all the parameters measured as well as increased survival after 4 weeks TAC as compared to WT mice.

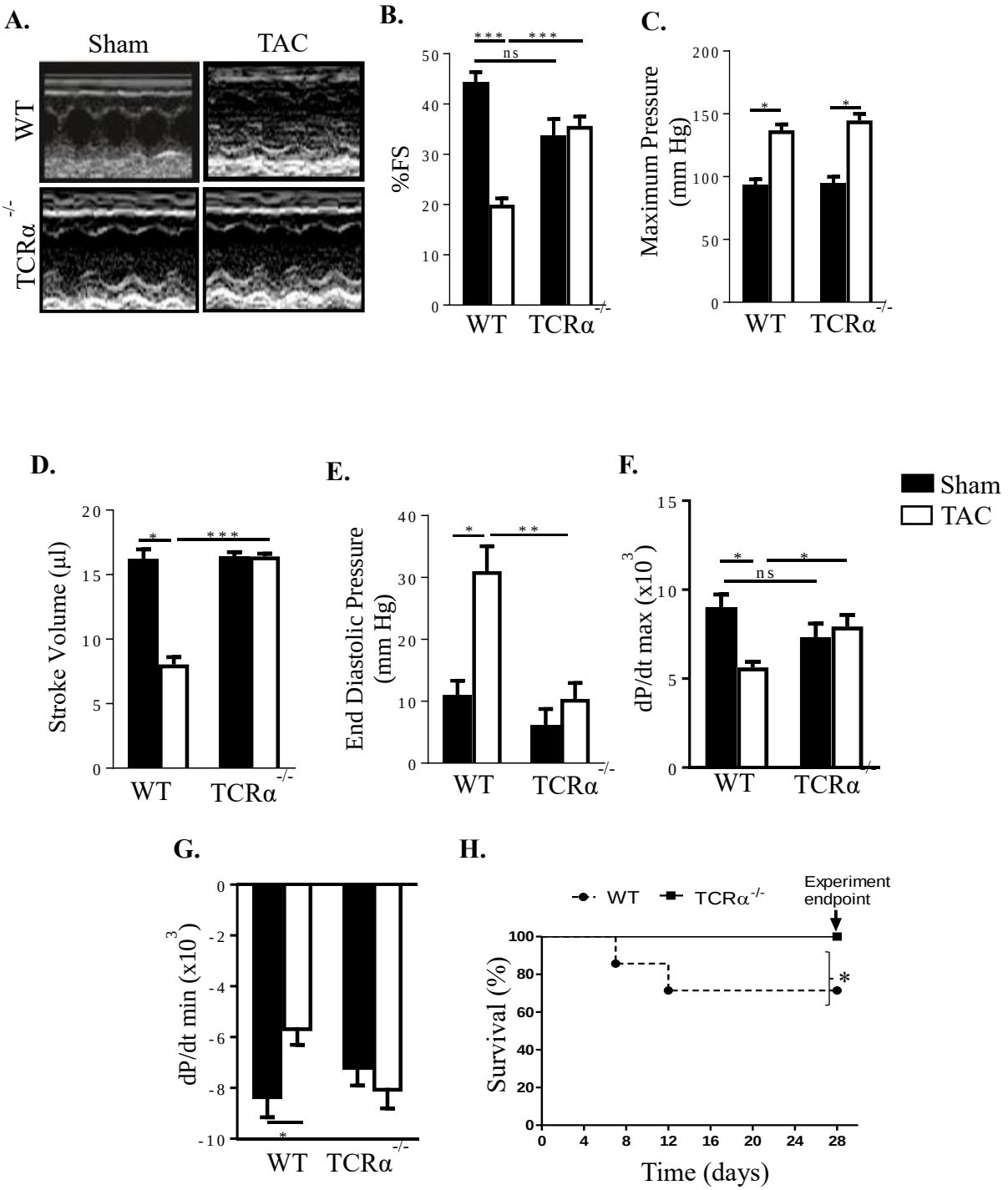

Figure 7.4. T-cell receptor deficient (TCRα$^{-/-}$) mice had preserved cardiac function and survival in response to pressure overload–induced HF. A-B. (A) Representative echocardiograms and **(B)** quantification of fractional shortening (%FS) 4 weeks after Sham or TAC surgery in WT and TCRα$^{-/-}$ mice. **C–G.** Invasive PV loop hemodynamic measurements in WT and TCRα$^{-/-}$ mice 4 weeks after Sham and TAC surgery (n= 3 Sham, 7 TAC). **H.** Kaplan–Meier

survival curves in WT (n=19) and TCRα$^{-/-}$ (n=10) mice after TAC. Mean ± SEM of independent experimental replicates is represented. Statistics unpaired t-test.

7.1.5 T lymphocytes regulate pathological myocardial remodeling, characterized by LV hypertrophy, fibrosis and cardiac inflammation

Given WT mice developed increased LV weight in response to 4 weeks TAC (Figure 7.2B), the same anatomic parameter was determined in TCRα$^{-/-}$ mice, where no increase in LV mass was observed 4 weeks after TAC (Figure 7.5A). In addition, cardiomyocyte (CM) area was determined in LV cross-sections stained with H&E,where a two-fold increase in CM area was determined in WT TAC mice as compared to Sham, while no CM area enhancement was developed in TCRα$^{-/-}$ mice after TAC (Figure 7.5B-C). Natriuretic peptides are considered markers of myocardial hypertrophy, since they are found increased in serum of HF patients, in a physiological effort to compensate the volume overload the myocardium faces in response to a reduced EF (173). Natriuretic peptide mRNA expression was determined in LV RNA samples isolated 4 weeks after TAC in both genotypes; while WT mice showed significant increase in both Brain Natriuretic Peptide (BNP) and Atrial Natriuretic Peptide (ANP) expression in response to TAC, TCRα$^{-/-}$ mice showed no increase of any of the natriuretic peptides (Figure 7.5D-E).

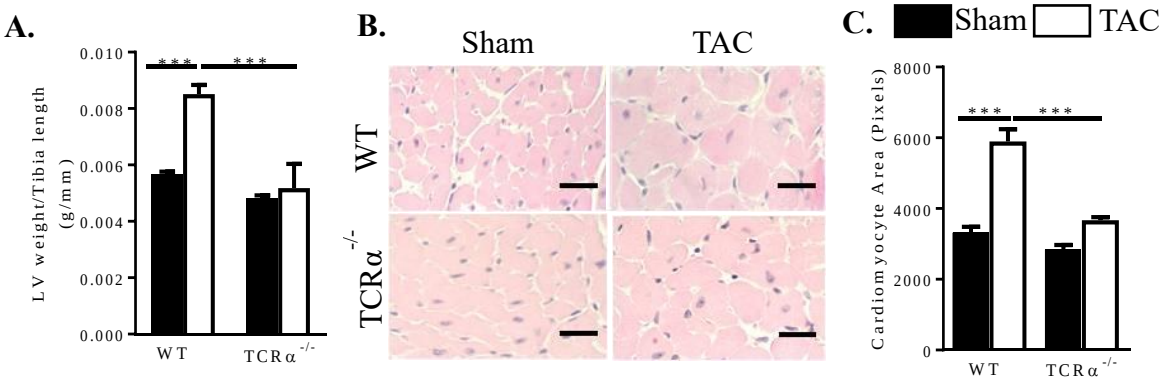

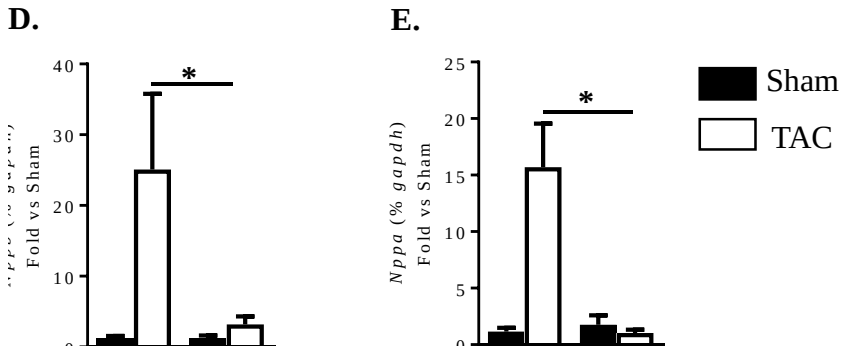

Figure 7.5. Absence of LV hypertrophy in response to pressure overload induced HF in TCRα$^{-/-}$ mice. A. LV weight, normalized to tibia length, in 4 week Sham or TAC operated mice. **B.** Representative H&E staining of WT and TCRα$^{-/-}$ LV cross-sections 4 weeks post Sham or TAC, scale bar 25μm. **C.** Quantification of CM area determined in LV cross sections stained with H&E. Mean ± SEM of independent experimental replicates is represented. Statistics unpaired t-test. **D-E.** qRT-PCR for pro-hypertrophic markers Brain Natriuretic Peptide (BNP, *nppb*) and Atrial Natriuretic Peptide (ANP, *nppa*). n= 6-11 WT Sham, 11-16 WT TAC, 5 TCRα$^{-/-}$ Sham, 8 TCRα$^{-/-}$ TAC. Mean ± SEM from a single qRT-PCR run containing samples collected in independent experimental replicates is represented. Statistics Mann-Whitney test.

Ventricular fibrosis is considered another hallmark of pathological cardiac remodeling, a process in which cardiac fibroblasts differentiate to myofibroblasts, which produce collagen that deposits in the myocardial tissue, increasing wall stiffness and decreasing cardiac function. First, LV cross-sections were stained with Picrosirius red to determine if collagen deposition and fibrosis were accounting for the increased in LV weight in response to TAC. While collagen matrix interstitial deposition was significantly increased in WT mice 4 weeks after TAC, TCRα$^{-/-}$ mice did not show matrix deposition and LV fibrosis in response to TAC (Figure 7.6A-B). In addition, several pro-fibrotic marker mRNA expression was determined through qRT-PCR. TGFβ, which induces transition of fibroblasts to myofibroblast, was found upregulated in WT TAC mice, while TCRα$^{-/-}$ mice had no

increase in TGFβ expression (Figure 7.6C). Along with the Picrosirius red staining data, collagen-I mRNA levels were found increased in WT TAC mice, opposite to the lack of upregulation determined in TCRα$^{-/-}$ TAC mice (Figure 7.6D). Finally, SMAα, which is a marker of fibroblast to myofibroblast transition, was significantly elevated in WT TAC mice while no upregulation was observed in TCRα$^{-/-}$ TAC mice (Figure 7.6E).

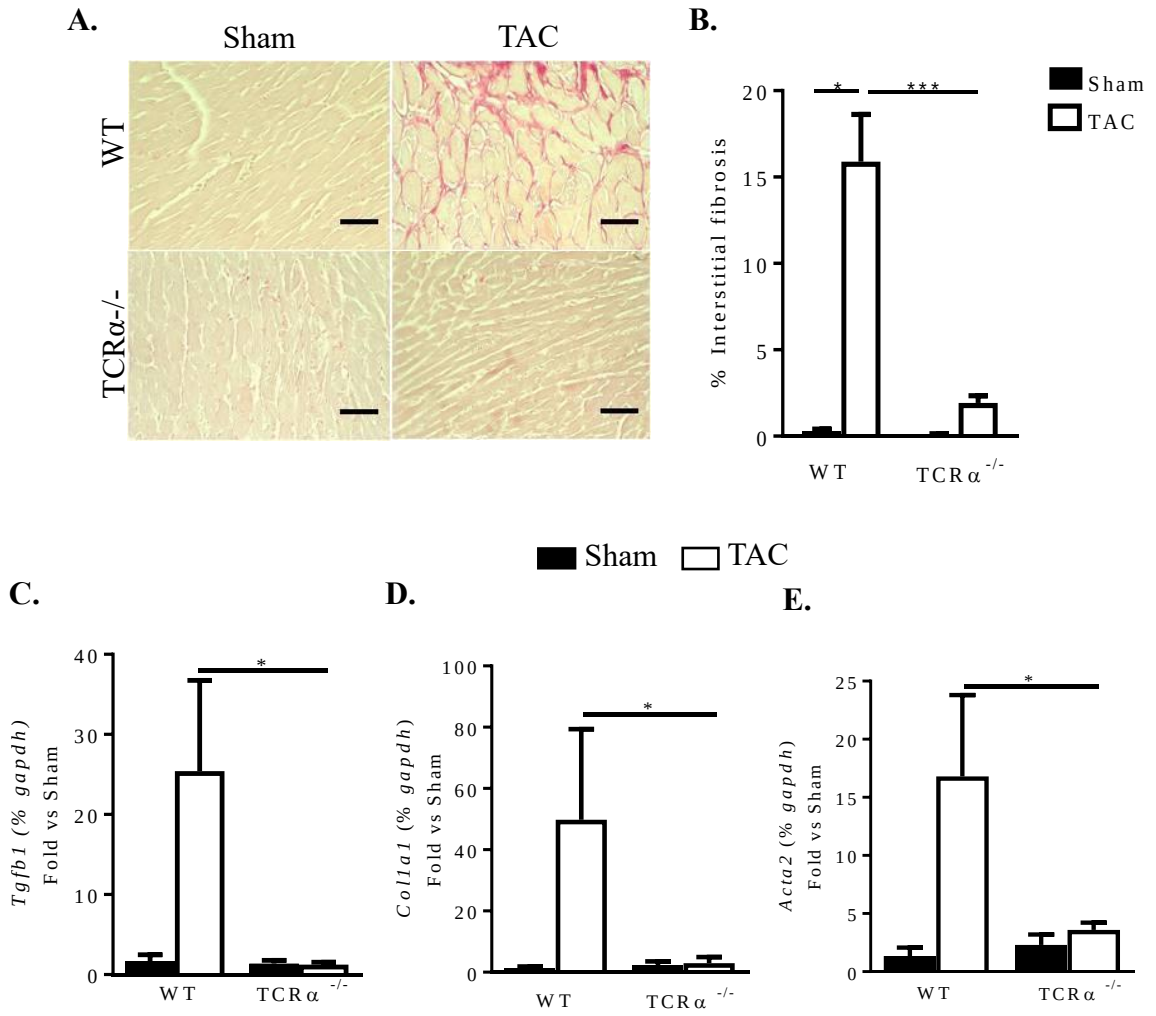

Figure 7.6. **Absence of LV fibrosis in response to pressure overload induced HF in TCRα$^{-/-}$ mice. A.** Representative 40x pictures and **(B)** quantification of myocardial interstitial fibrosis determined in LV cross sections stained with Picrosirius red 4 weeks after Sham or TAC surgery, scale bar 25μm. Mean ± SEM of independent experimental replicates is represented. Statistics unpaired t-test. **C-E.** qRT-PCR for pro-fibrotic markers Transforming Growth Factor β (*Tgfb1*),

collagen I (*Col1a1*) and Smooth Muscle Actin α (*Acta2*). n= 3-5 WT Sham, 6 WT TAC, 4 TCRα$^{-/-}$ Sham, 8 TCRα$^{-/-}$ TAC. Mean ± SEM from a single qRT-PCR run containing samples collected in independent experimental replicates is represented. Statistics Mann-Whitney test.

Another feature of pathological cardiac remodeling is ventricular inflammation characterized by an increase in pro-inflammatory cytokine LV expression. In order to evaluate whether T cells contribute to the inflammatory environment in the LV after TAC, LV mRNA levels of three well known pro-inflammatory cytokines linked to HF, TNFα, IL-1β and IL-6 were determined. All three cytokines were found significantly upregulated in the LV of WT mice after 4 weeks from TAC (Figure 7.7). On the contrary, TCRα$^{-/-}$ mice did not present such an increase in any of these pro-inflammatory cytokines at the same time point post-TAC, suggesting that T cell infiltration into the LV favors the generation and maintenance of a pro-inflammatory environment in the myocardium.

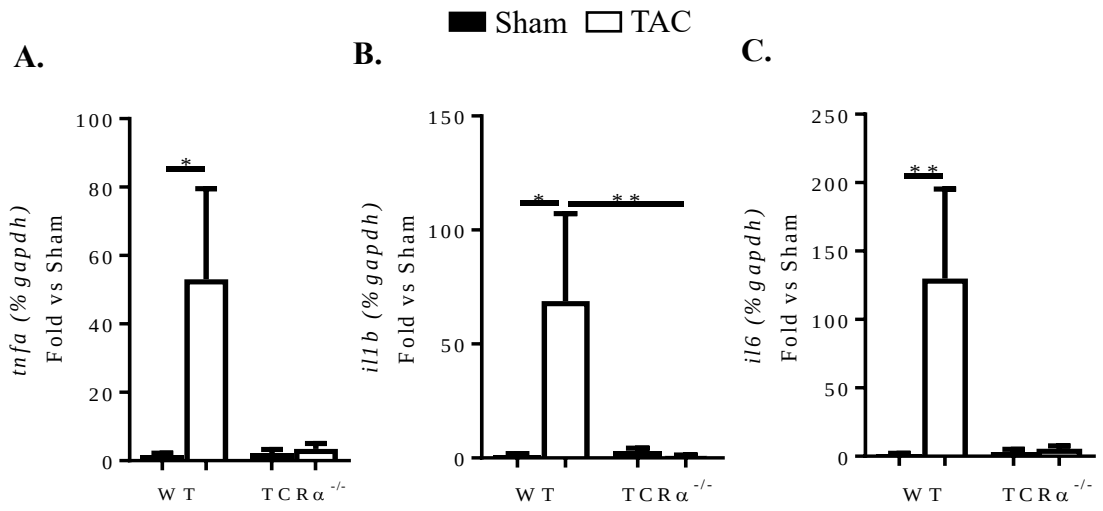

Figure 7.7. A-C. qRT-PCR pro-inflammatory cytokines **(A)** TNFα, **(B)** IL-1β and **(C)** IL-6. n= 5 WT Sham, 10 WT TAC, 3 TCRα$^{-/-}$ Sham, 7 TCRα$^{-/-}$ TAC. Mean ± SEM from a single qRT-PCR run containing samples collected in independent experimental replicates is represented. Statistics Mann-Whitney test.

All together, these data indicate that CD4+ T lymphocytes infiltrate the LV in response to TAC, the intramyocardial LV endothelium is activated, and mice lacking T cells do not develop maladaptive cardiac remodeling, including cardiac hypertrophy, cardiac fibrosis, cardiac inflammation and cardiac dysfunction in response to TAC. These data place T lymphocytes as major players in pathological cardiac remodeling in non-ischemic pressure overload induced HF.

7.2 Role of ICAM1 in T lymphocyte recruitment to the left ventricle and pathological cardiac remodeling in heart failure

Leukocyte recruitment from the blood stream to the inflamed tissues is a tightly regulated process that has been thoroughly characterized for the last decades. In addition, we and others have recently characterized the importance of T cell recruitment in to the LV for pathological cardiac remodeling in HF induced by pressure overload in mice (Chapter 7.1), and demonstrated the recruitment of T lymphocytes in the human LV in patients with chronic end stage HF (174, 175). However, the specific adhesion molecules involved in pro-inflammatory leukocyte LV recruitment in HF has not been studied in detail to date. Based on our initial characterization of the vascular EC activation in response to TAC (Figure 7.3A), we further investigated the role of ICAM1 in T cell activation, recruitment to the LV and maladaptive cardiac remodeling in HF progression using ICAM1$^{-/-}$ mice.

7.2.1 ICAM1 becomes sequentially upregulated in the LV in response to TAC

In order to determine the kinetics of EC activation during HF progression, ICAM1 expression in the LV of WT mice was measured 48 hours, 2 and 4 weeks after inducing cardiac ventricular pressure overload by TAC. ICAM1 mRNA was significantly upregulated in the LV of TAC mice as compared to Sham mice as early as 48h after TAC, which progressively increased 2 and 4 weeks after TAC (Figure 7.8A). EC ICAM1 protein expression was increased specifically in large and small vessels' EC following similar kinetics as the total LV mRNA upregulation, during the progression of systolic dysfunction and T lymphocyte recruitment (174). Platelet endothelial cell adhesion molecule- 1 (PECAM1) was used to stain the myocardial ECs parallel with ICAM1 in consecutive sections, and was, as expected, constitutively expressed and not induced in response to

TAC (Figure 7.8B). Taken together, these data demonstrate that the expression of endothelial ICAM1 is increased during the course of TAC as HF progresses and raises the question of whether ICAM1 mediates T cell recruitment to the LV as HF progresses and contributes to local cardiac inflammation, remodeling and systolic dysfunction in response to LV pressure overload.

A.

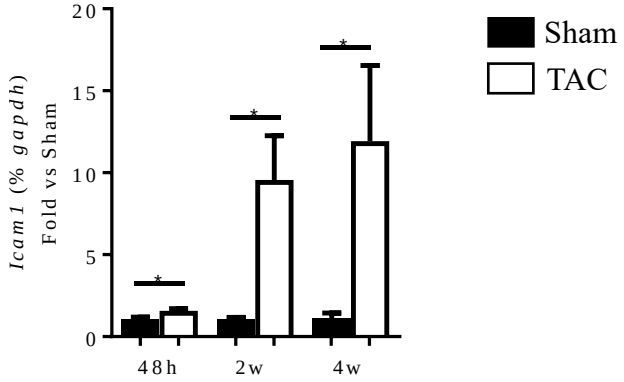

B.

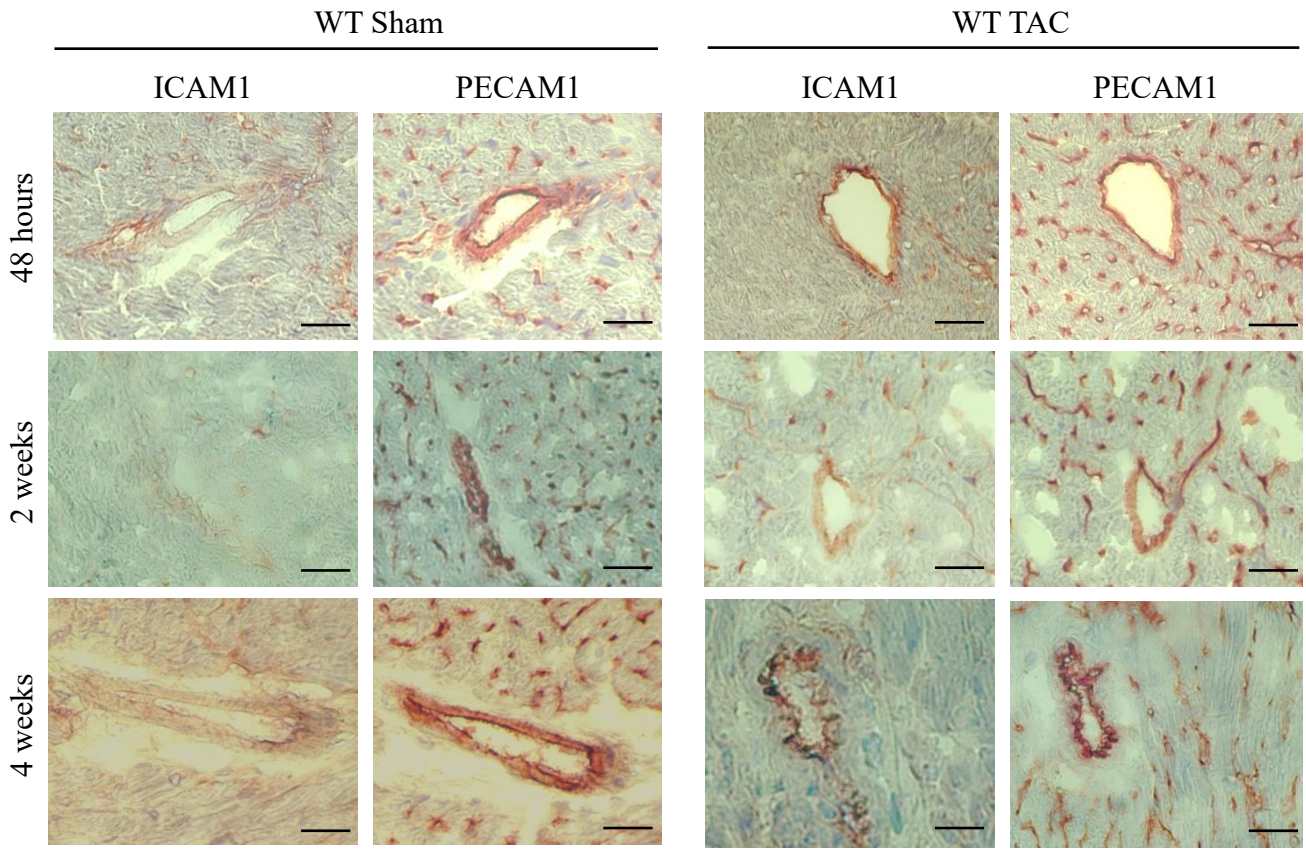

Figure 7.8. Upregulation of ICAM1 in the mRNA and protein level in the LV, specifically in the vascular endothelium, in response to TAC. A. ICAM1 mRNA expression in the WT mice LV determined by qRT-PCR represented as fold change TAC vs Sham control 48h, 2 and 4 weeks after surgery. Mean ± SEM from a single qRT-PCR run containing samples collected in independent experimental replicates is represented. Statistics Mann-Whitney test. **B.** Representative immunohistochemistry staining for ICAM1 and PECAM1 (used as positive control for endothelial cell staining in the same sections) in Sham and TAC mice 48 hours, 2 and 4 weeks after surgery. Scale bar= 50μm. n= 4 Sham, 6-9 TAC.

7.2.2 ICAM1 mediates leukocyte infiltration into the LV in response to TAC

ICAM1 has thoroughly been described as an endothelial CAM that mediates leukocyte recruitment into tissues. The observed upregulation of ICAM1 in the intramyocardial vessels in response to TAC (Figure 7.8), and previous findings indicating that T lymphocytes infiltrate the LV and contribute to HF pathogenesis in response to TAC (Chapter 7.1) (174, 175) led us to next investigate whether ICAM1 mediates T lymphocyte recruitment to the LV in response to TAC, using WT and $ICAM1^{-/-}$ mice. In contrast to WT mice, where CD45.2+ leukocyte infiltration to the LV was enhanced in response to TAC, pressure overload did not induce a significant increase in LV leukocyte infiltration in $ICAM1^{-/-}$ mice (Figure 7.9A) as measured by flow cytometry. These CD45.2+ leukocytes included CD3+ T lymphocytes and specifically CD4+ T helper cells (Figure 7.9B-C), which regulate cardiac dysfunction in response to TAC (Chapter 7.1) (174, 175). $Ly6C^{high}$ pro-inflammatory monocytes were also found infiltrated in the LV of WT mice but not in $ICAM1^{-/-}$ mice after 4 weeks of TAC (Figure 7.9D-E).

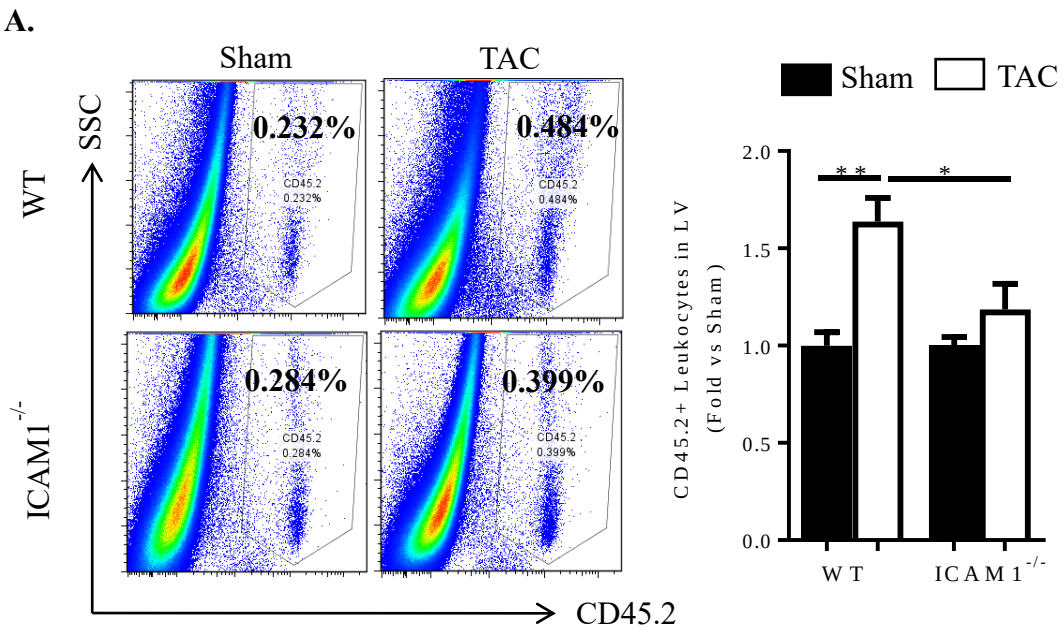
A.
Sham
TAC
WT
ICAM1 -/-
SSC
CD45.2
0.232%
0.484%
0.284%
0.399%
Sham
TAC
CD45.2+ Leukocytes in LV
(Fold vs Sham)
2.0
1.5
1.0
0.5
0.0
* *
*
WT
ICAM1 -/-

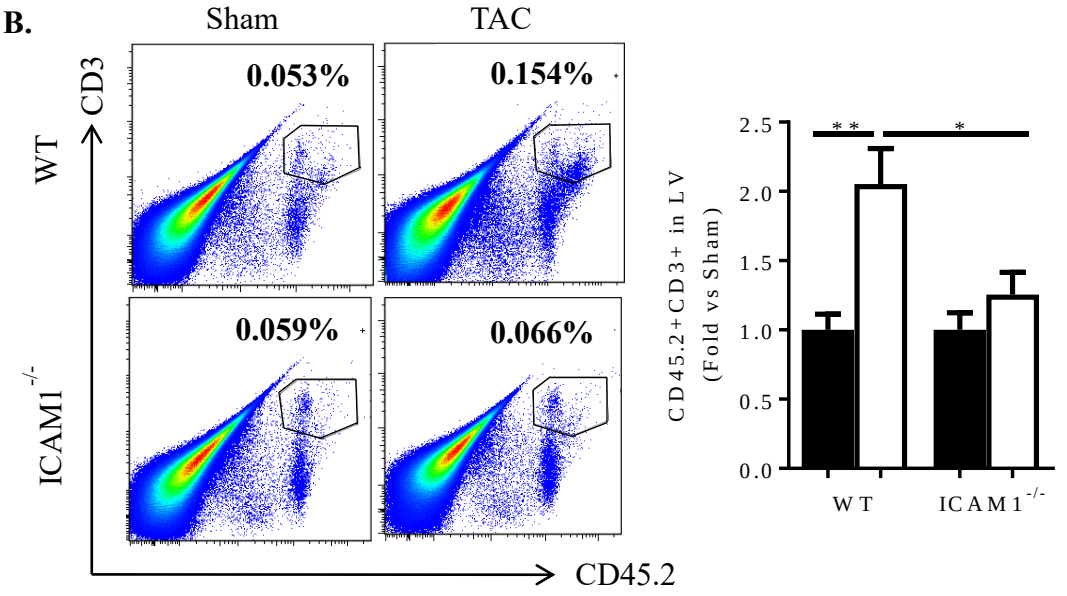
B.
Sham
TAC
WT
ICAM1 -/-
CD3
CD45.2
0.053%
0.154%
0.059%
0.066%
CD45.2+CD3+ in LV
(Fold vs Sham)
2.5
2.0
1.5
1.0
0.5
0.0
* *
*
WT
ICAM1 -/-

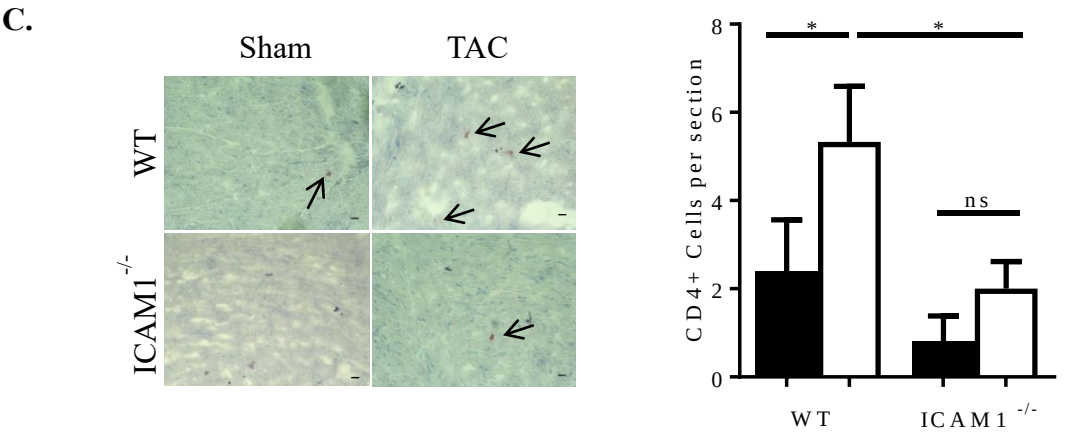
C.
Sham
TAC
WT
ICAM1 -/-
CD4+ Cells per section
8
6
4
2
0
*
*
ns
WT
ICAM1 -/-

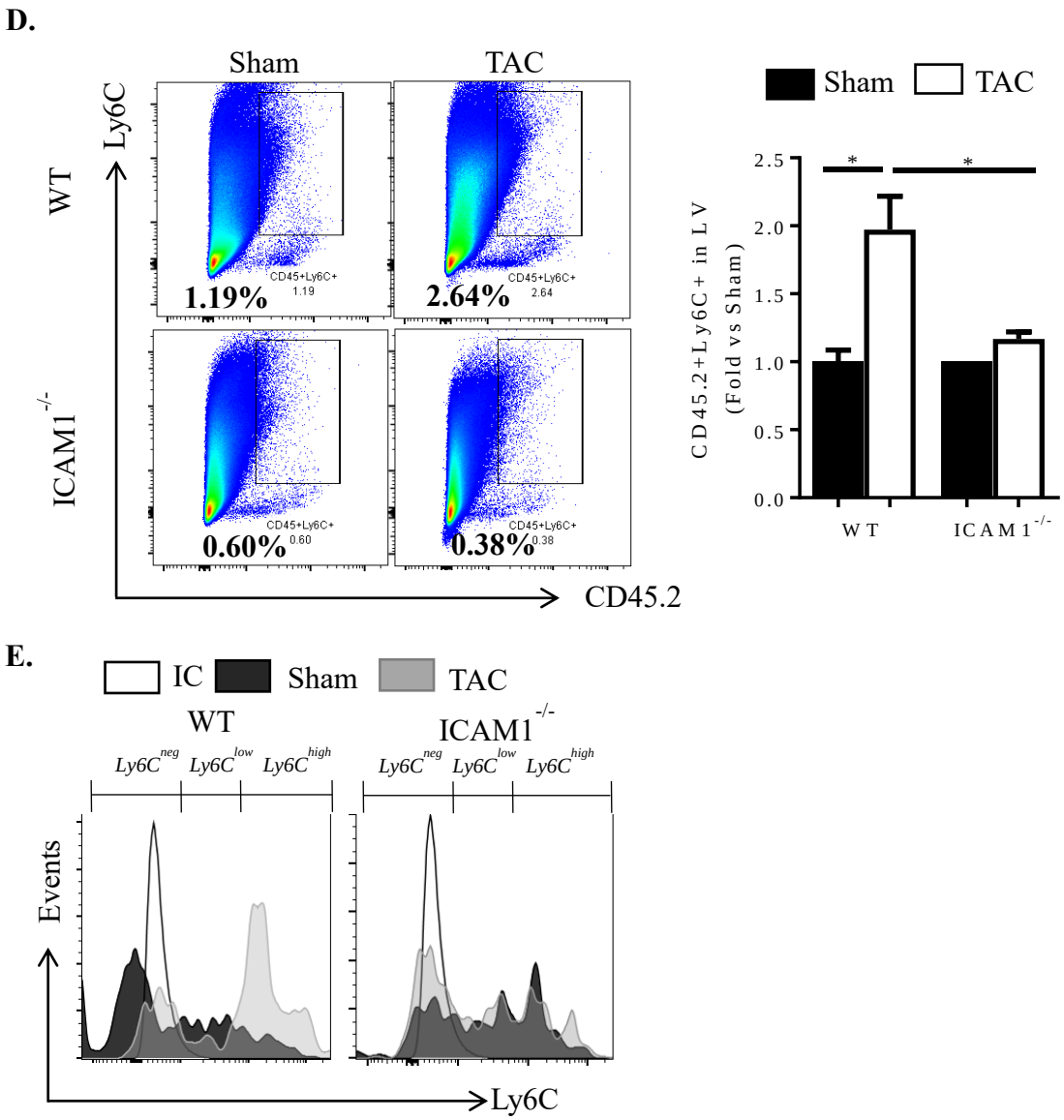

Figure 7.9. ICAM1 mediates CD45.2+, CD3+, CD4+ and Ly6C+ leukocyte infiltration into the LV in response to TAC. A-B. Representative flow cytometry plots of **(A)** LV CD45.2+ leukocytes and **(B)** CD3+ T lymphocyte infiltration in response to 4 week TAC or Sham controls, in WT and ICAM1$^{-/-}$ mice. Bar graph on the right represent fold change quantification of the indicated leukocytes normalized to Sham controls. **(C)** Representative 40x staining pictures CD4+ T helper lymphocytes infiltrated into the LV in Sham and TAC operated WT and ICAM1$^{-/-}$ mice. Quantification of CD4+ cells per 5µm LV cross-sections is represented. Scale bar= 10µm. **D.** Representative flow cytometry plots of Ly6C+ monocyte infiltration in response to 4 week TAC or

Sham controls, in WT and ICAM1$^{-/-}$ mice. Bar graph on the right represent fold change quantification of the Ly6C+ monocytes infiltrated normalized to Sham controls. **E.** Histogram for Ly6C+ low and high populations, gated on CD45.2+CD11b+ myeloid cells infiltrated into the LV of Sham and TAC operated WT and ICAM1$^{-/-}$ mice. Ly6C^{neg} cells represent non-monocyte myeloid cells, Ly6C^{low} represent patrolling monocytes and Ly6C^{high} represent pro-inflammatory monocytes. n= 8 WT Sham, 13 WT TAC, 7 ICAM1$^{-/-}$ Sham, 13 ICAM1$^{-/-}$ TAC. Mean ± SEM of independent experimental replicates is represented. Statistics unpaired t-test.

Altogether this data indicates that ICAM1 contributes to the infiltration of CD45.2+ leukocytes, including CD3+, CD4+ T cells and Ly6C^{high} pro-inflammatory monocytes into the LV in response to 4 week TAC.

7.2.3 T lymphocytes are equally activated in the heart draining lymph nodes and circulate in similar percentages in both WT and ICAM1$^{-/-}$ mice 4 weeks after TAC

Since ICAM1 is also expressed by the Antigen Presenting Cells (APC) and can play a role in the immune synapse during the presentation of some antigens (176), we next investigated whether the decreased LV lymphocyte infiltration observed in ICAM1$^{-/-}$ mice was a result of endothelial ICAM1 mediating their recruitment or additionally as a consequence of deficient T lymphocyte activation due to the lack of ICAM1 in APC in the immune synapse of ICAM1$^{-/-}$ mice in response to TAC. First, T lymphocyte activation was determined in the mediastinal lymph nodes, the heart draining lymph nodes where T lymphocytes are activated in response to TAC (174, 175), by evaluating the levels of CD62L^{low}CD44^{high} activated lymphocytes through flow cytometry (Figure 7.10A). Both WT and ICAM1$^{-/-}$ mice had similar frequency of CD62L^{low}CD44^{high} activated T lymphocyte in the cardiac draining lymph nodes in response to 4 weeks TAC (Figure 7.10B). The frequency of

circulating CD4+ T lymphocytes in peripheral blood was also similar between WT and ICAM1$^{-/-}$ mice in response to TAC (Figure 7.10C). Thus, these observations indicate that ICAM1 does not regulate T lymphocyte activation in the cardiac draining lymph nodes in response to TAC. These data, together with the similar frequencies of circulating T lymphocytes observed in WT and ICAM1$^{-/-}$ mice, supports that the reduced T lymphocyte infiltration observed in the ICAM1$^{-/-}$ mice LV in response to TAC is likely due to reduced recruitment mediated by endothelial ICAM1, not to impaired T lymphocyte activation in the absence of ICAM1.

A.

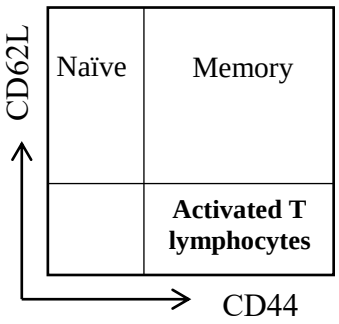

B.

Mediastinal lymph nodes

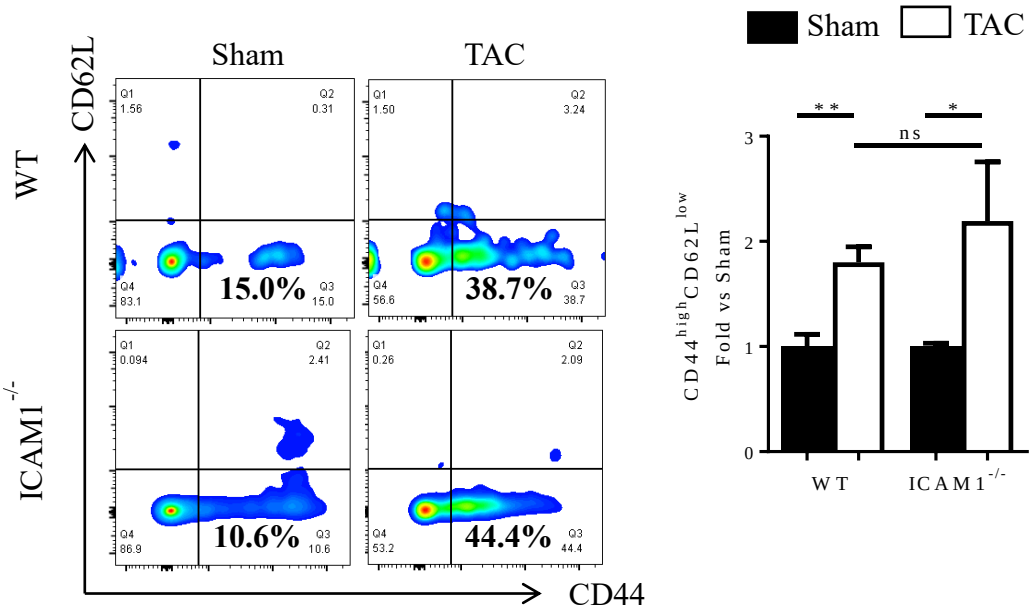

C.

Blood

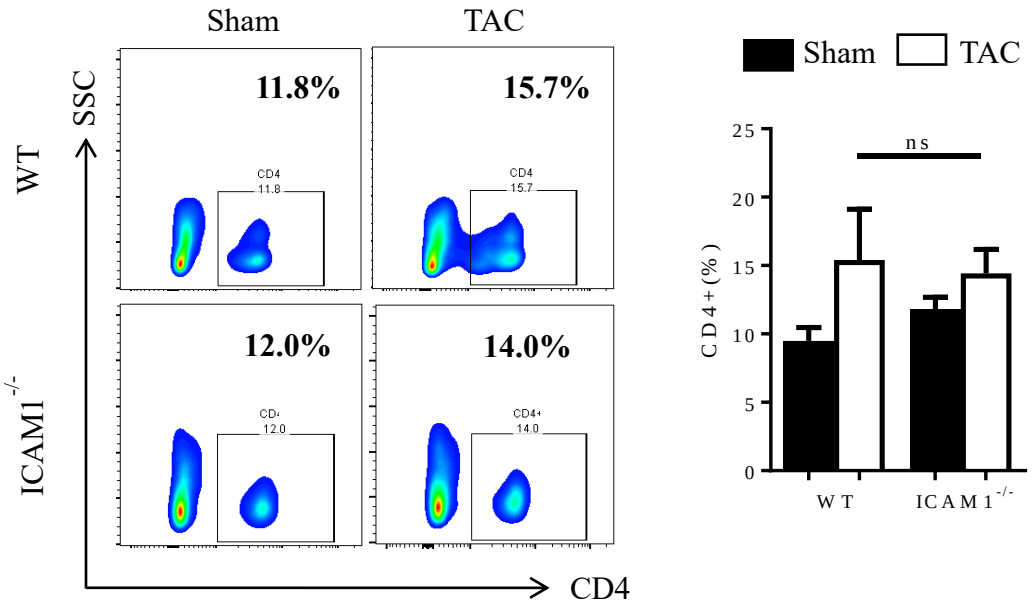

Figure 7.10. **T lymphocyte activation in the cardiac draining mediastinal lymph nodes and circulating CD4+ T cells in WT and ICAM1$^{-/-}$ mice in response to TAC. A.** Diagram indicating T lymphocyte subpopulations using activation markers. **B.** Representative flow cytometry plots showing naïve, memory and activated T lymphocytes in the mediastinal lymph nodes, pre-gated on lymphocytes, 4 weeks after TAC or Sham surgery. Quantification of activated T lymphocytes (CD44^{high}CD62L^{low}) is shown in the right bar graph with values normalized to Sham control. **C.** Representative flow cytometry plots showing circulating CD4+ T lymphocytes 4 weeks after TAC or Sham surgery. CD4+ T lymphocytes are represented as percentages in the graph bar on the right. n= 5 WT Sham, 8 WT TAC, 5 ICAM1$^{-/-}$ Sham, 7 ICAM1$^{-/-}$ TAC. Mean ± SEM of independent experimental replicates is represented. Statistics unpaired t-test.

7.2.4 ICAM1$^{-/-}$ mice have reduced LV cardiomyocyte hypertrophy as compared to WT mice in response to TAC

Next, we evaluated LV hypertrophy after 4 weeks of TAC, as a hallmark of pathological cardiac remodeling in response to TAC. LV mass increased to the same extent in WT and ICAM1$^{-/-}$ mice in response pressure overload (Figure 7.11A). Furthermore, the length and width dimensions of CM isolated from the LV of both WT and ICAM1$^{-/-}$ mice undergoing 4 weeks TAC was increased as compared to Sham, but these values were significantly higher in WT mice as compared to ICAM1$^{-/-}$ (Figure 7.11B). Interestingly, while WT TAC LVs exhibited an increase of natriuretic peptides ANP and BNP mRNA levels 4 weeks after pressure overload, ICAM1$^{-/-}$ mice TAC LVs did not show such upregulation (Figure 7.11C-D). Moreover, other hallmark of pathologic remodeling such as increased ratio of myosin heavy chain (MHC) β/ MHCα isoform expression levels (177), was found elevated in WT TAC LVs, but it was not significantly increased in ICAM1$^{-/-}$ mice (Figure 7.11E). Altogether, ICAM1$^{-/-}$ mice develop significantly less CM hypertrophy and exhibited decreased fetal gene re-expression and pathological hypertrophy in response to TAC.

A.

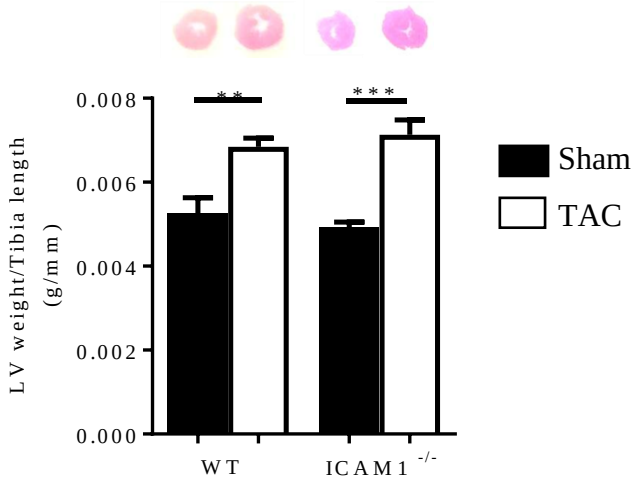

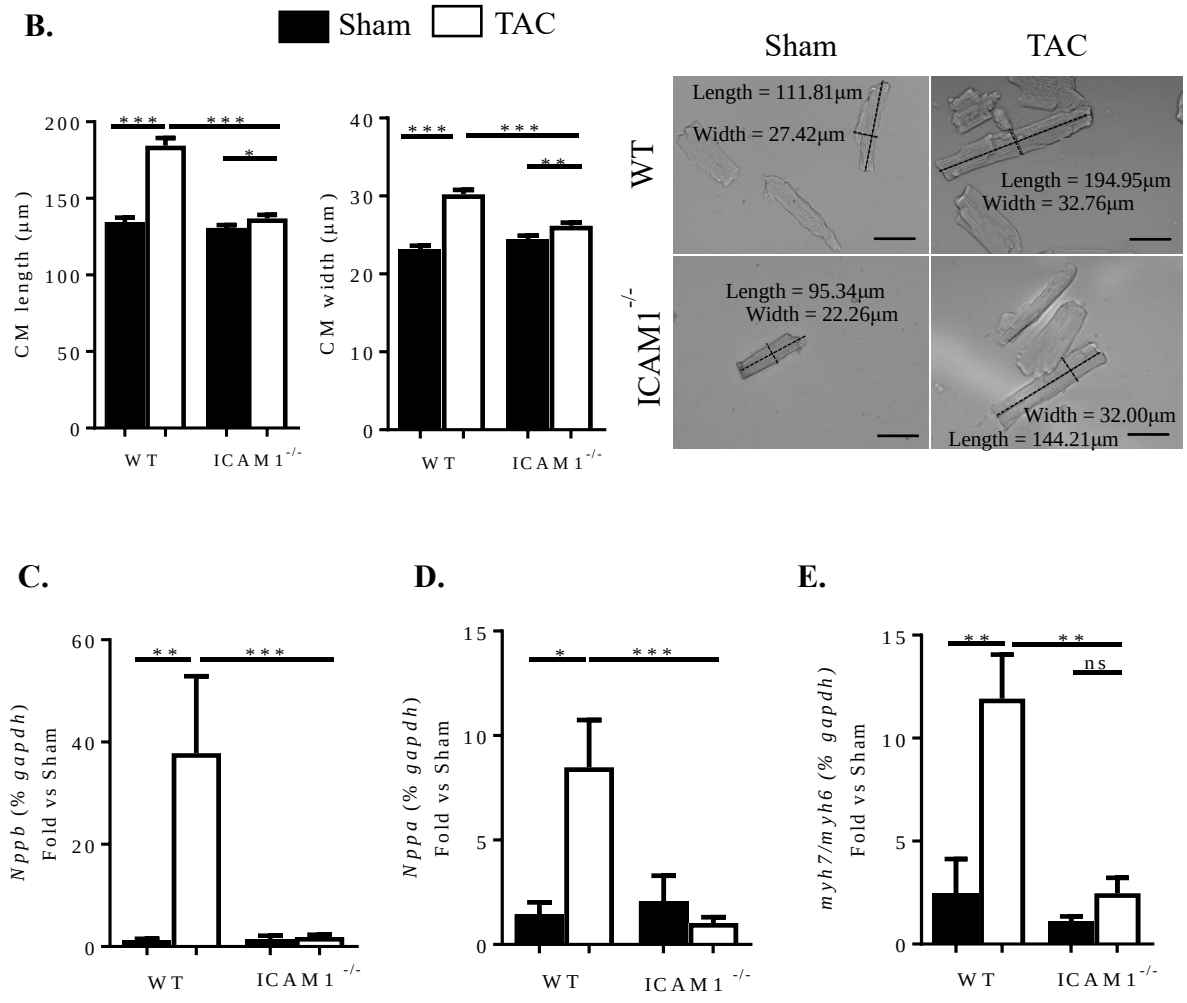

Figure 7.11. LV mass, CM dimensions, and mRNA expression of natriuretic peptides and myosin heavy chain isoforms in response to TAC in WT and ICAM1$^{-/-}$ mice. A. LV weight of WT and ICAM1$^{-/-}$ 4 weeks after TAC, normalized to tibia length. **B.** Length and width dimensions of CM isolated from WT and ICAM1$^{-/-}$ mice 4 weeks after TAC or Sham surgery. n= 100-200 cells per group, from two independent cardiac myocyte isolations. Representative pictures are shown (magnification 20x). Scale bar represents 50µm. Mean ± SEM of independent experimental replicates is represented. Statistics unpaired t-test. **C- E.** qRT-PCR of the hypertrophy markers **(C)** BNP and **(D)** ANP, and the **(E)** ratio of MHCβ and MHCα mRNA expression normalized to Sham in the LV in response to 4 weeks TAC or Sham surgery. n= 4 WT Sham, 9 WT TAC, 4 ICAM1$^{-/-}$ Sham, 7 ICAM1$^{-/-}$ TAC. Mean ± SEM from a single qRT-PCR run containing samples collected in independent experimental replicates is represented. Statistics Mann-Whitney test.

7.2.5 ICAM1$^{-/-}$ mice do not develop LV fibrosis in response to TAC

Cardiac fibrosis, another hallmark of maladaptive cardiac remodeling along with hypertrophy, likely promotes ventricular wall stiffness, and thus cardiac dysfunction and HF in response to pressure overload induced by TAC. Based on the findings that ICAM1$^{-/-}$ mice had decreased T lymphocyte infiltration in the LV in response to TAC (Figure 7.9), and given the role of T lymphocytes in cardiac fibrosis in this model (Figure 7.6) (174), we hypothesized that ICAM1$^{-/-}$ mice would not develop cardiac fibrosis in response to TAC. Pressure overload induced an expected increase in both LV interstitial (Figure 7.12A) and perivascular (Figure 7.12B) fibrosis in WT mice. On the contrary, LV fibrosis, including interstitial and perivascular, was completely absent in ICAM1$^{-/-}$ mice in response to TAC (Figure 7.12A-B).

A.

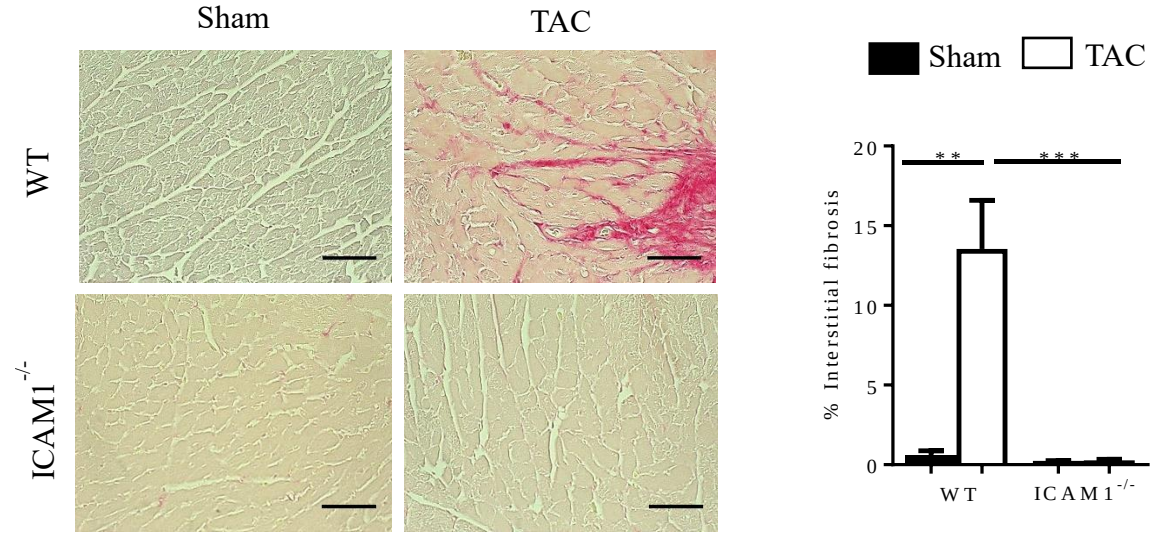

B.

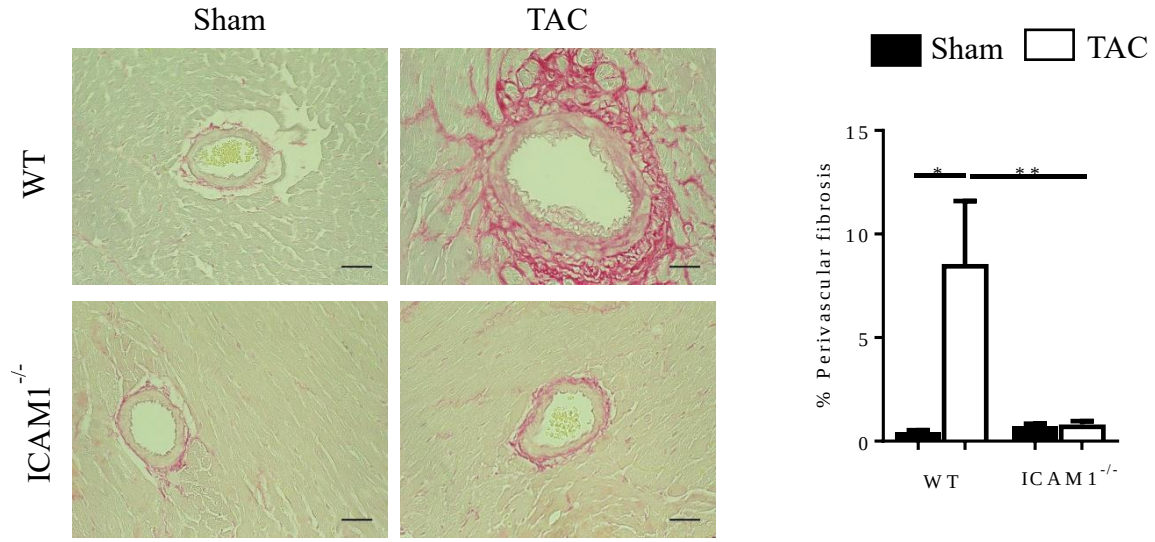

Figure 7.12. **Absence of fibrosis in ICAM1$^{-/-}$ mice in response to TAC. A.** Representative photomicrographs (40x magnification) and quantification (bar graph on the right) of myocardial interstitial fibrosis evaluated by Picrosirius red staining of LV sections from 4 week Sham and TAC mice. **B.** Representative 20x pictograms shown on the left and percent perivascular fibrosis quantification on the right. Scale bar= 50μm. n= 3 WT Sham, 3 WT TAC, 5 ICAM1$^{-/-}$ Sham, 8 ICAM1$^{-/-}$ TAC. Mean ± SEM of independent experimental replicates is represented. Statistics unpared t-test.

Markers of fibrosis such as TGFβ, collagen type I and αSMA were also elevated in the mRNA level in WT mice in response to 4 week TAC, but not in ICAM1$^{-/-}$ mice (Figure 7.13A-C). To investigate the specific cellular mechanism by which ICAM1 deletion prevents LV fibrosis in response to TAC, we next determined whether ICAM1 expressed in bone marrow derived monocytes or cardiac fibroblasts could contribute to the observed pro-fibrotic response in WT mice by measuring M2 macrophage and myofibroblast phenotypes from the ICAM1$^{-/-}$ mice. Differentiation of bone marrow monocytes from ICAM1$^{-/-}$ mice towards the M2 pro-fibrotic macrophage phenotype expressing Arginase 1, or towards the

M1 pro-inflammatory macrophage phenotype expressing inducible nitric oxide synthase (iNOS) was similar to WT monocytes (Figure 7.13D-E). Moreover, WT and ICAM1$^{-/-}$ adult cardiac fibroblasts differentiated similarly towards pro-fibrotic myofibroblasts *in vitro* in response to TGFβ (Figure 7.13F). Taken together, these data indicate that ICAM1 expression in bone marrow derived monocytes or in cardiac fibroblast does not regulate their transition towards a pro-fibrotic phenotype *in vitro*, and support the concept that ICAM1 contributes to LV fibrosis by mediating LV T lymphocyte recruitment in response to pressure overload *in vivo*.

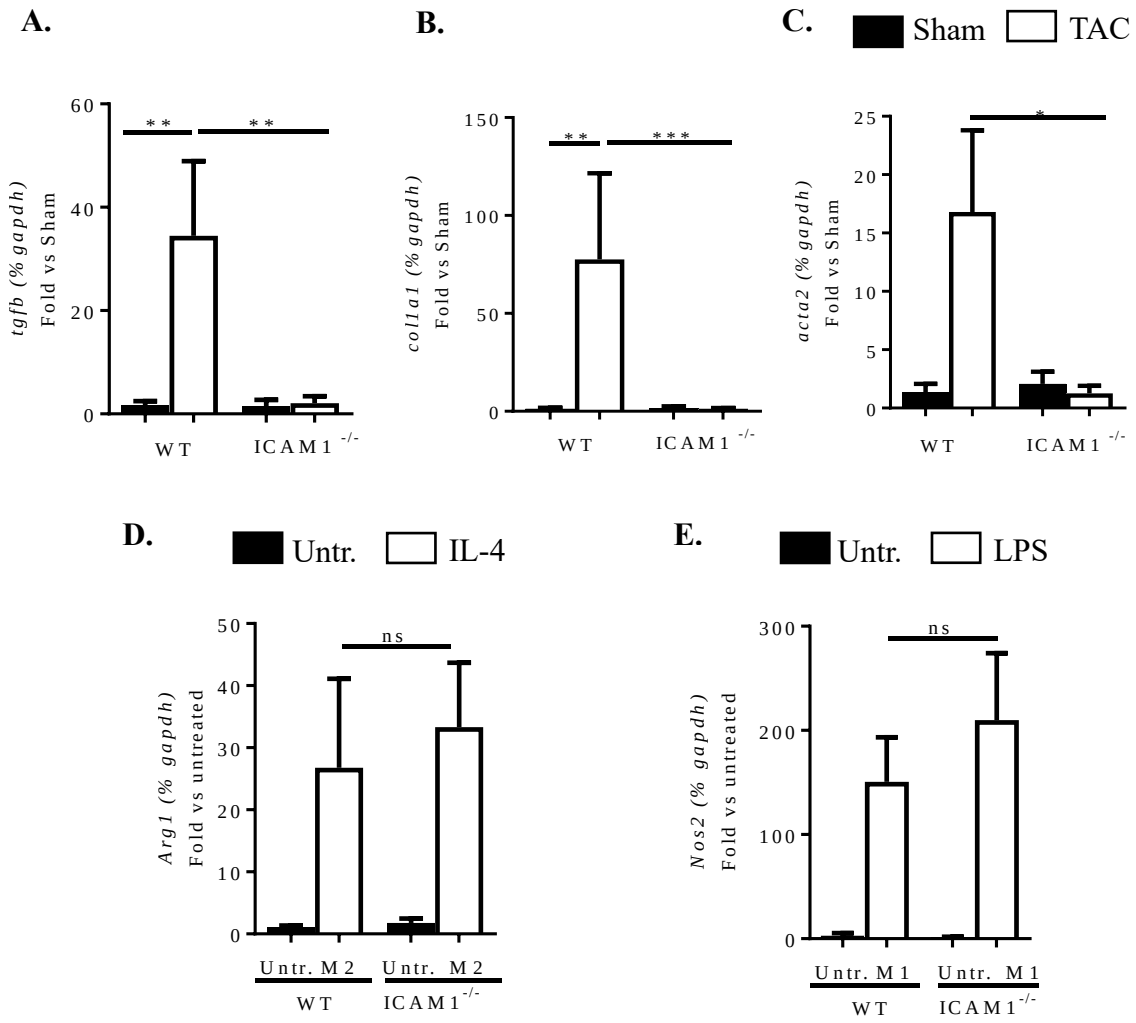

F.

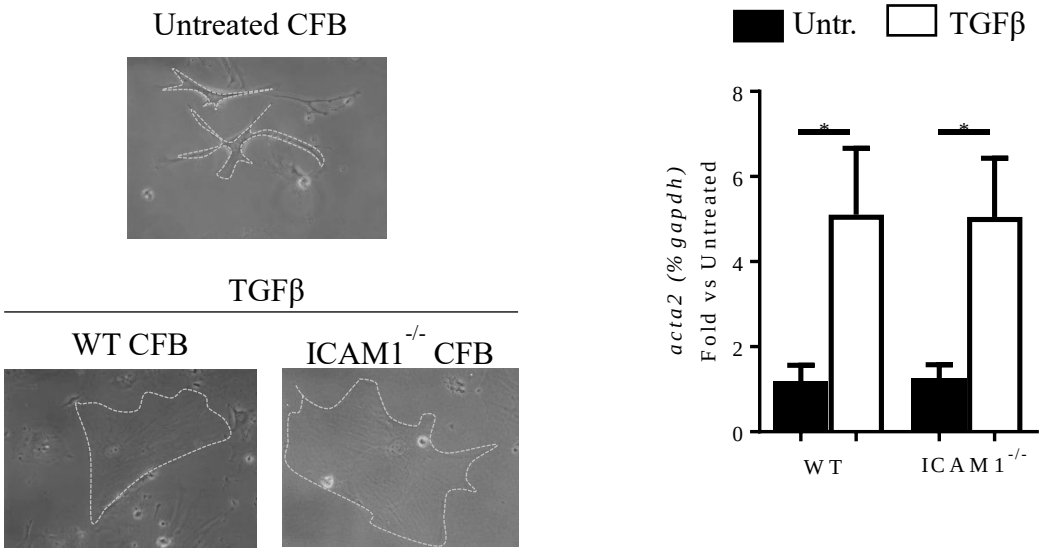

Figure 7.13. Absence of fibrosis mRNA marker upregulation in ICAM1$^{-/-}$ mice in response to TAC, despite equal capacity for M2 pro-fibrotic macrophage and myofibroblast differentiation *in vitro*. A- C. qRT-PCR in the LV for the fibrosis markers **(A)** TGFβ, **(B)** collagen-I and **(C)** SMAα. mRNA expression normalized to Sham. n= 4 WT Sham, 8 WT TAC, 3 ICAM1$^{-/-}$ Sham, 8 ICAM1$^{-/-}$ TAC. **D-E.** WT and ICAM1$^{-/-}$ bone marrow derived monocytes polarized to M2 and M1 macrophages, in the presence of 20ng/mL IL-4 or 1μg/mL LPS respectively, for three days. Polarization was determined by mRNA expression of **(D)** ArgI for M2 and **(E)** iNOS for M1 macrophages. n= 3 untreated, 3-4 IL-4 or LPS treated. **F**. WT and ICAM1$^{-/-}$ cardiac fibroblast polarized to myofibroblast in the presence of 100ng/mL TGFβ for 16h. Transition determined by mRNA expression of SMAα, 20x representative pictures of each condition are shown on the left. n= 4-6 untreated, 6-7 TGFβ treated. Mean ± SEM from a single qRT-PCR run containing samples collected in independent experimental replicates is represented. Statistics Mann-Whitney test.

7.2.6 ICAM1$^{-/-}$ mice do not develop cardiac dysfunction and heart failure in response to TAC

We next sought to determine the effect of ICAM1 deletion in cardiac function in the TAC model of HF, using invasive hemodynamics and non-invasive echocardiography studies.

LV end diastolic pressure (EDP), which is found elevated in HF, increased three-fold in WT mice in after TAC. Despite equal increases in LV pressure overload, EDP was significantly reduced in ICAM1$^{-/-}$ mice as compared to WT in response to TAC (Figure 7.14A-B). Cardiac systolic and diastolic function determined by the dp/dt_{max} and dp/dt_{min} indexes obtained from the hemodynamics studies, remained completely preserved in ICAM1$^{-/-}$ mice after TAC (Figure 7.14C-D). Finally, while ICAM1$^{-/-}$ mice showed a significant reduction in fractional shortening (FS) determined by echocardiography in response to 4 weeks TAC (27.15±4.89 TAC vs. 35.32±4.02 Sham) due to an increase in End Systolic Diameter (ESD) (Table 7.1), this reduction was not as severe as in WT mice after TAC (19.96±2.864 TAC vs. 44.37±3.405 Sham) (Figure 7.14E). Thus, these studies demonstrate that ICAM1 contributes to cardiac dysfunction in response to pressure overload induced by TAC.

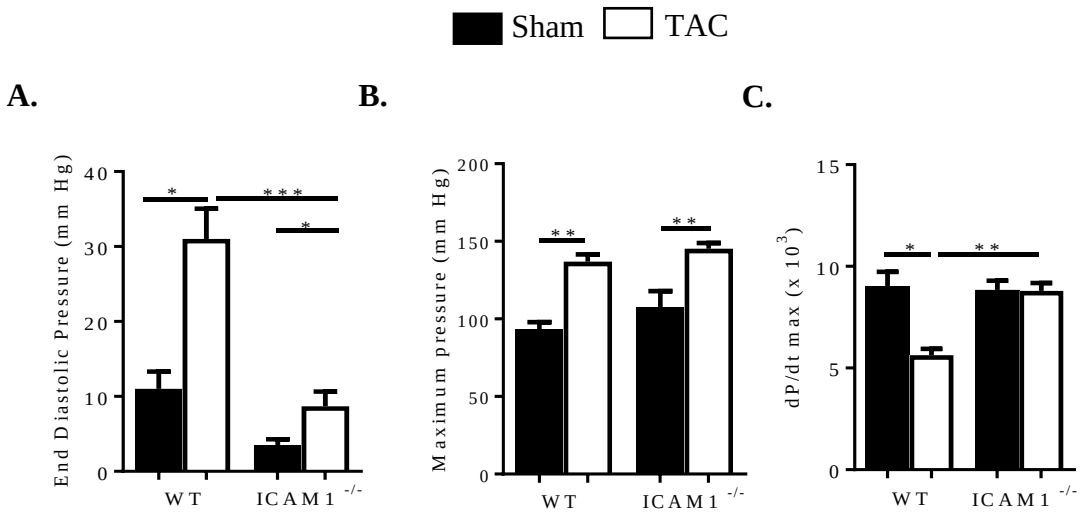

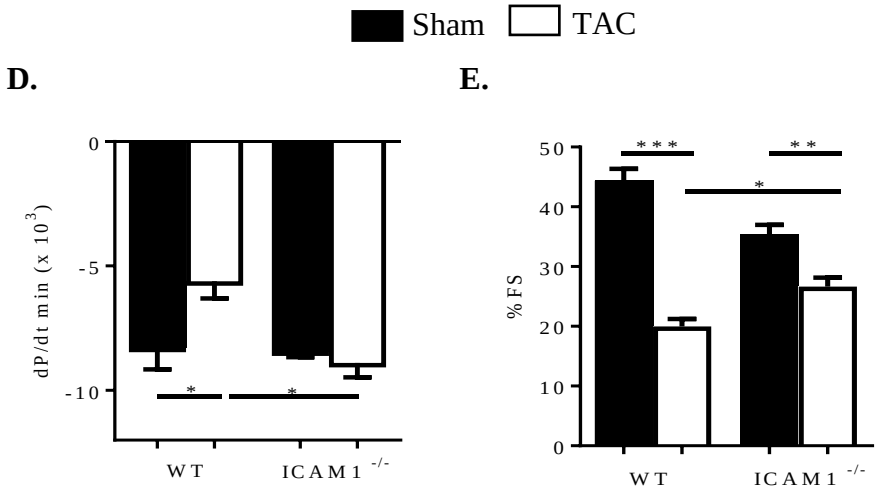

Figure 7.14. Improved cardiac function in response to TAC induced HF in ICAM1$^{-/-}$ mice. A-C. Invasive hemodynamic measurements in WT and ICAM1$^{-/-}$ mice measured 4 weeks after TAC and Sham surgery, **(A)** end diastolic pressure, **(B)** maximum pressure **(C)** contractile function (dP/dt_{max}) and **(D)** relaxation function **(dP/dt_{min}). E.** Fractional shortening (%FS) 4 weeks after Sham or TAC surgery in WT and ICAM1$^{-/-}$ mice. n= 3 WT Sham, 3-5 WT TAC, 6 ICAM1$^{-/-}$ Sham, 10 ICAM1$^{-/-}$ TAC. Mean ± SEM of independent experimental replicates is represented. Statistics, unpaired t-test.

	WT		**ICAM1$^{-/-}$**	
	Sham (n= 3)	TAC (n= 5)	Sham (n=6)	TAC (n=10)
ESD (mm)	1.880 ± 0.078	*3.191 ± 0.247***	2.464±0.14	*3.044±0.123***
EDD (mm)	3.375 ± 0.043	3.983 ± 0.257	3.802±0.148	4.137±0.088

Table 7.1. Cardiac anatomic dimensions determined by non-invasive echocardiography of WT and ICAM1$^{-/-}$ mice after 4 weeks from TAC. Mean±SEM of independent experimental replicates is represented. Statistics unpaired t-test. **p<0.01 TAC vs Sham within the same genotype.

7.2.7 ICAM1 upregulation in the pressure overloaded LV is independent of endothelial cell mineralocorticoid receptor signaling and associated with early upregulation of cardiac IL-1β and IL-6

We next explored potential mechanisms that may be driving the upregulation of ICAM1 expression in EC in response to pressure overload induced by TAC. Mineralocorticoid receptor (MR) signaling is known to be activated in HF and prior studies demonstrate that endothelial MR (EC-MR) activation upregulates the expression of ICAM1 *in vitro* in human coronary EC (96) and in the heart *in vivo* in response to constriction of the ascending aorta (178). Based on this data we hypothesized that EC-MR signaling drives cardiac endothelial ICAM1 upregulation in response to TAC. We used EC specific MR deficient mice that were previously generated by crossing VE-Cadherin Cre recombinase mice with mice that had LoxP sites flanking the MR. Thus, the MR gene of the progeny (EC-MR$^{-/-}$) had specific recombination exclusively in EC (168). EC-MR$^{-/-}$ mice are therefore optimal to evaluate whether ICAM1 is upregulated in the LV in response to TAC through aldosterone-MR signaling, and also allow us to explore the specific role of EC-MR in cardiac remodeling in TAC induced HF. Male EC-MR$^{-/-}$ and EC-MR$^{+/+}$ intact littermates were subjected to TAC. Both groups developed the same LV maximum pressure, supporting comparable degree of pressure overload in each group. Polymerase chain reaction, using DNA from EC-containing tissues four weeks post-TAC, confirmed selective recombination of the MR gene only in Cre positive mice (right ventricle-RV- and lung tissue Figure 7.15A, upper band), but not in leukocytes within inguinal and axillary lymph nodes of such mice subjected to TAC (Figure 7.15A). The intensity of the recombined band in EC-MR$^{-/-}$ was proportional to the expected presence of ECs in each organ with no recombination observed in DNA isolated from the lymph nodes of the same mice. Thus,

this model enables selective exploration of the specific role of EC-MR in cardiac remodeling and function in response to TAC in the presence of intact leukocyte MR.

After four weeks of TAC, EC ICAM1 was upregulated in EC-MR$^{-/-}$ to the same extent as in EC-MR$^{+/+}$ littermates (Figure 7.15B), and this correlated with a similar increase in CD4^{+} T lymphocyte recruitment independent of the presence of EC-MR (Figure 7.15C). Moreover the mRNA expression of the pro-inflammatory cytokines IL-6 and IL-1β, known to be endothelial cell activators leading to endothelial CAM upregulation (179, 180), were significantly increased to the same extent in the LV of both EC-MR$^{-/-}$ and EC-MR$^{+/+}$ mice (Figure 7.15D). Furthermore, the time course of IL-1β and IL-6 upregulation in the LV of WT mice (Figure 7.15E)correlated with the upregulation of ICAM1 over the course of TAC (Figure 7.8A), starting as early as 48h after TAC and remaining upregulated as pathological cardiac remodeling progressed. Taking together, our studies demonstrate that EC-MR does not play a role in endothelial LV ICAM1 upregulation in response to TAC, and suggest a mechanism by which IL-1β and IL-6 produced by resident LV cells as early as 48h after TAC induce endothelial ICAM1, which drives LV leukocyte infiltration, further cardiac inflammation and adverse cardiac remodeling in an EC-MR independent manner.

A.

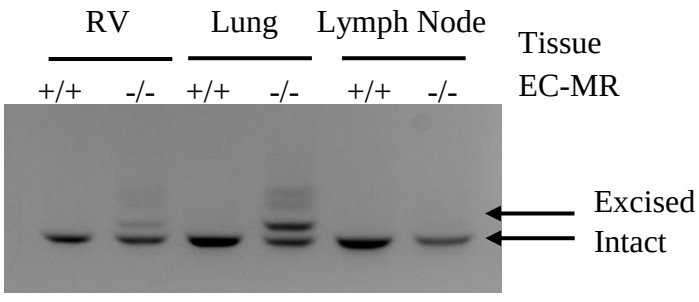

B.

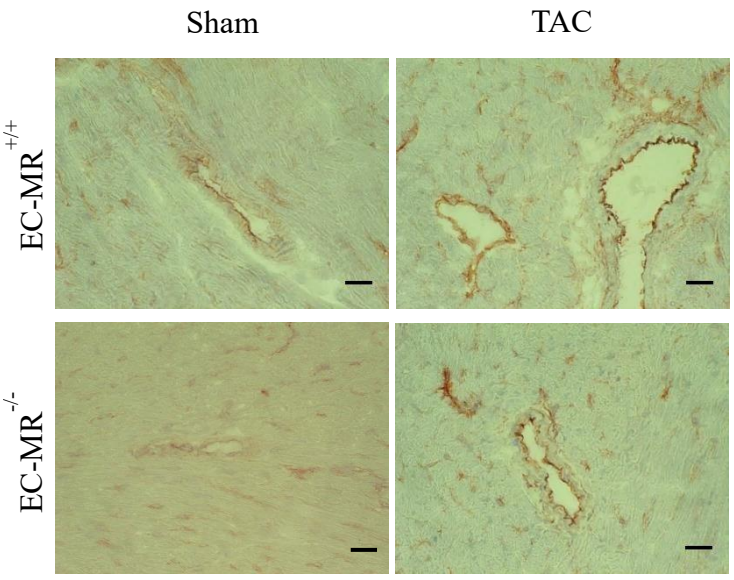
Sham
TAC
EC-MR+/+
EC-MR-/-

C.

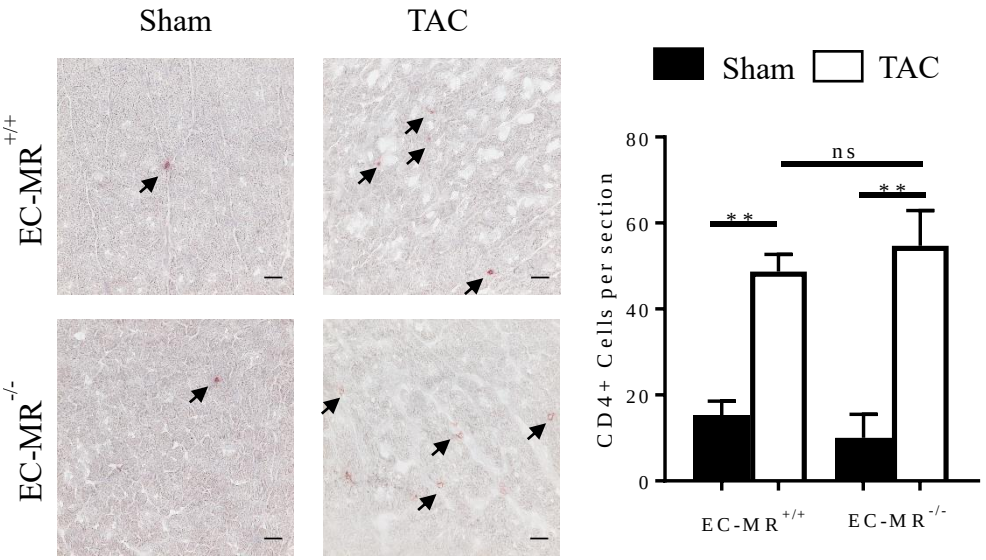
Sham
TAC
EC-MR+/+
EC-MR-/-
Sham
TAC
CD4+ Cells per section
ns
**
**
0
20
40
60
80
EC-MR+/+
EC-MR-/-

D.

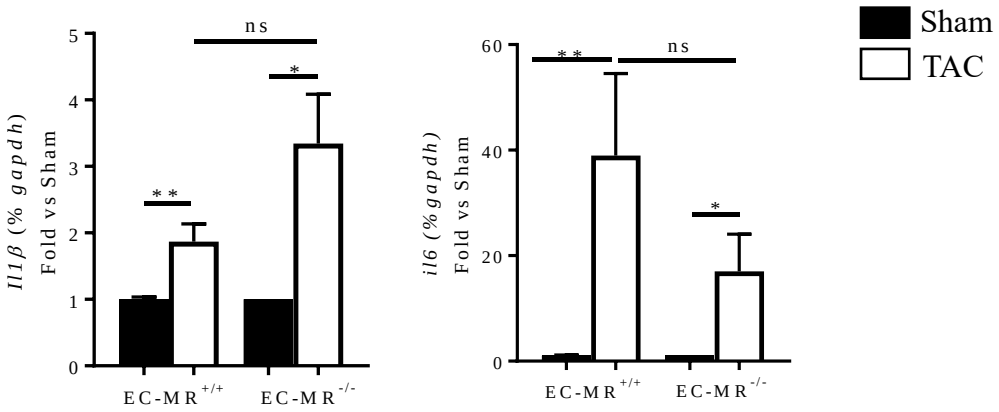
Il1β (% gapdh)
Fold vs Sham
ns
*
**
0
1
2
3
4
5
EC-MR+/+
EC-MR-/-
il6 (% gapdh)
Fold vs Sham
**
ns
*
0
20
40
60
EC-MR+/+
EC-MR-/-
Sham
TAC

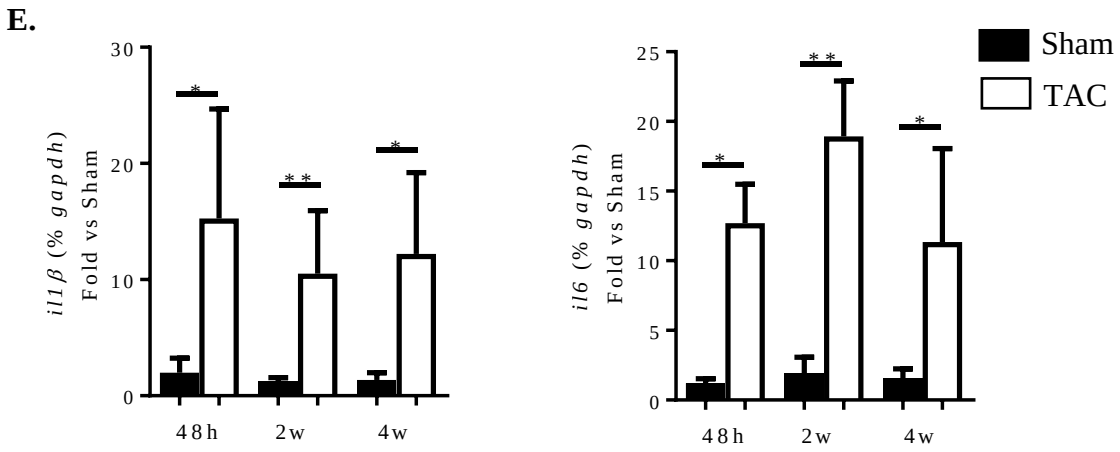

Figure 7.15. EC-MR signaling does not regulate ICAM1 expression, LV T cell recruitment and LV cytokine expression 4 weeks after TAC. A. MR recombination in VE-Cad-Cre+ EC-MR$^{-/-}$ mice specifically in endothelial cell (EC)-containing tissues (heart and lung) but not in leukocytes (lymph node cells) four weeks after TAC. RV= Right Ventricle, MR= Mineralocorticoid Receptor. **B-C.** Representative immunohistochemistry staining for **(B)** ICAM1 and **(C)** CD4+ in Sham and TAC operated EC-MR$^{+/+}$ and EC-MR$^{-/-}$ mice 4 weeks after surgery. On the right, quantification of CD4+ T cells per LV section after TAC. Scale bar= 50μm. Mean ± SEM of independent experimental replicates is represented. Statistics unpaired t-test. **D.** mRNA expression of the cytokines IL-1β and IL-6 on the LV of EC-MR$^{-/-}$ and EC-MR$^{+/+}$ littermates in response to 4 weeks TAC normalized to Sham. n= 5 Sham, 8 TAC EC-MR$^{+/+}$, 3 Sham, 8 TAC EC-MR$^{-/-}$. **E**. mRNA expression of the cytokines IL-1β and IL-6 on the LV of WT mice in response to 48h, 2 and 4 weeks TAC normalized to Sham. n= 3 WT Sham 48h, 4 WT TAC 48h, 6 WT Sham 2 weeks, 10 WT TAC 2w, 5 WT Sham 4 weeks, 7 WT TAC 4w. Mean ± SEM from a single qRT-PCR run containing samples collected in independent experimental replicates is represented. Statistics Mann-Whitney test.

7.3 Role of endothelial cell mineralocorticoid receptor (EC-MR) in cardiac inflammation, remodeling and dysfunction in heart failure

Left ventricular (LV) dysfunction and HF are strongly associated in humans with increased circulating levels of aldosterone and systemic inflammation (86, 87). Mineralocorticoid receptor (MR) antagonists are indeed an efficient therapeutic option for patients with congestive HF (90). However, the molecular mechanisms and cellular targets underlying the therapeutic benefits of MR antagonists through specific cell targets involved in the pathological cardiac modeling associated with pressure overload induced HF remains not fully understood (181). Our data indicate that EC-MR does not mediate ICAM1 upregulation in the intramyocardial EC and CD4+ T cell recruitment into the LV after TAC (Figure 7.15) (170); however, the cardiac phenotype of EC-MR$^{-/-}$ mice in resting conditions or in response to TAC remain unknown. Therefore, we next evaluated whether other pathological cardiac remodeling features associated with systolic and diastolic dysfunction and HF are regulated by EC-MR by characterizing the detailed cardiac remodeling phenotype of EC-MR$^{-/-}$ mice and their EC-MR$^{+/+}$ littermate controls in response to pressure overload induced by TAC (Figure 7.15A) (168).

7.3.1 Mice lacking MR in ECs have preserved systolic function in response to TAC

To begin exploring the cardiac effects of MR deletion in EC, transthoracic echocardiography was performed on 10-12 week old adult male EC-MR$^{-/-}$ and EC-MR$^{+/+}$ intact littermates. No differences in basal LV structure or function were observed between genotypes (Figure 7.16A-B and Table 7.2). Therefore, male EC-MR$^{-/-}$ and EC-MR$^{+/+}$ intact littermates were subjected to TAC in order to explore the specific role of EC-MR in the cardiac remodeling response to pressure overload. The effect of EC-MR deletion on LV

structure and function in response to pressure overload by performing TAC was first studied through echocardiography and invasive hemodynamic analysis. TAC induced equal increases in LV pressure overload in both EC-MR$^{+/+}$ and EC-MR$^{-/-}$ littermates as compared to their respective Sham EC-MR$^{+/+}$ and EC-MR$^{-/-}$ controls, determined by LV systolic pressure and arterial elastance (Ea) (Table 7.3). Complete LV hemodynamic data are presented in Table 7.3. Echocardiography revealed that, as expected, LV %FS and EF, indices of systolic function, declined in EC-MR$^{+/+}$ mice after TAC. By contrast, EC-MR$^{-/-}$ mice had preserved %FS and EF compared to EC-MR$^{+/+}$ exposed to same degree and duration of TAC, and similar to Sham EC-MR$^{-/-}$ controls (Figure 7.16C-E). However, indices of diastolic function, including dP/dtmin and tau (time constant of LV relaxation), did not differ between genotypes. Further, LV end diastolic pressure increased significantly in EC-MR$^{+/+}$ TAC mice compared with EC-MR$^{+/+}$ Sham controls, indicating LV decompensation which marks the clinical syndrome of HF. However, EC-MR$^{-/-}$ TAC mice developed LV end diastolic pressures comparable with the EC-MR$^{+/+}$ TAC mice, indicating that LV decompensation occurred in both genotypes. Thus, these findings demonstrate that deletion of EC-MR improves indices of systolic function but not diastolic function or LV compensation in response to pressure overload.

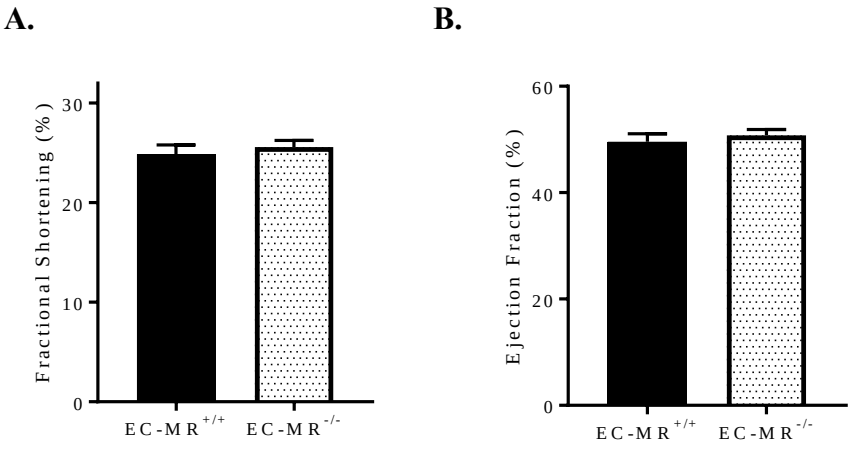

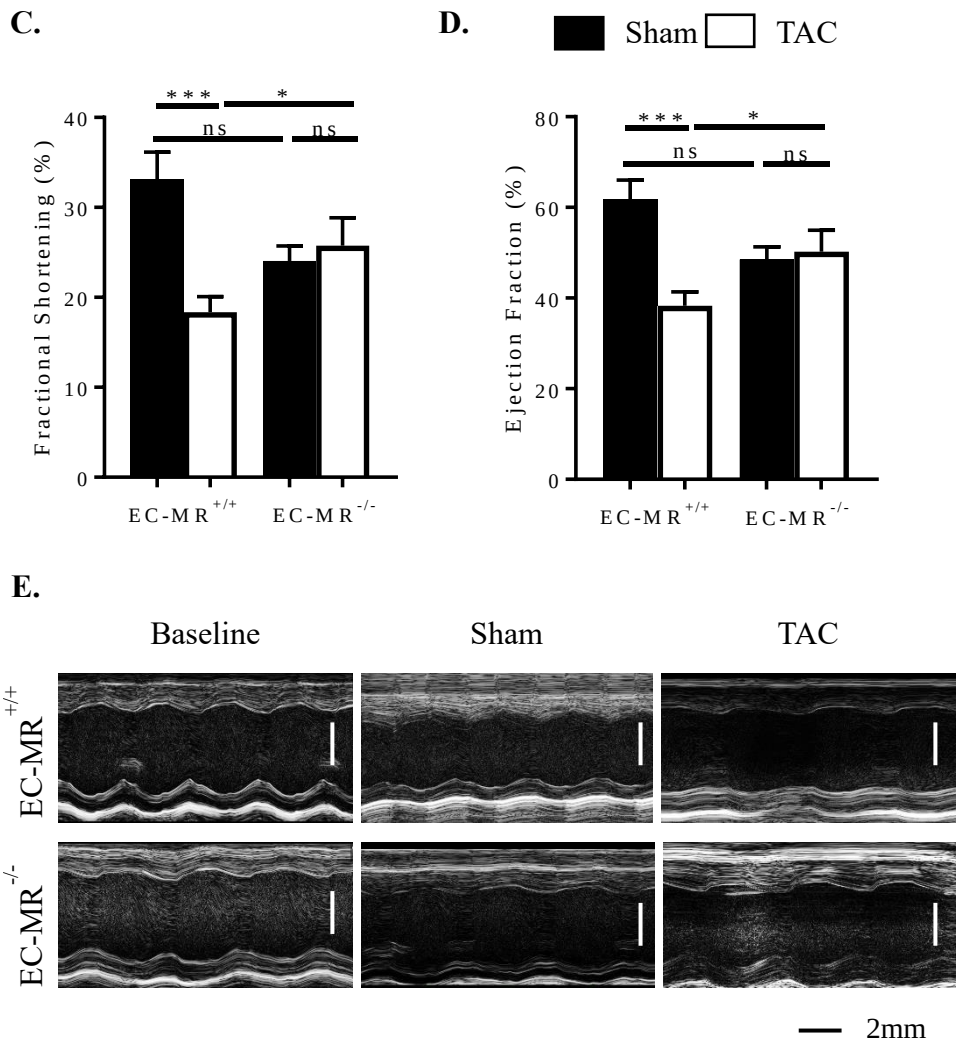

Figure 7.16. EC-MR contributes to LV systolic dysfunction in response to TAC. A-B. Baseline echocardiography measurements of the **(A)** fractional shortening (%FS) and **(B)** ejection fraction (EF) of EC-MR$^{+/+}$ and EC-MR$^{-/-}$ mice. **(C)** %FS and **(D)** EF of EC-MR$^{+/+}$ and EC-MR$^{-/-}$ mice measured by non-invasive echocardiography after TAC. % FS is calculated by [(LVEDD-LVESD)/ LVEDD] x 100. **(E)** Representative echocardiography images of baseline, Sham and 4 week operated TAC EC-MR$^{+/+}$ and EC-MR$^{-/-}$ mice. n: 6 baseline EC-MR$^{+/+}$ and 6 baseline EC-MR$^{-/-}$, 5 Sham and 8 TAC EC-MR$^{+/+}$, 3 Sham and 8 TAC EC-MR$^{-/-}$. Mean ± SEM of independent experimental replicates is represented. Statistics unpaired t-test.

	EC-MR$^{+/+}$	**EC-MR$^{-/-}$**
Anterior Wall Thickness (μm)	0.8647 ± 0.044	0.841 ± 0.045
Posterior Wall Thickness (μm)	0.7638 ± 0.022	0.8165 ± 0.065
End Diastolic Diameter (μm)	4.137 ± 0.163	4.195 ± 0.049
End Systolic Diameter (μm)	3.106 ± 0.118	3.087 ± 0.039
Fractional Shortening (%)	24.86 ± 0.944	25.57 ± 0.686
Ejection Fraction (%)	49.6 ± 1.469	50.77 ± 1.087
Heart Rate (bpm)	433.5 ± 19.07	423.3 ± 8.713

Table 7.2. Baseline cardiac function characterization of EC-MR$^{+/+}$ and EC-MR$^{-/-}$ through echocardiographic studies. Mean ± SEM from data collected in a single adquisition by a blinded investigator is indicated for each parameter. n: 6 baseline EC-MR$^{+/+}$ and 6 baseline EC-MR$^{-/-}$.

	EC-MR$^{+/+}$		**EC-MR$^{-/-}$**	
	Sham	TAC	Sham	TAC
Hemodynamics				
Systolic Pressure (mm Hg)	106.2 ± 2.676	*164.5* ± *4.435****	105.4 ± 3.925	*163* ± *8.4***
End Diastolic Pressure (mm Hg)	4.44 ± 0.74	*14.86* ± *2.834**	5.267 ± 1.317	13.13 ± 3.506
Arterial Elastance	8.776 ± 2.03	11.27 ± 1.041	8.22 ± 2.934	11.98 ±

(mm Hg/μL)				1.482
dP/dt_{max}	9119 ± 468.3	8235 ± 653.1	8861 ± 728.2	7818 ± 761.7
dP/dt_{min}	-9715 ± 793.2	-8985 ± 1043	-8940 ± 670.7	-8863 ± 655
End Diastolic Volume (μL)	35.78 ± 9.259	42.13 ± 5.101	35.8 ± 11.1	36.79 ± 4.56
End Systolic Volume (μL)	25.11 ± 5.786	31.91 ± 3.811	23.99 ± 5.615	30.1 ± 3.881
Cardiac Output (μL/min)	7544 ± 1890	7136 ± 558.5	7475 ± 2085	5810 ± 815.7
ESPVR (mm Hg/μL)	4.078 ± 0.892	4.888 ± 0.763	3.65 ± 0.496	6.135 ± 1.355
PRSW (mmHg/μL)	44.9 ± 11.73	70.02 ± 10.17	65.14 ± 9.932	81.09 ± 16.05
Tau ½ (msec)	4.54 ± 0.21	4.625 ± 0.30	4.367 ± 0.37	4.65 ± 0.237
Heart Rate (bpm)	490.4 ± 17.57	493.9 ± 10.34	481.7 ± 45.08	449.3 ± 21.27
Echocardiography				
End Diastolic Diameter (μm)	3.88 ± 0.14	3.92 ± 0.12	3.946 ± 0.10	4.05 ± 0.14

End Systolic Diameter (μm)	2.61 ± 0.19	3.21 ± 0.12*	2.99 ± 0.01	3.03 ± 0.21

Table 7.3. Cardiac function characterization through echocardiographic and hemodynamic studies. n= 5 EC-MR$^{+/+}$ Sham, 8 EC-MR$^{+/+}$ TAC, 3 EC-MR$^{-/-}$ Sham, 8 EC-MR$^{-/-}$ TAC. * vs Sham per genotype. Mean ± SEM of independent experimental replicates is represented. Statistics unpaired t-test.

7.3.2 EC-MR does not contribute to LV hypertrophy but regulates some aspects of fetal gene re-expression associated with maladaptive cardiac remodeling in response to TAC

Next, cardiac hypertrophy was evaluated after 4 weeks of pressure overload induced by TAC as an early structural marker of pathological cardiac remodeling. As expected, LV mass increased in EC-MR$^{+/+}$ mice in response to TAC compared to Sham surgery. Moreover, LV mass increased to the same extent in EC-MR$^{-/-}$ and EC-MR$^{+/+}$ mice in response to TAC (Figure 7.17A). LV anterior wall thickness was increased in both genotypes after TAC as compared to Sham controls, and no difference was observed between genotypes after TAC (Figure 7.17B). Analysis of the CM area from LV cross sections stained with H&E showed increased myocyte area after TAC compared to Sham that did not differ between EC-MR$^{-/-}$ and EC-MR$^{+/+}$ littermates (Figure 7.17C). Fetal gene expression was also determined, which represents a molecular signature correlating with pathologic, as opposed to adaptive, cardiac hypertrophy. In response to TAC, both EC-MR$^{+/+}$ and EC-MR$^{-/-}$ LVs showed an isoform switch from adult to fetal myosin heavy chain (MHC) isoform (MHCβ/α isoform ratio) in response to TAC as compared to their Sham controls (Figure 7.17D). However, while EC-MR$^{+/+}$ exhibited an expected increase in mRNA level of the natriuretic peptides ANP (Figure 7.17E) and BNP (Figure 7.17F) in

TAC vs Sham, there was no such increase observed in these genes in EC-MR$^{-/-}$ after TAC, and the expression was significantly decreased as compared to TAC EC-MR$^{+/+}$.

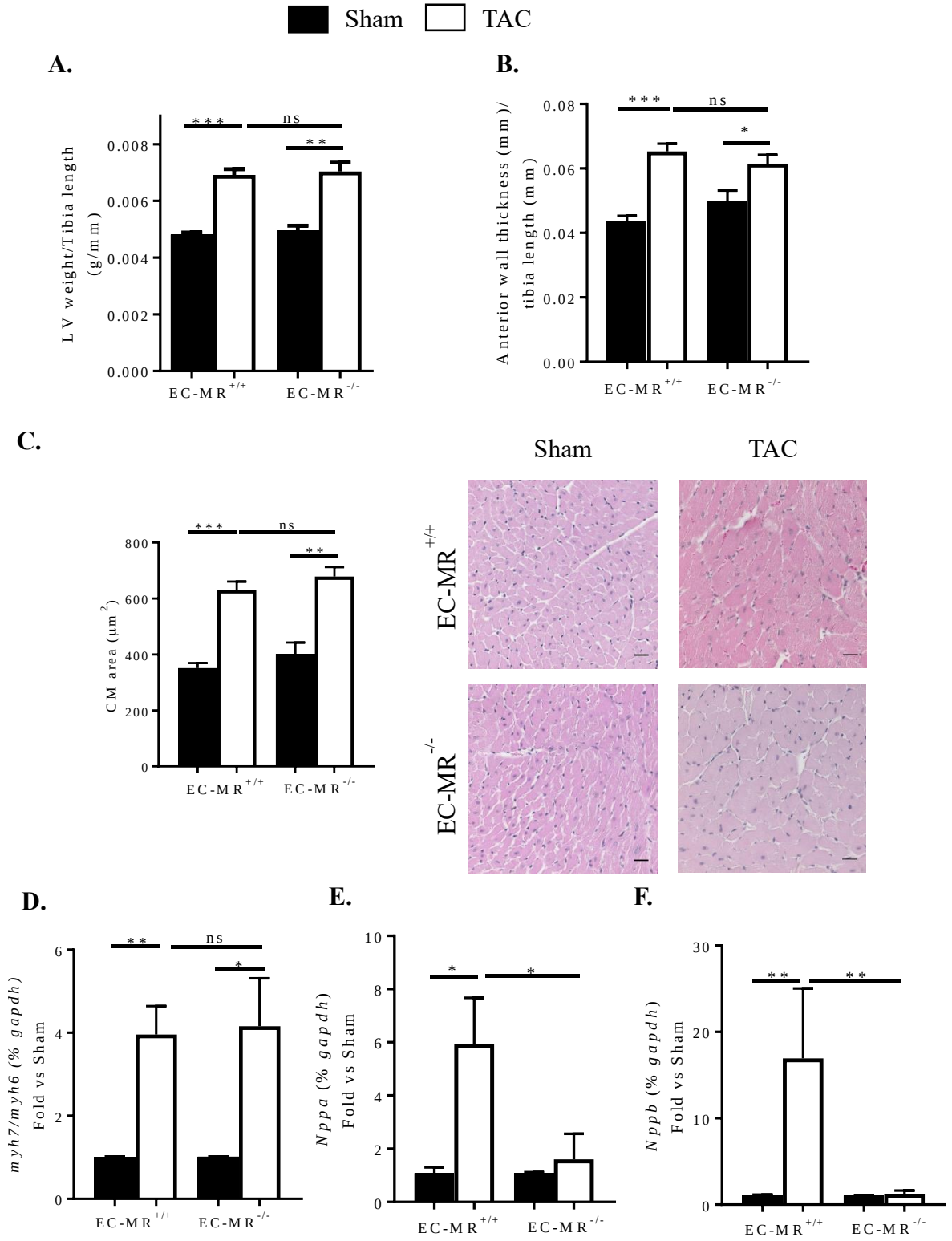

Figure 7.17. EC-MR contributes to some aspects of cardiac hypertrophy and fetal gene re-expression associated with pathological remodeling in response to TAC. A. LV weight normalized with the tibia length (g/mm). **B.** LV anterior wall thicknesses determined by non-invasive echocardiography normalized to tibia length. **C.** CM area measured in H&E stained LV cross-sections; quantification is shown on the left and 40x representative pictures are shown on the right. Scale bar 25μm. Mean ± SEM of independent experimental replicates is represented. Statistics unpaired t-test. **D.** Ratio of mRNA levels of MHCβ isoform over MHCα, represented as fold vs respective Sham. LV **(E)** ANP and **(F)** BNP mRNA levels, represented as fold vs respective Sham. n= 5 EC-MR$^{+/+}$ Sham, 8 EC-MR$^{+/+}$ TAC, 3 EC-MR$^{-/-}$ Sham, 6-8 EC-MR$^{-/-}$ TAC. Mean ± SEM from a single qRT-PCR run containing samples collected in independent experimental replicates is represented. Statistics Mann-Whitney test.

Taken together, these data confirm the induction of pathologic LV hypertrophy in this model and further reveal that EC-MR$^{-/-}$ mice are not protected from pressure overload-induced LV hypertrophy. However, the reduced induction of some fetal genes that are associated with maladaptive cardiac remodeling in EC-MR$^{-/-}$ TAC LVs supports that EC-MR promotes a more pathological hypertrophic phenotype in response to TAC.

7.3.3 EC-MR is not essential for LV endothelial cell activation and myeloid cell recruitment in response to TAC

It has previously been reported that MR activation by aldosterone upregulates ICAM1 in human coronary ECs (96), and that ICAM1 mediates T lymphocyte and CD11b+ myeloid cell recruitment into the LV after TAC (Chapter 7.2) (170). Thus, the requirement of EC-MR for ICAM1 mRNA expression in response to TAC was next evaluated. As expected, ICAM1 mRNA levels increased in EC-MR$^{+/+}$ LVs in response to TAC as compared to Sham. However, ICAM1 mRNA levels also increased to the same extent in EC-MR$^{-/-}$ TAC LVs, indicating that ICAM1 mRNA expression was not affected by deletion of EC-MR

(Figure 7.18A). In contrast, vascular cell adhesion molecule 1 (VCAM1) mRNA expression was not altered in any of the groups in response to TAC (Figure 7.18B). Despite this lack of differential EC adhesion molecule upregulation after TAC, whether recruitment of immune cells was impaired in EC-MR$^{-/-}$ mice was evaluated, which could justify the observed preserved systolic function (Figure 7.16) and reduced natriuretic peptide gene expression (Figure 7.17). As determined in previous studies, EC-MR$^{-/-}$ mice have similar T lymphocyte infiltration as EC-MR$^{+/+}$ littermates after TAC (Figure 7.15). Further immunohistochemistry analysis was performed to visualize infiltrating monocytes and neutrophils in LV cross-sections subjected to 4 week TAC. Quantification of the staining demonstrated that CD11b+ myeloid cell (Figure 7.18C) infiltration was increased in EC-MR$^{+/+}$ mice in response to TAC and surprisingly, this was unaffected by EC-MR deletion. Additionally, Gr1+ neutrophil infiltration did not change between Sham and TAC EC-MR$^{+/+}$ mice, as previously demonstrated in WT mice, neither was altered in TAC EC-MR$^{-/-}$ mice (Figure 7.18D).

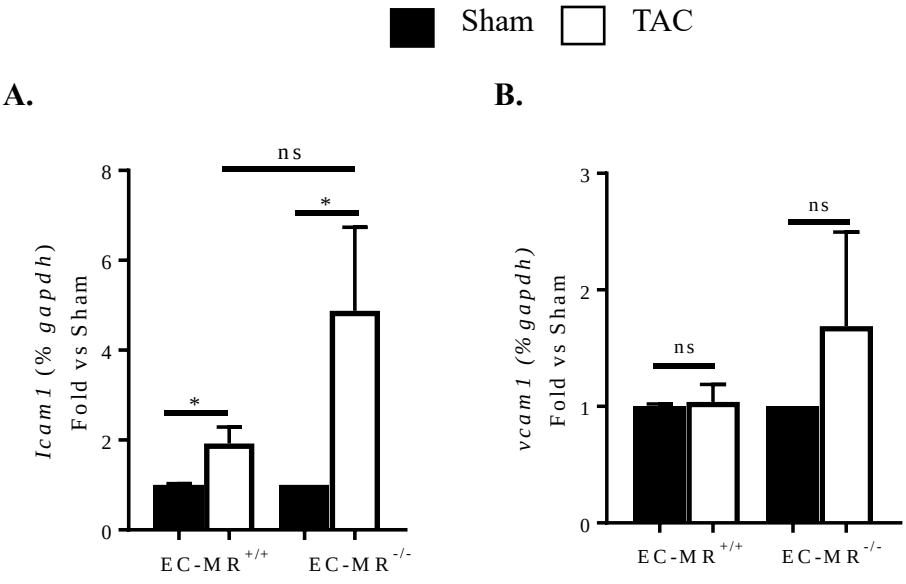

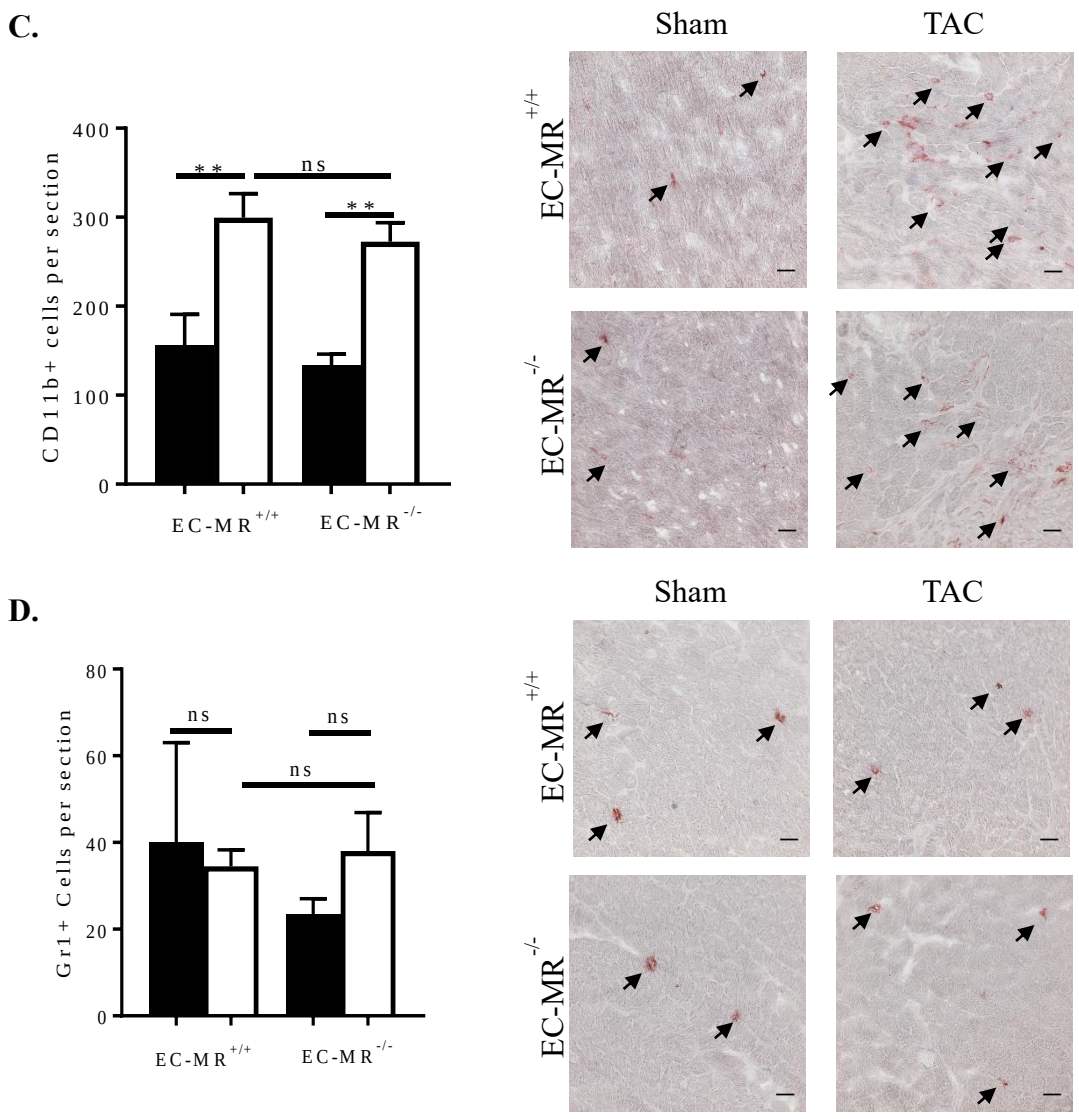

Figure 7.18. EC-MR does not regulate LV adhesion molecule expression and CD11b+ myeloid cell and Gr1+ neutrophil recruitment in response to TAC. (A) ICAM1 and **(B)** VCAM1 mRNA levels determined by qRT-PCR represented as fold vs respective Sham. Mean ± SEM from a single qRT-PCR run containing samples collected in independent experimental replicates is represented. Statistics Mann-Whitney test. **C.** CD11b+ myeloid cell recruitment determined by immunohistochemitry as number of positive cells per section. Arrows indicate representative staining. Quantification of infiltrated cells is shown on the left and representative 40x pictures are shown on the right. **C.** LV Gr1+ cell recruitment, determined by immunohistochemistry as number Gr1+ cells per section. Quantification of infiltrated cells is shown on the left and representative 40x pictures are shown on the right. Scale bar 25µm. n= 5 EC-MR$^{+/+}$ Sham, 8 EC-MR$^{+/+}$ TAC, 3 EC-MR

Sham, 8 EC-MR$^{-/-}$ TAC. Mean ± SEM of independent experimental replicates is represented. Statistics unpaired t-test.

7.3.4 EC-MR deletion does not affect the degree of perivascular and interstitial fibrosis in response to TAC

Both perivascular and interstitial collagen deposition are hallmarks of maladaptive cardiac remodeling in response to pressure overload (182). We next evaluated whether any of these were altered by the lack of EC-MR, potentially contributing to the preservation of systolic function in EC-MR$^{-/-}$ mice in response to TAC. First, the areas surrounding the vessels were specifically examined, thus evaluating the role of EC-MR in perivascular inflammation and fibrosis which is known to be influenced by aldosterone and MR in response hypertensive pressure overload (183). Perivascular areas with high collagen deposition co-localized with significant immune cell infiltration after TAC. However, the degree of perivascular inflammatory infiltration and fibrosis were not affected by deletion of EC-MR (Figure 7.19A).

Additionally, interstitial fibrosis was measured by quantifying collagen deposition in the LV tissue stained with Picrosirius red, and similar degree of tissue fibrosis was determined in EC-MR$^{+/+}$ mice and EC-MR$^{-/-}$ (Figure 7.19B) in response to TAC.

Taken together these data indicate that EC-MR deletion does not prevent the development of either perivascular inflammation or perivascular and interstial fibrosis in response to pressure overload.

A.

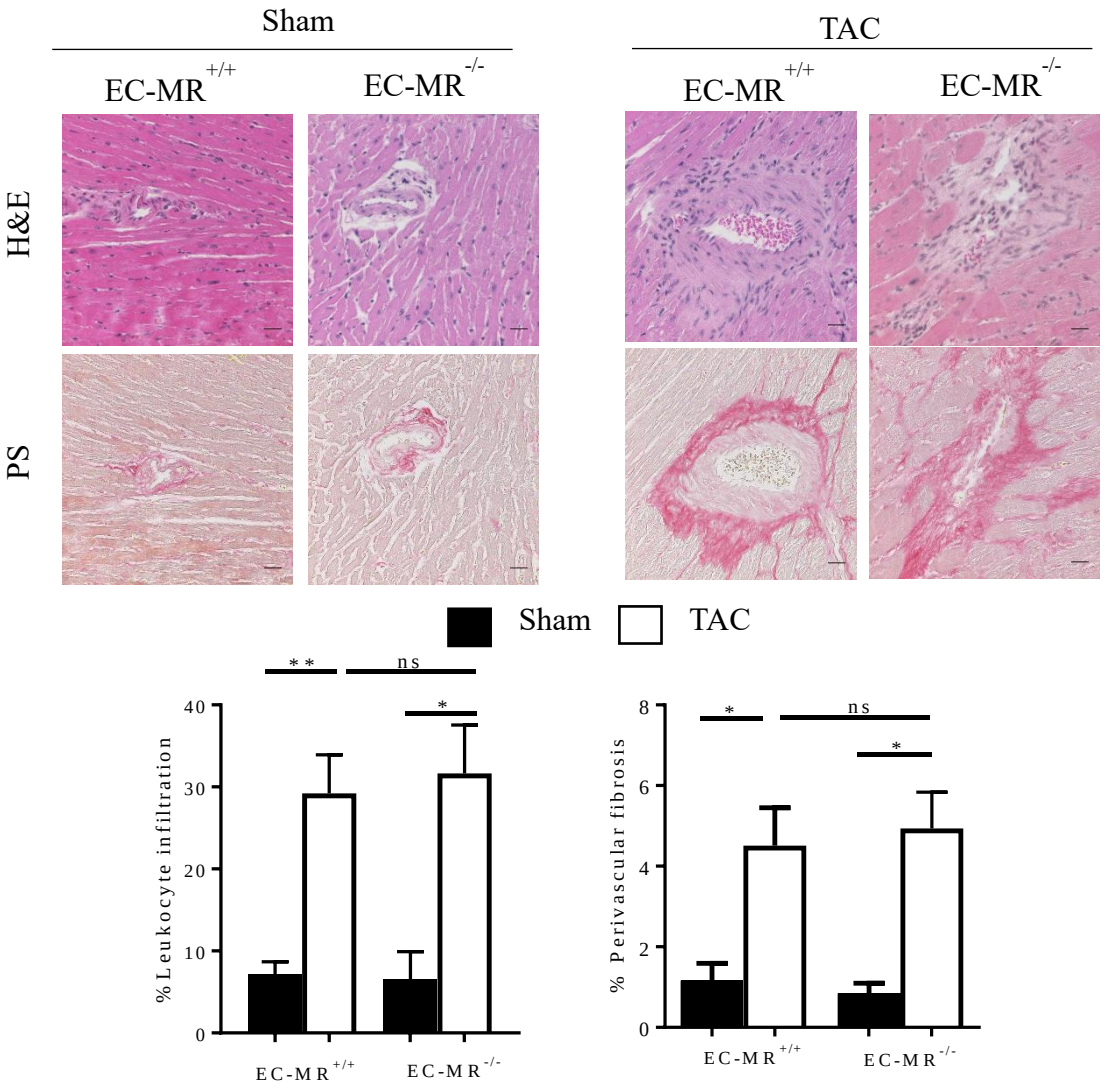
Sham
TAC
EC-MR+/+
EC-MR-/-
EC-MR+/+
EC-MR-/-
H&E
PS
Sham
TAC
** ns
* ns
% Leukocyte infiltration
% Perivascular fibrosis
EC-MR+/+
EC-MR-/-
EC-MR+/+
EC-MR-/-

B.

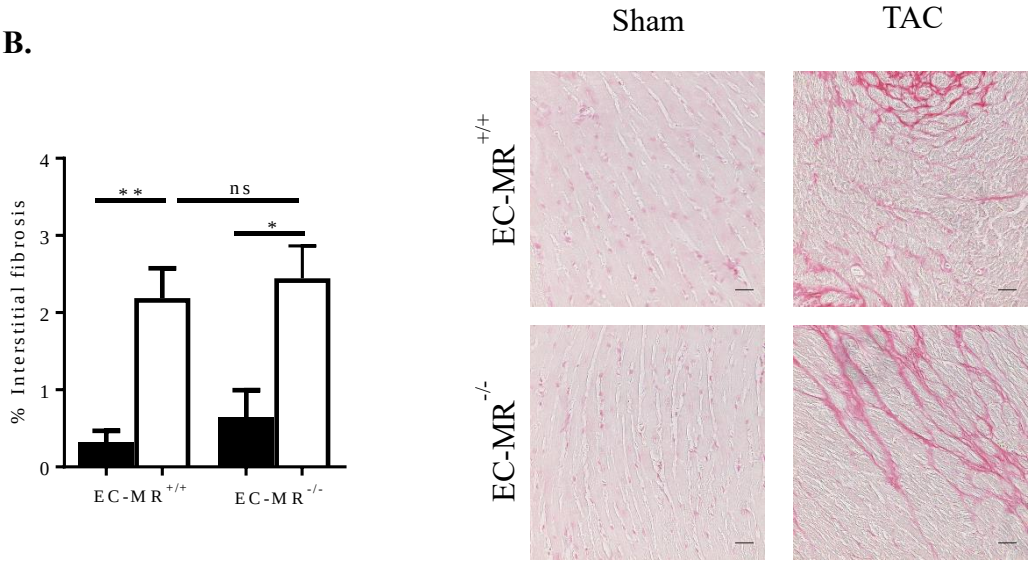
Sham
TAC
** ns
* ns
% Interstitial fibrosis
EC-MR+/+
EC-MR-/-
EC-MR+/+
EC-MR-/-

Figure 7.19. EC-MR deletion does not affect total leukocyte recruitment, perivascular and interstitial collagen deposition in response to TAC. A. Representative H&E and Picrosirius red stained LV sections, showing areas with elevated leukocyte infiltration co-localizing with areas presenting high percentage of perivascular fibrosis; quantifications of infiltrates and perivascular collagen deposition are shown below. Scale bar 25μm. **B.** LV interstitial collagen deposition quantified as percent fibrosis on the left. Representative 40x pictures of Picrosirius red stained LV sections are shown on the right. Scale bar 25μm. n= 5 EC-MR$^{+/+}$ Sham, 8 EC-MR$^{+/+}$ TAC, 3 EC-MR$^{-/-}$ Sham, 8 EC-MR$^{-/-}$ TAC. Mean ± SEM of independent experimental replicates is represented. Statistics unpaired t-test.

7.3.5 EC-MR does not regulate capillary rarefraction and CM apoptosis after TAC

Further characterizing the role of EC-MR in cardiac remodeling in response to pressure overload, we determined capillary density and CM death as potential mechanisms that could explain the preserved systolic function observed in EC-MR$^{-/-}$ mice after TAC. LV cross-sections were first stained with PECAM1 to quantify intramyocardial capillaries relative to the CM area as a measurement of capillary density in the LV. EC-MR$^{-/-}$ and EC-MR$^{+/+}$ both had the same decrease in LV capillary density in response to TAC as compared to their respective Sham control mice (Figure 7.20A). Despite CM apoptosis is not routinely observed in the TAC pressure overload model until longer time points, CM death was next examined through the TUNEL staining as apotential mechanism that could explain the improve cardiac function phenotype in EC-MR$^{-/-}$ TAC mice. However, 4 week TAC did not induce a significant increase in CM apoptosis, with no difference among genotypes (Figure 7.20B). Altogether these data indicate that EC-MR does not play a role in either decreasing capillary density or in CM death in response to pressure overload.

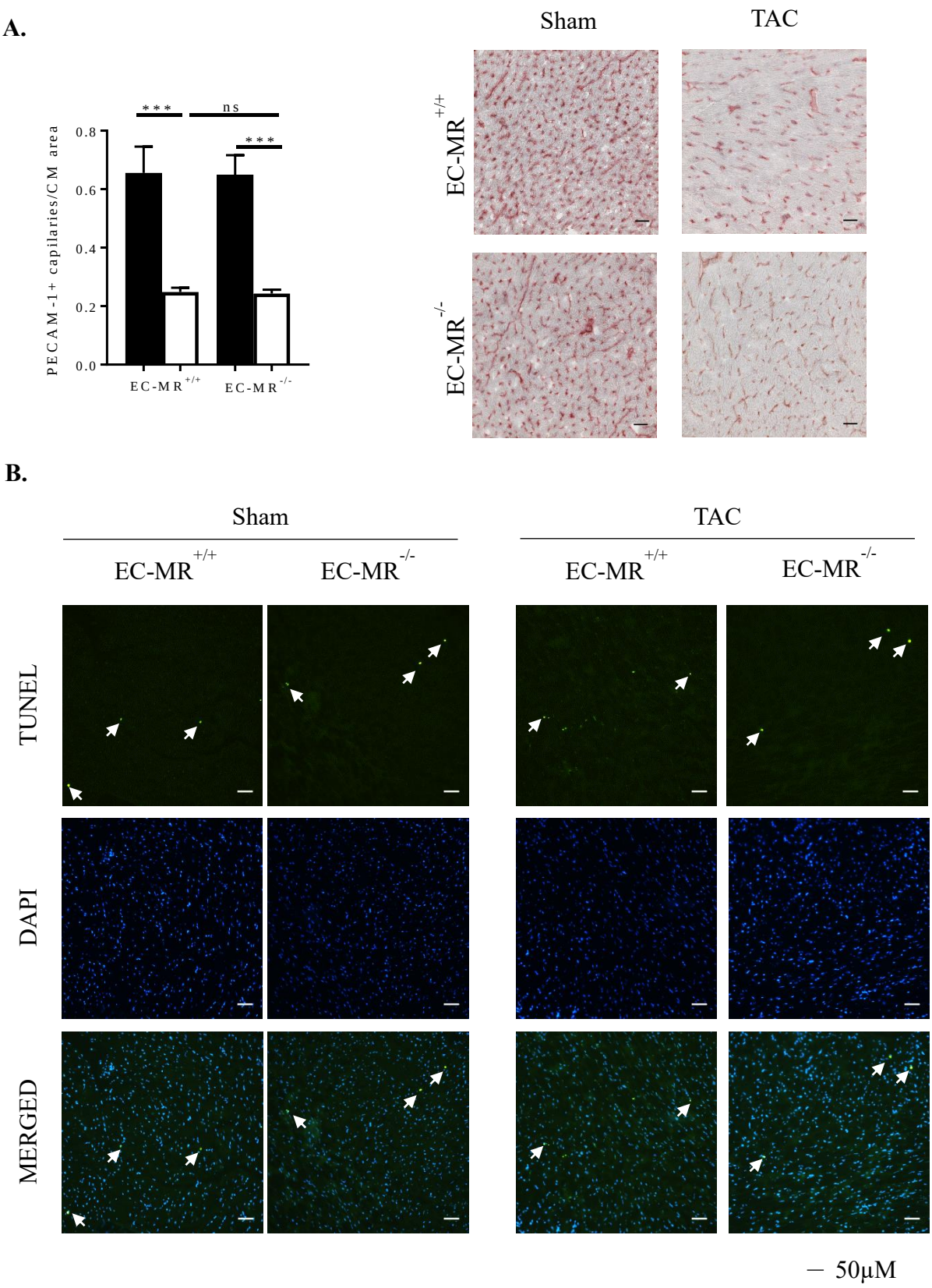

Figure 7.20.EC-MR deletion does not affect LV angiogenesis and CM apoptosis in response to TAC. A. LV capillary density, determined by immunohistochemistry as PECAM1+ (CD31)

capillary number normalized by CM area. Quantification is shown on the left and representative 40x pictures are shown on the right. n= 5 EC-MR$^{+/+}$ Sham, 8 EC-MR$^{+/+}$ TAC, 3 EC-MR$^{-/-}$ Sham, 8 EC-MR$^{-/-}$ TAC. Mean ± SEM of independent experimental replicates is represented. Statistics unpaired t-test. **B.** Representative pictures showing CM death through the TUNEL staining (ApopTag®). Arrows indicate representative apoptotic CM.

7.3.6 EC-MR regulates the expression of TNFα and endothelin receptor type B in response to TAC

Aldosterone and MR have been implicated in vascular and systemic inflammation (184) in response to hypertension (183). We had previously postulated that T cell infiltration in the LV in response to TAC was a driver of a pro-inflammatory cytokine environment in the LV that contributes to development of HF (174). Thus, the LV expression of the pro-inflammatory cytokine TNFα was evaluated as a potential mechanism involved in the observed preserved systolic function in EC-MR$^{-/-}$ mice. TNFα mRNA expression did not follow the same pattern as IL-1β and IL-6 (Figure 7.15D) and was increased in TAC EC-MR$^{+/+}$ but not in TAC EC-MR$^{-/-}$ mice after TAC (Figure 7.21A). Therefore, these data indicate that while EC-MR is essential for LV TNFα expression, it is not necessary for IL-1β and IL-6 mediated myocardial inflammation and adhesion molecule expression in response to TAC, and indicates that the lack of myocardial TNFα expression may contribute to the ameliorated systolic dysfunction in EC-MR$^{-/-}$ mice, while supporting that IL-1β and IL-6 may be the inducers of ICAM1, as we have previously reported (Figure 7.15) (170). We also determined the mRNA expression of the endothelin receptor type B (*ednrb*, ETB), a fetal gene known to regulate endothelin mediated vasoconstriction, as a potential mechanism involved in the observed improved systolic function. Whereas *ednrb* increased in the LV of EC-MR$^{+/+}$ mice in response to TAC, such increase was not observed

in EC-MR$^{-/-}$ mice after TAC and remained similar as the expression observed in EC-MR$^{-/-}$ Sham mice (Figure 7.21B).

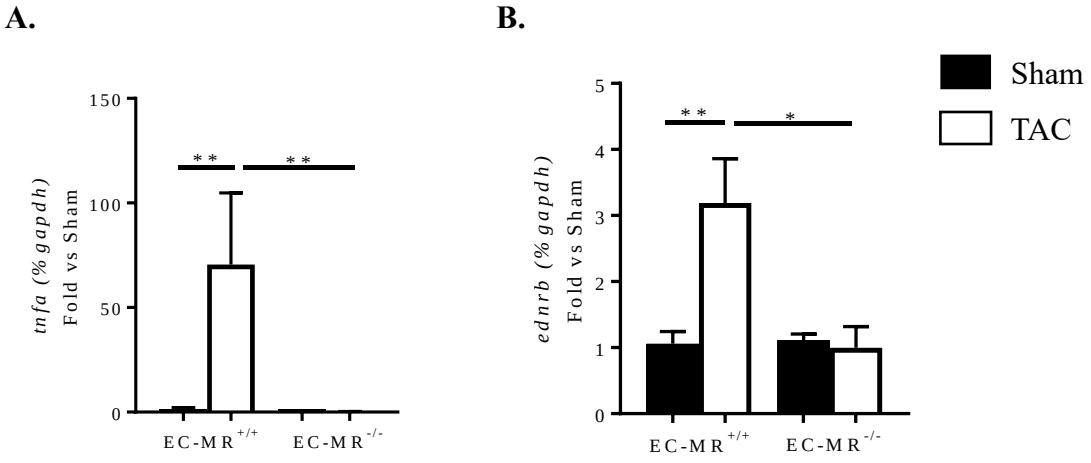

Figure 7.21. LV pro-inflammatory cytokine TNFα and ETB expressions are regulated by EC-MR in response to TAC. (A) TNFα and **(B)** ETB mRNA levels determined by qRT-PCR represented as fold vs respective Sham. n= 5 EC-MR$^{+/+}$ Sham, 8 EC-MR$^{+/+}$ TAC, 3 EC-MR$^{-/-}$ Sham, 6 EC-MR$^{-/-}$ TAC. Mean ± SEM from a single qRT-PCR run containing samples collected in independent experimental replicates is represented. Statistics Mann-Whitney test.

Altogether, our data indicate on one hand a differential pro-inflammatory cytokine expression in the presence or absence of EC-MR, suggesting an alternative pathway of NFκB activation triggered by MR expressed in cells different than EC in response to TAC, other than aldosterone activation of EC-MR. On the other hand, EC-MR seems to regulate ETB expression, suggesting that it may regulate endothelin-ETB mediated vasoconstriction and therefore the cardiac perfusion in response to pressure overload. These two observations could contribute to the observed preservation in systolic function in the absence of EC-MR.

7.4 T cell cardiotropism in heart failure – role of chemokines CXCL9 and CXCL10 and the CXCR3 chemokine receptor

In addition to endothelial CAM, chemokines and chemokine receptors are small proteins involved in leukocyte chemo attraction to the sites of inflammation. Each chemokine receptor and ligand is quite specific in the recruitment of either innate or adaptive immune cell subsets. Given the critical role of T lymphocytes in LV remodeling (Chapter 7.1) and the ICAM1 mediated T lymphocyte recruitment (Chapter 7.2), we next investigated the role of specific chemokines and chemokine receptors involved in effector T lymphocyte LV infiltration during HF development. We focused on the chemokines CXCL9 and CXCL10, which are found elevated in circulation of humans and mice with HF (185, 186). Additionally, the expression of their receptor, CXCR3 in circulating T cells is associated with disease progression and LV dysfunction in HF patients (139).

Genes encoding for CXCL9 and CXCL10 are expressed in various tissues in mice in response to tissue injury (187), induced mainly by IFNγ, and in a lower extent by IFNα/β and TNF. *In vitro* experiments using human cells have indicated that upon inflammatory stimuli many cell types, including monocytes, EC and fibroblasts (188), can produce CXCR3 ligands, although the source of these chemokines *in vivo* is still unclear.

Interestingly, the (a) chemokine- (b) chemokine receptor- (c) integrin- (d) integrin ligand axis in T lymphocytes has thoroughly been characterized in the last decades in their chemotaxis and recruitment to inflamed tissues.

We tested the hypothesis that CXCR3 signaling in T lymphocytes facilitates their adhesion to ICAM1 expressed in the intramyocardial ECs and contributes to the progression of HF.

7.4.1 CXCR3 ligands' expression is increased in the LV 2 and 4 weeks after TAC

Recent investigations indicate that CXCL10 promoter's histone acetylation is increased in the myocardium and circulating levels of CXCL9 and CXCL10 are elevated during cardiac remodeling after TAC (189, 190). Given the well stablished association between CD4+ T lymphocytes LV recruitment and cardiac dysfunction in response to TAC (Chapter 7.1) (174), we first evaluated the sequential expression of CXCL9 and CXCL10 at different time points after pressure overload. TAC was induced in WT mice, which were sacrificed after 48h, 1, 2 and 4 weeks to determine the kinetics of the CXCR3 ligands CXCL9 and CXCL10 expression by qRT-PCR in the LV (Figure 7.22A-B). It was not until 2 and 4 weeks after TAC, but not at earlier time points (48h and 1 week), that the mRNA levels of CXCL9 and CXCL10 were significantly upregulated in the LV. The mRNA expression of TNFα and IFNγ, known to induce CXCL9 and CXCL10 expression in various cell types (132), followed similar expression kinetics as CXCL9 and CXCL10 (Figure 7.22C-D). Thus, this initial screening at different time points during cardiac remodeling indicated that both CXCL9 and CXCL10 become upregulated in the LV, probably in response to local IFNγ and TNFα release, at the same time points after TAC in which CD4+ T cell are found infiltrated in the myocardium and cardiac dysfunction is observed (Figure 7.2) (174).

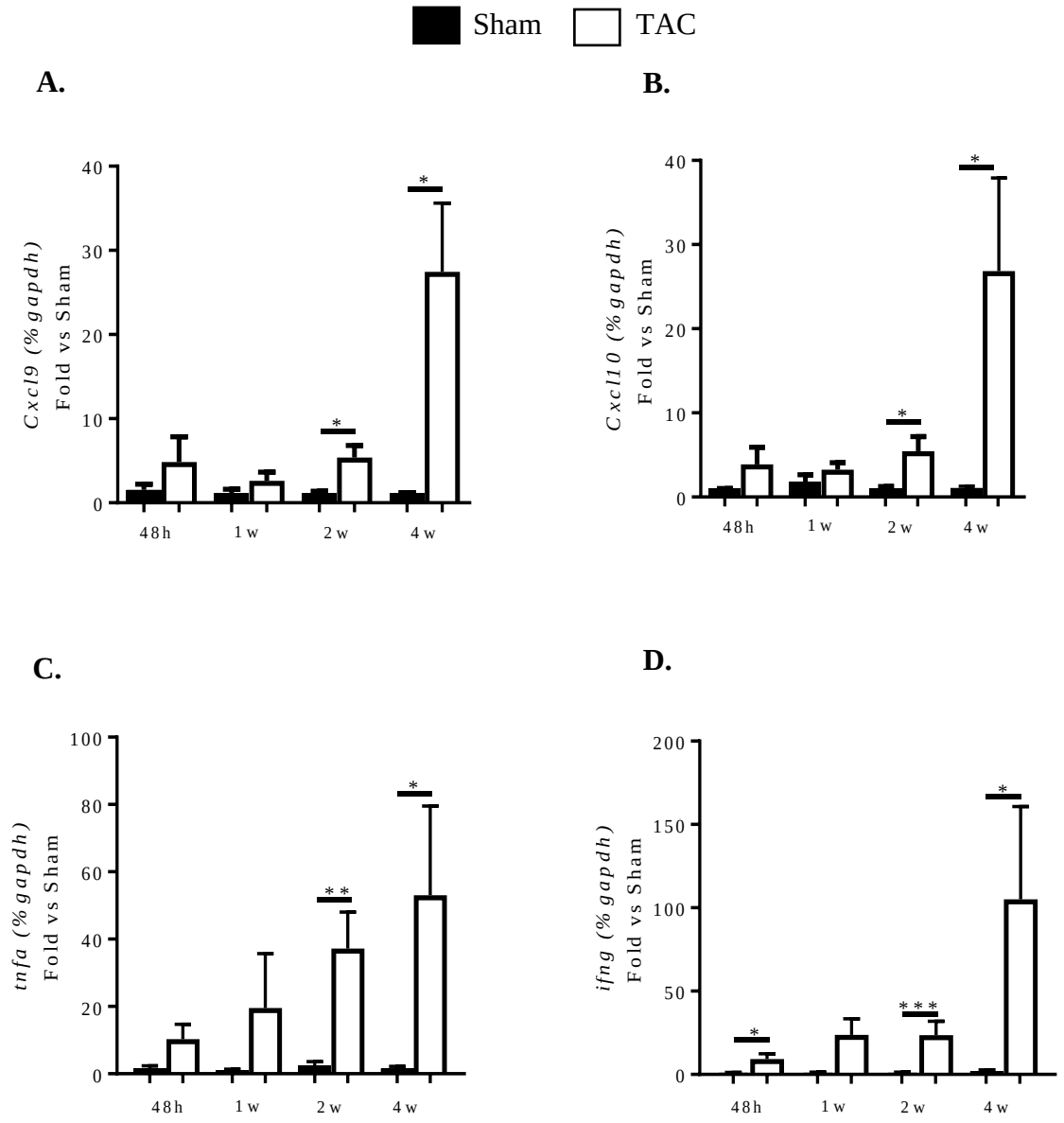

Figure 7.22. LV mRNA expression of CXCR3 ligands and their inducers, cytokines TNFα and IFNγ, in WT mice at different times points after TAC. Chemokine and cytokine mRNA expression in the LV of WT mice subjected to TAC, or Sham control, at different time points. **(A)** CXCL9, **(B)** CXCL10, **(C)** TNFα and **(D)** IFNγ mRNA expression. n= 3 Sham 48h, 5 TAC 48h; 4 Sham 1w, 5 TAC 1w; 5 Sham 2w, 9 TAC 2w; 6 Sham 4w, 8 TAC 4w. Mean ± SEM from a single qRT-PCR run containing samples collected in independent experimental replicates is represented. Statistics Mann-Whitney test.

7.4.2 CXCR3+ T lymphocyte frequency is increased in the cardiac draining lymph nodes after TAC and express higher levels of ICAM1's ligand LFA1

Mediastinal lymph nodes (MLN) are the secondary lymphoid organ where T lymphocyte response is initiated after TAC (170, 174). Indeed, it has recently been described that in response to TAC total CD4+ and CD4+IFNγ+ T lymphocyte counts are significantly inceased as compared to Sham mice (175). Thus, the levels of CXCR3+ CD4+ T lymphocyte in the cardiac draining lymph nodes over the time course of TAC were determined. CXCR3+ T lymphocyte were found expanded in the cardiac draining lymph nodes at 1, 2 and 4 weeks after TAC as compared to Sham operated mice (upper right quadrant Figure 7.23A). The total percentages of CXCR3+LFA1+ T lymphocytes were found increased in all three time points after TAC as compared to Sham operated mice (upper right quadrant Figure 7.23B). Given that CD4+ T lymphocytes are expanded in the mediastinal lymph nodes in response to TAC (175), it is likely that the total number of CXCR3 expressing T lymphocytes is increased as well in the mediastinal lymph nodes based on our data showing an increase in their percentage. Interestingly, in contrast to CXCR3+ T lymphocytes, which expressed high levels of LFA1, CXCR3- mediastinal lymph node T lymphocytes expressed low levels of LFA1, and no difference between TAC and Sham operated mice was observed (Figure 7.23C). This indicates that TAC induces an increase in CXCR3 expression in T lymphocytes making them more prone to abandon the lymph node following chemotactic gradients mediated by CXCL9 and CXCL10 released from the LV after TAC. This correlation suggests that CXCR3+ T lymphocyte carditropism and LV recruitment is initially mediated by LV released CXCL9 and CXCL10 chemotactic gradients, followed by ventricular migration regulated by integrin LFA1.

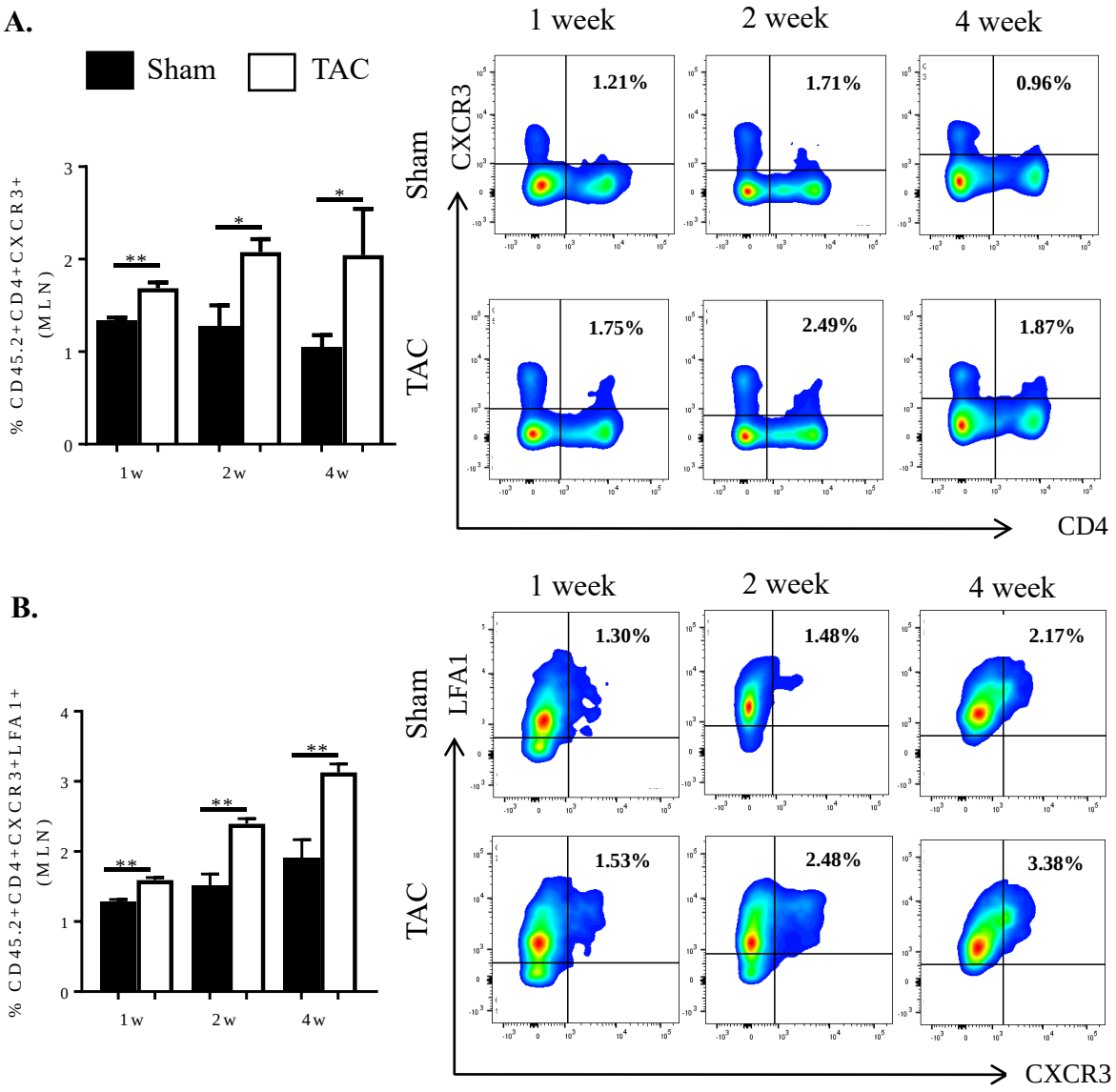
A.
Sham
TAC
% CD45.2+CD4+CXCR3+ (MLN)
1w
2w
4w
1 week
2 week
4 week
CXCR3
Sham
TAC
1.21%
1.71%
0.96%
1.75%
2.49%
1.87%
CD4
B.
% CD45.2+CD4+CXCR3+LFA1+ (MLN)
LFA1
1.30%
1.48%
2.17%
1.53%
2.48%
3.38%
CXCR3
C.
CD4+CXCR3-
CD4+CXCR3+
LFA1

Figure 7.23. CXCR3+LFA1+ T lymphocyte percentages in MLN after TAC. MLN from WT mice subjected to TAC, or Sham control, for different time points were and stained for CD4, CXCR3 and LFA1. **A.** Percent of CXCR3+ T helper lymphocytes in MLN of WT mice after 1, 2 or 4 weeks from TAC surgery is represented in the graph. On the right, representative FACS plots are shown for each time point. **B.** Percent of CXCR3+LFA1+ T helper lymphocytes in MLN of WT mice after 1, 2 or 4 weeks from TAC surgery is represented in the graph. On the right, representative FACS plots within the CD4+ gate are shown for each time point. **C.** Representative histograms indicating the differential LFA1 expression between CXCR3+ and CXCR3- T lymphocytes. Percent of LFA1+ T helper lymphocytes in MLN, classified in CXCR3+ and CXCR3- CD4+ T lymphocytes. n= 3 Sham 1w, 3 TAC 1w; 3 Sham 2w, 4 TAC 2w; 3 Sham 4w, 5 TAC 4w. Mean ± SEM of independent experimental replicates is represented. Statistics unpaired t-test.

7.4.3 CXCR3+ and LFA1+ T lymphocytes infiltrate the LV in response to 2 and 4 weeks TAC and correlate with increased LV Tbet and MHCβ expression

Based on the kinetics of expansion of CXCR3+ T lymphocytes in the cardiac draining lymph nodes in response to TAC, we hypothesized that CXCR3+ T lymphocytes will sequentially traffic to the LV resulting in progressive CXCR3+ T lymphocyte LV infiltration in response to TAC. Therefore at the same time points post TAC (1, 2 and 4 weeks), the presence of CXCR3+ T lymphocytes in the LV was evaluated by flow cytometry. CXCR3+ T lymphocytes were found recruited in the LV after 2 weeks post TAC and further infiltrated significantly at 4 weeks of TAC (Figure 7.24A), the same time points in which CXCL9 and CXCL10, CXCR3 ligands, were found increased in the LV (Figure 7.22) and when total CD3+ T lymphocyte infiltration occurs after TAC (Figure 7.2) (174). In addition, within the CD3+ infiltrated T lymphocytes, LFA1 was found to be highly expressed 2 and 4 weeks after TAC, as LFA1+ CD3+ lymphocyte frequency in the LV was increased as compared to Sham operated mice starting 2 weeks post TAC and

continuing at 4 weeks (Figure 7.24B). As the transcription factor Tbet has been shown to regulate CXCR3 expression in immune cells, the mRNA expression of Tbet over time after TAC was next determined. Tbet was found upregulated in the LV as early as 1 week after TAC, and was further upregulted 2 and 4 weeks after TAC (Figure 7.24C). MHCβ fetal isotype upregultation was also increased 2 and 4 weeks post TAC (Figure 7.24D). Thus, this data indicate that in response to CXCR3 ligands expressed in the LV 2 and 4 weeks after TAC, CXCR3+ and LFA1+ T lymphocytes are recruited into the LV and possibly contribute to pathological cardiac remodeling features observed at this time points post TAC.

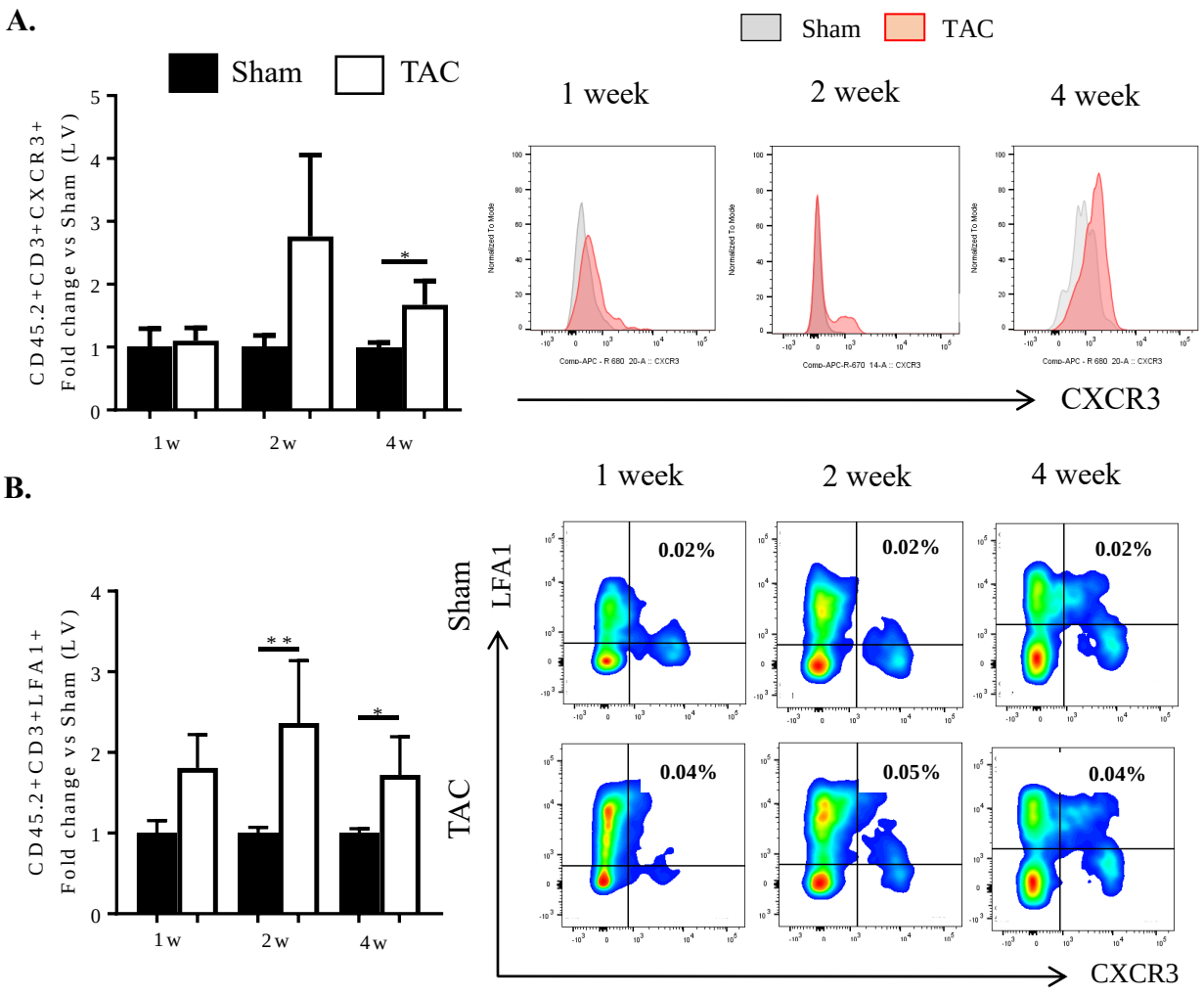

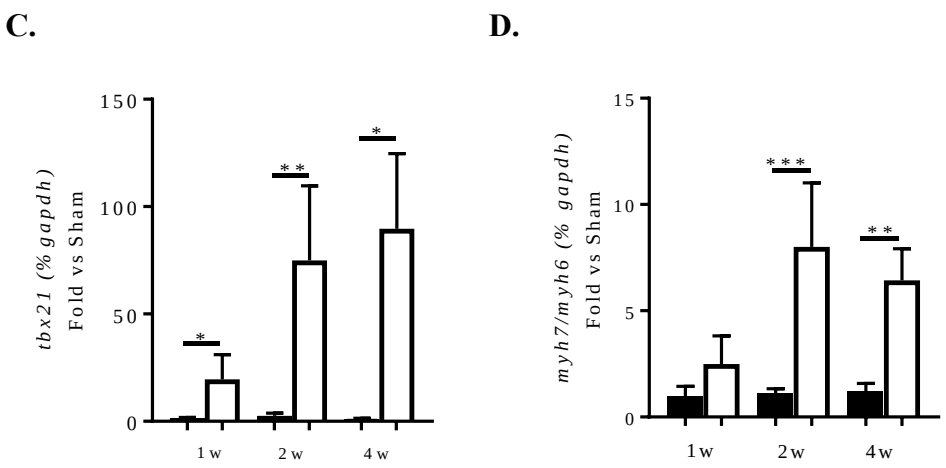

Figure 7.24. CXCR3+ and LFA1+ T lymphocyte infiltration in the LV at different time points after TAC. A. Fold change vs Sham of CXCR3+CD3+ lymphocytes infiltrated in the LV of WT mice after 1, 2 or 4 weeks from TAC surgery is represented in the graph. On the right, representative FACS histograms are shown for each time point. **B.** Fold change vs Sham of LFA1+CD3+ lymphocytes infiltrated in the LV of WT mice after 1, 2 or 4 weeks from TAC surgery is represented in the graph. On the right, representative FACS plots are shown for each time point. Mean ± SEM of independent experimental replicates is represented. Statistics unpaired t-test. **C.** qRT-PCR of Tbet expression in the LV of WT mice at different time points after TAC. **D.** qRT-PCR of the MHCβ/α expression ratio in the LV of WT mice at different time points after TAC. n= 3-4 Sham 1w, 3-6 TAC 1w; 7 Sham 2w, 5-10 TAC 2w; 4-6 Sham 4w, 8-9 TAC 4w. Mean ± SEM from a single qRT-PCR run containing samples collected in independent experimental replicates is represented. Statistics Mann-Whitney test.

7.4.4 CXCR3+ T lymphocytes circulate in similar frequency in TAC and Sham operated mice, but express higher levels of LFA1 than CXCR3- T lymphocytes

CXCR3+ T lymphocyte frequency in circulation has been shown to be an effective marker of HF prognosis since patients suffering from it have elevated circulating levels, which correlated with disease progression (139). Thus, the presence of blood circulating CXCR3+ and CXCR3- T lymphocytes as well as their LFA1 expression was next evaluated. Unlike

in the mediastinal lymph nodes, no systemic expansion of CXCR3+ T lymphocytes was observed at 1, 2 and 4 weeks after TAC as compared to Sham operated mice in the circulation (Figure 7.25A). The frequency of CXCR3+LFA1+ T lymphocytes was not significantly different between Sham and TAC mice over the time course tested (Figure 7.25B). Circulating CXCR3+ T lymphocytes, however, maintained higher expression levels of LFA1, as compared to CXCR3- T lymphocytes (Figure 7.25C). Thus, the lack of circulating expansion suggests that there may be a direct mediastinal lymph node – LV trafficking, with absence of significant CXCR3+ T lymphocytes mediated systemic inflammation.

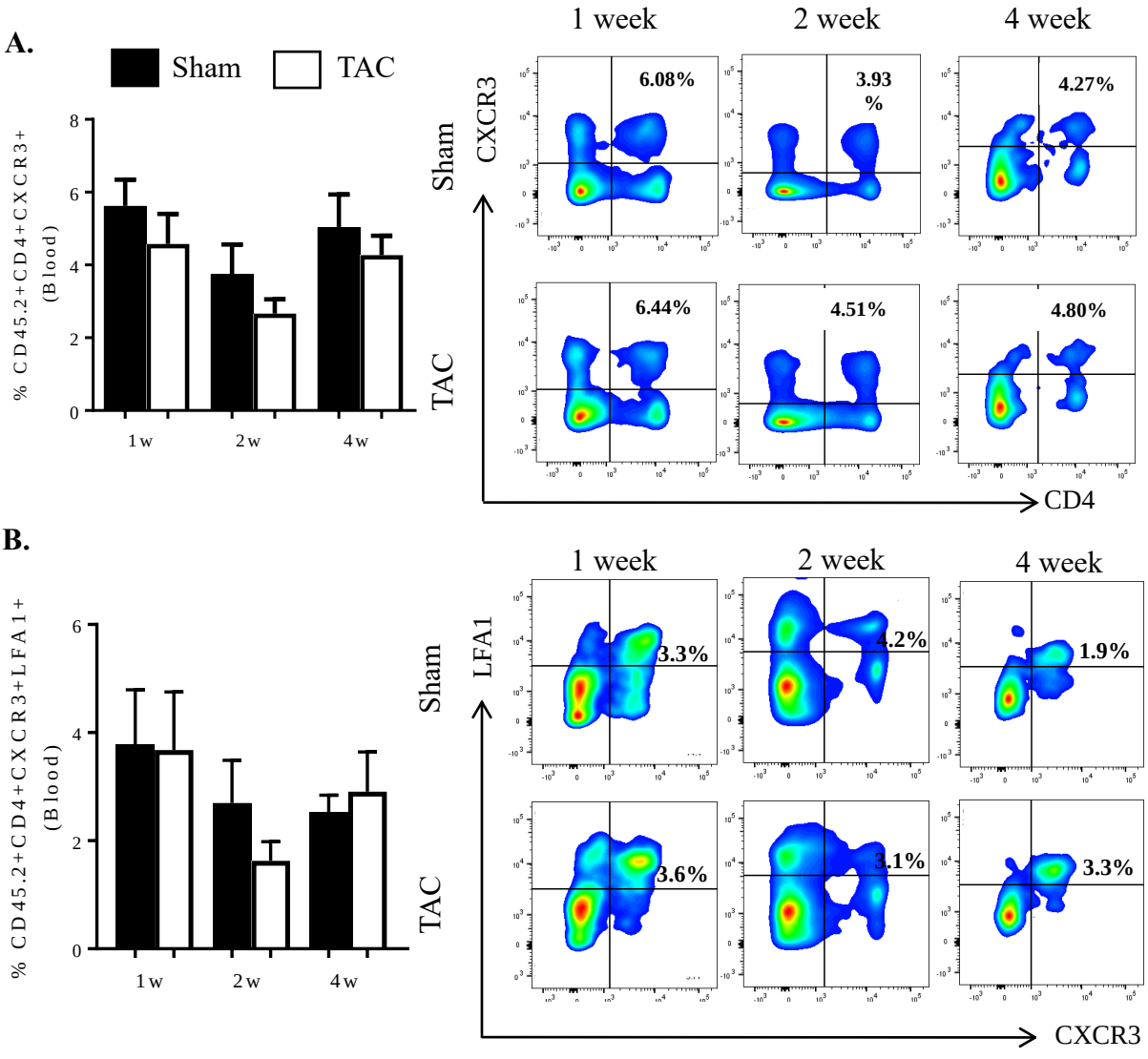

C.

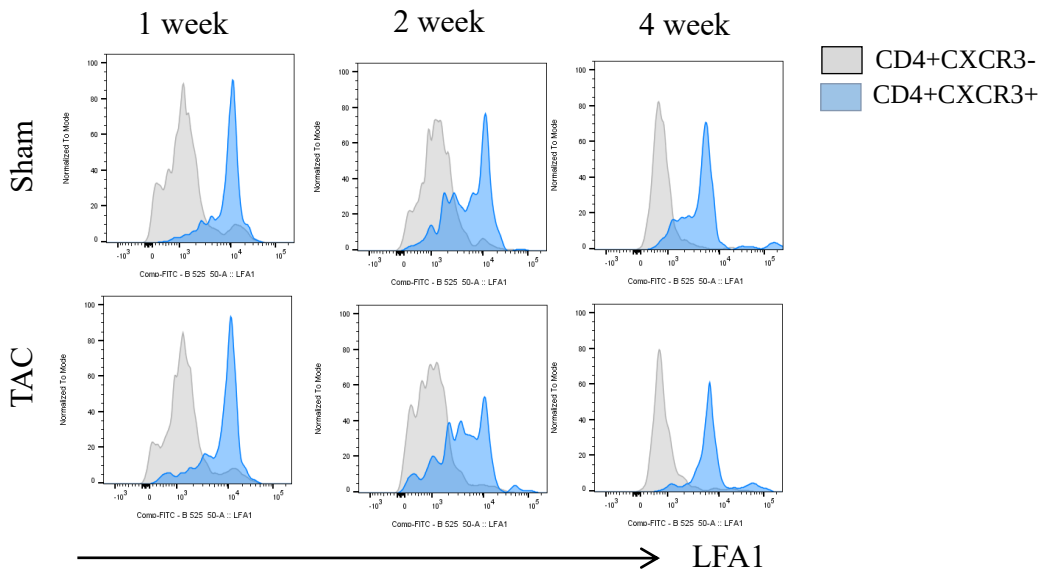

Figure 7.25. CXCR3+LFA1+ T lymphocyte frequencies in systemic circulation after TAC. A. Percent of CXCR3+ T helper lymphocytes in blood of WT mice after 1, 2 or 4 weeks from TAC surgery is represented in the graph. On the right, representative FACS plots are shown for each time point. **B.** Percent of CXCR3+LFA1+ T helper lymphocytes in blood of WT mice after 1, 2 or 4 weeks from TAC surgery is represented in the graph. On the right, representative FACS plots are shown for each time point. **C.** Representative histograms indicating the differential percentage of LFA1 expression between CXCR3+ and CXCR3- T lymphocytes in blood. n= 3 Sham 1w, 3 TAC 1w; 7 Sham 2w, 6 TAC 2w; 6 Sham 4w, 8 TAC 4w. Mean ± SEM of independent experimental replicates is represented. Statistics unpaired t-test.

Taken together, these data indicate that CXCR3+ T lymphocytes expand locally in the mediastinal lymph nodes, mobilize towards the cardiac tissue facilitated by the CXCR3 ligand gradient, and are prone to adhere to the cardiac endothelial ICAM1 through LFA1 and transmigrate into the myocardial tissue.

7.4.5 CXCL9 and CXCL10 induce an increase of Th1 lymphocyte adhesion to ICAM1 under flow conditions *in vitro,* in a LFA1 dependent manner

The above shown *in vivo* data indicate that there is a consistent correlation between CXCR3 and LFA1 expression in effector T lymphocytes both locally in the mediastinal lymph nodes and systemically in circulation after TAC. In addition, there are several reports showing that CXCR3 ligands play a key role in T lymphocytes adhesion to ICAM1 by increasing LFA1 affinity leading to optimal adhesion to ICAM1 and ECs under flow conditions *in vitro*. Thus, we hypothesized that CXCL9 and/or CXCL10 induce adhesion of CXCR3+ effector Th1 lymphocytes to immobilized ICAM1 under flow conditions *in vitro,* as a potential mechanism involved in CXCR3+ T lymphocytes LV infiltration during TAC. A parallel plate flow chamber set up was used and PMA as a positive control of integrin activation that leads to increased T lymphocyte arrest to ICAM1 (191). As expected, PMA induced an increase of Th1 lymphocyte adhesion to ICAM1 (Figure 7.26A). Interestingly, both CXCL9 and CXCL10 induced an increase in T lymphocyte arrest to ICAM1 as compared to unstimulated T lymphocytes, regardless of the chemokine been directly incubated with the T lymphocytes or immobilized on the coverslip with ICAM1 (Figure 7.26B); this last condition is more physiologically relevant since it mimics the apical surface of the vessels that are sensed by the circulating T lymphocytes when they flow by. Moreover, CXCL9 induced a stronger effect on Th1 arrest on ICAM1 than CXCL10.

A.

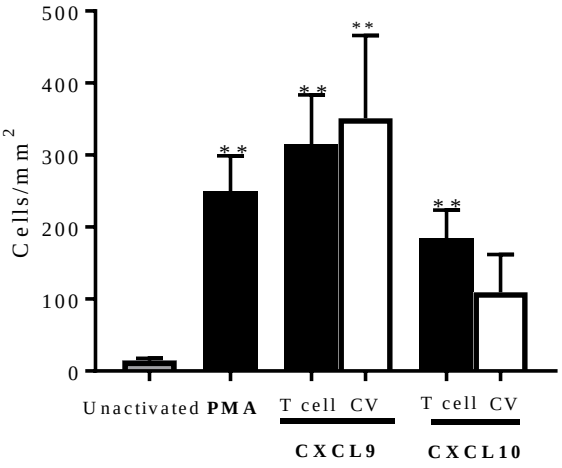

B.

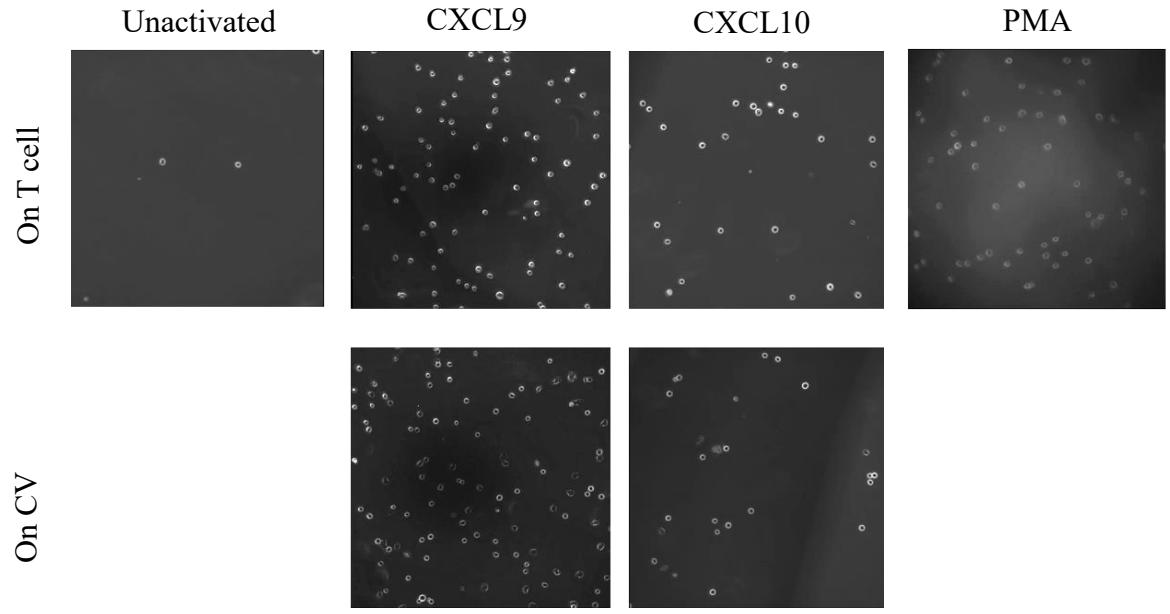

Figure 7.26 CXCR3 ligand mediated effector Th1 lymphocyte adhesion to ICAM1. 10^6 *in vitro* differentiated WT Th1 lymphocytes were flown in a parallel flow chamber (shear stress 1 dyne/cm^2) over 8µg of immobilized ICAM1. Th1 lymphocytes were incubated with either 50ng/mL of PMA for 5 minute at 37C or with 100ng/mL of either CXCL9 or CXCL10 for 5 minute at 37C, prior to the adhesion studies. When coverslips were treated, 2µg/mL of chemokine were added for 15 minutes at 37C. Six different fields of view were recorded for 1 minute. **A.** Bar graph indicating the number of lymphocytes per mm^2 adhered per condition at 1 dyne/cm^2 shear stress. Cells per field were counted, averaged per condition and divided by 0.13 to convert from cells/field to cells/mm^2.

Statistics compare the T lymphocytes activated conditions with the unactivated T lymphocytes data. Mean ± SEM of independent experimental replicates is represented.Statistics unpaired t-test. **B.** Representative pictures of Th1 lymphocytes adhesion to ICAM1 per condition.

In order to determine the LFA1 dependence of the chemokine mediated adhesion, we next incubated effector Th1 lymphocytes expressing CXCR3 with function blocking antibody to LFA1 (αLFA1). In all stimulation cases, either with PMA, CXCL9 or CXCL10, Th1 cell adhesion to ICAM1 was significantly diminished after αLFA1 treatment (Figure 7.27A). We then determined if the chemokine induced increase in adhesion to ICAM1 was due to an increase in LFA1 expression mediated by CXCR3 ligands. To test this, Th1 cells were incubated for 5 minutes with each chemokine, mimicking the treatment done for the adhesion studies under flow conditions. As expected, a short incubation of 5 minutes with the chemokine did not lead to a significant increase in LFA expression (Figure 7.27B), indicating that the observed effect in adhesion to ICAM1 is due to an increase of LFA1 affinity, as suggested by previous reports (192). Thus, this data indicate that CXCR3 ligands´ pro-adhesive properties to ICAM1 are dependent on integrin LFA1. Interestingly, CXCL9 mediated increase in Th1 addition to ICAM1 is higher than CXCL10. CXCL10 has been shown to have anti-fibrotic effects in MI that are independent of CXCR3 (110), and our *in vitro* data indicates that CXCL9-CXCR3 axis may potentailly be a more relevant chemokine in LV T cell infiltration and cardiac dysfunction *in vivo*.

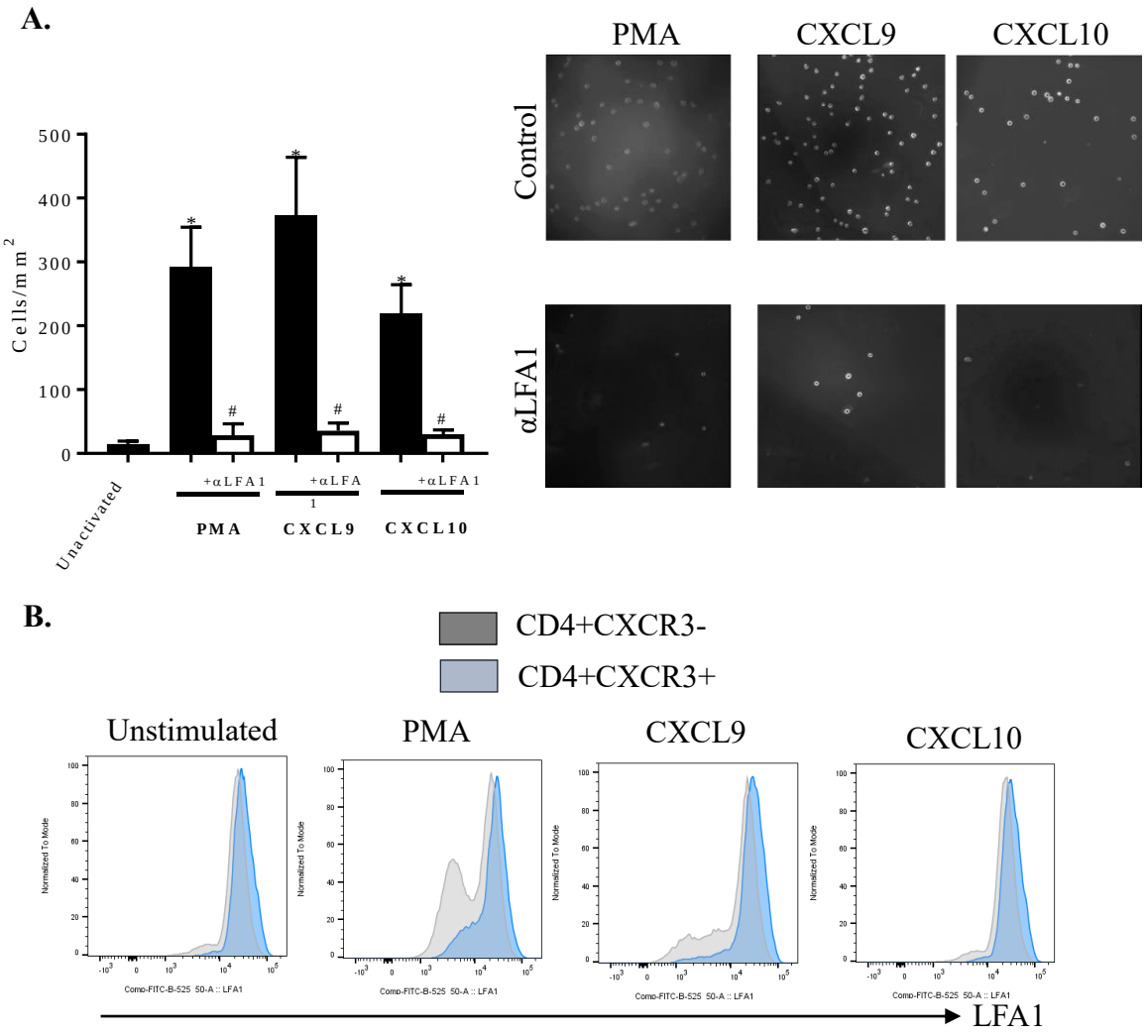

Figure 7.27. CXCR3 ligand mediated and LFA1 dependent effector T lymphocyte adhesion to ICAM1. 10^6 *in vitro* differentiated WT Th1 lymphocytes were flown in a parallel flow chamber over 8µg of immobilized ICAM1. Th1 lymphocytes were incubated with either 50ng/mL of PMA for 5 minute at 37C or with 100ng/mL of either CXCL9 or CXCL10 for 5 minute at 37C, prior to the adhesion studies. LFA1 blocking was done for 30 minutes at 37C using 40µg/mL αLFA1 (Biolegend M1714). Six different fields of view were recorded for 1 minute. **A.** Bar graph indicating the number of cells per mm^2 adhered per condition at 1 dyne/cm^2 shear stress. Cells per field were counted, averaged per condition and divided by 0.13 to convert from cells/field to cells/mm^2. Representative pictures of Th1 cell adhesion to ICAM1 per conditions indicated on the right. Statistics compare the (*) T cell activated conditions with the unactivated T lymphocyte data

and (#) T lymphocyte activated conditions with αLFA1 respectively. Mean ± SEM of independent experimental replicates is represented. Statistics unpaired t-test. **B.** Representative flow cytometry histograms showing LFA1 expression in Th1 cells after the indicated treatment conditions.

7.5 CRISPR/Cas9 mediated insertion of loxP sites flanking the mouse *icam1* gene

With the aim of studying *in vivo* gene functions and their role in disease, phenotypic characterization of the mutated genes of interest has widely been used in biomedical research. However, in some cases the genes of interest are expressed by a variety of cell types, with different role in each tissue, adding to the complexity of the interpretation of the phenotypic studies. In order to be able to determine the role of a specific gene expressed by an individual cell type, mice carrying tissue-specific gene mutations have been generated in recent years, enabling a more accurate understanding of the role of the gene of interest expressed by a particular cell type.

Thus, in line with the project described in Chapter 7.2, and with the aim of better understanding the role of ICAM1 expressed by different cell types in leukocyte activation and their recruitment into inflammed tissues, we started to develop a mouse with the *icam1* gene flanked by loxP sites. For this purpose, the CRISPR/Cas9 technology was used, as an alternative for successfull conditional gene targeting and thus modification of the mouse genome (193, 194). The CRISPR system (Clustered Regularly Interspaced Short Palindromic Repeats) is a bacterial antiviral defense mechanisms providing immunity against extrachromosomal genetic material (195). This bacterial immune system has three steps: acquisition of the foreign genetic material, synthesis of CRISPR RNA (single guide RNA, or sgRNA) followed by formation RNA-Cas nuclease protein complex, and target recognition and destruction of foreign genetic material mediated by Cas nuclease (196). The CRISPR/Cas9 based technology for targeted gene mutation in mice offers many advantages over traditional directed mutagenesis method, as lower cost, shorter developing time and the posibility to modify various genes simultaneously (Figure 7.28). Thus, we

decided to use this approach as a first step to create ICAM1 tissue specific knock out mice in the future.

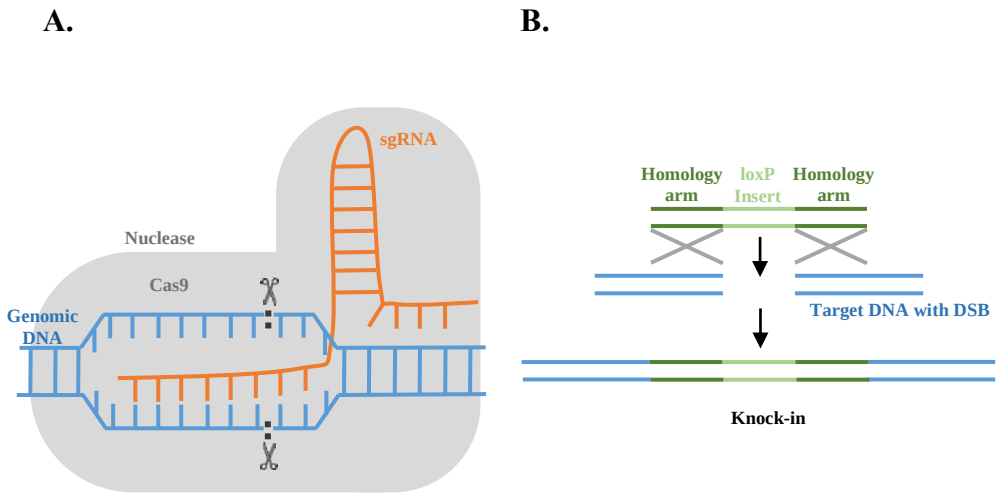

Figure 7.28. A. Cas9 unwinds the dsDNA allowing sgRNA to basepair with one strand and subsequently cleave both strands. **B.** Insertion of the loxP site in the targeted DNA break through homologous recombination.

7.5.1 sgRNA production and CRISPR/Cas9 validation

For the development of the loxP flanked ICAM1 mouse, the whole body ICAM1$^{-/-}$ was used as reference, which was the strain used in the project exploring the role of ICAM1 in ventricular leukocyte recruitment and pathological cardiac remodeling in HF (Chapter 7.2) (167, 170). This mouse consists on a *neo* casette inserted within exon 5 of the *icam1* gene. For the insertion of the loxP sites, the upstream (US) and downstream (DS) regions of exon 5 were targeted with specific sgRNA for each site (see Sections 6.2.3 and 6.2.4).

7.5.2 Genotyping founder pups

A total of 17 pups were born from the first microinjection (Section 6.2.4), from which none of the pups had the US site inserted, and just one has the DS loxP site inserted (Figure 7.29).

US expected bands:

- Expected Upstream wild-type band size: 1276bp
- Expected Upstream targeted integration band size: 1316bp
- Expected targeted integration RE digest cut bands: 252bp, 1064bp

DS expected bands:

- Expected Downstream wild-type band size: 869bp
- Expected Downstream targeted integration band size: 907bp
- Expected targeted integration RE digest cut bands: 272bp, 635bp

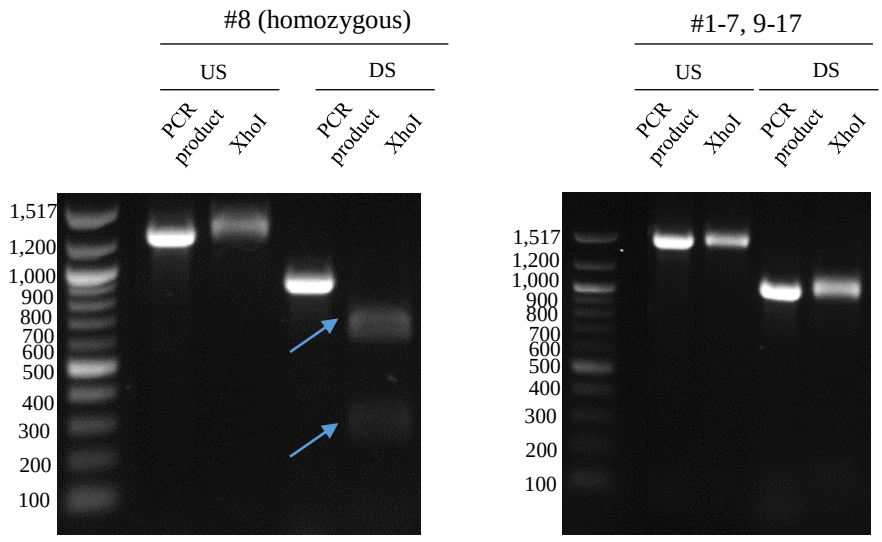

Figure 7.29. Electrophoresis gels of the PCR products and XhoI digested samples, showing on the left the mouse having an insertion in the DS region with the corresponding XhoI mediated cleavage

(pointed by blue arrow). On the right, a represenatative gel shows lack of insertion and digestion of the US and DS regions.

Based on the results obtained from the progeny (Figure 7.29), female mouse #8 was bred with a WT male in order to determine if the DS knock-in (KI) was germline transmited. From the first 17 mice born from this cross, two of them were heterozygous for the DS-KI (Figure 7.30), indicating that, despite in a low frequency, the DS insertion is germline trasmited.

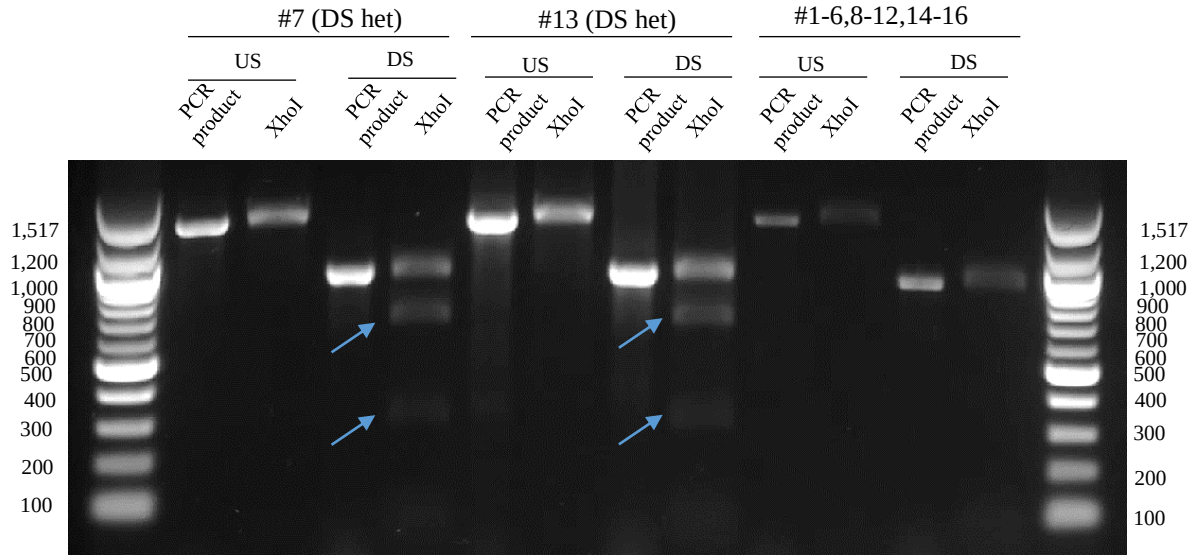

Figure 7.30. Electrophoresis gel of the PCR product and XhoI digested DS samples, showing the PCR product and the XhoI mediated cleavage of the offspring resulted from crossing female #8 (DS insertion) and a WT male. The DS insertion can be observed in the heterozygous mice #7 and #13 (blue arrow). Representative bands of mice without the DS insertion are shown on the right.

To date, the generation of the mouse containing the *icam1* flanked with loxP sites continues under development. For this aim, on one hand female mouse #8 that contains the DS-KI is still breeding with a WT male mouse, in order to microinject with the US sgRNA and respective oligonucleotide sequence any offspring that may carry the DS-KI. On the other hand, we have additionally consider and alternative approach consisting on miroinjecting a

single plasmid containing both the US and the DS loxP insertion sequences, which, if successfully recombined with the WT genome, will result in the mouse having both KIs. This alternative approach prevents any mutation as well as oligonucleotide digestion. Within the upcoming months, we expect to have further advances in the generation of the *icam1*$^{fl/fl}$ mouse.

8 DISCUSSION

In the present doctoral thesis dissertation, several mechanisms involved in T lymphocyte mediated pathological cardiac remodeling during HF have been investigated using a mouse model of non-ischemic HF induced by LV pressure overload (TAC). First, the role of T lymphocytes in cardiac hypertrophy, fibrosis, inflammation and dysfunction has been characterized using T lymphocyte deficient mice ($TCR\alpha^{-/-}$ mice). Second, we have identified ICAM1 as a critical adhesion molecule that regulates effector T lymphocyte recruitment to the LV after TAC using $ICAM1^{-/-}$ mice. Third, we have evaluated the mechanisms that induce ICAM1 expression in the endothelium and found that this is likely dependent on pro-inflammatory cytokine release and independent of EC-MR. Fourth, we have further characterized the role of EC-MR in pressure overload induced LV remodeling and HF. Lastly, we report that the chemokines CXCL9 and CXCL10 and their chemokine receptor CXCR3 are involved in T lymphocyte adhesion to ICAM1 and their cardiotropism to the LV during HF progression. While these findings significantly contribute to the knowledge of T cell mediated immune response and inflammation in the myocardium in non-ischemic HF, they also open new routes of exciting investigation that will shed more light into the role the adaptive immunity plays in HF. Thus, we have initiated the generation of a novel transgenic mouse that will allow investigating the role of ICAM1 expressed by different cell types both in HF progression as well as in other inflammatory diseases. Altogether, the present doctoral thesis work thoroughly investigates and characterizes the cellular and molecular mechanisms taking place during the adaptive immune response in pressure overload induced HF.

8.1 T lymphocyte mediated adaptive immune responses mediate pathological cardiac remodeling and heart failure

The initial studies evaluating the adaptive immune response taking place in non-ischemic HF identified CD4+ T lymphocyte recruitment into the LV as a detrimental contributor to pathological cardiac remodeling in HF. Thus, these findings support a model in which LV recruitment of effector T lymphocytes in response to pressure overload contributes to myocardial dysfunction, pathological remodeling, and ultimately HF, placing effector CD4+ T lymphocytes as a potential target for the prevention or treatment of this deadly syndrome (Figure 8.1).

8.1.1 Effector T lymphocytes are recruited into the LV in response to pressure overload leading to HF

T lymphocyte mediated immune responses targeting the myocardium have classically been associated to pathologies with an autoimmune component, in which T lymphocytes are found recruited in both humans and experimental mouse models (197). Recent evidence suggests that HF patients, with non-ischemic or non-infectious cause, present chronic systemic inflammation possibly mediated by T lymphocytes (198, 199). In line with this observation, we demonstrate for the first time that CD3+ T lymphocytes are recruited to the WT mice LV responding to pressure overload, unlike Gr1+ neutrophil and F4/80 macrophages. The antigens inducing this T lymphocyte immune response is still a subject of investigation. The possibility that T lymphocytes are activated by cardiac peptide antigens resulting from cardiac cell death, as it has suggested in response to myocardial infarction (200) is unlikely, given that TAC does not induce significant CM apoptosis 4 weeks and even 8 weeks after TAC (201), and

we found T lymphocytes infiltrated in the LV as early as 2 weeks post TAC, when cardiac cell death is not evident. Thus, LV pressure overload could disrupts the myocardial immune tolerance allowing self-cardiac antigens to induce a T lymphocyte mediated immune response, similar to what has been described in autoimmune myocarditis (202). Such self-cardiac antigens may include α-myosin, which is neither expressed in the thymus, nor negatively selected by clonal deletion (203), nor positively selected by α- myosin–specific natural T regulatory cells. An alternative possibility is that T lymphocyte activation and infiltration in the heart occurs in a non-specific and antigen-independent manner, through alarmin signals (204, 205). Our data supports a role for activated T lymphocytes in pathological cardiac remodeling and HF, but how T lymphocytes become activated in such context requires further investigation.

Although we and others have also found that in addition to T lymphocytes, $CD11b^{+}$ myeloid cells are recruited to the LV in response to TAC (74) , the F4/80+ macrophage counts were found to be similar in TAC and Sham operated mice, therefore leading to the conclusion that the macrophages in the LV may not be fully activated. Among the CD4+ T lymphocytes infiltrated into the LV, both IFNγ and Tbet, the signature cytokine and transcription factor of Th1 lymphocytes, were found upregulated four weeks after TAC. These markers are also expressed by other immune cell types and therefore are not exclusive of Th1 lymphocytes (206), but given that neither IFNγ not Tbet were found upregulated in $TCR\alpha^{-/-}$, it suggests that Th1 lymphocytes may be the main subset of T lymphocytes recruited in the LV, potentially impacting the function of cardiac resident cells via IFNγ (207). Further adoptive transfer studies of T lymphocytes subsets into $TCR\alpha^{-/-}$ mice are needed to define the specific T lymphocyte subset that infiltrate the LV and may be responsible for cardiac dysfunction. Altogether, these data suggest on one hand, that in response to pressure

overload self-cardiac antigens are presented to the T lymphocytes in the mediastinal lymph nodes that drain the heart, inducing T lymphocyte activation. Once activated, T lymphocytes are recruited to the LV where they release pro-inflammatory cytokines as TNFα and IFNγ, and DAMPS that could potentially contribute to further leukocyte recruitment and cardiac dysfunction.

8.1.2 T lymphocyte mediated immune response is necessary for pathological cardiac remodeling and HF

The potential association between activated T lymphocyte LV infiltration and cardiac function worsening was analyzed and proved in the studies using TCRα$^{-/-}$ mice, which showed lack of pathological cardiac remodeling, including cardiac hypertrophy, fibrosis, and function in response to TAC. The role of CD4+ T lymphocytes in pressure overload induced HF was also studied by others using different genetic T lymphocyte deficient mouse strains, including recombination activating gene 2 null mice (*Rag2*$^{-/-}$) and the major histocompatibility complex II knock out (*MHCII*$^{-/-}$), both proving blunted adverse cardiac remodeling and preserved LV function after six week TAC (175). In those studies, Laroumanie et al. demonstrated that CD4+ T lymphocyte systemic activation in the cardiac draining lymph nodes is essential for T lymphocyte mediated immune response observed in response to pressure overload (175). Our studies using TCRα$^{-/-}$, a different strain of T lymphocyte –deficient mice, and subjecting them to 4 week TAC both confirm the importance of T lymphocytes in adverse remodeling and HF, and also demonstrate for the first time that T lymphocyte LV recruitment occurs as early as 2 weeks post TAC in WT mice, suggesting a much earlier T lymphocyte activation contributing to HF progression. Unlike Laroumanie et al., cardiac function studies were also performed in the current work through invasive

hemodynamic pressure-volume loops in TCR$\alpha^{-/-}$ mice and importantly implicated T lymphocytes in diastolic HF (determined by the parameter dP/dt_{min}), a clinical condition for which there are no treatments available to date. Thus, the protected systolic and diastolic cardiac function phenotype resulted in 100% survival in TCR$\alpha^{-/-}$. Together with the lack of an LV pro-inflammatory milieu observed in T lymphocyte deficient mice, these studies support a mechanism in which cytokine production by infiltrated activated T lymphocytes have a negative effect in LV function and survival in response to TAC. Altogether, our data provide evidence that activated T lymphocytes and their infiltration to the LV are essential regulators of pathological cardiac remodeling in HF in the setting of pressure overload induced by TAC.

8.2 ICAM1 regulates T lymphocyte recruitment to the left ventricle and maladaptive cardiac remodeling in heart failure

We next sought to decipher how T lymphocytes are recruited to the LV, with the aim of potentially preventing cardiac dysfunction by blocking LV T lymphocyte recruitment. Given that we previously showed that the mRNA levels of ICAM1, VCAM1 and E-Selectin are upregulated in response to TAC, and the well stablished literature highlighting a link between ICAM1 and chronic HF and immune cell infiltration (72, 74), we hypothesized that ICAM1 mediates leukocyte infiltration into the LV after TAC and therefore contributes to cardiac remodeling and dysfunction. Our data support a model in which LV pressure overload initially results pro-inflammatory cytokine release by cardiac resident cells that induces endothelial ICAM1 upregulation, which promotes later leukocyte recruitment to the LV in response to TAC. In the absence of ICAM1, leukocyte recruitment, cardiac inflammation and fibrosis are significantly

diminished, resulting in improved cardiac function as compared to WT mice. Therefore, these studies position ICAM1 as a critical player in pressure overload induced HF.

8.2.1 ICAM1 upregulation by myocardial endothelial cells is necessary for pro-inflammatory leukocyte recruitment into the LV

It has thoroughly been characterized over the last decades the fact of ICAM1 being a central regulator of both leukocyte adhesion to ECs and subsequent transendothelial migration that allow leukocyte infiltration into tissues in a variety of cardiovascular diseases (145, 179, 208). In the human myocardium, endothelial ICAM1 expression is found increased after myocardial infarction (MI), associated with high infiltration of inflammatory leukocytes (172). We and others have demonstrated that endothelial cell ICAM1 is upregulated in the onset of pressure overload induced by either TAC or suprarenal abdominal aortic constriction in rodents, correlating with increased cardiac inflammation and T lymphocyte infiltration to the LV (74, 174, 209). These data corroborated by different authors led us to hypothesize that ICAM1 mediates T lymohocyte recruitment to the LV during pathological cardiac remodeling in HF. Our data demonstrates that endothelial ICAM1 expression two and four weeks after inducing LV pressure overload correlates with a highly pro-inflammatory cytokine milieu that can result in intramyocardial endothelial cell activation and T lymphocyte infiltration to the LV. Moreover, we demonstrate that endothelial ICAM1 expression is upregulated as early as 48h after TAC, which precedes LV leukocyte infiltration (174).

Our studies using quantitative flow cytometry indicate for the first time that Ly-6C^{high} pro-inflammatory monocytes, known to play a role in cardiac remodeling after MI (210, 211), also get recruited to the LV together with T lymphocytes in response to 4 weeks TAC. These results are in line with a recent report that suggests Ly6C^{hi} monocytes play

a role in maladaptive cardiac remodeling 3 weeks after TAC whereas Ly6C^{low} participate in early adaptive cardiac remodeling to TAC (212). We furthermore demonstrate that pro-inflammatory leukocyte recruitment into the LV is an ICAM1 dependent process and positions ICAM1 as an important contributor to cardiac inflammation, likely contributing to HF progression in this model of pressure overload induced HF (Figure 8.1).

8.2.2 ICAM1 expressed in antigen presenting cells is not essential for T lymphocyte activation in response to LV pressure overload

Even though ICAM1 was originally cloned from ECs, it is today known that it is also expressed by essentially all leukocyte subsets (213). Among these leukocytes, several antigen presenting cells (APC) could be mentioned, in which ICAM1 functions as an accessory molecule in the immune synapse in the presentation of specific antigens (214). Therefore, ICAM1 expressed in non-endothelial cells likely contributes as well to the phenotype of the ICAM1$^{-/-}$ mice. However, our data support that ICAM1 expressed by APC is not essential in T lymphocyte activation in response to TAC, as they get activated similarly in the cardiac draining mediastinal lymph nodes of WT and ICAM1$^{-/-}$ mice in response to pressure overload. It is still unclear whether T lymphocyte activation in response to TAC is antigen dependent or independent or which antigens activate T lymphocyte responses in case of being an antigen-dependent response (174, 175). However, our data support that whichever antigens are involved in this response do not require ICAM1 in the immune synapse for optimal presentation to achieve T lymphocyte activation. In addition, the similar frequencies of blood circulating CD4+ T lymphocytes in Sham WT and ICAM1$^{-/-}$ mice are in agreement with the initial description of ICAM1$^{-/-}$ mice indicating no differences in circulating T cells as

compared to WT mice (167). Furthermore, the percentages of circulating CD4+ T lymphocytes were also similar between WT and ICAM1$^{-/-}$ mice after TAC, supporting the concept that the reduced LV T lymphocyte infiltration observed in ICAM1$^{-/-}$ mice is not due to a defect in T lymphocyte activation due to APC expressed ICAM1, but rather due to a defect in LV T lymphocyte infiltration mediated by endothelial ICAM1.

8.2.3 ICAM1$^{-/-}$ mice are protected from pathological cardiac hypertrophy, fibrosis and myocardial inflammation in response to TAC

ICAM1$^{-/-}$ mice develop LV hypertrophy but not fibrosis, systolic and diastolic dysfunction in response to TAC, supporting the possibility that ICAM1 promotes pathological cardiac hypertrophic mechanisms, whereas its deletion is sufficient to retain a compensatory physiological hypertrophic phenotype during pressure overload. This possibility is supported by the lack of upregulation of fetal or pathological gene expression pattern, including atrial and brain natriuretic peptides (ANP and BNP) and myosin heavy chain β observed in ICAM1$^{-/-}$ mice after TAC (173, 215). In addition, cardiac myocytes isolated from mice lacking ICAM1 in response to 4 week pressure overload are smaller in length and width dimensions than WT cardiac myocytes, suggesting the previously unknown role for ICAM1 in cardiac hypertrophy. This role could be directly associated with infiltrated LV T lymphocytes, since we and others have shown that T lymphocyte deficient mice do not develop cardiac hypertrophy in response to TAC (Chapter 7.1) (174, 175). We speculate that in ICAM1$^{-/-}$ mice the few T lymphocytes that infiltrate the LV can still contribute to hypertrophy by secreting pro-hypertrophic mediators such as angiotensin II (216). Interestingly, when investigating further cardiac remodeling features, we observe blunted LV interstitial and perivascular fibrosis in response to TAC. Our *in vitro* data demonstrate that ICAM1 expressed in

bone marrow derived monocytes and cardiac fibroblasts is not required for their transition to pro-fibrotic macrophages or myofibroblasts, respectively. Taking together, our data support that the lack of fibrosis in ICAM1$^{-/-}$ mice *in vivo* is due to lack of cardiac endothelial ICAM1 that reduces T lymphocyte infiltration which is necessary for cardiac fibrosis during HF progression. However, we cannot determine the role for non-EC ICAM1 *in vivo* and this possibility will require further investigation in tissue specific ICAM1 deficient mice, which we are currently working on developing (Chapter 7.5). Alternatively, soluble ICAM1 (sICAM1) which results from matrix metalloproteases (MMPs) and elastases cleavage of membrane bound ICAM1 (213) could contribute as well to cardiac inflammation in response to TAC by acting on beta-2 integrins of infiltrated leukocytes and inducing their pro-inflammatory actions, as described in a model of lung injury (217). sICAM1 has also been shown to bind to unknown receptors in the central nervous system and trigger Src activation (218), and Src, p38 MAPK and ERK-1/2 which are involved in cardiac hypertrophy and fibrosis (219-221). Therefore, sICAM1 could function through similar mechanisms in cardiac resident macrophages (by engaging beta-2 integrins) and in other cardiac resident cells (by engaging an unknown receptor) in the onset of pressure overload and hemodynamic stress, contributing to signaling cascades that result in adverse cardiac remodeling, in addition to membrane bound ICAM1 engagement by infiltrated LV leukocytes. These actions of sICAM1 require further investigation and are highly significant clinically, since sICAM1 is significantly increased in plasma of HF patients (222).

8.2.4 ICAM1$^{-/-}$ mice have improved cardiac function in response to TAC as compared to WT mice

Our echocardiography cardiac function results demonstrate that despite ICAM1$^{-/-}$ mice having a slight increase in end diastolic diameter (EDD) in response to TAC, and thus a decrease in Fractional Shortening (FS) as compared to Sham, these values are within the healthy myocardium range and are significantly different from those of WT. Our results are in agreement with a recent study in which treatment of WT mice with an ICAM1 function blocking antibody resulted in increased FS as compared to mice treated with control antibody in response to two weeks TAC (209). Furthermore, our detailed pressure-volume loop hemodynamics analyses demonstrate that both the systolic and diastolic functions, determined by dP/dt_{max} and dP/dt_{min} respectively, remain preserved in ICAM1$^{-/-}$ in the onset of TAC. One mechanism for preserved cardiac function phenotype in ICAM1$^{-/-}$ mice is explained by the lack of interstitial fibrosis as a result of a decreased LV leukocyte infiltration. Interestingly, ICAM1 has been found to be expressed in human, dog and rat cardiac myocytes (145, 172, 223) and shown to adhere to neutrophils via Mac-1 in *in vitro* experiments leading to an impaired cardiac myocyte contractility and cardiac myocyte oxidative injury (224, 225). Given the complete preservation of contractility and relaxation functions in ICAM1$^{-/-}$ mice in response to TAC, we speculate that ICAM1 expressed by cardiac myocytes may adhere to LV infiltrated leukocytes and trigger signals that lead to an impaired cardiac myocyte function. This hypothesized mechanism, however, requires further investigation, ideally using cardiac myocyte specific ICAM1$^{-/-}$ mice (ICAM1$^{flox/flox}$ x Myh6-Cre).

8.2.5 Pro-inflammatory cytokines released by cardiac resident cells after TAC induce intramyocardial endothelial cell ICAM1 upregulation

Deciphering the mechanisms and/or molecules that induce the upregulation of endothelial ICAM1 represent an important avenue in our understanding of the contribution of ICAM1 and pro-inflammatory leukocyte recruitment to pathological cardiac remodeling and failure. The mineralocorticoid receptor (MR) is engaged by the hormone aldosterone which is found elevated in serum of humans with HF and in animal models of HF induced by aortic constriction (226-228). Aldosterone is known to induce ICAM1 upregulation in human coronary artery endothelial cells *in vitro* through its actions via EC specific MR signaling (96). Despite, our results demonstrate that ICAM1, IL-1β and IL-6 LV levels as well as LV CD4+ T lymphocyte and $CD11b^{+}$ myeloid cell infiltration are similarly induced in EC-$MR^{-/-}$ and EC-$MR^{+/+}$ in response to TAC, suggesting that ICAM1 is upregulated independently of endothelial MR signaling in the onset of LV pressure overload (157, 229). Altogether, our data support that EC-ICAM1 gets upregulated in response to the pro-inflammatory cytokines IL-1β and IL-6, previously shown to be expressed by cardiac resident cells under stress (157, 230), and also known to mediate EC activation (180).

Collectively, our investigations demonstrate for the first time that ICAM1 is necessary for pressure overload induced cardiac inflammation, fibrosis, and the resulting cardiac dysfunction and HF (Figure 8.1). Our data supports an ICAM1 dependent mechanism through which effector T lymphocytes are recruited into the LV in response to pressure overload perhaps due to pro-inflammatory cytokine expression by cardiac resident cells that activate the cardiac endothelium and increase ICAM1 expression. This understanding supports the potential to target ICAM1 mediated T lymphocyte

recruitment into the LV to improve the function of the failing heart. Future studies using tissue specific ICAM1 deficient mice under development (Chapter 7.5) will explore whether ICAM1 expressed in other cell compartments in the myocardium in addition to EC also contributes to maladaptive cardiac remodeling in HF.

8.3 Endothelial cell mineralocorticoid receptor contributes to systolic dysfunction in pressure overload induced cardiac remodeling

With the aim of fully characterizing the role of EC-MR in vascular activation, leukocyte LV recruitment and cardiac remodeling in HF, the initial studies indicated in Figure 7.15 were expanded, using EC-MR$^{-/-}$ mice and the well-established mouse model of HF induced by TAC. Overall, our study demonstrates for the first time that EC-MR does not impact systolic function during homeostasis but contributes to the development of systolic dysfunction in response to LV pressure overload induced by TAC. EC-MR$^{-/-}$ mice display decreaments in some indices of systolic dysfunction after TAC, and develop an adaptive pattern of reduced natriuretic peptide, endothelin receptor B and TNFα LV gene expression, compared with EC-MR$^{+/+}$ TAC mice. However, the EC-MR$^{-/-}$ mice develop similar cardiac hypertrophy as EC-MR$^{+/+}$, and displayed similar pathologic features that include LV MHC isoform switching, LV fibrosis, LV ICAM1, IL-1β and IL-6 cytokine expression, and LV leukocyte infiltration as EC-MR$^{+/+}$ littermates in response to TAC (Figure 8.2). These findings unveil a novel role for MR in the vascular endothelium in contributing to systolic dysfunction and cardiac remodeling in response to pressure overload.

MR antagonists reduce mortality for patients with HF with depressed ejection fraction (90-92). Despite the clinical benefit of MR antagonists, their specific cellular target(s)

and the precise mechanism for these benefits have not yet been fully uncovered. A meta-analysis of randomized clinical trials revealed that pharmacological blockade of MR has beneficial effects on cardiac remodeling and improves parameters of LV function in HF patients (231). Delineating the precise tissues through which MR modulates these effects has been an area of active investigation and overall suggests that MR signaling in different cell types plays distinct roles. While overexpression of MR generally induces spontaneous development of classical features of HF such as cardiac hypertrophy and fibrosis (232, 233), cell specific deletion of MR has provided variable results depending on the cell targeted and the HF model used. For example, MR deletion in CM did not affect cardiac hypertrophy or fibrosis in response to TAC but resulted in improved systolic function. This was in contrast to selective MR deletion in CFB, which did not have any beneficial effect (181). The data in Chapter 7.3 indicate that deletion of EC-MR does not affect systolic function during homeostasis, but contributes to the development of systolic dysfunction and to some aspects of cardiac hypertrophy without modulating cardiac fibrosis or diastolic dysfunction in response to TAC. This outcome is similar to the findings in CM specific MR deficient mice, and supports that MR in EC and in CM regulates other aspects of pressure overload-induced HF that are independent of these maladaptive cardiac remodeling features classically associated with the pathology of HF. These findings also raise the possibility that the benefits of MR antagonists in patients with cardiac dysfunction may arise independently of effects on cardiac fibrosis and hypertrophy.

8.3.1 Lack of EC-MR does not affect LV EC activation and leukocyte recruitment after TAC

The findings indicating that EC-MR deletion did not affect LV EC activation and leukocyte recruitment after TAC were unexpected for several reasons. Prior work from our group and others demonstrated that EC-MR regulates ICAM1 expression, which contributes to leukocyte adhesion to EC, a necessary step for cardiac leukocyte infiltration. Moreover, we and others have recently demonstrated that T lymphocytes are necessary for cardiac inflammation, hypertrophy and fibrosis in HF induced by TAC, as T lymphocyte deficient mice are protected from these cardiac responses to pressure overload (Chapter 7.1) (174, 175). In the present study, we proposed the straightforward hypothesis that EC-MR contributes to cardiac remodeling by promoting cardiac T lymphocyte infiltration, inflammation, and fibrosis. However, our findings support that EC-MR in fact does not mediate TAC-induced leukocyte infiltration and fibrosis, but rather that MR in other cell types regulate these processes. These unexpected findings therefore provide novel insights into the specific processes regulated by EC-MR in HF.

The findings indicated in the present dissertation are especially relevant in light of previous studies in which the Tie2 promotor drove MR deletion in both the EC and leukocyte lineages. For example, mice with MR deleted from both EC and leukocytes have decreased cardiac inflammatory infiltration and fibrosis in response to deoxycorticosterone/salt-induced hypertension (101). The lack of complete inflammatory attenuation in our selective EC-MR deletion model, compared with the reduction in these processes in the above combined EC and leukocyte deletion model supports that MR regulates these phenotypes through its function in leukocytes, rather

than in ECs. It is not clear whether the low expression of MR in T lymphocytes (234) is sufficient to mediate such an effect, but one could speculate that this could be a potential mechanism. Additionally, we found that CD11b+ monocytes also infiltrated the LV of EC-MR$^{-/-}$ mice in similar numbers as in their WT littermates exposed to TAC. Given the critical role of monocyte/macrophage MR in promoting macrophage polarization to the pro-inflammatory M1 phenotype and in the development of cardiac fibrosis in two separate models of hypertension-induced cardiac remodeling (98, 235), these data support the notion that EC-MR does not regulate cardiac fibrosis, but rather that MR in leukocytes infiltrating into the LV mediate this pro-fibrotic effect. Indeed, we demonstrate that leukocyte infiltration in perivascular areas co-localize with perivascular fibrosis in EC-MR$^{-/-}$ and EC-MR$^{+/+}$ mice. It has previously been demonstrated that EC-MR signaling is required to induce upregulation of ICAM1 and leukocyte adhesion to human coronary endothelial cells *in vitro* (96), however this was not the case *in vivo* in response to TAC (170). Here we confirm that ICAM1 is upregulated in response to TAC independent of EC-MR *in vivo* and additionally report, for the first time to our knowledge, that the production of the pro-inflammatory cytokine TNFα is prevented in the LV of mice lacking EC-MR. The lack of TNFα induction in the LV of EC-MR$^{-/-}$ in response to TAC can partially explain the amelioration of systolic function in an MR EC specific way, in line with studies where MR antagonism reduces plasma TNF levels in rodent models of ischemic HF (236, 237). This may also imply that TNFα in the LV is in part produced by EC in response to MR signaling thereby negatively regulating CM function and inducing systolic dysfunction. These data additionally suggest the possibility that IL-1β and/or IL-6 may be responsible for inducing ICAM1 upregulation in the LV independently of MR signaling in HF (71, 180).

8.3.2 EC-MR contributes to systolic dysfunction in response to TAC

It is striking that although EC-MR$^{-/-}$ and EC-MR$^{+/+}$ mice subjected to the same LV pressure overload developed similar cardiac fibrosis, which is intimately associated with pathological cardiac remodeling and cardiac dysfunction, EC-MR$^{-/-}$ mice displayed an ejection fraction and fractional shortening very similar to Sham operated EC-MR$^{-/-}$ mice and preserved as compared to EC-MR$^{+/+}$ mice exposed to TAC. In contrast, other parameters of LV function and structure were similar in both genotypes. Therefore, these data suggest that EC-MR deletion selectively preserves systolic function during pressure overload yet does not affect other pathologic mechanisms mentioned above. One possibility is that the improved phenotype of EC-MR$^{-/-}$ mice arises from an improved aortic compliance as a consequence of the lack or EC-MR. However, this hypothesis is unlikely because effective arterial elastance did not differ between EC-MR$^{+/+}$ and $^{-/-}$ littermates after TAC (Table 7.3). The possibility of EC-MR regulating CM apoptosis is also unlikely, as 4 weeks TAC does not induce significant apoptosis in EC-MR$^{+/+}$ and $^{-/-}$ mice in line with what has been reported in WT mice (174, 201). Alternatively, EC-MR may contribute to the cardiac functional response to pressure overload by modulating coronary blood flow. It was recently reported that EC-MR contributes to vascular contractile function particularly in the coronary vasculature. Specifically, EC-MR deletion attenuated coronary vasoconstriction in response to endothelin-1 (168), which is increased in HF (238, 239). Thus, an intriguing possibility is that EC-MR mediates endothelin-1-induced vasoconstriction of coronary vessels in TAC mice through the upregulated ETB, thereby contributing to impaired systolic function. If so, the lack of EC-MR may preserve coronary flow by preventing coronary vasoconstriction mediated by endothelin-ETB interaction and therefore contributing to

the maintenance of the ejection fraction. The data indicating that the expression of ETB is not induced by TAC in the LV of EC-MR$^{-/-}$ mice is in support of this mechanism. This concept correlates with recent reports demonstrating that SMC-MR contributes to coronary dysfunction in mice subjected to experimental myocardial infarction (240), that overexpression of MR in CM impairs coronary vasodilation (241), and also consistent with clinical data demonstrating that MR blockade improves coronary vascular function in patient with diabetes (242). However, since coronary function was not evaluated in these studies, this potential mechanism remains speculative and future studies are needed to test this novel hypothesis. Besides this, there are some other limitations to consider in this study. First, evidence from animal models and HF patients treated with MR antagonists support a contribution of the aldosterone-MR axis in both systolic and diastolic dysfunction (90-92, 243). Because EC-MR$^{-/-}$ are mainly protected from systolic dysfunction, MR expressed by other cell types could be the mediator of diastolic dysfunction, however, this possibility has not been evaluated in mice with multiple genetic deficiency of MR in other cells besides EC in the context of TAC. Thus, additional studies are needed to characterize the role of EC-MR in conjunction with MR expressed in other cells types.

In conclusion, this study reveals that EC-MR contributes to LV systolic dysfunction in response to pressure overload induced HF without affecting cardiac fibrosis or hypertrophy (Figure 8.2). Despite a known role for EC-MR in promoting inflammation, and a role for inflammation in progression of HF, EC-MR deletion also did not impact pro-inflammatory leukocyte recruitment in the TAC model of HF. These results, together with the growing body of literature evaluating MR signaling in other cell types involved in HF, enhance the global understanding of the role of MR in the development

of HF. These findings further suggest that some of the beneficial effects of MR antagonists in improving cardiac function and preventing mortality in HF patients could be independent of effects on cardiac hypertrophy or fibrosis.

8.4 CXCR3 mediates effector T lymphocyte cardiotropism and left ventricular recruitment during heart failure development

Increased numbers of CXCR3+ T lymphocytes in circulation as well as elevated levels of circulating chemokine ligands have been suggested as biomarkers and thus predictors of HF progression (139, 186). In this chapter we focused on the better understanding of the T lymphocyte CXCR3-endothelial ICAM1 axis contribution to T lymphocyte cardiotropism during the progression of HF.

Of interest, CXCR3 is mainly expressed by Th1 effector lymphocytes since its expression is regulated by transcription factor Tbet, which was found upregulated in the LV 4 weeks after TAC in our initial studies (Figure 7.1). Additionally, extensive literature indicates a direct link between CXCR3 activation by ligand engagement and increase in LFA1 affinity to ICAM1 (192, 244, 245), which we have found to be critical in T lymphocyte recruitment and pathological cardiac remodeling in HF (Chapter 7.2.).

8.4.1 Locally produced IFNγ and TNFα associated with CXCL9 and CXCL10 release in the LV contribute to CXCR3+ T lymphocytes cardiotropism

Our studies indicate that cytokines IFNγ and TNFα are released in the LV *in vivo*. *In vitro* findings using monocytes co-cultured with CD4+ T lymphocytes indicate that CXCL9 and CXCL10 depend non-linearly on both IFNγ and TNFα levels (246). We speculate that both cardiac resident cells and also LV recruited leukocytes release IFNγ

and TNFα in response to 2 and 4 weeks TAC, which in turn induce CXCL9 and CXCL10 production that target effector T lymphocyte recruitment to the LV in a temporal manner as HF progresses, since we observe CXCR3+ T lymphocyte LV infiltration at the same time points in which CXCL9 and CXCL10 are found upregulated in the LV but not before that. Several cardiac resident cells may the potential source of these chemokines, including cardiac fibroblasts or monocytes as previously described in the DOCA/Salt hypertension rodent model for CXCL9 (99).

Simultaneously, T lymphocytes expressing CXCR3 were found expanded in the cardiac draining lymph nodes as early as 1 week after TAC, and were further found expanded over time, suggesting that T lymphocytes are continuously being primed in the cardiac draining lymph nodes after the initial stimulation after 1 week TAC. Of note, CXCR3+ T lymphocytes showed significantly higher levels of the integrin LFA1, ICAM1's main ligand in T lymphocytes. This interesting finding suggests that in addition to CXCR3 signaling regulating integrin activation (192, 244) in the setting of TAC it can regulate LFA1 expression. The mechanisms of how this signaling takes place remain to be investigated.

Opposite to humans diagnosed with HF where circulating CXCR3+ T lymphocyte levels are found increased (247), CXCR3 levels of circulating T lymphocytes were found unchanged in TAC mice. However, CXCR3+ T lymphocytes still expressed higher levels of LFA1 when compared to CXCR3- circulating T lymphocytes, indicating that the CXCR3+ T lymphocytes that left the cardiac draining lymph nodes following their chemokine ligand gradient, still kept and increased probability of getting recruited into the LV through ICAM1.

8.4.2 CXCR3+ and LFA+ T lymphocytes are recruited into the LV and contribute to Tbet upregulation in the myocardium after TAC

The time points in which CXCL9 and CXCL10 expression was found upregulated in the LV, 2 and 4 week post-surgery, correlated in time with both CXCR3+ and LFA1+ CD3+ T lymphocyte infiltration, when pathological cardiac remodeling has been described to take place (174, 175). Our observation that CXCR3+ T lymphocytes infiltrate the LV 2 weeks after TAC suggest that it takes at least one week from the priming and expansion of CXCR3+ T lymphocytes in the cardiac draining lymph node until their recruitment in the LV. These T lymphocytes express adhesion molecules such as LFA1 whose affinity towards ICAM1 is enhanced when CXCL9 and CXCL10 are upregulated in the LV (2 weeks), allowing CXCR3+ T lymphocyte adhesion to ICAM and LV infiltration. Indeed, integrin blocking in mice undergoing TAC has been shown to reduce cardiac inflammation and dysfunction (209). Others have shown that the axis CXCL10-CXCR3 expressed in CFB does not play a role in cardiac remodeling after MI, since CXCL10 mediated anti-fibrotic effects are CXCR3-independent (110); however that study did not evaluate T lymphocytes specifically. Our data suggests that CXCR3 could potentially be blocked with no effects in CXCL10 regulated anti-fibrotic effects, but with significant differences in T lymphocyte infiltration.

Interestingly, the LV expression of Tbet, the signature transcription factor of Th1 lymphocytes and regulator of CXCR3 expression was significantly increased in these same time points in the LV. One could speculate that TAC induced myocardial remodeling is an immune condition in which the tolerance towards self-antigens has been disrupted. The kinase mammalian target of rapamycin (mTOR) configures cellular metabolism and regulates cytokine release, antigen presentation and cell migration,

among other functions (248). mTOR has been described as a regulator of Tbet and CXCR3 expression under T cell inactivation or tolerance, and therefore mTOR, Tbet and CXCR3 levels are low when immune tolerance is present and high when disrupted, as potentially in the TAC model (249). In line with LV Tbet expression, it must be mentioned that not only T lymphocytes express this transcription factor. Indeed, Tbet expression at early time points after TAC, 48h and 1 week, could correspond to newly recruited or cardiac resident DCs responding to IFNγ stimulation, as previously described (206). The additional increase in Tbet LV expression at later time points, from 2 weeks on, could be directly associated to Th1 lymphocytes (Figure 7.24). Whether the observed increased levels of Tbet and CXCR3 are a result of Th1 cardiotropism towards CXCL9 and/or CXCL10 expressed in the myocardium, a result of mTOR disregulation, or both, are possibilities that require further investigation.

8.4.3 CXCL9 and CXCL10 induce an increase in T lymphocyte adhesion to ICAM1 through an increase in LFA1 affinity but not its expression

In the *in vitro* adhesion studies performed, we observed that both CXCL9 and CXCL10 induce an increase of LFA1 dependent CXCR3+ Th1 lymphocyte adhesion to immobilized ICAM1. As indicated by others (192), this increase in T lymphocyte interaction with ICAM1 was due to an increase in LFA1 affinity in the presence of CXCL9 and CXCL10, with no change in its expression. Our results further indicate that even though both CXCL9 and CXCL10 induce LFA1 dependent Th1 arrest to ICAM1, CXCL9 is a stronger inducer. Thus, our studies indicated that CXCR3 and its ligands, particularly CXCL9, could be potentially targeted in order to reduce effector T lymphocyte recruitment into the LV, and therefore prevent pathological cardiac

remodeling. These findings, if confirmed *in vivo*, will be novel since the role of CXCL9, in contrast to CXCL10 (110), has not been evaluated in HF models.

Altogether, our studies describe a novel CXCL9/10-CXCR3-LFA1-ICAM1 axis being involved in effector T lymphocyte chemotaxis and recruitment into the LV in response to TAC, which could potentially be targeted in order to reduce od prevent pathological cardiac remodeling and HF (Figure 8.1).

8.5 CRISPR/Cas9 mediated insertion of loxP sites flanking the mouse *icam1* gene

As an effort for a better understanding the role of cell specific ICAM1 in leukocyte recruitment and pathological cardiac remodeling in pressure overload induced HF, and with the aim of contributing to the inflammatory disease and immune cell recruitment field, we decided to generate the first mouse to our knowledge containing the ICAM1 gene flanked with loxP sites. For this purpose, we considered the CRISPR/Cas9 mediated gene editing technology as the optimal one in order to generate the new transgene mouse efficiently, in a short period of time and having the least off-target mutations possible.

Thus, the strategy we chose consisted on a single injection of fertilized oocytes containing the srRNAs targeting both the upstream (US) and downstream (DS) regions of the ICAM1 gene, together with Cas9 and the loxP sites containing oligonucleotide sequences. This initial strategy did not result optimal since none of the mice offspring from the treated oocytes contained the US knock in (KI), and just 5% of contained the DS site insertion. The lack of US site insertion could be due to a degradation of the sgRNA by the Cas9 enzyme within the injection cocktail due to its endonuclease

capacity, which once injected would have prevented the recognition and subsequent excision of the target genomic site. Additionally, the probability of efficient insertions is decreased when increasing the number of targeted sites on a single injection (250). Altogether, our results indicate that the first approach chosen was not optimal; thus, subsequent approaches will consider and avoid these limitations. An alternative approach would be to initially microinject oocytes targeting the US site, with a microinjection cocktail containing a single sgRNA; once having successfully knocked in the US site and proved to be germ line transmitted, a second injection containing the sgRNA targeting the DS site would be performed to US-KI containing oocytes. This approach is currently under investigation with the 5% mice that successfully received the DS insertion.

An alternative plausible strategy consists on a single donor plasmid containing both loxP sites as well as the ICAM1 gene's exon 1 sequence flanked, which by homologous recombination would be inserted in the ICAM1 gene site when injected with Cas9 and the two sgRNAs targeting the 5'and 3'sites, respectively. Restriction sites introduced US of each LoxP sites would help to distinguish modified allele from WT and it would protect plasmid template from sgRNA targeting. If successful, as previously reported for other sites, this strategy would allow us to generate cell-specific ICAM1$^{-/-}$ mice upon crossing with cell type-specific Cre recombinase.

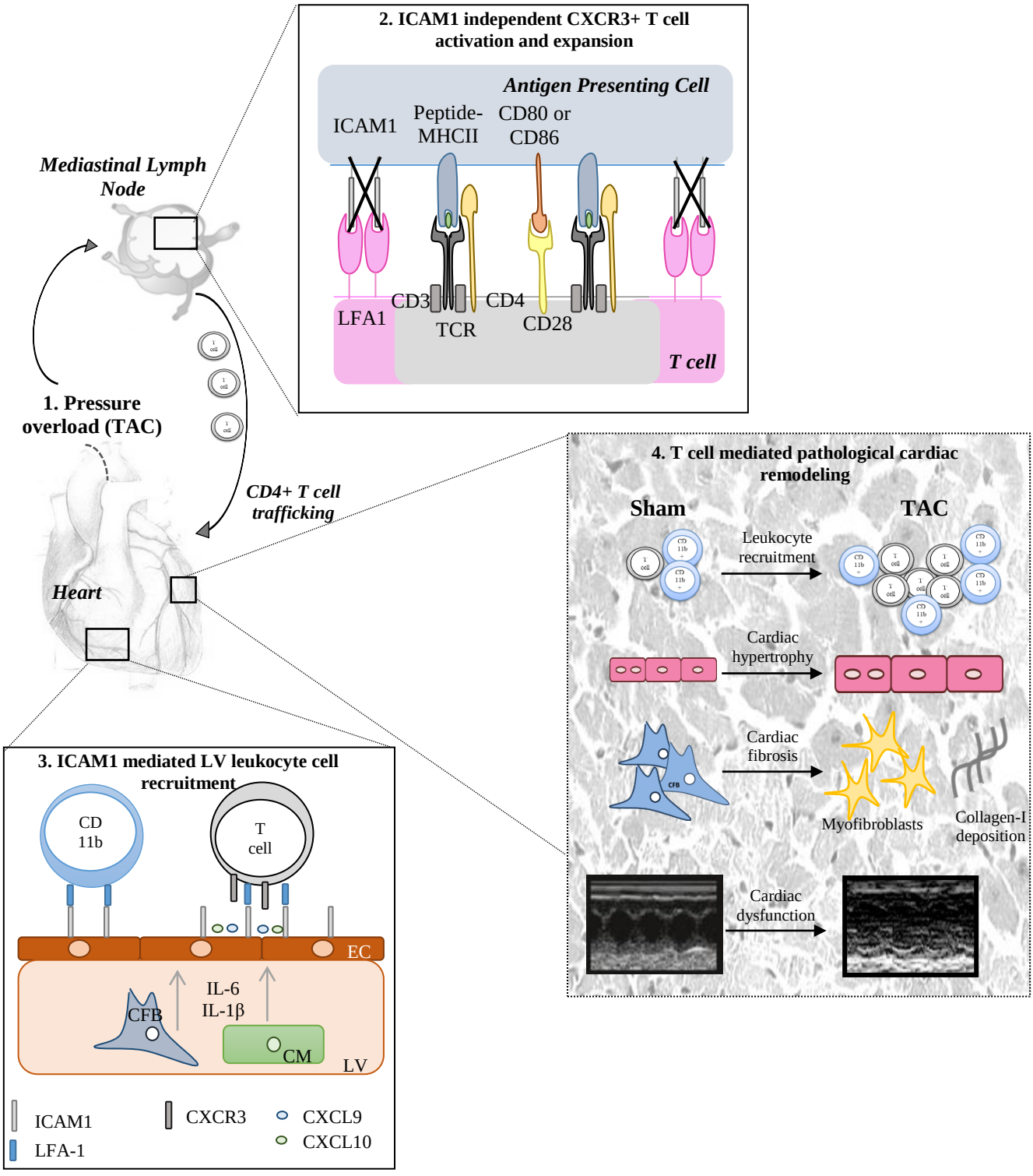

Figure 8.1. In response to LV pressure overload induced by TAC (1), T cells become activated and increase their CXCR3 expression in the mediastinal lymph nodes (2). Following CXCL9 and CXCL10 chemokine gradient, CXCR3+ are recruited into the LV in a process mediated by EC-ICAM1, which is found upregulated in the myocardial EC in response to pro-inflammatory

cytokines released by cardiac resident cells after TAC (3). Once in the LV (4) T cells mediate the development of pathological cardiac remodeling, characterized by cardiac inflammation, hypertrophy, fibrosis and dysfunction.

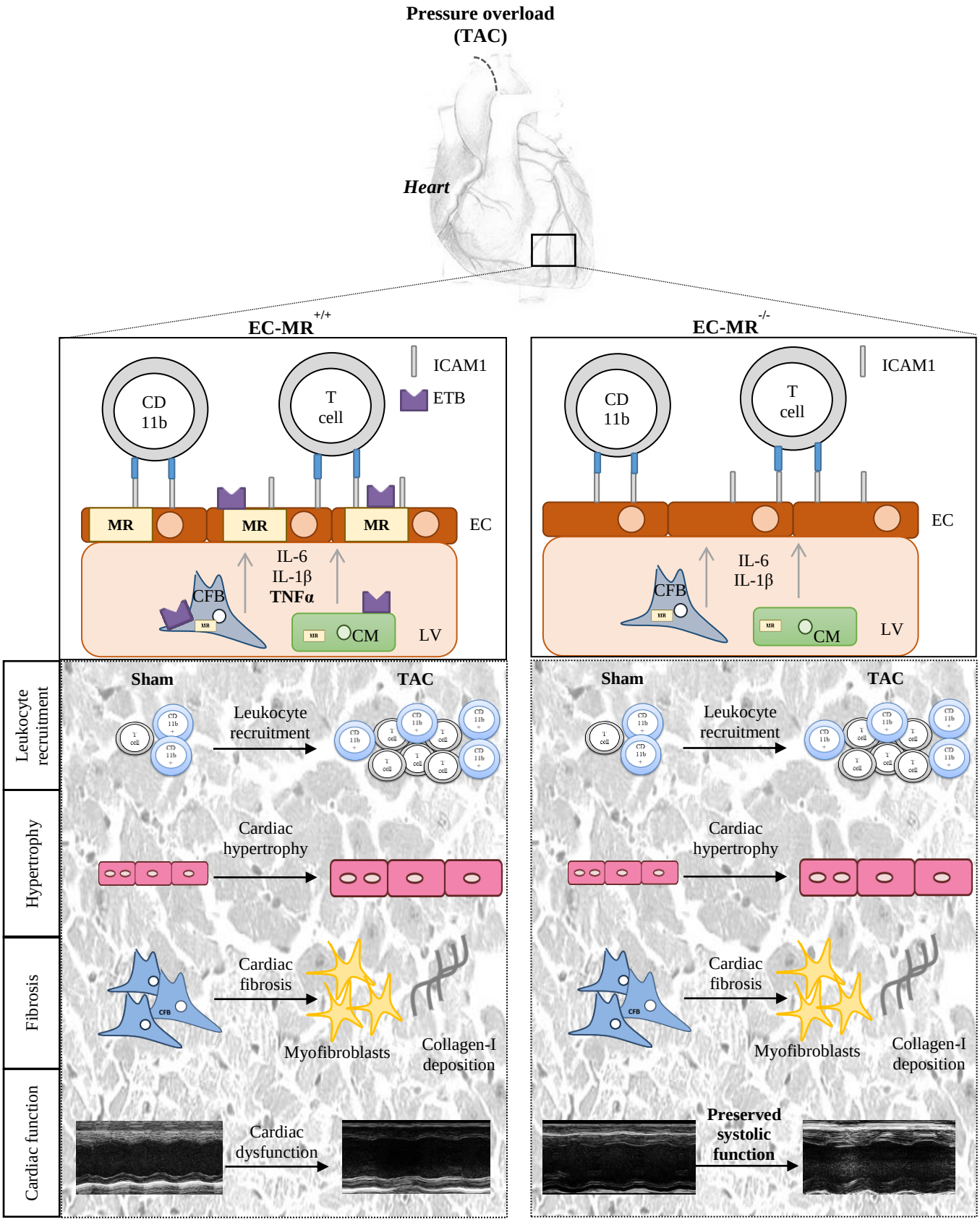
Pressure overload
(TAC)
Heart
EC-MR+/+
EC-MR-/-
ICAM1
ETB
CD 11b
T cell
MR
EC
IL-6
IL-1β
TNFα
CFB
CM
LV
Leukocyte recruitment
Hypertrophy
Fibrosis
Cardiac function
Sham
TAC
Cardiac hypertrophy
Cardiac fibrosis
Myofibroblasts
Collagen-I deposition
Cardiac dysfunction
Preserved systolic function

Figure 8.2. EC-MR$^{-/-}$ mice have partially preserved cardiac function in response to TAC despite presenting similar degree of cardiac hypertrophy and inflammation and same fibrotic remodeling as compared to EC-MR$^{+/+}$ mice. EC-MR seems to regulate cardiac ETB expression, suggesting that it may regulate endothelin-ETB mediated vasoconstriction and cardiac perfusion, contributing to the preserved systolic function of EC-MR$^{-/-}$ mice in response to pressure overload.

9 CONCLUSIONS- *CONCLUSIONES*

1. T lymphocytes get gradually infiltrated to the LV of the heart during non-ischemic HF progression. Lymphocyte recruitment is significantly increased two and four weeks after the surgery, correlating with cardiac hypertrophy, fibrosis, inflammation and dysfunction, which characterize HF development. Mice lacking T lymphocytes do not show a pathological cardiac remodeling phenotype in response to ventricular pressure overload, since they do not develop either hypertrophy, fibrosis, inflammation or ventricular dysfunction.
2. The expression of the endothelial cell adhesion molecule ICAM1 is increased in the LV during HF development, induced by pro-inflammatory cytokines released in the ventricle. ICAM1 mediates leukocyte recruitment, CD4+ lymphocyte and pro-inflammatory $Ly6C^{hi}$ monocyte infiltration specifically, to the LV in HF. Mice lacking ICAM1 develop hypertrophy, fibrosis and cardiac dysfunction in a lower degree than WT mice in response to ventricular pressure overload, despite having similar lymphocyte activation and circulating lymphocyte percentage as compared to WT mice.
3. Even though the endothelial cell mineralocorticoid receptor (EC-MR) does not play a role in leukocyte recruitment and endothelial ICAM upregulation in response to pressure overload, it contributes to cardiac dysfunction, since mice lacking EC-MR have preserved systolic function, despite the fact of developing same degree of ventricular hypertrophy, fibrosis and inflammation as WT mice.
4. The chemokines CXCL9 and CXCL10 are produced in the LV correlating in a temporal manner with local TNFα and IFNγ released in response to ventricular pressure overload. The expression of CXCR3, CXCL9 and CXCL10's main receptor, in lymphocytes present in the cardiac draining lymph nodes is increased in response to pressure overload, and express higher levels of the

integrin LFA1, which is ICAM1's main ligand. Two and four weeks after inducing ventricular pressure overload, CXCR3+ and LFA1+ lymphocyte are found recruited in the myocardium, which correlates with an increase of Th1 lymphocytes signature transcription factor Tbet expression, which is known to regulate the expression of CXCR3. *In vitro* studies using a parallel flow chamber apparatus indicate that the chemokines CXCL9 and CXCL10 increase Th1 lymphocyte adhesion to ICAM1 through an increase of LFA1's affinity without affecting its expression.

5. The study of the role of ICAM1 expressed exclusively in the ECs or in other cardiac resident cells will be possible in a near future using the mouse under development based on the CRISPR/Cas9 technology; this mouse will have loxP sites in the 5' and 3' regions of the gene that encodes for ICAM1. These mice will be crossed with mice expressing Cre recombinase in the cell type of interest, thus generating cell type specific ICAM1 knock out mice.

The conclusions indicated in these five points highlight the importance of both the T lymphocyte mediated adaptive immune response and the local myocardial inflammatory processes, during pathological cardiac remodeling in HF development. Additionally, the remarkable role of the EC adhesion molecule ICAM1 and the chemokine receptor CXCR3 is emphasized in mediating lymphocyte recruitment into the LV during HF progression. Altogether, the work presented in this doctoral thesis dissertation contributes to the better understanding of the local pathological inflammatory mechanisms taking place in HF development, and positions the adaptive immune response as well as the molecules that mediate immune cell recruitment as potential therapeutic targets for HF treatment.

1. *Los linfocitos T infiltran de forma gradual al ventrículo izquierdo del corazón durante el desarrollo de insuficiencia cardíaca (IC) no isquémica. El reclutamiento linfocitario es detectable dos y cuatro semanas tras la cirugía, correlacionando con procesos de hipertrofia, fibrosis, inflamación y disfunción ventricular, lo cuales caracterizan el desarrollo de IC. Ratones deficientes en linfocitos T no presentan dicho remodelado cardíaco patológico en respuesta a sobrecarga de presión ventricular, ya que no desarrollan ni hipertrofia, ni fibrosis, ni inflamación, ni disfunción ventricular.*
2. *La expresión de la molécula de adhesión endotelial ICAM1 se encuentra incrementada en el ventrículo izquierdo durante el desarrollo de IC, en respuesta a citoquinas pro-inflamatorias liberadas desde el ventrículo. ICAM1 media el reclutamiento de leucocitos, linfocitos CD4+ y monocitos pro-inflamatorios Ly6C^{hi} en concreto, al ventrículo izquierdo en IC. Ratones deficientes en ICAM1 desarrollan menor grado de hipertrofia, fibrosis y disfunción cardíaca durante el desarrollo de IC, a pesar de presentar similar grado de activación linfocitaria y porcentaje de linfocitos circulantes que los ratones WT.*
3. *A pesar de que el receptor mineralocorticoide endotelial (EC-MR) no juegue un papel decisivo en el reclutamiento leucocitario e incremento de expresión de ICAM1 en el endotelio en respuesta a sobrecarga de presión, contribuye a la disfunción cardíaca, ya que ratones deficientes en EC-MR presentan función sistólica preservada, a pesar de desarrollar el mismo grado de fibrosis, inflamación e hipertrofia ventricular que ratones WT.*
4. *Las quimioquinas CXCL9 y CXCL10 son producidas en el ventrículo izquierdo cardíaco de forma temporal correlacionando con la producción local de TNFα*

e IFNγ en el ventrículo en respuesta a sobrecarga de presión. A su vez, los linfocitos presentes en los nódulos linfáticos que drenan el corazón incrementan su expresión del receptor de CXCL9 y CXCL10, CXCR3, los cuales expresan elevados niveles de la integrina LFA1, la cual es el principal ligando de ICAM1. Dos y cuatro semanas después de la inducción de a sobrecarga de presión ventricular, cuando se observa disfunción ventricular se comienzan a detectar linfocitos CXCR3+ y LFA1+ reclutados en el tejido miocárdico, coincidiendo con el incremento de expresión del principal factor de trascripción de linfocitos Th1, Tbet, el cual regula la expresión de CXCR3. Estudios en cámara de flujo laminar in vitro indican que las quimioquinas CXCL9 y CXCL10 aumentan la adhesión de células Th1 a ICAM1, mediante un aumento de la afinidad de LFA de las células Th1 sin afectar su expresión.

5. *El estudio del papel de ICAM1 expresado exclusivamente en el endotelio u otras células residentes cardiacas, será posible en un futuro próximo gracias al ratón que estamos generando mediante la tecnología CRISPR/Cas9 el cual tendrá secuencias loxP en las regiones 5' y 3' del gen que que codifica para ICAM1. Dichos ratones se podrán cruzar con ratones que expresen Cre recombinasa en el tipo celular de interés para generar ratones knock-out específicos de tipo celular.*

Las conclusiones indicadas en estos cinco puntos ponen de relieve la importancia de ambos la respuesta inmunitaria adaptativa mediada por linfocitos T y de los procesos inflamatorios locales en el miocardio, durante el remodelado cardíaco patológico durante el desarrollo de IC, así como el remarcable papel de la molécula de adhesión endotelial ICAM1 y el receptor de quimioquinas CXCR3 que median el reclutamiento

de linfocitos al ventrículo izquierdo. Todo ello contribuye a la mejor comprensión de los mecanismos inflamatorios locales patológicos relevantes en el desarrollo de IC, y posiciona la respuesta inmunitaria adaptativa así como las moléculas que median el reclutamiento celular como potenciales dianas terapéuticas en el tratamiento de IC.

10 REFERENCES

1. Maillet M, van Berlo JH, Molkentin JD. Molecular basis of physiological heart growth: fundamental concepts and new players. Nat Rev Mol Cell Biol. 2013;14(1):38-48.

2. Mohrman DE, Heller LJ. Cardiovascular physiology. 8th edition. ed. New York: McGraw-Hill, Education/Medical; 2014. ix, 276 pages p.

3. Xin M, Olson EN, Bassel-Duby R. Mending broken hearts: cardiac development as a basis for adult heart regeneration and repair. Nat Rev Mol Cell Biol. 2013;14(8):529-41.

4. Epelman S, Liu PP, Mann DL. Role of innate and adaptive immune mechanisms in cardiac injury and repair. Nat Rev Immunol. 2015;15(2):117-29.

5. Lavine KJ, Epelman S, Uchida K, Weber KJ, Nichols CG, Schilling JD, et al. Distinct macrophage lineages contribute to disparate patterns of cardiac recovery and remodeling in the neonatal and adult heart. Proc Natl Acad Sci U S A. 2014;111(45):16029-34.

6. Epelman S, Lavine KJ, Beaudin AE, Sojka DK, Carrero JA, Calderon B, et al. Embryonic and adult-derived resident cardiac macrophages are maintained through distinct mechanisms at steady state and during inflammation. Immunity. 2014;40(1):91-104.

7. Pinto AR, Ilinykh A, Ivey MJ, Kuwabara JT, D'Antoni ML, Debuque R, et al. Revisiting Cardiac Cellular Composition. Circ Res. 2016;118(3):400-9.

8. Harvey PA, Leinwand LA. The cell biology of disease: cellular mechanisms of cardiomyopathy. J Cell Biol. 2011;194(3):355-65.

9. Guha K, McDonagh T. Heart failure epidemiology: European perspective. Curr Cardiol Rev. 2013;9(2):123-7.

10. Ambrosy AP, Fonarow GC, Butler J, Chioncel O, Greene SJ, Vaduganathan M, et al. The global health and economic burden of hospitalizations for heart failure: lessons learned from hospitalized heart failure registries. J Am Coll Cardiol. 2014;63(12):1123-33.

11. Ziaeian B, Fonarow GC. Epidemiology and aetiology of heart failure. Nat Rev Cardiol. 2016;13(6):368-78.

12. Writing Group M, Mozaffarian D, Benjamin EJ, Go AS, Arnett DK, Blaha MJ, et al. Heart Disease and Stroke Statistics-2016 Update: A Report From the American Heart Association. Circulation. 2016;133(4):e38-360.

13. Kubo SH, Schulman S, Starling RC, Jessup M, Wentworth D, Burkhoff D. Development and validation of a patient questionnaire to determine New York Heart Association classification. J Card Fail. 2004;10(3):228-35.

14. Lam CS, Donal E, Kraigher-Krainer E, Vasan RS. Epidemiology and clinical course of heart failure with preserved ejection fraction. Eur J Heart Fail. 2011;13(1):18-28.

15. Yancy CW, Jessup M, Bozkurt B, Butler J, Casey DE, Jr., Colvin MM, et al. 2016 ACC/AHA/HFSA Focused Update on New Pharmacological Therapy for Heart Failure: An Update of the 2013 ACCF/AHA Guideline for the Management of Heart Failure: A Report of the American College of Cardiology/American Heart Association Task Force on Clinical Practice Guidelines and the Heart Failure Society of America. J Am Coll Cardiol. 2016;68(13):1476-88.

16. Kuhl U, Pauschinger M, Seeberg B, Lassner D, Noutsias M, Poller W, et al. Viral persistence in the myocardium is associated with progressive cardiac dysfunction. Circulation. 2005;112(13):1965-70.

17. Bock CT, Klingel K, Kandolf R. Human parvovirus B19-associated myocarditis. N Engl J Med. 2010;362(13):1248-9.

18. Kuhl U, Noutsias M, Seeberg B, Schultheiss HP. Immunohistological evidence for a chronic intramyocardial inflammatory process in dilated cardiomyopathy. Heart. 1996;75(3):295-300.

19. Fujinami RS, von Herrath MG, Christen U, Whitton JL. Molecular mimicry, bystander activation, or viral persistence: infections and autoimmune disease. Clin Microbiol Rev. 2006;19(1):80-94.

20. Lawson CM, O'Donoghue HL, Reed WD. Mouse cytomegalovirus infection induces antibodies which cross-react with virus and cardiac myosin: a model for the study of molecular mimicry in the pathogenesis of viral myocarditis. Immunology. 1992;75(3):513-9.

21. Kaya Z, Leib C, Katus HA. Autoantibodies in heart failure and cardiac dysfunction. Circ Res. 2012;110(1):145-58.

22. Rossi MA, Bestetti RB. The challenge of chagasic cardiomyopathy. The pathologic roles of autonomic abnormalities, autoimmune mechanisms and microvascular changes, and therapeutic implications. Cardiology. 1995;86(1):1-7.

23. Yancy CW, Jessup M, Bozkurt B, Butler J, Casey DE, Jr., Drazner MH, et al. 2013 ACCF/AHA guideline for the management of heart failure: a report of the American College of Cardiology Foundation/American Heart Association Task Force on Practice Guidelines. J Am Coll Cardiol. 2013;62(16):e147-239.

24. Iwai LK, Juliano MA, Juliano L, Kalil J, Cunha-Neto E. T-cell molecular mimicry in Chagas disease: identification and partial structural analysis of multiple cross-reactive epitopes between Trypanosoma cruzi B13 and cardiac myosin heavy chain. J Autoimmun. 2005;24(2):111-7.

25. Girones N, Cuervo H, Fresno M. Trypanosoma cruzi-induced molecular mimicry and Chagas' disease. Curr Top Microbiol Immunol. 2005;296:89-123.

26. Dorn GW, 2nd. Novel pharmacotherapies to abrogate postinfarction ventricular remodeling. Nat Rev Cardiol. 2009;6(4):283-91.

27. Grossman W, Jones D, McLaurin LP. Wall stress and patterns of hypertrophy in the human left ventricle. J Clin Invest. 1975;56(1):56-64.

28. American College of Cardiology/American Heart Association Task Force on Practice G, Society of Cardiovascular A, Society for Cardiovascular A, Interventions, Society of Thoracic S, Bonow RO, et al. ACC/AHA 2006 guidelines for the management of patients with valvular heart disease: a report of the American College of Cardiology/American Heart Association Task Force on Practice Guidelines (writing committee to revise the 1998 Guidelines for the Management of Patients With Valvular Heart Disease): developed in collaboration with the Society of Cardiovascular Anesthesiologists: endorsed by the Society for Cardiovascular Angiography and Interventions and the Society of Thoracic Surgeons. Circulation. 2006;114(5):e84-231.

29. Grundy SM. Pre-diabetes, metabolic syndrome, and cardiovascular risk. J Am Coll Cardiol. 2012;59(7):635-43.

30. Abel ED, Litwin SE, Sweeney G. Cardiac remodeling in obesity. Physiol Rev. 2008;88(2):389-419.

31. Piano MR. Alcoholic cardiomyopathy: incidence, clinical characteristics, and pathophysiology. Chest. 2002;121(5):1638-50.

32. Walsh CR, Larson MG, Evans JC, Djousse L, Ellison RC, Vasan RS, et al. Alcohol consumption and risk for congestive heart failure in the Framingham Heart Study. Ann Intern Med. 2002;136(3):181-91.

33. Chakko S, Myerburg RJ. Cardiac complications of cocaine abuse. Clin Cardiol. 1995;18(2):67-72.
34. Bovelli D, Plataniotis G, Roila F, Group EGW. Cardiotoxicity of chemotherapeutic agents and radiotherapy-related heart disease: ESMO Clinical Practice Guidelines. Ann Oncol. 2010;21 Suppl 5:v277-82.
35. Mohan SB, Parker M, Wehbi M, Douglass P. Idiopathic dilated cardiomyopathy: a common but mystifying cause of heart failure. Cleve Clin J Med. 2002;69(6):481-7.
36. Dorn GW, 2nd. The fuzzy logic of physiological cardiac hypertrophy. Hypertension. 2007;49(5):962-70.
37. Mihl C, Dassen WR, Kuipers H. Cardiac remodelling: concentric versus eccentric hypertrophy in strength and endurance athletes. Neth Heart J. 2008;16(4):129-33.
38. Burchfield JS, Xie M, Hill JA. Pathological ventricular remodeling: mechanisms: part 1 of 2. Circulation. 2013;128(4):388-400.
39. Nass RD, Aiba T, Tomaselli GF, Akar FG. Mechanisms of disease: ion channel remodeling in the failing ventricle. Nat Clin Pract Cardiovasc Med. 2008;5(4):196-207.
40. Goligorsky MS. Microvascular rarefaction: the decline and fall of blood vessels. Organogenesis. 2010;6(1):1-10.
41. Mohammed SF, Hussain S, Mirzoyev SA, Edwards WD, Maleszewski JJ, Redfield MM. Coronary microvascular rarefaction and myocardial fibrosis in heart failure with preserved ejection fraction. Circulation. 2015;131(6):550-9.
42. Dick SA, Epelman S. Chronic Heart Failure and Inflammation: What Do We Really Know? Circ Res. 2016;119(1):159-76.
43. Mann DL, Topkara VK, Evans S, Barger PM. Innate immunity in the adult mammalian heart: for whom the cell tolls. Trans Am Clin Climatol Assoc. 2010;121:34-50; discussion -1.
44. Mezzaroma E, Toldo S, Farkas D, Seropian IM, Van Tassell BW, Salloum FN, et al. The inflammasome promotes adverse cardiac remodeling following acute myocardial infarction in the mouse. Proc Natl Acad Sci U S A. 2011;108(49):19725-30.
45. Gordon S, Martinez FO. Alternative activation of macrophages: mechanism and functions. Immunity. 2010;32(5):593-604.

46. Biswas SK, Mantovani A. Macrophage plasticity and interaction with lymphocyte subsets: cancer as a paradigm. Nat Immunol. 2010;11(10):889-96.

47. Sica A, Mantovani A. Macrophage plasticity and polarization: in vivo veritas. J Clin Invest. 2012;122(3):787-95.

48. Weinberger T, Schulz C. Myocardial infarction: a critical role of macrophages in cardiac remodeling. Front Physiol. 2015;6:107.

49. Nahrendorf M, Swirski FK. Monocyte and macrophage heterogeneity in the heart. Circ Res. 2013;112(12):1624-33.

50. Kalra D, Sivasubramanian N, Mann DL. Angiotensin II induces tumor necrosis factor biosynthesis in the adult mammalian heart through a protein kinase C-dependent pathway. Circulation. 2002;105(18):2198-205.

51. Murray DR, Prabhu SD, Chandrasekar B. Chronic beta-adrenergic stimulation induces myocardial proinflammatory cytokine expression. Circulation. 2000;101(20):2338-41.

52. Zhu J, Paul WE. CD4 T cells: fates, functions, and faults. Blood. 2008;112(5):1557-69.

53. Williams MA, Tyznik AJ, Bevan MJ. Interleukin-2 signals during priming are required for secondary expansion of CD8+ memory T cells. Nature. 2006;441(7095):890-3.

54. Sokol CL, Chu NQ, Yu S, Nish SA, Laufer TM, Medzhitov R. Basophils function as antigen-presenting cells for an allergen-induced T helper type 2 response. Nat Immunol. 2009;10(7):713-20.

55. Luckheeram RV, Zhou R, Verma AD, Xia B. CD4(+)T cells: differentiation and functions. Clin Dev Immunol. 2012;2012:925135.

56. Gaffen SL. Structure and signalling in the IL-17 receptor family. Nat Rev Immunol. 2009;9(8):556-67.

57. Manel N, Unutmaz D, Littman DR. The differentiation of human T(H)-17 cells requires transforming growth factor-beta and induction of the nuclear receptor RORgammat. Nat Immunol. 2008;9(6):641-9.

58. Volpe E, Servant N, Zollinger R, Bogiatzi SI, Hupe P, Barillot E, et al. A critical function for transforming growth factor-beta, interleukin 23 and proinflammatory cytokines in driving and modulating human T(H)-17 responses. Nat Immunol. 2008;9(6):650-7.

59. Chen W, Jin W, Hardegen N, Lei KJ, Li L, Marinos N, et al. Conversion of peripheral CD4+CD25- naive T cells to CD4+CD25+ regulatory T cells by TGF-beta induction of transcription factor Foxp3. J Exp Med. 2003;198(12):1875-86.

60. Rojas AI, Ahmed AR. Adhesion receptors in health and disease. Crit Rev Oral Biol Med. 1999;10(3):337-58.

61. Aricescu AR, Jones EY. Immunoglobulin superfamily cell adhesion molecules: zippers and signals. Curr Opin Cell Biol. 2007;19(5):543-50.

62. Barclay AN. Membrane proteins with immunoglobulin-like domains--a master superfamily of interaction molecules. Semin Immunol. 2003;15(4):215-23.

63. Bevilacqua MP, Nelson RM, Mannori G, Cecconi O. Endothelial-leukocyte adhesion molecules in human disease. Annu Rev Med. 1994;45:361-78.

64. Arnaout MA, Goodman SL, Xiong JP. Structure and mechanics of integrin-based cell adhesion. Curr Opin Cell Biol. 2007;19(5):495-507.

65. Askari JA, Buckley PA, Mould AP, Humphries MJ. Linking integrin conformation to function. J Cell Sci. 2009;122(Pt 2):165-70.

66. Shimaoka M, Takagi J, Springer TA. Conformational regulation of integrin structure and function. Annu Rev Biophys Biomol Struct. 2002;31:485-516.

67. Vestweber D. VE-cadherin: the major endothelial adhesion molecule controlling cellular junctions and blood vessel formation. Arterioscler Thromb Vasc Biol. 2008;28(2):223-32.

68. McEver RP. Selectins: initiators of leucocyte adhesion and signalling at the vascular wall. Cardiovasc Res. 2015;107(3):331-9.

69. Ley K. The role of selectins in inflammation and disease. Trends Mol Med. 2003;9(6):263-8.

70. Hope SA, Meredith IT. Cellular adhesion molecules and cardiovascular disease. Part I. Their expression and role in atherogenesis. Intern Med J. 2003;33(8):380-6.

71. Schnoor M, Alcaide P, Voisin MB, van Buul JD. Crossing the Vascular Wall: Common and Unique Mechanisms Exploited by Different Leukocyte Subsets during Extravasation. Mediators Inflamm. 2015;2015:946509.

72. Devaux B, Scholz D, Hirche A, Klovekorn WP, Schaper J. Upregulation of cell adhesion molecules and the presence of low grade inflammation in human chronic heart failure. Eur Heart J. 1997;18(3):470-9.

73. Franssen C, Chen S, Unger A, Korkmaz HI, De Keulenaer GW, Tschope C, et al. Myocardial Microvascular Inflammatory Endothelial Activation in Heart Failure With Preserved Ejection Fraction. JACC Heart Fail. 2016;4(4):312-24.

74. Kuwahara F, Kai H, Tokuda K, Niiyama H, Tahara N, Kusaba K, et al. Roles of intercellular adhesion molecule-1 in hypertensive cardiac remodeling. Hypertension. 2003;41(3 Pt 2):819-23.

75. Pigott R, Dillon LP, Hemingway IH, Gearing AJ. Soluble forms of E-selectin, ICAM-1 and VCAM-1 are present in the supernatants of cytokine activated cultured endothelial cells. Biochem Biophys Res Commun. 1992;187(2):584-9.

76. Leeuwenberg JF, Smeets EF, Neefjes JJ, Shaffer MA, Cinek T, Jeunhomme TM, et al. E-selectin and intercellular adhesion molecule-1 are released by activated human endothelial cells in vitro. Immunology. 1992;77(4):543-9.

77. Fonsatti E, Altomonte M, Coral S, Cattarossi I, Nicotra MR, Gasparollo A, et al. Tumour-derived interleukin 1alpha (IL-1alpha) up-regulates the release of soluble intercellular adhesion molecule-1 (sICAM-1) by endothelial cells. Br J Cancer. 1997;76(10):1255-61.

78. Tarin C, Gomez M, Calvo E, Lopez JA, Zaragoza C. Endothelial nitric oxide deficiency reduces MMP-13-mediated cleavage of ICAM-1 in vascular endothelium: a role in atherosclerosis. Arterioscler Thromb Vasc Biol. 2009;29(1):27-32.

79. Champagne B, Tremblay P, Cantin A, St Pierre Y. Proteolytic cleavage of ICAM-1 by human neutrophil elastase. J Immunol. 1998;161(11):6398-405.

80. Hwang SJ, Ballantyne CM, Sharrett AR, Smith LC, Davis CE, Gotto AM, Jr., et al. Circulating adhesion molecules VCAM-1, ICAM-1, and E-selectin in carotid atherosclerosis and incident coronary heart disease cases: the Atherosclerosis Risk In Communities (ARIC) study. Circulation. 1997;96(12):4219-25.

81. Ridker PM, Hennekens CH, Roitman-Johnson B, Stampfer MJ, Allen J. Plasma concentration of soluble intercellular adhesion molecule 1 and risks of future myocardial infarction in apparently healthy men. Lancet. 1998;351(9096):88-92.

82. Kitagawa K, Matsumoto M, Sasaki T, Hashimoto H, Kuwabara K, Ohtsuki T, et al. Involvement of ICAM-1 in the progression of atherosclerosis in APOE-knockout mice. Atherosclerosis. 2002;160(2):305-10.

83. Alexiou D, Karayiannakis AJ, Syrigos KN, Zbar A, Kremmyda A, Bramis I, et al. Serum levels of E-selectin, ICAM-1 and VCAM-1 in colorectal cancer patients:

correlations with clinicopathological features, patient survival and tumour surgery. Eur J Cancer. 2001;37(18):2392-7.

84. Otto VI, Heinzel-Pleines UE, Gloor SM, Trentz O, Kossmann T, Morganti-Kossmann MC. sICAM-1 and TNF-alpha induce MIP-2 with distinct kinetics in astrocytes and brain microvascular endothelial cells. J Neurosci Res. 2000;60(6):733-42.

85. Lawson C, Wolf S. ICAM-1 signaling in endothelial cells. Pharmacol Rep. 2009;61(1):22-32.

86. Girerd N, Pang PS, Swedberg K, Fought A, Kwasny MJ, Subacius H, et al. Serum aldosterone is associated with mortality and re-hospitalization in patients with reduced ejection fraction hospitalized for acute heart failure: analysis from the EVEREST trial. Eur J Heart Fail. 2013;15(11):1228-35.

87. Guder G, Bauersachs J, Frantz S, Weismann D, Allolio B, Ertl G, et al. Complementary and incremental mortality risk prediction by cortisol and aldosterone in chronic heart failure. Circulation. 2007;115(13):1754-61.

88. Rogerson FM, Fuller PJ. Mineralocorticoid action. Steroids. 2000;65(2):61-73.

89. McCurley A, Pires PW, Bender SB, Aronovitz M, Zhao MJ, Metzger D, et al. Direct regulation of blood pressure by smooth muscle cell mineralocorticoid receptors. Nat Med. 2012;18(9):1429-33.

90. Pitt B, Zannad F, Remme WJ, Cody R, Castaigne A, Perez A, et al. The effect of spironolactone on morbidity and mortality in patients with severe heart failure. Randomized Aldactone Evaluation Study Investigators. N Engl J Med. 1999;341(10):709-17.

91. Pitt B, Reichek N, Willenbrock R, Zannad F, Phillips RA, Roniker B, et al. Effects of eplerenone, enalapril, and eplerenone/enalapril in patients with essential hypertension and left ventricular hypertrophy: the 4E-left ventricular hypertrophy study. Circulation. 2003;108(15):1831-8.

92. Zannad F, McMurray JJ, Krum H, van Veldhuisen DJ, Swedberg K, Shi H, et al. Eplerenone in patients with systolic heart failure and mild symptoms. N Engl J Med. 2011;364(1):11-21.

93. Lombes M, Alfaidy N, Eugene E, Lessana A, Farman N, Bonvalet JP. Prerequisite for cardiac aldosterone action. Mineralocorticoid receptor and 11 beta-hydroxysteroid dehydrogenase in the human heart. Circulation. 1995;92(2):175-82.

94. Bunda S, Wang Y, Mitts TF, Liu P, Arab S, Arabkhari M, et al. Aldosterone stimulates elastogenesis in cardiac fibroblasts via mineralocorticoid receptor-independent action involving the consecutive activation of Galpha13, c-Src, the insulin-like growth factor-I receptor, and phosphatidylinositol 3-kinase/Akt. J Biol Chem. 2009;284(24):16633-47.

95. Jaffe IZ, Mendelsohn ME. Angiotensin II and aldosterone regulate gene transcription via functional mineralocortocoid receptors in human coronary artery smooth muscle cells. Circ Res. 2005;96(6):643-50.

96. Caprio M, Newfell BG, la Sala A, Baur W, Fabbri A, Rosano G, et al. Functional mineralocorticoid receptors in human vascular endothelial cells regulate intercellular adhesion molecule-1 expression and promote leukocyte adhesion. Circ Res. 2008;102(11):1359-67.

97. Bene NC, Alcaide P, Wortis HH, Jaffe IZ. Mineralocorticoid receptors in immune cells: emerging role in cardiovascular disease. Steroids. 2014;91:38-45.

98. Rickard AJ, Morgan J, Tesch G, Funder JW, Fuller PJ, Young MJ. Deletion of mineralocorticoid receptors from macrophages protects against deoxycorticosterone/salt-induced cardiac fibrosis and increased blood pressure. Hypertension. 2009;54(3):537-43.

99. Shen JZ, Morgan J, Tesch GH, Rickard AJ, Chrissobolis S, Drummond GR, et al. Cardiac Tissue Injury and Remodeling Is Dependent Upon MR Regulation of Activation Pathways in Cardiac Tissue Macrophages. Endocrinology. 2016;157(8):3213-23.

100. Lother A, Furst D, Bergemann S, Gilsbach R, Grahammer F, Huber TB, et al. Deoxycorticosterone Acetate/Salt-Induced Cardiac But Not Renal Injury Is Mediated By Endothelial Mineralocorticoid Receptors Independently From Blood Pressure. Hypertension. 2016;67(1):130-8.

101. Rickard AJ, Morgan J, Chrissobolis S, Miller AA, Sobey CG, Young MJ. Endothelial cell mineralocorticoid receptors regulate deoxycorticosterone/salt-mediated cardiac remodeling and vascular reactivity but not blood pressure. Hypertension. 2014;63(5):1033-40.

102. Lawrence T. The nuclear factor NF-kappaB pathway in inflammation. Cold Spring Harb Perspect Biol. 2009;1(6):a001651.

103. Jaisser F, Farman N. Emerging Roles of the Mineralocorticoid Receptor in Pathology: Toward New Paradigms in Clinical Pharmacology. Pharmacol Rev. 2016;68(1):49-75.

104. Damas JK, Eiken HG, Oie E, Bjerkeli V, Yndestad A, Ueland T, et al. Myocardial expression of CC- and CXC-chemokines and their receptors in human end-stage heart failure. Cardiovasc Res. 2000;47(4):778-87.

105. Aukrust P, Ueland T, Muller F, Andreassen AK, Nordoy I, Aas H, et al. Elevated circulating levels of C-C chemokines in patients with congestive heart failure. Circulation. 1998;97(12):1136-43.

106. Behr TM, Wang X, Aiyar N, Coatney RW, Li X, Koster P, et al. Monocyte chemoattractant protein-1 is upregulated in rats with volume-overload congestive heart failure. Circulation. 2000;102(11):1315-22.

107. Frangogiannis NG. Chemokines in the ischemic myocardium: from inflammation to fibrosis. Inflamm Res. 2004;53(11):585-95.

108. Frangogiannis NG, Mendoza LH, Lewallen M, Michael LH, Smith CW, Entman ML. Induction and suppression of interferon-inducible protein 10 in reperfused myocardial infarcts may regulate angiogenesis. FASEB J. 2001;15(8):1428-30.

109. Frangogiannis NG, Entman ML. Chemokines in myocardial ischemia. Trends Cardiovasc Med. 2005;15(5):163-9.

110. Saxena A, Bujak M, Frunza O, Dobaczewski M, Gonzalez-Quesada C, Lu B, et al. CXCR3-independent actions of the CXC chemokine CXCL10 in the infarcted myocardium and in isolated cardiac fibroblasts are mediated through proteoglycans. Cardiovasc Res. 2014;103(2):217-27.

111. Pyo RT, Sui J, Dhume A, Palomeque J, Blaxall BC, Diaz G, et al. CXCR4 modulates contractility in adult cardiac myocytes. J Mol Cell Cardiol. 2006;41(5):834-44.

112. Tarzami ST, Cheng R, Miao W, Kitsis RN, Berman JW. Chemokine expression in myocardial ischemia: MIP-2 dependent MCP-1 expression protects cardiomyocytes from cell death. J Mol Cell Cardiol. 2002;34(2):209-21.

113. Chen J, Chemaly E, Liang L, Kho C, Lee A, Park J, et al. Effects of CXCR4 gene transfer on cardiac function after ischemia-reperfusion injury. Am J Pathol. 2010;176(4):1705-15.

114. Birdsall HH, Green DM, Trial J, Youker KA, Burns AR, MacKay CR, et al. Complement C5a, TGF-beta 1, and MCP-1, in sequence, induce migration of monocytes into ischemic canine myocardium within the first one to five hours after reperfusion. Circulation. 1997;95(3):684-92.

115. Frangogiannis NG, Youker KA, Rossen RD, Gwechenberger M, Lindsey MH, Mendoza LH, et al. Cytokines and the microcirculation in ischemia and reperfusion. J Mol Cell Cardiol. 1998;30(12):2567-76.

116. Nossuli TO, Frangogiannis NG, Knuefermann P, Lakshminarayanan V, Dewald O, Evans AJ, et al. Brief murine myocardial I/R induces chemokines in a TNF-alpha-independent manner: role of oxygen radicals. Am J Physiol Heart Circ Physiol. 2001;281(6):H2549-58.

117. Montecucco F, Braunersreuther V, Lenglet S, Delattre BM, Pelli G, Buatois V, et al. CC chemokine CCL5 plays a central role impacting infarct size and post-infarction heart failure in mice. Eur Heart J. 2012;33(15):1964-74.

118. Libby P. Inflammation and cardiovascular disease mechanisms. Am J Clin Nutr. 2006;83(2):456S-60S.

119. de Jager SC, Bongaerts BW, Weber M, Kraaijeveld AO, Rousch M, Dimmeler S, et al. Chemokines CCL3/MIP1alpha, CCL5/RANTES and CCL18/PARC are independent risk predictors of short-term mortality in patients with acute coronary syndromes. PLoS One. 2012;7(9):e45804.

120. Finsen AV, Ueland T, Sjaastad I, Ranheim T, Ahmed MS, Dahl CP, et al. The homeostatic chemokine CCL21 predicts mortality in aortic stenosis patients and modulates left ventricular remodeling. PLoS One. 2014;9(11):e112172.

121. Lo JC, Chin RK, Lee Y, Kang HS, Wang Y, Weinstock JV, et al. Differential regulation of CCL21 in lymphoid/nonlymphoid tissues for effectively attracting T cells to peripheral tissues. J Clin Invest. 2003;112(10):1495-505.

122. Montecucco F, Lenglet S, Braunersreuther V, Pelli G, Pellieux C, Montessuit C, et al. Single administration of the CXC chemokine-binding protein Evasin-3 during ischemia prevents myocardial reperfusion injury in mice. Arterioscler Thromb Vasc Biol. 2010;30(7):1371-7.

123. Damas JK, Gullestad L, Ueland T, Solum NO, Simonsen S, Froland SS, et al. CXC-chemokines, a new group of cytokines in congestive heart failure--possible role of platelets and monocytes. Cardiovasc Res. 2000;45(2):428-36.

124. Kukielka GL, Smith CW, LaRosa GJ, Manning AM, Mendoza LH, Daly TJ, et al. Interleukin-8 gene induction in the myocardium after ischemia and reperfusion in vivo. J Clin Invest. 1995;95(1):89-103.

125. Elmas E, Lang S, Dempfle CE, Kalsch T, Hannak D, Sueselbeck T, et al. High plasma levels of tissue inhibitor of metalloproteinase-1 (TIMP-1) and interleukin-8 (IL-8) characterize patients prone to ventricular fibrillation complicating myocardial infarction. Clin Chem Lab Med. 2007;45(10):1360-5.

126. Nogueira LG, Santos RH, Ianni BM, Fiorelli AI, Mairena EC, Benvenuti LA, et al. Myocardial chemokine expression and intensity of myocarditis in Chagas cardiomyopathy are controlled by polymorphisms in CXCL9 and CXCL10. PLoS Negl Trop Dis. 2012;6(10):e1867.

127. Waehre A, Vistnes M, Sjaastad I, Nygard S, Husberg C, Lunde IG, et al. Chemokines regulate small leucine-rich proteoglycans in the extracellular matrix of the pressure-overloaded right ventricle. J Appl Physiol (1985). 2012;112(8):1372-82.

128. Larocca TJ, Jeong D, Kohlbrenner E, Lee A, Chen J, Hajjar RJ, et al. CXCR4 gene transfer prevents pressure overload induced heart failure. J Mol Cell Cardiol. 2012;53(2):223-32.

129. Waehre A, Halvorsen B, Yndestad A, Husberg C, Sjaastad I, Nygard S, et al. Lack of chemokine signaling through CXCR5 causes increased mortality, ventricular dilatation and deranged matrix during cardiac pressure overload. PLoS One. 2011;6(4):e18668.

130. Xuan W, Liao Y, Chen B, Huang Q, Xu D, Liu Y, et al. Detrimental effect of fractalkine on myocardial ischaemia and heart failure. Cardiovasc Res. 2011;92(3):385-93.

131. Streblow DN, Kreklywich C, Yin Q, De La Melena VT, Corless CL, Smith PA, et al. Cytomegalovirus-mediated upregulation of chemokine expression correlates with the acceleration of chronic rejection in rat heart transplants. J Virol. 2003;77(3):2182-94.

132. Groom JR, Luster AD. CXCR3 ligands: redundant, collaborative and antagonistic functions. Immunol Cell Biol. 2011;89(2):207-15.

133. Paust HJ, Riedel JH, Krebs CF, Turner JE, Brix SR, Krohn S, et al. CXCR3+ Regulatory T Cells Control TH1 Responses in Crescentic GN. J Am Soc Nephrol. 2016;27(7):1933-42.

134. Taub DD, Lloyd AR, Conlon K, Wang JM, Ortaldo JR, Harada A, et al. Recombinant human interferon-inducible protein 10 is a chemoattractant for human monocytes and T lymphocytes and promotes T cell adhesion to endothelial cells. J Exp Med. 1993;177(6):1809-14.

135. Curbishley SM, Eksteen B, Gladue RP, Lalor P, Adams DH. CXCR 3 activation promotes lymphocyte transendothelial migration across human hepatic endothelium under fluid flow. Am J Pathol. 2005;167(3):887-99.

136. Whiting D, Hsieh G, Yun JJ, Banerji A, Yao W, Fishbein MC, et al. Chemokine monokine induced by IFN-gamma/CXC chemokine ligand 9 stimulates T lymphocyte proliferation and effector cytokine production. J Immunol. 2004;172(12):7417-24.

137. Groom JR, Richmond J, Murooka TT, Sorensen EW, Sung JH, Bankert K, et al. CXCR3 chemokine receptor-ligand interactions in the lymph node optimize CD4+ T helper 1 cell differentiation. Immunity. 2012;37(6):1091-103.

138. Bujak M, Dobaczewski M, Gonzalez-Quesada C, Xia Y, Leucker T, Zymek P, et al. Induction of the CXC chemokine interferon-gamma-inducible protein 10 regulates the reparative response following myocardial infarction. Circ Res. 2009;105(10):973-83.

139. Altara R, Manca M, Brandao RD, Zeidan A, Booz GW, Zouein FA. Emerging importance of chemokine receptor CXCR3 and its ligands in cardiovascular diseases. Clin Sci (Lond). 2016;130(7):463-78.

140. Francis GS. Neurohormonal control of heart failure. Cleve Clin J Med. 2011;78 Suppl 1:S75-9.

141. Torre-Amione G, Kapadia S, Lee J, Durand JB, Bies RD, Young JB, et al. Tumor necrosis factor-alpha and tumor necrosis factor receptors in the failing human heart. Circulation. 1996;93(4):704-11.

142. Vasan RS, Sullivan LM, Roubenoff R, Dinarello CA, Harris T, Benjamin EJ, et al. Inflammatory markers and risk of heart failure in elderly subjects without prior myocardial infarction: the Framingham Heart Study. Circulation. 2003;107(11):1486-91.

143. Mann DL. Innate immunity and the failing heart: the cytokine hypothesis revisited. Circ Res. 2015;116(7):1254-68.

144. Tracey KJ, Beutler B, Lowry SF, Merryweather J, Wolpe S, Milsark IW, et al. Shock and tissue injury induced by recombinant human cachectin. Science. 1986;234(4775):470-4.

145. Mann DL. Inflammatory mediators and the failing heart: past, present, and the foreseeable future. Circ Res. 2002;91(11):988-98.

146. Bozkurt B, Kribbs SB, Clubb FJ, Jr., Michael LH, Didenko VV, Hornsby PJ, et al. Pathophysiologically relevant concentrations of tumor necrosis factor-alpha promote progressive left ventricular dysfunction and remodeling in rats. Circulation. 1998;97(14):1382-91.

147. Kubota T, McTiernan CF, Frye CS, Slawson SE, Lemster BH, Koretsky AP, et al. Dilated cardiomyopathy in transgenic mice with cardiac-specific overexpression of tumor necrosis factor-alpha. Circ Res. 1997;81(4):627-35.

148. Moe KT, Khairunnisa K, Yin NO, Chin-Dusting J, Wong P, Wong MC. Tumor necrosis factor-alpha-induced nuclear factor-kappaB activation in human cardiomyocytes is mediated by NADPH oxidase. J Physiol Biochem. 2014;70(3):769-79.

149. Finkel MS, Oddis CV, Jacob TD, Watkins SC, Hattler BG, Simmons RL. Negative inotropic effects of cytokines on the heart mediated by nitric oxide. Science. 1992;257(5068):387-9.

150. Chung ES, Packer M, Lo KH, Fasanmade AA, Willerson JT, Anti TNFTACHFI. Randomized, double-blind, placebo-controlled, pilot trial of infliximab, a chimeric monoclonal antibody to tumor necrosis factor-alpha, in patients with moderate-to-severe heart failure: results of the anti-TNF Therapy Against Congestive Heart Failure (ATTACH) trial. Circulation. 2003;107(25):3133-40.

151. Mann DL, McMurray JJ, Packer M, Swedberg K, Borer JS, Colucci WS, et al. Targeted anticytokine therapy in patients with chronic heart failure: results of the Randomized Etanercept Worldwide Evaluation (RENEWAL). Circulation. 2004;109(13):1594-602.

152. Van Tassell BW, Abouzaki NA, Oddi Erdle C, Carbone S, Trankle CR, Melchior RD, et al. Interleukin-1 Blockade in Acute Decompensated Heart Failure: A Randomized, Double-Blinded, Placebo-Controlled Pilot Study. J Cardiovasc Pharmacol. 2016;67(6):544-51.

153. Zhao L, Cheng G, Jin R, Afzal MR, Samanta A, Xuan YT, et al. Deletion of Interleukin-6 Attenuates Pressure Overload-Induced Left Ventricular Hypertrophy and Dysfunction. Circ Res. 2016;118(12):1918-29.

154. Wang H, Hou L, Kwak D, Fassett J, Xu X, Chen A, et al. Increasing Regulatory T Cells With Interleukin-2 and Interleukin-2 Antibody Complexes Attenuates Lung Inflammation and Heart Failure Progression. Hypertension. 2016;68(1):114-22.

155. Peng H, Sarwar Z, Yang XP, Peterson EL, Xu J, Janic B, et al. Profibrotic Role for Interleukin-4 in Cardiac Remodeling and Dysfunction. Hypertension. 2015;66(3):582-9.

156. Wu L, Ong S, Talor MV, Barin JG, Baldeviano GC, Kass DA, et al. Cardiac fibroblasts mediate IL-17A-driven inflammatory dilated cardiomyopathy. J Exp Med. 2014;211(7):1449-64.

157. Saxena A, Chen W, Su Y, Rai V, Uche OU, Li N, et al. IL-1 induces proinflammatory leukocyte infiltration and regulates fibroblast phenotype in the infarcted myocardium. J Immunol. 2013;191(9):4838-48.

158. Agnoletti L, Curello S, Bachetti T, Malacarne F, Gaia G, Comini L, et al. Serum from patients with severe heart failure downregulates eNOS and is proapoptotic: role of tumor necrosis factor-alpha. Circulation. 1999;100(19):1983-91.

159. Tang TT, Ding YJ, Liao YH, Yu X, Xiao H, Xie JJ, et al. Defective circulating CD4CD25+Foxp3+CD127(low) regulatory T-cells in patients with chronic heart failure. Cell Physiol Biochem. 2010;25(4-5):451-8.

160. Li N, Bian H, Zhang J, Li X, Ji X, Zhang Y. The Th17/Treg imbalance exists in patients with heart failure with normal ejection fraction and heart failure with reduced ejection fraction. Clin Chim Acta. 2010;411(23-24):1963-8.

161. Guzik TJ, Hoch NE, Brown KA, McCann LA, Rahman A, Dikalov S, et al. Role of the T cell in the genesis of angiotensin II induced hypertension and vascular dysfunction. J Exp Med. 2007;204(10):2449-60.

162. Yan X, Anzai A, Katsumata Y, Matsuhashi T, Ito K, Endo J, et al. Temporal dynamics of cardiac immune cell accumulation following acute myocardial infarction. J Mol Cell Cardiol. 2013;62:24-35.

163. Weirather J, Hofmann UD, Beyersdorf N, Ramos GC, Vogel B, Frey A, et al. Foxp3+ CD4+ T cells improve healing after myocardial infarction by modulating monocyte/macrophage differentiation. Circ Res. 2014;115(1):55-67.

164. Kvakan H, Kleinewietfeld M, Qadri F, Park JK, Fischer R, Schwarz I, et al. Regulatory T cells ameliorate angiotensin II-induced cardiac damage. Circulation. 2009;119(22):2904-12.

165. Kanellakis P, Dinh TN, Agrotis A, Bobik A. CD4(+)CD25(+)Foxp3(+) regulatory T cells suppress cardiac fibrosis in the hypertensive heart. J Hypertens. 2011;29(9):1820-8.

166. Frieler RA, Mortensen RM. Immune cell and other noncardiomyocyte regulation of cardiac hypertrophy and remodeling. Circulation. 2015;131(11):1019-30.

167. Sligh JE, Jr., Ballantyne CM, Rich SS, Hawkins HK, Smith CW, Bradley A, et al. Inflammatory and immune responses are impaired in mice deficient in intercellular adhesion molecule 1. Proc Natl Acad Sci U S A. 1993;90(18):8529-33.

168. Mueller KB, Bender SB, Hong K, Yang Y, Aronovitz M, Jaisser F, et al. Endothelial Mineralocorticoid Receptors Differentially Contribute to Coronary and Mesenteric Vascular Function Without Modulating Blood Pressure. Hypertension. 2015;66(5):988-97.

169. Rockman HA, Ross RS, Harris AN, Knowlton KU, Steinhelper ME, Field LJ, et al. Segregation of atrial-specific and inducible expression of an atrial natriuretic factor transgene in an in vivo murine model of cardiac hypertrophy. Proc Natl Acad Sci U S A. 1991;88(18):8277-81.

170. Salvador AM, Nevers T, Velazquez F, Aronovitz M, Wang B, Abadia Molina A, et al. Intercellular Adhesion Molecule 1 Regulates Left Ventricular Leukocyte Infiltration, Cardiac Remodeling, and Function in Pressure Overload-Induced Heart Failure. J Am Heart Assoc. 2016;5(3):e003126.

171. Kouranova E, Forbes K, Zhao G, Warren J, Bartels A, Wu Y, et al. CRISPRs for Optimal Targeting: Delivery of CRISPR Components as DNA, RNA, and Protein into Cultured Cells and Single-Cell Embryos. Hum Gene Ther. 2016;27(6):464-75.

172. Niessen HW, Lagrand WK, Visser CA, Meijer CJ, Hack CE. Upregulation of ICAM-1 on cardiomyocytes in jeopardized human myocardium during infarction. Cardiovasc Res. 1999;41(3):603-10.

173. McMullen JR, Jennings GL. Differences between pathological and physiological cardiac hypertrophy: novel therapeutic strategies to treat heart failure. Clin Exp Pharmacol Physiol. 2007;34(4):255-62.

174. Nevers T, Salvador AM, Grodecki-Pena A, Knapp A, Velazquez F, Aronovitz M, et al. Left Ventricular T-Cell Recruitment Contributes to the Pathogenesis of Heart Failure. Circ Heart Fail. 2015;8(4):776-87.

175. Laroumanie F, Douin-Echinard V, Pozzo J, Lairez O, Tortosa F, Vinel C, et al. CD4+ T cells promote the transition from hypertrophy to heart failure during chronic pressure overload. Circulation. 2014;129(21):2111-24.

176. Huppa JB, Davis MM. T-cell-antigen recognition and the immunological synapse. Nat Rev Immunol. 2003;3(12):973-83.

177. Miyata S, Minobe W, Bristow MR, Leinwand LA. Myosin heavy chain isoform expression in the failing and nonfailing human heart. Circ Res. 2000;86(4):386-90.

178. Kuster GM, Kotlyar E, Rude MK, Siwik DA, Liao R, Colucci WS, et al. Mineralocorticoid receptor inhibition ameliorates the transition to myocardial failure and decreases oxidative stress and inflammation in mice with chronic pressure overload. Circulation. 2005;111(4):420-7.

179. Alcaide P, Auerbach S, Luscinskas FW. Neutrophil recruitment under shear flow: it's all about endothelial cell rings and gaps. Microcirculation. 2009;16(1):43-57.

180. Luscinskas FW, Cybulsky MI, Kiely JM, Peckins CS, Davis VM, Gimbrone MA, Jr. Cytokine-activated human endothelial monolayers support enhanced neutrophil transmigration via a mechanism involving both endothelial-leukocyte adhesion molecule-1 and intercellular adhesion molecule-1. J Immunol. 1991;146(5):1617-25.

181. Lother A, Berger S, Gilsbach R, Rosner S, Ecke A, Barreto F, et al. Ablation of mineralocorticoid receptors in myocytes but not in fibroblasts preserves cardiac function. Hypertension. 2011;57(4):746-54.

182. Tsagalou EP, Anastasiou-Nana M, Agapitos E, Gika A, Drakos SG, Terrovitis JV, et al. Depressed coronary flow reserve is associated with decreased myocardial capillary density in patients with heart failure due to idiopathic dilated cardiomyopathy. J Am Coll Cardiol. 2008;52(17):1391-8.

183. Rocha R, Rudolph AE, Frierdich GE, Nachowiak DA, Kekec BK, Blomme EA, et al. Aldosterone induces a vascular inflammatory phenotype in the rat heart. Am J Physiol Heart Circ Physiol. 2002;283(5):H1802-10.

184. McGraw AP, Bagley J, Chen WS, Galayda C, Nickerson H, Armani A, et al. Aldosterone increases early atherosclerosis and promotes plaque inflammation through

a placental growth factor-dependent mechanism. J Am Heart Assoc. 2013;2(1):e000018.

185. Altara R, Gu YM, Struijker-Boudier HA, Thijs L, Staessen JA, Blankesteijn WM. Left Ventricular Dysfunction and CXCR3 Ligands in Hypertension: From Animal Experiments to a Population-Based Pilot Study. PLoS One. 2015;10(10):e0141394.

186. Altara R, Manca M, Hessel MH, Gu Y, van Vark LC, Akkerhuis KM, et al. CXCL10 Is a Circulating Inflammatory Marker in Patients with Advanced Heart Failure: a Pilot Study. J Cardiovasc Transl Res. 2016;9(4):302-14.

187. Farber JM. Mig and IP-10: CXC chemokines that target lymphocytes. J Leukoc Biol. 1997;61(3):246-57.

188. Luster AD, Ravetch JV. Biochemical characterization of a gamma interferon-inducible cytokine (IP-10). J Exp Med. 1987;166(4):1084-97.

189. Ooi JY, Tuano NK, Rafehi H, Gao XM, Ziemann M, Du XJ, et al. HDAC inhibition attenuates cardiac hypertrophy by acetylation and deacetylation of target genes. Epigenetics. 2015;10(5):418-30.

190. Altara R, Manca M, Hessel MH, Janssen BJ, Struijker-Boudier HH, Hermans RJ, et al. Improving membrane based multiplex immunoassays for semi-quantitative detection of multiple cytokines in a single sample. BMC Biotechnol. 2014;14:63.

191. Ye F, Kim C, Ginsberg MH. Reconstruction of integrin activation. Blood. 2012;119(1):26-33.

192. Pasvolsky R, Grabovsky V, Giagulli C, Shulman Z, Shamri R, Feigelson SW, et al. RhoA is involved in LFA-1 extension triggered by CXCL12 but not in a novel outside-in LFA-1 activation facilitated by CXCL9. J Immunol. 2008;180(5):2815-23.

193. Jinek M, Chylinski K, Fonfara I, Hauer M, Doudna JA, Charpentier E. A programmable dual-RNA-guided DNA endonuclease in adaptive bacterial immunity. Science. 2012;337(6096):816-21.

194. Yang H, Wang H, Shivalila CS, Cheng AW, Shi L, Jaenisch R. One-step generation of mice carrying reporter and conditional alleles by CRISPR/Cas-mediated genome engineering. Cell. 2013;154(6):1370-9.

195. Horvath P, Barrangou R. CRISPR/Cas, the immune system of bacteria and archaea. Science. 2010;327(5962):167-70.

196. Sander JD, Joung JK. CRISPR-Cas systems for editing, regulating and targeting genomes. Nat Biotechnol. 2014;32(4):347-55.

197. Lichtman AH. The heart of the matter: protection of the myocardium from T cells. J Autoimmun. 2013;45:90-6.

198. Yu Q, Watson RR, Marchalonis JJ, Larson DF. A role for T lymphocytes in mediating cardiac diastolic function. Am J Physiol Heart Circ Physiol. 2005;289(2):H643-51.

199. Li J, Wang L, Wang S, Zhu H, Ye P, Xie A, et al. The Treg/Th17 imbalance in patients with idiopathic dilated cardiomyopathy. Scand J Immunol. 2010;71(4):298-303.

200. Hofmann U, Beyersdorf N, Weirather J, Podolskaya A, Bauersachs J, Ertl G, et al. Activation of CD4+ T lymphocytes improves wound healing and survival after experimental myocardial infarction in mice. Circulation. 2012;125(13):1652-63.

201. Li XM, Ma YT, Yang YN, Liu F, Chen BD, Han W, et al. Downregulation of survival signalling pathways and increased apoptosis in the transition of pressure overload-induced cardiac hypertrophy to heart failure. Clin Exp Pharmacol Physiol. 2009;36(11):1054-61.

202. Tarrio ML, Grabie N, Bu DX, Sharpe AH, Lichtman AH. PD-1 protects against inflammation and myocyte damage in T cell-mediated myocarditis. J Immunol. 2012;188(10):4876-84.

203. Lv H, Havari E, Pinto S, Gottumukkala RV, Cornivelli L, Raddassi K, et al. Impaired thymic tolerance to alpha-myosin directs autoimmunity to the heart in mice and humans. J Clin Invest. 2011;121(4):1561-73.

204. Mills KH. TLR-dependent T cell activation in autoimmunity. Nat Rev Immunol. 2011;11(12):807-22.

205. Peine M, Marek RM, Lohning M. IL-33 in T Cell Differentiation, Function, and Immune Homeostasis. Trends Immunol. 2016;37(5):321-33.

206. Alcaide P, Jones TG, Lord GM, Glimcher LH, Hallgren J, Arinobu Y, et al. Dendritic cell expression of the transcription factor T-bet regulates mast cell progenitor homing to mucosal tissue. J Exp Med. 2007;204(2):431-9.

207. Marko L, Kvakan H, Park JK, Qadri F, Spallek B, Binger KJ, et al. Interferon-gamma signaling inhibition ameliorates angiotensin II-induced cardiac damage. Hypertension. 2012;60(6):1430-6.

208. de Gaetano M, Dempsey E, Marcone S, James WG, Belton O. Conjugated linoleic acid targets beta2 integrin expression to suppress monocyte adhesion. J Immunol. 2013;191(8):4326-36.

209. Yoshida Y, Shimizu I, Katsuumi G, Jiao S, Suda M, Hayashi Y, et al. p53-Induced inflammation exacerbates cardiac dysfunction during pressure overload. J Mol Cell Cardiol. 2015;85:183-98.

210. Hilgendorf I, Gerhardt LM, Tan TC, Winter C, Holderried TA, Chousterman BG, et al. Ly-6Chigh monocytes depend on Nr4a1 to balance both inflammatory and reparative phases in the infarcted myocardium. Circ Res. 2014;114(10):1611-22.

211. Dutta P, Nahrendorf M. Monocytes in myocardial infarction. Arterioscler Thromb Vasc Biol. 2015;35(5):1066-70.

212. Weisheit C, Zhang Y, Faron A, Kopke O, Weisheit G, Steinstrasser A, et al. Ly6C(low) and not Ly6C(high) macrophages accumulate first in the heart in a model of murine pressure-overload. PLoS One. 2014;9(11):e112710.

213. Ramos TN, Bullard DC, Barnum SR. ICAM-1: isoforms and phenotypes. J Immunol. 2014;192(10):4469-74.

214. Bullard DC, Hu X, Crawford D, McDonald K, Ramos TN, Barnum SR. Expression of a single ICAM-1 isoform on T cells is sufficient for development of experimental autoimmune encephalomyelitis. Eur J Immunol. 2014;44(4):1194-9.

215. Krenz M, Robbins J. Impact of beta-myosin heavy chain expression on cardiac function during stress. J Am Coll Cardiol. 2004;44(12):2390-7.

216. Hoch NE, Guzik TJ, Chen W, Deans T, Maalouf SA, Gratze P, et al. Regulation of T-cell function by endogenously produced angiotensin II. Am J Physiol Regul Integr Comp Physiol. 2009;296(2):R208-16.

217. Schmal H, Czermak BJ, Lentsch AB, Bless NM, Beck-Schimmer B, Friedl HP, et al. Soluble ICAM-1 activates lung macrophages and enhances lung injury. J Immunol. 1998;161(7):3685-93.

218. Otto VI, Gloor SM, Frentzel S, Gilli U, Ammann E, Hein AE, et al. The production of macrophage inflammatory protein-2 induced by soluble intercellular adhesion molecule-1 in mouse astrocytes is mediated by src tyrosine kinases and p42/44 mitogen-activated protein kinase. J Neurochem. 2002;80(5):824-34.

219. Zhu X, Fang J, Jiang DS, Zhang P, Zhao GN, Zhu X, et al. Exacerbating Pressure Overload-Induced Cardiac Hypertrophy: Novel Role of Adaptor Molecule Src Homology 2-B3. Hypertension. 2015;66(3):571-81.

220. Zhang S, Weinheimer C, Courtois M, Kovacs A, Zhang CE, Cheng AM, et al. The role of the Grb2-p38 MAPK signaling pathway in cardiac hypertrophy and fibrosis. J Clin Invest. 2003;111(6):833-41.

221. Wang Y. Mitogen-activated protein kinases in heart development and diseases. Circulation. 2007;116(12):1413-23.

222. Yin WH, Chen JW, Jen HL, Chiang MC, Huang WP, Feng AN, et al. The prognostic value of circulating soluble cell adhesion molecules in patients with chronic congestive heart failure. Eur J Heart Fail. 2003;5(4):507-16.

223. Gwechenberger M, Mendoza LH, Youker KA, Frangogiannis NG, Smith CW, Michael LH, et al. Cardiac myocytes produce interleukin-6 in culture and in viable border zone of reperfused infarctions. Circulation. 1999;99(4):546-51.

224. Davani EY, Dorscheid DR, Lee CH, van Breemen C, Walley KR. Novel regulatory mechanism of cardiomyocyte contractility involving ICAM-1 and the cytoskeleton. Am J Physiol Heart Circ Physiol. 2004;287(3):H1013-22.

225. Entman ML, Youker K, Shoji T, Kukielka G, Shappell SB, Taylor AA, et al. Neutrophil induced oxidative injury of cardiac myocytes. A compartmented system requiring CD11b/CD18-ICAM-1 adherence. J Clin Invest. 1992;90(4):1335-45.

226. Morris BJ, Davis JO, Zatzman ML, Williams GM. The renin-angiotensin-aldosterone system in rabbits with congestive heart failure produced by aortic constriction. Circ Res. 1977;40(3):275-82.

227. Young M, Head G, Funder J. Determinants of cardiac fibrosis in experimental hypermineralocorticoid states. Am J Physiol. 1995;269(4 Pt 1):E657-62.

228. Somanna NK, Yariswamy M, Garagliano JM, Siebenlist U, Mummidi S, Valente AJ, et al. Aldosterone-induced cardiomyocyte growth, and fibroblast migration and proliferation are mediated by TRAF3IP2. Cell Signal. 2015;27(10):1928-38.

229. Mann DL, Young JB. Basic mechanisms in congestive heart failure. Recognizing the role of proinflammatory cytokines. Chest. 1994;105(3):897-904.

230. Suzuki S, Shishido T, Funayama A, Netsu S, Ishino M, Kitahara T, et al. Long pentraxin PTX3 exacerbates pressure overload-induced left ventricular dysfunction. PLoS One. 2013;8(1):e53133.

231. Li X, Qi Y, Li Y, Zhang S, Guo S, Chu S, et al. Impact of mineralocorticoid receptor antagonists on changes in cardiac structure and function of left ventricular

dysfunction: a meta-analysis of randomized controlled trials. Circ Heart Fail. 2013;6(2):156-65.

232. Le Menuet D, Isnard R, Bichara M, Viengchareun S, Muffat-Joly M, Walker F, et al. Alteration of cardiac and renal functions in transgenic mice overexpressing human mineralocorticoid receptor. J Biol Chem. 2001;276(42):38911-20.

233. Ouvrard-Pascaud A, Sainte-Marie Y, Benitah JP, Perrier R, Soukaseum C, Nguyen Dinh Cat A, et al. Conditional mineralocorticoid receptor expression in the heart leads to life-threatening arrhythmias. Circulation. 2005;111(23):3025-33.

234. Herrada AA, Contreras FJ, Marini NP, Amador CA, Gonzalez PA, Cortes CM, et al. Aldosterone promotes autoimmune damage by enhancing Th17-mediated immunity. J Immunol. 2010;184(1):191-202.

235. Usher MG, Duan SZ, Ivaschenko CY, Frieler RA, Berger S, Schutz G, et al. Myeloid mineralocorticoid receptor controls macrophage polarization and cardiovascular hypertrophy and remodeling in mice. J Clin Invest. 2010;120(9):3350-64.

236. Francis J, Weiss RM, Johnson AK, Felder RB. Central mineralocorticoid receptor blockade decreases plasma TNF-alpha after coronary artery ligation in rats. Am J Physiol Regul Integr Comp Physiol. 2003;284(2):R328-35.

237. Kang YM, Zhang ZH, Johnson RF, Yu Y, Beltz T, Johnson AK, et al. Novel effect of mineralocorticoid receptor antagonism to reduce proinflammatory cytokines and hypothalamic activation in rats with ischemia-induced heart failure. Circ Res. 2006;99(7):758-66.

238. Lehmann LH, Rostosky JS, Buss SJ, Kreusser MM, Krebs J, Mier W, et al. Essential role of sympathetic endothelin A receptors for adverse cardiac remodeling. Proc Natl Acad Sci U S A. 2014;111(37):13499-504.

239. Ito H, Hiroe M, Hirata Y, Fujisaki H, Adachi S, Akimoto H, et al. Endothelin ETA receptor antagonist blocks cardiac hypertrophy provoked by hemodynamic overload. Circulation. 1994;89(5):2198-203.

240. Gueret A, Harouki N, Favre J, Galmiche G, Nicol L, Henry JP, et al. Vascular Smooth Muscle Mineralocorticoid Receptor Contributes to Coronary and Left Ventricular Dysfunction After Myocardial Infarction. Hypertension. 2016;67(4):717-23.

241. Favre J, Gao J, Zhang AD, Remy-Jouet I, Ouvrard-Pascaud A, Dautreaux B, et al. Coronary endothelial dysfunction after cardiomyocyte-specific mineralocorticoid receptor overexpression. Am J Physiol Heart Circ Physiol. 2011;300(6):H2035-43.

242. Garg R, Rao AD, Baimas-George M, Hurwitz S, Foster C, Shah RV, et al. Mineralocorticoid receptor blockade improves coronary microvascular function in individuals with type 2 diabetes. Diabetes. 2015;64(1):236-42.

243. Ayuzawa N, Nagase M, Ueda K, Nishimoto M, Kawarazaki W, Marumo T, et al. Rac1-Mediated Activation of Mineralocorticoid Receptor in Pressure Overload-Induced Cardiac Injury. Hypertension. 2016;67(1):99-106.

244. Shamri R, Grabovsky V, Gauguet JM, Feigelson S, Manevich E, Kolanus W, et al. Lymphocyte arrest requires instantaneous induction of an extended LFA-1 conformation mediated by endothelium-bound chemokines. Nat Immunol. 2005;6(5):497-506.

245. Piali L, Weber C, LaRosa G, Mackay CR, Springer TA, Clark-Lewis I, et al. The chemokine receptor CXCR3 mediates rapid and shear-resistant adhesion-induction of effector T lymphocytes by the chemokines IP10 and Mig. Eur J Immunol. 1998;28(3):961-72.

246. Schrier SB, Hill AS, Plana D, Lauffenburger DA. Synergistic Communication between CD4+ T Cells and Monocytes Impacts the Cytokine Environment. Scientific Reports. 2016;6:34942.

247. Athanassopoulos P, Vaessen LM, Balk AH, Weimar W, Sharma HS, Bogers AJ. Altered chemokine receptor profile on circulating leukocytes in human heart failure. Cell Biochem Biophys. 2006;44(1):83-101.

248. Weichhart T, Hengstschlager M, Linke M. Regulation of innate immune cell function by mTOR. Nat Rev Immunol. 2015;15(10):599-614.

249. Chen W, Wan X, Ukah TK, Miller MM, Barik S, Cattin-Roy AN, et al. Antigen-Specific Immune Modulation Targets mTORC1 Function To Drive Chemokine Receptor-Mediated T Cell Tolerance. J Immunol. 2016;197(9):3554-65.

250. Bishop KA, Harrington A, Kouranova E, Weinstein EJ, Rosen CJ, Cui X, et al. CRISPR/Cas9-Mediated Insertion of loxP Sites in the Mouse Dock7 Gene Provides an Effective Alternative to Use of Targeted Embryonic Stem Cells. G3 (Bethesda). 2016;6(7):2051-61.